Durham E-Theses

From the bottom to the top: Assessing the potential subsurface migration of fracking-related fluids along natural geological pathways

WILSON, MILES,PERRY

From the bottom to the top:

Assessing the potential subsurface migration of fracking-related fluids along natural geological pathways

Miles Perry Wilson

Department of Earth Sciences

A thesis submitted to Durham University in fulfilment of the requirements for the

degree of Doctor of Philosophy (PhD)

March 2020

Abstract

Over the last century humans have increasingly gone from just extracting fluids from the subsurface to also injecting them, for example hydraulic fracturing (fracking) for shale gas. Concurrently, there has been increased environmental interest in how injected fluids might interact with natural groundwater systems. One potential environmental impact of fracking is the contamination of shallow groundwater from the upward migration of injected and formation fluids along natural geological pathways. High-permeability fault and fracture zones have generally been regarded as the highest-risk pathway. Therefore, the first aim of this thesis was to determine a horizontal respect distance between fluid injection locations and known faults. Using published microseismic data a horizontal respect distance of ~900 m was proposed. The second aim of this thesis was to consider complex geological structure in numerical models to investigate hydrogeological factors which might increase the vulnerability of shallow groundwater resources to the potential upward migration of fracking-related fluids. Using 2D and 3D numerical models four hydrogeological factors increased the vulnerability of a shallow aquifer to upward fluid migration from an underlying shale reservoir: increased stimulated fracture extent; greater amounts of overpressure; the presence of low-permeability faults; and the absence of deep high-permeability formations. Low-permeability faults acted to compartmentalise groundwater, thereby discouraging regional horizontal flow whilst encouraging upward flow through strata. The integration of groundwater quality and seismic reflection data provided a novel method for identifying compartmentalisation, but compartmentalisation could not be identified from surface water quality data in the studied basin. However, analysis of surface water quality data could demonstrate regional-scale groundwater-surface water interactions. Importantly, this thesis highlights the need to understand and model interactions between deep groundwater, shallow groundwater, and surface waters by integrating data from a variety of industry and environmental regulatory sources.

Table of contents

Declaration

No part of this thesis has previously been submitted for a degree at this or any other university. The work described in this thesis is entirely that of the author, except where reference is made to previously published or unpublished work. Work for this thesis was conducted from October 2016 to March 2020 under the supervision of Professor Fred Worrall at Durham University, UK.

Miles Perry Wilson

Durham University

March 2020

Acknowledgements

Supervisory team

First and foremost I would like to acknowledge and thank my supervisory team of Fred Worrall, Richard Davies and Alwyn Hart. Not only have they guided the analyses and put up with my regular proof-reading requests, but they supported me in the years leading up to my PhD and continue to do so now it is complete. I have thoroughly enjoyed working with them and look forward to our future work together. I would also like to thank Gillian Foulger, Jon Gluyas, Bruce Julian and Theresa Jezierski for their support and guidance through the Human-Induced Earthquake Database project, which ran alongside my PhD.

Family and friends

Thank you to my wonderful partner Sarah Clancy for her constant support and positivity throughout my PhD. From when I first sat next to her in the months before my PhD she has been an ever-friendly face and tower of strength, even in the face of adversity. We've shared some incredible experiences together, both inside and outside our PhD work, and I look forward to many more over the coming years. Thank you also to my parents and brother for their support during my PhD. Although the following thesis content probably means very little to them, all of this would not have been possible without their support in the background. I would also like to extend my thanks to my flatmate Ollie Barker and my close Durham-related friends from the Department of Earth Sciences and St Aidan's College Boat Club: Katy Burrows; Kate Horan; Jack Lee; Jordan Phethean; Chris Ward; Paddy Alton; Evan Bolle-Jones; James Hammond; Jack Pooley; and Henry Scott. We've spent far too long together either in boats, climbing walls, coffee rooms, gyms, hotels, pubs, tents or vans, but I wouldn't have had it any other way.

Funding

This thesis is dedicated to Professor Neil Goulty (1949 to 2018)

Neil, the most attentive and patient lecturer I have known in my time in academia, first planted the idea of a PhD in my head as a geophysics undergraduate. Although this thesis expands well beyond the world of geophysics, I thank Neil for his unrivalled teaching, his inspiration, and for planting that initial seed.

There is no magic to achievement. It's really about hard work, choices, and persistence.

Michelle Obama

1 Introduction

Below the water table rocks in the Earth's crust are saturated by fluids, predominantly comprising of water. The flow and pressure of these fluids play a critical role in many natural subsurface processes [*Cathles*, 1990]: earthquake nucleation [*Sibson*, 1974]; rock weakening and deformation [*Griggs*, 1967]; ore-body formation [*Hedenquist & Lowenstern*, 1994]; accumulation of oil and gas [*Gussow*, 1954]; and water supply to surface water systems [*Sear et al.*, 1999]. Subsurface fluids also form important resources exploited globally by humans. Historically, exploitation either made use of naturally rising fluids (e.g. thermal springs for bathing and heating) or artificially extracting fluids from the subsurface (e.g. freshwater for drinking or petroleum for energy production). However, over the last century humans have increasingly gone from just extracting fluids from the subsurface to also injecting them for a range of purposes [*Foulger et al.*, 2018]: carbon capture and storage; gas storage; geothermal energy production; reservoir stimulation; salt mining; secondary oil recovery; and waste-water disposal. As a result, on a global scale there has been increased commercial and environmental interest in understanding groundwater systems and how injected fluids interact with such systems.

1.1 Hydraulic fracturing

Hydraulic fracturing (fracking) is a process used to recover commercial quantities of oil and gas from low-permeability unconventional reservoirs such as shale. Fracking involves the subsurface injection of a pressurised fluid which usually consists of water, chemical additives and a proppant, for example sand [*King*, 2012]. Chemical additives typically form 0.5 to 2.0% of the injected fluid and are added for a number of reasons: to reduce friction and thereby reduce injection pressures (slickwater); to help carry proppants to the reservoir; to prevent biological growth and metal corrosion; and to remove drilling mud damage surrounding the borehole [*FracFocus*, 2019]. The fluid is

1

injected at a pressure greater than the strength of the reservoir rock, resulting in tensile and shear failure of the rock and the creation of a network of hydraulic fractures. This network is often referred to as a stimulated reservoir volume (SRV) [*Mayerhofer et al.*, 2010]. The purpose of the proppant is to prevent the newly created fractures from closing, thereby increasing the reservoir permeability and allowing oil and gas to flow more easily back to the surface via the borehole. Although fracking has been used for decades, the application to shale reservoirs using multiple horizontal boreholes and injection stages is a more recent development [*King,* 2012]; using the widespread application of fracking the United States of America (USA) increased gas production from shale reservoirs from $\sim3.7\times10^{10}$ m^3 (1293 bcf) in 2007 to $\sim5.3\times10^{11}$ m^3 (18589 bcf) in 2017 (Figure 1.1) [*US EIA,* 2019]. This growth in production turned the USA from a net gas importer to a net exporter. Other countries have looked to follow suit with commercial shale gas production also occurring in Canada, China and Argentina. Elsewhere, including in the United Kingdom (UK), shale gas resources have been identified and licenses issued, but only a few exploratory boreholes drilled.
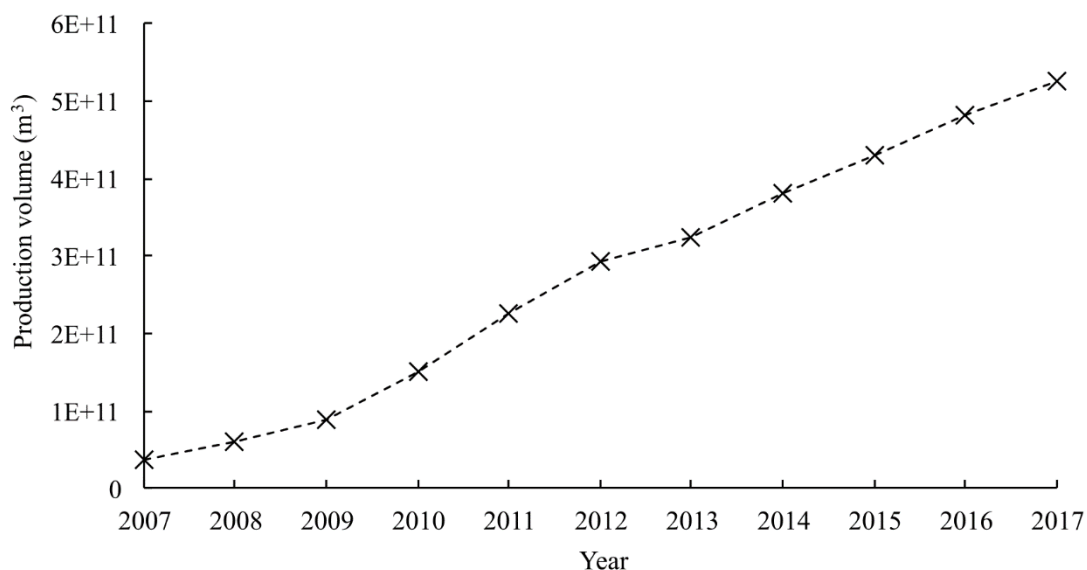
Figure 1.1
USA annual shale gas production volumes from 2007 to 2017. Data from US EIA [2019].

1.2   Fracking in the UK

The development of shale gas has been slow in the UK and moratoriums now exist in England, Scotland, Wales and Northern Ireland. Only in England has there been exploratory drilling, but only three boreholes targeting shale gas have been fracked to date and resource estimates still vary widely [e.g. *Andrews*, 2013; *Whitelaw et al.*, 2019]. All three of these boreholes targeted the Bowland Shale in the Bowland Basin, northwest England (Figure 1.2). The first borehole to be drilled and fracked was Preese Hall 1 (PH-1) in 2011. However, following the injection of 2245 m^3 of fluid a series of earthquakes occurred from the reactivation of a previously unknown natural geological fault [*Clarke et al.*, 2014a]. The largest earthquake in the sequence reached local magnitude (M_L) 2.3 and was felt by the local population [*BGS*, 2019a]. As a result of the induced seismicity a government enquiry was carried out and a temporary ban on fracking was enforced for 18 months. PH-1 was plugged, abandoned and the site remediated.

In October 2018 fracking recommenced at the nearby Preston New Road site (Figure 1.2) under a new regulatory traffic light system (TLS) designed to mitigate the risk of induced seismicity (Figure 1.3). The TLS had a red-light threshold of M_L 0.5 and on detecting an earthquake of this magnitude the operator must suspend injection, reduce pressure and monitor seismicity and ground motion for 18 hours for any further earthquakes before potentially resuming injection [*OGA*, 2019]. During the fracking of the Preston New Road 1z borehole (PNR-1z) the British Geological Survey (BGS) detected 57 earthquakes with magnitudes ranging from M_L -0.8 to 1.5 [*BGS*, 2019b]. The two largest earthquakes in the sequence were felt by local residents. The nature of the TLS and the induced seismicity meant that only 17 of the planned 41 stages were injected and, of these, only two were injected with the planned injection volume of 400 m^3 of slickwater and 50 tons of proppant [*Clarke et al.*, 2019].
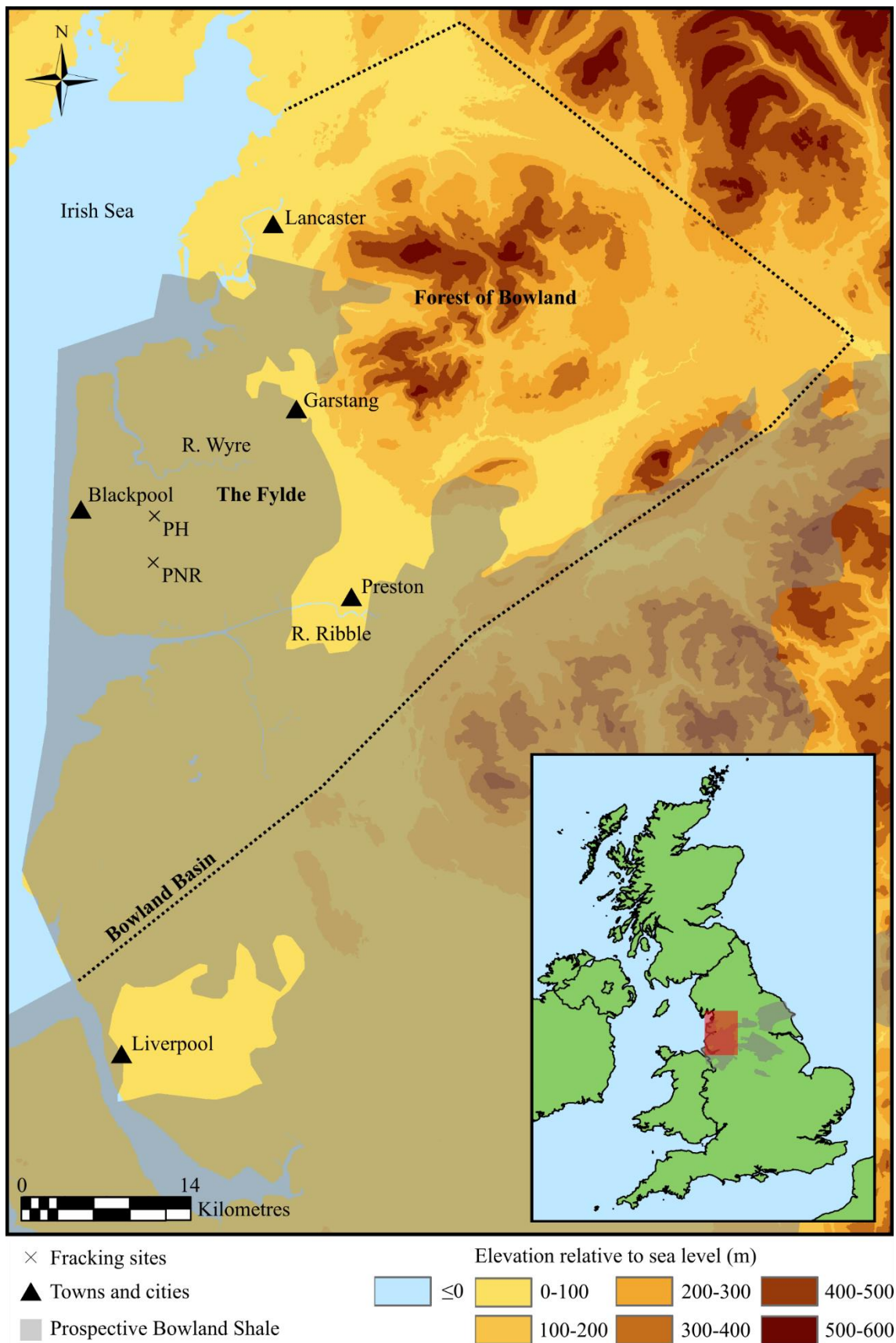
Figure 1.2
Map showing the approximate extent of the Bowland Basin and the fracking sites of
Preese Hall (PH) and Preston New Road (PNR). Contains Ordnance Survey (OS) ©
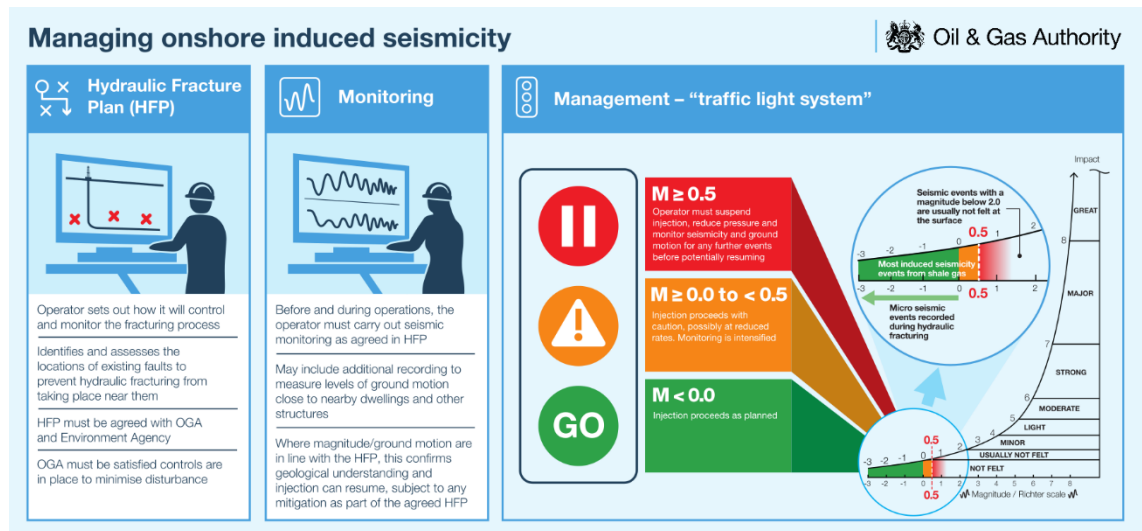
Figure 1.3
The traffic light system used by the UK Oil & Gas Authority (OGA) to mitigate the risk of induced seismicity. Image from OGA [2019].

The third shale gas borehole to be fracked was Preston New Road 2 (PNR-2), also located at the Preston New Road site (Figure 1.2). Fluid injection began on the 15th August 2019 with the same planned injection volumes and proppant tonnage as PNR-1z [*Cuadrilla Resources Ltd.*, 2018a]. The fluid injection resulted in a further 134 earthquakes, including a M_L 2.9 earthquake on the 26th August [*BGS*, 2019b]. The M_L 2.9 earthquake was felt widely across the surrounding local area and given an intensity of six (slightly damaging – objects fall off shelves) on the European Macroseismic Intensity Scale by the BGS. The M_L 2.9 earthquake is now the largest fracking-induced earthquake recorded in the UK, although it was substantially smaller than the largest fracking-induced earthquake recorded globally; a M_L 5.7 earthquake in the Sichuan Province, China [*Lei et al.*, 2019; *Wilson et al.*, 2017a]. Nevertheless, the M_L 2.9 earthquake neared the "low likelihood" expected maximum magnitude for the Preston New Road site [*Ove Arup and Partners Ltd.*, 2014a] and, following an investigation by

the regulatory body (the UK Oil and Gas Authority), fracking has been suspended nationwide until further notice [*BEIS*, 2019].

1.3 Potential environmental impacts of fracking

Alongside induced seismicity the potential environmental impacts of fracking for shale gas and oil have been a global topic of discussion. As a result, initial fracking operations in England have been met by substantial public opposition. Other potential environmental impacts include: water usage and contamination [*Vengosh et al.*, 2013; 2014; *Kondash et al.*, 2018]; fugitive methane (CH_4) emissions [*Boothroyd et al.*, 2016; 2018]; health effects [*Currie et al.*, 2017]; air quality and noise [*Goodman et al.*, 2016]; and surface footprint [*Clancy et al.*, 2018].

1.3.1 Groundwater contamination

Although the public focus in England has primarily been on the impact of induced seismicity, the potential contamination of shallow groundwater ($\leq$400 m below the surface [*UKTAG*, 2011]) has been a key concern for the environmental regulatory body of England; the Environment Agency (EA) [*EA*, 2013]. Groundwater contamination can in theory occur via a number of sources and pathways, for example, surface spills and downward seepage into groundwater; direct leakage from borehole integrity failure; or the migration of fluids from the reservoir along natural geological pathways [*Vengosh et al.*, 2014]. Contaminating fracking-related fluids could consist of chemicals of anthropogenic origin, downhole-altered chemicals (anthropogenic chemicals altered by subsurface conditions such as temperature and pressure) [e.g. *Kahrilas et al.*, 2016] and natural formation fluids such as brines and gas.

1.3.2 Observed groundwater contamination

Observed groundwater contamination from fracking sites is relatively rare and often disputed. For example, in Susquehanna County, Pennsylvania, USA, *Osborn et al.* [2011] and *Jackson et al.* [2013] found that shallow groundwater CH_4 concentrations increased with proximity to the nearest shale gas well. Conversely, it was argued that CH_4 is naturally ubiquitous in groundwater and elevated CH_4 concentrations relate to topography and groundwater geochemistry [*Molofsky et al.*, 2011; 2013; 2016]. It is generally accepted that potential cases of shallow groundwater contamination relate to fluid migration in faulty cements of borehole annuli, either directly into shallow aquifers or via hydraulic connections with intermediate geological formations [*Darrah et al.*, 2014; *Llewellyn et al.*, 2015]. It has been argued that there is no indisputable evidence for the contamination of shallow groundwater by fluids migrating from several kilometres depth along natural geological pathways [*Vengosh et al.*, 2014]. Nevertheless, groundwater contamination via natural geological pathways remains a shared concern amongst stakeholders.

1.3.3 Potential natural geological pathways

Direct hydraulic connection between an exploited shale reservoir and overlying shallow groundwater resources via stimulated hydraulic fractures is considered an unlikely scenario, particularly in the UK [*Flewelling & Sharma*, 2014; *Royal Society and Royal Academy of Engineering*, 2012]. Using microseismic datasets from the USA, *Davies et al.* [2012] reported a maximum observed stimulated fracture height of ~588 m and an ~1% probability of a stimulated fracture exceeding 350 m. Groundwater abstractions in England typically do not descend more than 200 m below ground level and it has been suggested that a reasonable maximum depth of ~400 m may be considered for

7

conventional fresh water aquifers [*UKTAG,* 2011]. UK fracking regulations ensure that fracking must occur at depths ≥1000 m below the surface and ≥1200 m below the surface in: specified groundwater areas; National Parks; Areas of Outstanding National Beauty; and World Heritage Sites [*Infrastructure Act*, 2015; *The Onshore Hydraulic Fracturing (Protected Areas) Regulations*, 2016]. Therefore, a vertical respect distance ≥600 m is always maintained between a subsurface injection point and shallow groundwater resources in the UK, substantially reducing the risk of direct hydraulic connection (Figure 1.4). However, it is possible that if stimulated hydraulic fractures provided an entry point to geological strata that were sufficiently hydraulically connected to shallow groundwater resources, upward migration of fracking-related fluids could occur under certain hydraulic conditions (Figure 1.5).

The other possible natural geological pathway to shallow groundwater is through high-permeability (i.e. high-hydraulic conductivity) fault or fracture zones (Figure 1.5). If fluids were injected directly into a high-permeability fault or fracture zone, or the SRV hydraulically connected with a fault or fracture zone, it is possible that fluids could migrate upwards if hydraulic conditions permitted, for example the fault maintained high-permeability along its length. Predicting flow properties along faults can be challenging because permeability can vary greatly from fault to fault [e.g. *Seymour et al.*, 2006] and along a single fault [e.g. *Fisher & Knipe*, 2001]. To overcome this uncertainty the precautionary principle can be applied; avoid injection or interaction with known faults from prior geological and geophysical surveys, for example those faults inferred from seismic reflection data. Although this approach is not without its problems, such as seismic reflection resolution and distinguishing strike slip faulting, avoiding known faults and fracture zones reduces the risk of hydraulic connections between deep shales and shallow groundwater resources.
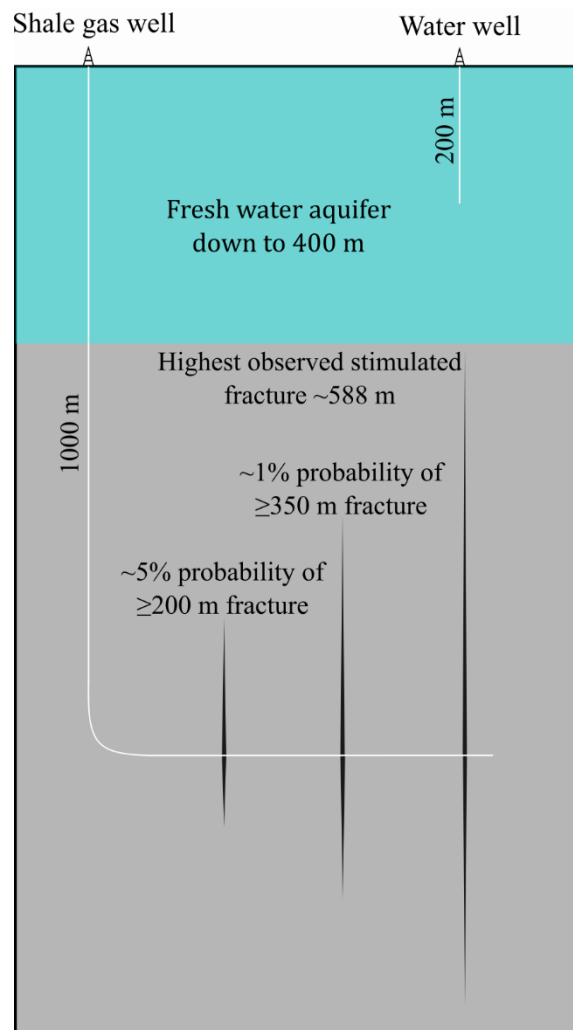
Figure 1.4
Schematic diagram showing the vertical fracture height probabilities of Davies et al. [2012] with respect to UK fracking regulation depth [Infrastructure Act, 2015], typical groundwater abstraction depth and the considered maximum depth of fresh water aquifers [UKTAG, 2011].
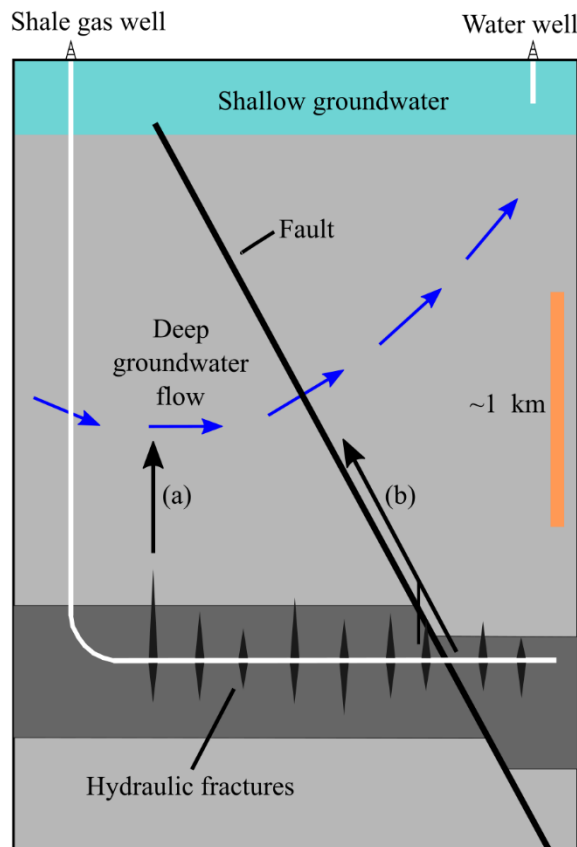
Figure 1.5
Schematic diagram showing potential natural geological pathways for fracking-related
fluids to migrate to shallow groundwater resources. (a) Stimulated fractures providing
an entry point to strata which are hydraulically connected to shallow groundwater. (b)
Stimulated fractures or borehole perforations connecting to a high-permeability fault.

1.3.4   Potential drivers of upward fluid flow from fracking

Birdsell et al. [2015] identified four mechanisms which could drive the upward flow of

fracking-related fluids: topography-driven groundwater flow; overpressure; injection

pressures; and buoyancy. Topography-driven groundwater flow results from differences

in elevation, which drive groundwater from recharge areas of higher elevation and

hydraulic head to discharge areas of lower elevation and hydraulic head. Topography-

driven flow is common in continental sedimentary basins [*Garven*, 1995] and could drive

the upward movement of fracking-related fluids in regional discharge zones.

Overpressure is a phenomenon whereby subsurface fluids are at higher pressures than hydrostatic pressure. Overpressure is common in shales because of their low permeabilities combined with rapid burial (disequilibrium compaction) and hydrocarbon generation [*Osborne & Swarbrick*, 1997; *Gassiat et al.*, 2013]. When a shale is fracked the overpressure, which had been maintained within the shale matrix by low permeabilities and capillary sealing effects, is released by the increase in fracture permeability, potentially causing upward fluid migration until the overpressure is dissipated [*Birdsell et al.*, 2015].

During fracking operations injected fluid pressures must be increased to at least the minimal principal stress acting on the shale so that the shale fractures and reservoir permeability is increased. The injection pressures drive fluid away from the borehole and, although flowback and production may reduce these pressures [*Brownlow et al.*, 2016], if boreholes are shut in for safety reasons or to increase gas production rates [e.g. *Cheng*, 2012; *King*, 2012; *Fakcharoenphol et al.*, 2013] then flow will continue away from the borehole until the pressure dissipates.

The buoyancy of fracking fluids or released oil and gas could also drive upward fluid migration from shale reservoirs. Oil and gas are less dense than fresh water and even more so than saline waters, which are commonly found at depth in the subsurface [*Dickey*, 1969; *Ferguson et al.*, 2018]. Similarly, fracking fluids are typically buoyant compared to formation waters because they are low-salinity, low-density slickwaters whereas formation waters at several kilometres depth are typically high-salinity, high-density brines [*Gassiat et al.*, 2013; *Engelder et al.*, 2014]. Consequently, injected fracking fluids will act as buoyant plumes until they have either mixed with formation waters so that there remains no density contrast or they are exceeded by pressure drawdown from the producing borehole [*Birdsell et al.*, 2015].

1.4   Evidence for deep to shallow natural geological pathways in England

Although it is debated whether there is any evidence of shallow groundwater contamination from fracking-related fluids migrating from several kilometres depth along natural geological pathways, it is well-known that natural fluids migrate along natural geological pathways over the same spatial scale. For example, conventional petroleum reservoirs are typically filled with petroleum generated at kilometre-scale depths where temperatures and pressures are high enough to convert buried kerogen [*Philippi*, 1965]. Likewise, thermal springs in non-volcanically active areas require fluid circulation to kilometre-scale depths to reach temperatures substantially warmer than shallow groundwater [e.g. *Andrews et al.*, 1982]. Therefore, petroleum seeps (surface outflows of oil or gas) and thermal springs can both provide evidence of fluid migration from kilometre-scale depths to the surface via natural geological pathways. The following sections provide an overview of notable petroleum seeps and thermal springs in England that provide evidence for deep to shallow fluid migration along natural geological pathways.

1.4.1   Petroleum seeps

There are ~170 petroleum seeps and impregnations (static occurrences of petroleum such as bitumen) known in Britain and ~110 of these occur in England [*Selley*, 1992; 2012]. Furthermore, *Boothroyd et al.* [2017] provided evidence that basin-bounding faults in England, including some in shale gas basins, can act as conduits for CH_4 to travel from the deep subsurface to the surface without anthropogenic disturbance. Examples of notable petroleum seeps from three geological basins are described in the following sections.

1.4.1.1   Abbeystead, Bowland Basin

The Abbeystead valve house and associated Wyresdale Tunnel in the Bowland Basin, Lancashire, northwest England, were constructed to pump water from the River Lune to the River Wyre. After concerns were raised related to the pumping operation and flooding at St Michael's on Wyre, 36 villagers from St Michael's on Wyre and eight Water Board officials were invited to visit the valve house on the 23rd May 1984. During the visit a fatal gas explosion occurred. Eight people died on the scene, eight later died in hospital and all survivors suffered injuries [*Jaffe et al.*, 1997].

Following the disaster North West Water commissioned a geological and geophysical investigation to determine the source of the gas and why the explosion had occurred [*NWW*, 1986]. The investigation concluded that the gas was CH_4 of natural thermogenic origin and the most prolific source rocks in the area were the Bowland Shales and the Tarnbrook Wyre Marine Beds. It was hypothesised that a complex fold and fault trap structure exists ~1100 m below the Wyresdale Tunnel and gas, likely generated during the Carboniferous, had been trapped in a geological reservoir probably composed of the Pendleside Limestone and Boulder Beds. Natural tectonic activity during the 20th Century (notable earthquakes occurred at Skipton in 1948, Kirby Stephen in 1970 and Carlisle in 1979) may have breached this reservoir and reopened the fault zone, leading to leakage of gas from the reservoir and subsequent migration to the Wyresdale Tunnel (Figure 1.6). This gas also mixed with groundwater, thought to be of deep origin and driven by topography or pressure differentials created by the generation of new porosity in the zone, resulting in a mix of free and dissolved gas entering the Wyresdale Tunnel [*NWW*, 1986; *Sibson*, 1975].
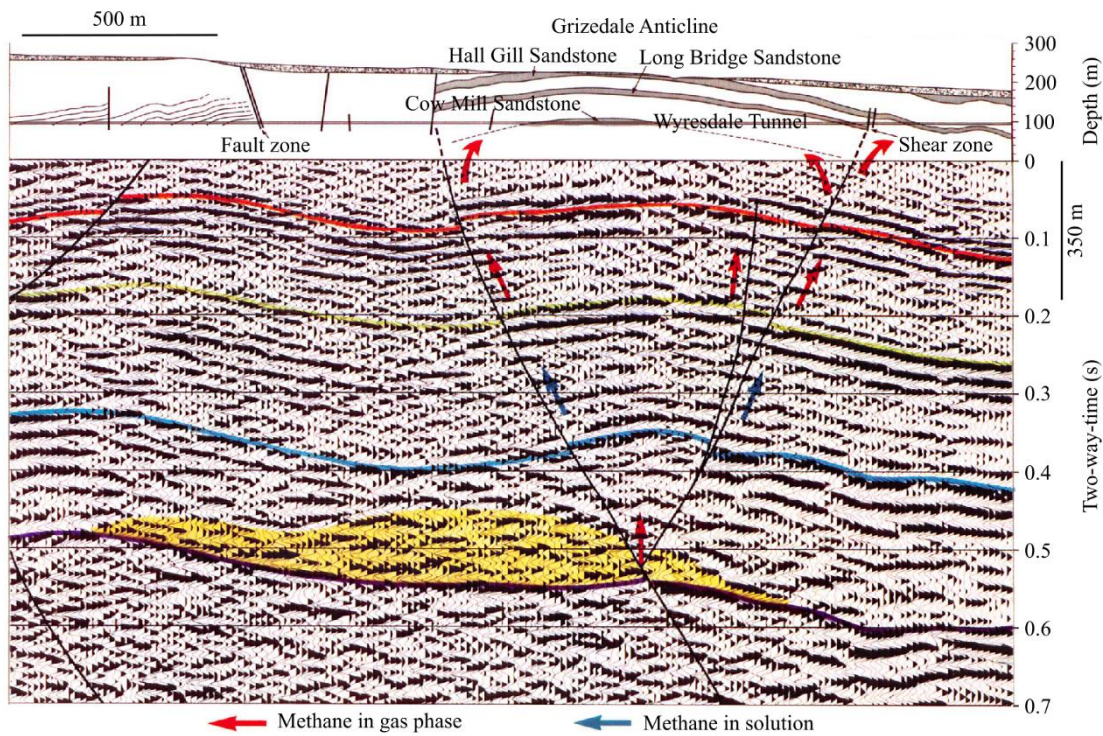
Figure 1.6
Interpreted seismic reflection line from NWW [1986] showing the proposed Pendleside
Limestone and Boulder Beds reservoir (yellow) and gas migration along faults to the
Wyresdale Tunnel (red arrows – methane in gas phase, blue arrows – methane in
solution). The coloured seismic horizons are the Top Pendle Grit (red), Base Pendle Grit
(green), Base Bowland Shales (blue) and Top Worston Shales (purple). The Base Pendle
Grit lies ~350 m below mean sea level based on an interval velocity of 3900 m/s.

1.4.1.2   Wessex Basin

The Wessex Basin is situated in the south of England and is defined to the west by the

Armorican and Cornubian Massifs, to the north by the London-Brabant Massif, to the

south by the Central Channel High and to the east by the Weald Basin [*Underhill &*

Stoneley, 1998]. The most well-known and documented seeps occur just offshore at Anvil

Point and onshore at Osmington Mills and Mupe Bay. At Anvil Point gas seeps from the

fractured Upper Jurassic Portland Limestone seabed [*Power*, 1978]. At Osmington Mills

and Mupe Bay oil flows slowly from the Upper Jurassic Bencliff Grit and Lower

Cretaceous Sandstones, respectively [*Lees & Cox*, 1937]. A number of other seeps also

occur at Dungy Head, Durdle Door, Lulworth Cove and Worbarrow Bay [*Selley*, 1992].

14

The source of the petroleum is considered to be Lower Jurassic (Liassic) shales which reached the oil window in the Early Cretaceous and reached peak generation in the Mid-Late Cretaceous [*Selley & Stoneley*, 1987; *Cornford et al.*, 1988]. Generated petroleum migrated upwards and across the Purbeck fault zone to backfill tilted footwall reservoirs (Figure 1.7) [*Underhill & Stoneley*, 1998]. The onset of tectonic compression and basin inversion in the Late Cretaceous then sealed the fault zones, which had acted previously as migration pathways [*Selley & Stoneley*, 1987]. Continued basin inversion in the Tertiary reactivated the Purbeck fault zone and led to reservoir leakage and the development of seeps in the Wessex Basin (Figure 1.7) [*Underhill & Stoneley*, 1998]. The present-day depth range of the proposed leaking reservoirs is ~600 to 2000 m [*Underhill & Stoneley*, 1998; see their figure 6]. At Anvil Point, if the assumption is made that gas is still migrating from the Liassic shales south of the Purbeck fault zone, the depth of origin may be up to 2500 m [*Stoneley*, 1982; see his figure 3].
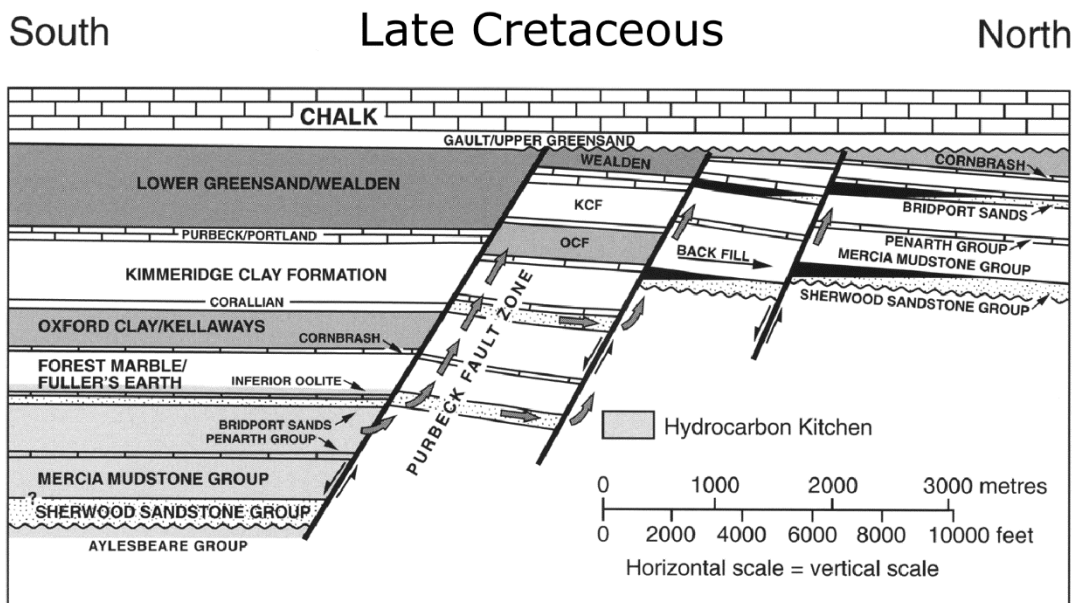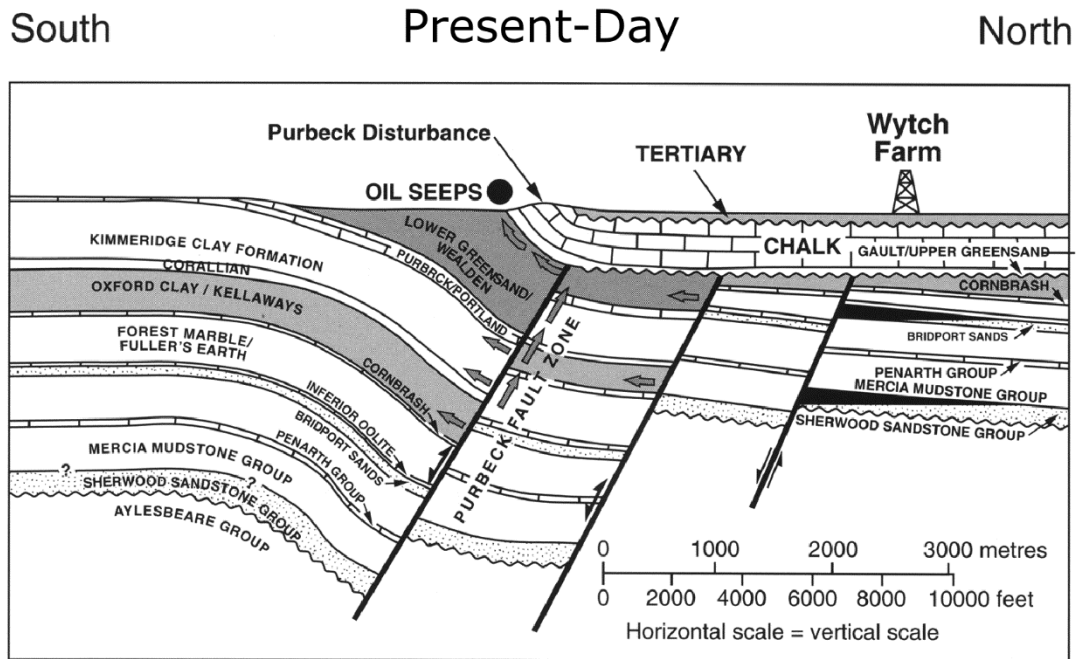
Figure 1.7
Present-day and Late Cretaceous petroleum migration and trapping in the Wessex Basin.
Image adapted from Underhill and Stoneley [1998].

1.4.1.3   Weald Basin

The Weald Basin lies east of the Wessex Basin and south of the London Platform, covering the English counties of Hampshire, Kent, Surrey, East Sussex and West Sussex. In East Sussex oil seeps have been recorded in the Cretaceous Turnbridge Wells Sandstone at Chilley, Down Ash, Halisham, Halisham Cemetery and the Horns [*Reeves*, 1948; *Selley*, 1992]. All these seeps appear to be related to faulting associated with the Pevensey anticline (Figure 1.8), suggesting that the faults act as natural geological pathways for oil migration. In the centre of the basin five Jurassic shale units (Kimmeridge Clay, Corallian Clay, Oxford Clay, and the Middle and Upper Lias Clays) are hypothesised to have reached oil maturation in the Late Cretaceous. It is the Middle and Upper Lias Clays that are considered to be the likely source of oil in the Weald Basin [*Andrews*, 2014]. If these formations are the source of oil seeping at the Pevensey anticline then oil may have migrated along the faults from the depths of ~1000 to 1400 m below the surface.
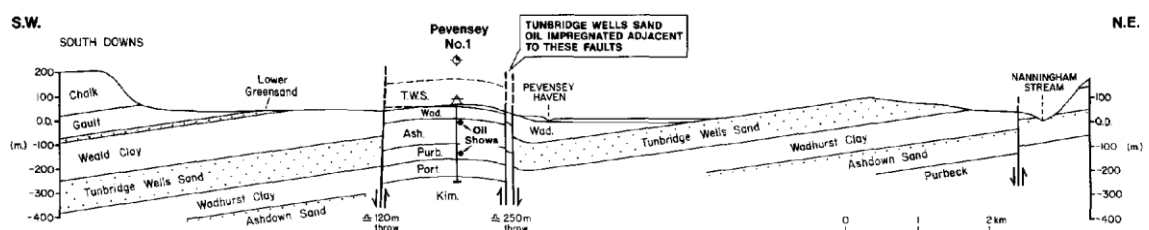
Figure 1.8
Cross-section through the Pevensey anticline showing the relationship of oil seeps to faulting. Image from Selley [1992].

No known gas seeps occur in the Weald Basin. However, there are several conventional gas fields across the basin and there have been a number of cases where gas has seeped into boreholes [*Reeves*, 1948; *Selley*, 1992]. The Jurassic shales in the Weald Basin are not considered to have reached gas maturity [*Andrews*, 2014] and so it has been

17

proposed that there is a source rock older than the Jurassic shales which has generated gas, for example the Carboniferous Coal Measures [*Selley*, 1992]. Gas may have migrated from depths >2500 m because in the central Weald Basin the potential Carboniferous source rocks lie below ~2500 m [*Andrews*, 2014; see his figure 17].

1.4.2   *Thermal springs*

Although cold water springs are common in England, thermal springs are much rarer. Only two known systems exist; the Mendips and Derbyshire [*Brassington*, 2007].

1.4.2.1   *Mendips system (Bath and Bristol)*

The thermal springs at Bath, Somerset, are the highest temperature springs in England, discharging at a temperature of 46.5ºC [*Mather*, 2013]. Three springs are located in close proximity within the oldest part of Bath: King's, Cross Bath and Hetling [*Gallois*, 2007]. A number of conceptual models exist to explain the occurrence of the thermal springs but the most favoured is the "Mendips Model" (Figure 1.9) [*Andrews et al.*, 1982], which is supported by numerical modelling and geochemical observations [*Atkinson & Davison*, 2002]. In the Mendips Model meteoric water recharges Carboniferous limestone which outcrops ~20 km to the southwest of Bath in the Mendip Hills. The Carboniferous limestone is in a syncline structure, allowing cold water to be transported down to depths of 2700 to 4300 m where it is heated by geothermal heat to temperatures of 64 to 96ºC [*Edmunds*, 2004]. The water is hypothesised to return to the surface at Bath via upward migration along a thrust fault fracture zone in the other limb of the synclinal Carboniferous limestone. The topographic difference between the Mendip Hills and Bath provides the main upward driving force, although the buoyancy of the heated water may also play a role. Circulation time from rainfall recharge in the Mendip Hills to emergence in Bath is hypothesised to be <10000 years [*Mather*, 2013].
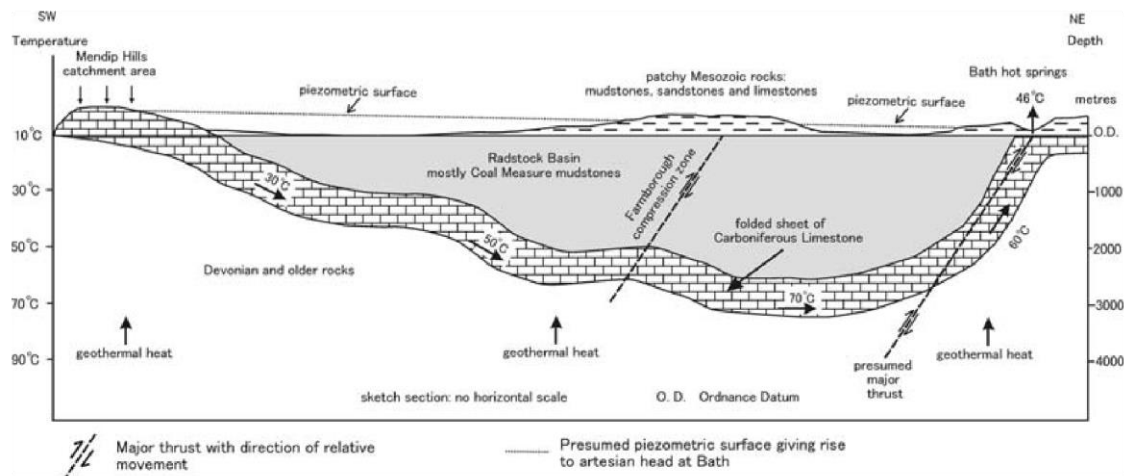
Figure 1.9
Cross-section of the Mendips Model showing the proposed origin of the thermal springs at Bath. Image from Gallois [2007].

Thermal springs also occur in the Avon Gorge, Bristol, where the Carboniferous limestone has been incised by the River Avon. The warmest of the springs is the Hotwells Spring which reaches 24ºC [*Atkinson & Davison*, 2002]. Geochemical analysis and numerical modelling suggests that the spring water at Hotwells is a mixture of thermal water from the Mendip system and more recent groundwater in the Carboniferous limestone [*Burgess et al.*, 1980; *Andrews et al.*, 1982; *Atkinson & Davison*, 2002]. Silica content analysis indicates that the thermal water component reached lower temperatures (49 to 72ºC) than those emerging at Bath [*Atkinson & Davison*, 2002], suggesting shallower circulation depths. Thrust faults and vertical fractures in the Carboniferous limestone are hypothesised to provide conduits for the upward migration of the thermal waters [*Hawkins & Kellaway*, 1991].

1.4.2.2   Derbyshire

Within Derbyshire there are seven recorded locations with thermal springs [*Edmunds*, 1971]. The Buxton Spring has the highest temperature (27.5ºC) and is the second warmest

thermal spring in England. The springs are located at the boundary between the Lower Carboniferous limestone and the Lower-Mid Carboniferous shales at the edge of an anticlinal dome structure called the "Derbyshire Dome" (Figure 1.10). The thermal waters are of meteoric origin [*Edmunds*, 1971] and the age of the water emerging at Buxton is dated at 3900 to 6400 years old, with a bulk age of 5000 years [*Barker et al.*, 2000]. *Brassington* [2007] proposed the following conceptual model (Figure 1.10): meteoric water recharges the limestone aquifer in the centre of the Derbyshire Dome; this water migrates downwards through a fracture system and is heated geothermally at depths of at least ≥950 m; fault structures at the limestone-shale boundary provide conduits to the surface which are enhanced by karst nearer the surface. Circulation depths for cooler springs at Bakewell and Matlock Bath are estimated at ~200 and 500 m below the surface, respectively, and tritium measurements imply a larger proportion of recent meteoric recharge than at Buxton [*Edmunds*, 1971; *Brassington*, 2007]. Temperature differences at the separate spring locations support the hypothesis that separate groundwater convection cells exist within fault block compartments [*Brassington*, 2007].
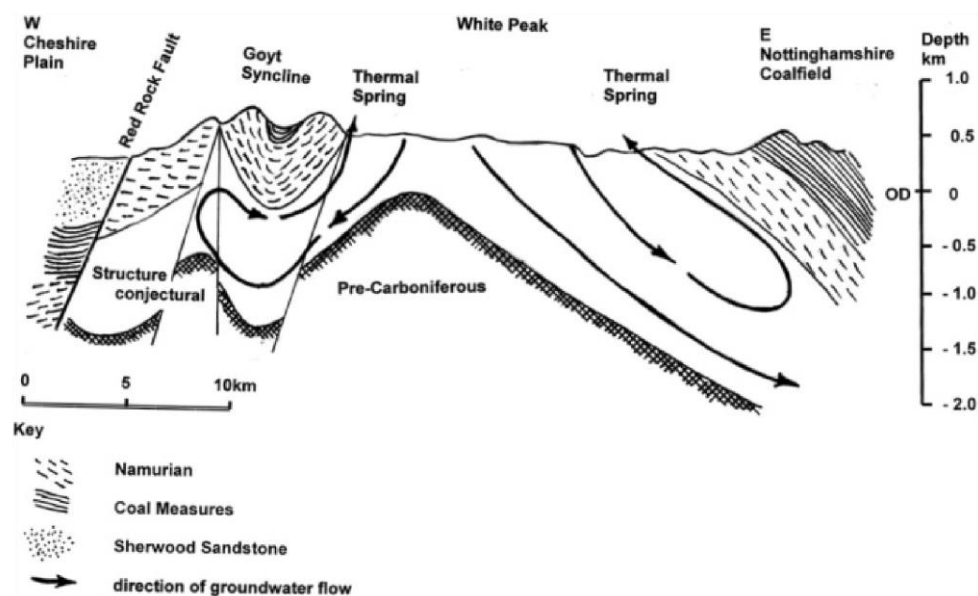
Figure 1.10
Cross-section through the Derbyshire Dome showing the conceptual model for the origin of the thermal springs in Derbyshire. Image from Brassington [2007].

1.5   Assessing fracking-related fluid migration along natural geological pathways

Section 1.4 highlighted that natural geological pathways, particularly those involving fault and fracture zones, do provide pathways for fluids between the deep subsurface and the surface in England. Consequently, assessing potential natural geological pathways from deep shales to shallow groundwater resources plays an important part of mitigating the risk of upward fluid migration and contamination of shallow groundwater resources by fracking-related fluids.

One approach to assessing this risk is to undertake field-based groundwater monitoring. By measuring groundwater properties prior to (i.e. establishing baseline conditions), during and after fracking operations, any upward fluid migration and contamination may be identified by comparison to baseline conditions. However, this approach requires baseline conditions to be known prior to fracking (not always possible in developed basins), tens of years of continuous monitoring and ultimately is not a predictive approach, i.e. a pathway is only inferred after a change in groundwater conditions has been detected and potential contamination has already occurred. A more practical solution offering quantitative predictions is numerical modelling. To date various numerical models have been produced to investigate the potential migration of fracking-related fluids via natural geological pathways. Many of these models use simplistic geological structure and focus on fluid injection into high-permeability fault and fracture zones as "worst-case scenarios".

Myers [2012] produced the first numerical model to assess upward fluid migration from fracking and simulated a range of scenarios. In scenarios with simple advection through shale and the overlying sandstone, tracked particles reached the surface within ~20 to 40000 years, depending on the specified hydraulic conductivities of the formations. Other scenarios, which included modelling a fault connecting to the surface,

21

resulted in travel times of less than 10 years to the surface [*Myers*, 2012]. However, the model was heavily criticised due to unrealistic geology and the chosen boundary conditions [e.g. *Cohen et al.*, 2013].

Gassiat et al. [2013] produced a more realistic model using global shale basin data to assess the potential for upward fluid migration along hydraulically conductive faults. Model results for a scenario with fracking at ~1800 m below the surface indicated a 500 year travel time to a depth of 500 m below the surface [*Gassiat et al.*, 2013]. *Kissinger et al.* [2013] also investigated upward fluid flow from fracking but instead focussed on specific basins; the Münsterland and Lower-Saxony basins in Germany. Three scenarios were designed to cover the migration of fracking fluids, brine and CH_4 on local and regional scales, as well as on short- and long-term temporal scales. Results indicated that fluid migration to shallow layers can occur if a combination of assumptions are met, for example the presence of high-permeability fault zones which connect the stimulated shale and aquifer [*Kissinger et al.*, 2013].

Prior to this thesis, *Cai and Ofterdinger* [2014] produced the only numerical model focussing on the Bowland Shale in Lancashire, northwest England. Their worst-case scenario, with fractures directly connecting the stimulated shale to the shallow aquifer, resulted in aquifer contamination in 100 years. Conversely, using faulted models of the North Perth Basin (Australia) and the North German Basin (Germany) *Palat et al.* [2015] and *Pfunt et al.* [2016] did not observe fracking fluids reaching the regional aquifers within the simulated timescales of 20 and 300 years, respectively.

Arguably the most advanced numerical model investigating fracking fluid migration is that by *Birdsell et al.* [2015]. *Birdsell et al.* [2015] reviewed previous numerical models and identified that no model had combined the effects of buoyancy, borehole operations and capillary imbibition. They constructed a numerical model to include these effects and

various scenarios were run with sensitivity analyses. No fracking fluid was observed to reach the shallow aquifer when a permeable pathway (modelled as either a fault or borehole) was not present. When a permeable pathway was present the effect of borehole production and capillary imbibition were to reduce the amount of fracking fluid reaching the aquifer by a factor of ten [*Birdsell et al.*, 2015].

1.6   Thesis aim and outline

Although evidence of fracking-related fluids migrating from shale reservoirs to shallow groundwater resources along natural geological pathways is debated, there is conclusive evidence that natural fluid migration between kilometre-scale depths and the surface does occur. As a result, there remains environmental concerns regarding possible natural pathways between shale reservoirs and shallow groundwater resources. Numerical models with simplistic geological structure have been built to address this concern, typically focussing on high-permeability fault and fracture zones as the highest risk natural pathways. Therefore, the first aim of this thesis was to apply the precautionary principle and establish a horizontal respect distance between subsurface injection points and known faults. The second aim of this thesis was to consider complex geological structure to further investigate and identify hydrogeological factors which may increase or decrease the vulnerability of shallow groundwater resources to the potential upward migration of fracking-related fluids. Potential fluid migration along anthropogenic pathways such as poorly constructed active and abandoned boreholes was not addressed in this thesis but has been considered by others [e.g. *Brownlow et al.*, 2016; *Taherdangkoo et al.*, 2019]. An important development this thesis makes to address the potential upward migration of fracking-related fluids is the highly multidisciplinary approach; this thesis integrates environmental water quality monitoring, geophysical methods and numerical modelling. Such an approach is essential for linking solid geology with subsurface fluid

flow to understand the potential migration of fracking-related fluids. The following sections provide a brief overview of the subsequent chapters which make up this thesis.

1.6.1   Chapter 2

The introduction demonstrated that fault and fracture zones are generally considered as the highest risk potential natural geological pathways between deep shale reservoirs and shallow groundwater resources. In this chapter an empirical methodology is used to establish a horizontal respect distance to known faults, thereby reducing the risk of injected fluids entering a potential pathway. The contents of this chapter contributed to the following publication:

Wilson, M. P., Worrall, F., Davies, R. J., & Almond, S. (2018). Fracking: How far from faults?. *Geomechanics and Geophysics for Geo-Energy and Geo-Resources*, 4(2), 193-199.

1.6.2   Chapter 3

In this chapter a real-life fracking operation in a complex sedimentary basin is numerically modelled to investigate hydrogeological factors which may increase or decrease the vulnerability of the overlying shallow aquifer to injected fluids. Importantly, this operation avoided fluid injection into known faults and was therefore situated between known faults. The contents of this chapter contributed to the following publication:

Wilson, M. P., Worrall, F., Davies, R. J., & Hart, A. (2017b). Shallow aquifer vulnerability from subsurface fluid injection at a proposed shale gas hydraulic fracturing site. *Water Resources Research*, 53(11), 9922-9940.

1.6.3   Chapter 4

In this chapter historic groundwater quality data are combined with two-dimensional (2D) seismic reflection data to interpret the groundwater system of a prospective shale gas basin and determine if groundwater compartmentalisation can be identified prior to fluid injection. The contents of this chapter contributed to the following publication:

Wilson, M. P., Worrall, F., Davies, R. J., & Hart, A. (2019a). Identifying groundwater compartmentalisation for hydraulic fracturing risk assessments. *Environmental Science: Processes & Impacts*, 21(2), 352-369.

1.6.4   Chapter 5

Spatially comprehensive groundwater data can be difficult to obtain because of the costs and logistics in drilling and monitoring numerous boreholes. As a result, interpreting groundwater systems in prospective shale gas basins can be challenging. Surface water quality data may provide a cheaper and more practical alternative. In this chapter a new surface water quality dataset is described and interpreted to investigate if surface water quality data can be used to identify groundwater compartmentalisation and groundwater-surface water interactions in a prospective shale gas basin. The contents of this chapter contributed to the following publication:

Wilson, M. P., Worrall, F., Clancy, S. A., Ottley, C. J., Hart, A., & Davies, R. J. (accepted). Compartmentalisation and groundwater-surface water interactions in a prospective shale gas basin: Assessment using variance analysis and multivariate statistics on water quality data. *Hydrological Processes*.

1.6.5   Chapter 6

Ultimately, predicting the long-term migration pathways and receptors of fracking-related fluids requires geologically realistic basin-scale numerical models. In this chapter a three-dimensional (3D) numerical model of a prospective shale gas basin is constructed and a variety of groundwater simulations run to investigate the long-term migration of injected fluids at the same site as in Chapter 3. This model is the first 3D basin-scale groundwater model created to address potential upward fluid migration from fracking in a real-life basin.

1.6.6   Chapter 7

In this chapter the conclusions and implications from all previous chapters are summarised and suggestions are made for further work.

1.6.7   References

A complete list of references cited within this thesis.

1.6.8   Appendices (A to D)

Supplementary material associated with the thesis chapters. Also included is an additional publication which was produced during this thesis but was considered outside the thesis narrative (Appendix A):

Wilson, M. P., Worrall, F., Davies, R. J., & Hart, A. (2019b). A dynamic baseline for dissolved methane in English groundwater. *Science of the Total Environment*, 134854.

1.7 The Bowland Basin

Chapters 3 to 6 use a prospective shale gas basin to investigate and identify hydrogeological factors which may increase or decrease the vulnerability of shallow groundwater resources to the potential upward migration of fracking-related fluids. This basin was the Bowland Basin which, as previously mentioned, has been one of the main target basins in England for shale gas exploration. The extent and formation of the basin have been described and modified by various authors in the literature [*Gawthorpe*, 1987; *Kirby et al.*, 2000; *Andrews*, 2013]. In this thesis the Bowland Basin is defined as the area bounded to the northeast by the Craven Fault System, to the southeast by the Pendle Fault System, and to the west by the East Irish Sea Basin (Figure 1.2) [*Andrews*, 2013]. Much of the Bowland Basin covers the Fylde coastal plain of Lancashire, which is where the Bowland Shale is prospective and fracking operations have been focussed (Figure 1.2). As reference for the Chapters 3 to 6, the following sections provide an overview of the geological history, stratigraphy and hydrology of the Bowland Basin.

1.7.1 Geological history and stratigraphy

The Bowland Basin initiated in the Early Carboniferous as a result of extensional rift faulting, leading to the deposition of basin-wide organic rich shales (Bowland Shale Group and Hodder Mudstone Formation) and carbonates (Figure 1.11) [*Kirby et al.*, 2000]. The Bowland Shale Group consists of the Upper and Lower Bowland Shale Formations (distinguished by a marine band), which lie conformably over the Worston Shale Group to which the Hodder Mudstone Formation belongs (Figure 1.12)

[*Anderson & Underhill*, 2020]. Together the Early Carboniferous shales and limestones, which partly form the bedrock geology in the east of the Bowland Basin (Figure 1.13), are commonly referred to as the Bowland High and Craven Groups. *Clarke et al.* [2014b] hypothesised that a minor period of inversion followed the deposition of the Bowland Shale Group based on reverse faults in the Bowland Shale Group terminating at the base of the overlying Millstone Grit Group [*Clarke et al.*, 2014b].
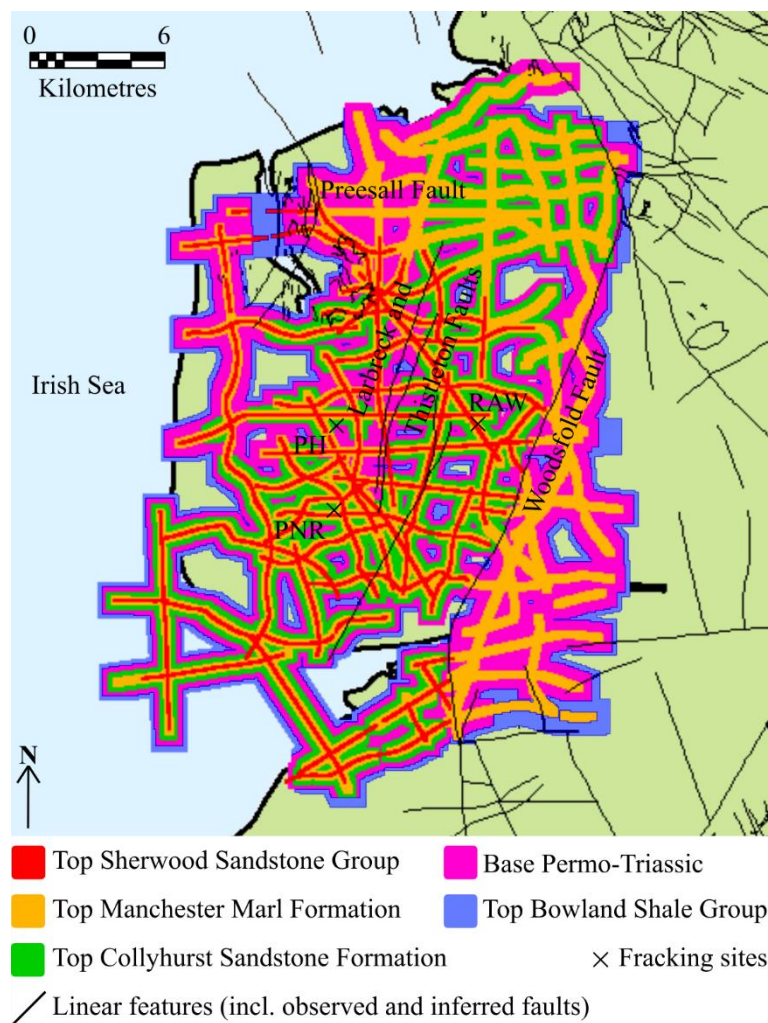
Figure 1.11
Map of the Fylde showing the subsurface extent of geological groups and formations interpreted from 2D seismic reflection data (see Chapter 4). Also shown are BGS mapped linear features, the fracking sites Preston New Road (PNR) and Preese Hall (PH), and the previously proposed fracking site Rose Acre Wood (RAW). The top of the Sherwood Sandstone Group is eroded in the north and east but is confined by the Mercia Mudstone Group towards the southwest. Contains British Geological Survey data © Crown copyright and database right (2018). A British Geological Survey/EDINA supplied service.
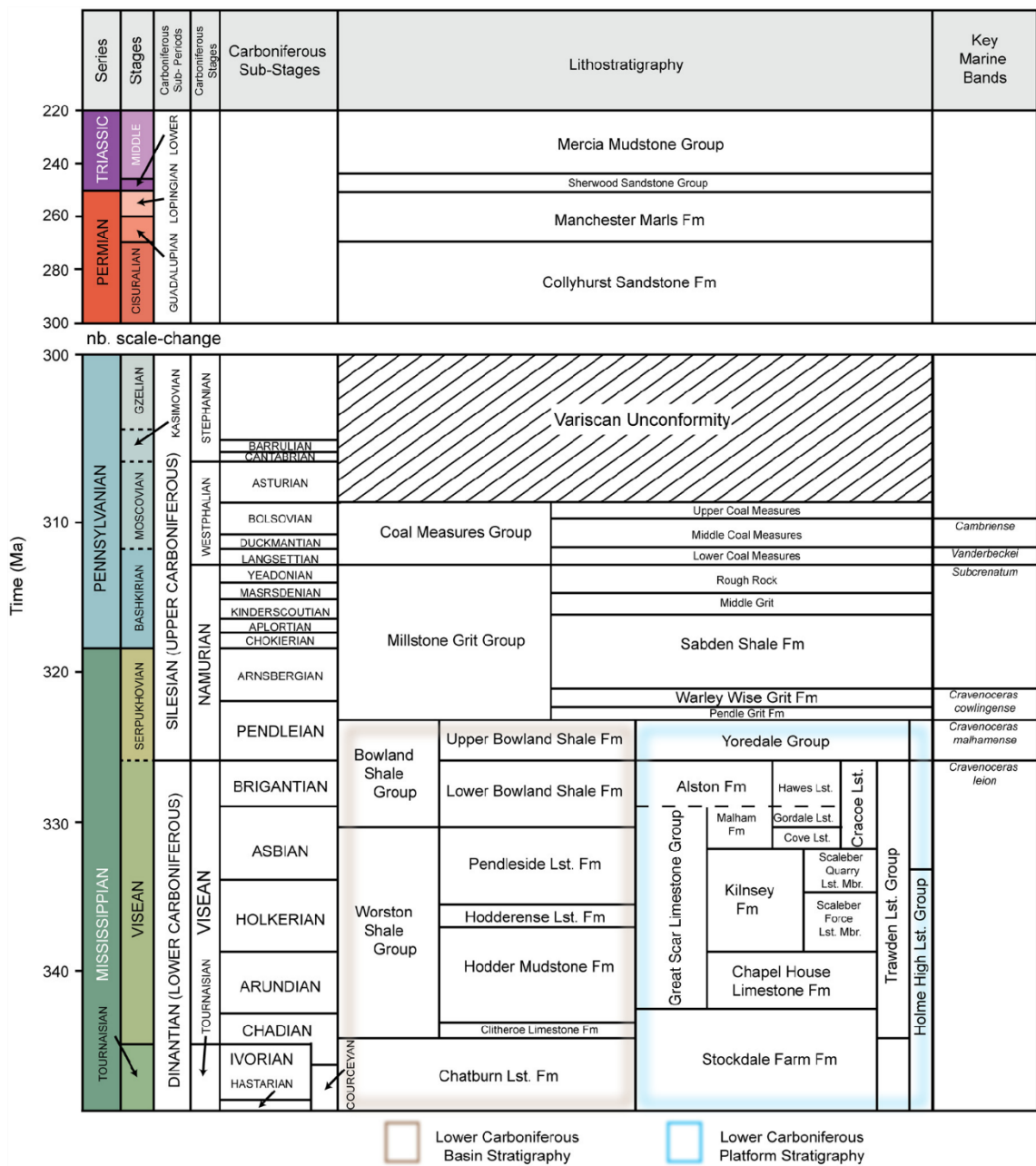
Figure 1.12
Stratigraphic chart for the Carboniferous, Permian and Triassic sequences of northwest England. Image adapted from Anderson and Underhill [2020].

The Millstone Grit and Coal Measures Groups are hypothesised to have formed during a thermal sag phase following the main rifting event and possible minor inversion [*Kirby et al.*, 2000]. The Millstone Grit Group, which consists of several shale and coarse sandstone formations (Figure 1.12), was deposited as a result of clastic sediment

29

progradation southwards throughout northern England [*Anderson & Underhill*, 2020]. The Millstone Grit Group forms the remaining bedrock geology in the east of the Bowland Basin (Figure 1.13). The deposition of the Coal Measures Group (predominantly consisting of cycles of sandstones, siltstones, mudstones and coals) in the Upper Carboniferous demonstrates the establishment of fluvial-deltaic conditions prior to basin inversion. The Late Carboniferous was marked by the Variscan Orogeny, which led to inversion of the Bowland Basin and substantial erosion of the Millstone Grit and Coal Measures Groups. The Variscan Unconformity (Figure 1.12) can be observed on seismic reflection data from the Bowland Basin where dipping Carboniferous sediments are truncated by sub-horizontal Permo-Triassic sediments [*UKOGL*, 2012].

Permian sediments in the Bowland Basin comprise of the Collyhurst Sandstone and Manchester Marl Formations (Figure 1.12). The Collyhurst Sandstone Formation is of mixed aeolian-fluvial origin and deposition at the margin of the East Irish Sea Basin in semi-arid conditions appears to have been controlled by a second phase of extensional faulting [*British Gas PLC.*, 1991; *Eukan Energy Ltd.*, 1994; *Kirby et al.*, 2000]. The Collyhurst Sandstone Formation is present in the Elswick Graben (bounded to the east by the Woodsfold Fault and to the west by the Larbreck and Thistleton Faults), but is absent on the structural high immediately west of the Thistleton and Larbreck Faults (Figure 1.11) [*Kirby et al.*, 2000]. However, the Collyhurst Sandstone Formation was observed in PH-1 further west of the structural high, supporting the hypothesis that it exists as a pinchout edge [*Eukan Consortium*, 1992]. No outcrops of the Collyhurst Sandstone Formation occur in the Bowland Basin. The Manchester Marl Formation (predominantly calcareous mudstone and siltstone) was deposited by marine incursion and is considered to exist across the Bowland Basin (Figure 1.11), forming a regional seal unit to the underlying strata [*Fraser & Gawthorpe*, 1990; *Ove Arup and Partners Ltd.*, 2014b]. The Manchester Marl Formation exists as bedrock on the faulted and

unconformable contact between the Carboniferous and Triassic sediments in the Bowland Basin (Figure 1.13).
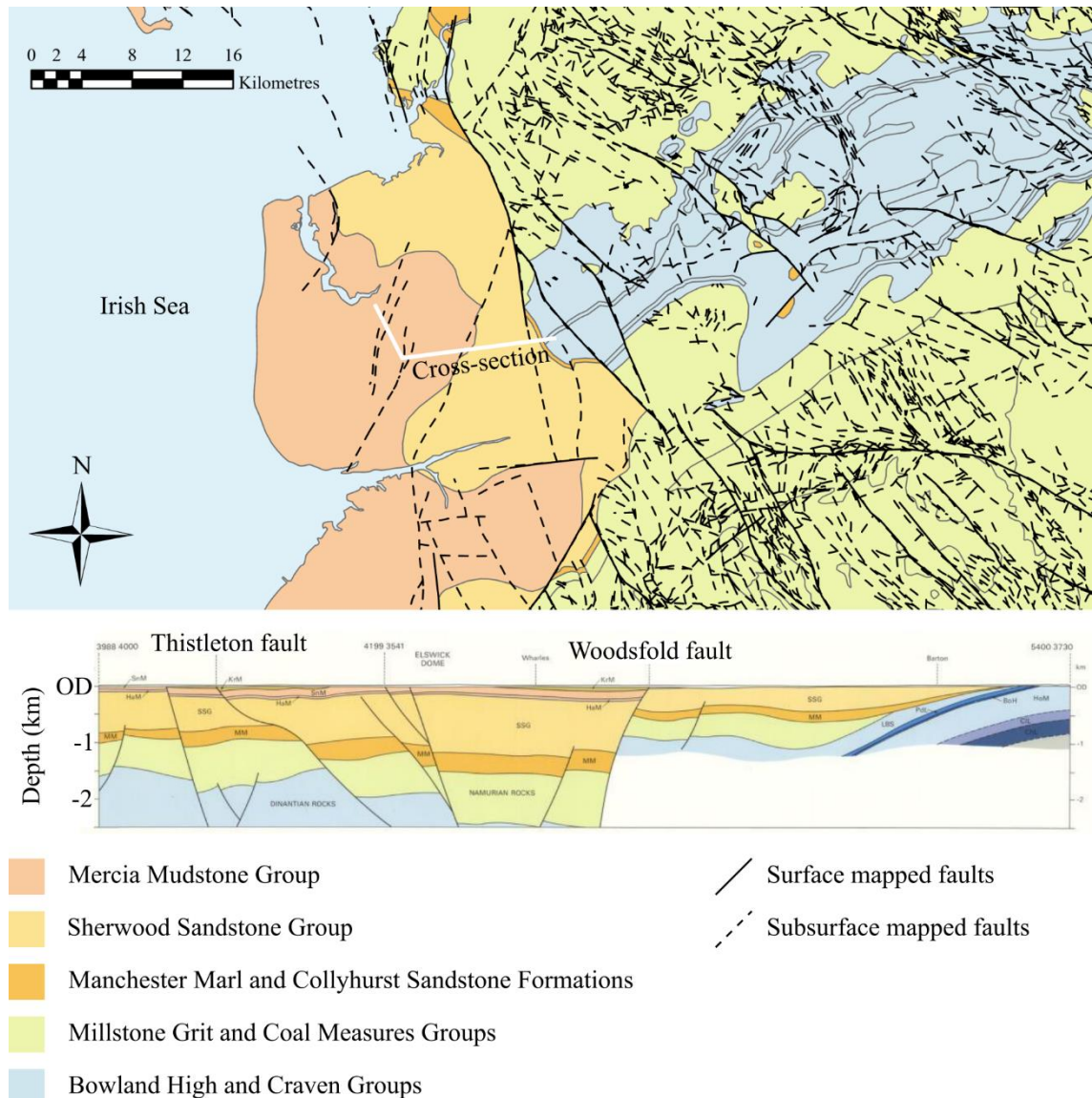
Figure 1.13
Bedrock geology map of the Bowland Basin including surface and subsurface mapped faults by the BGS. The geological cross-section is adapted from BGS [1990]. Contains British Geological Survey data © Crown copyright and database right (2018). A British Geological Survey/EDINA supplied service.

Episodes of crustal extension continued during the Triassic, resulting in the deposition of the Sherwood Sandstone Group and the overlying Mercia Mudstone Group (Figure 1.12). The Sherwood Sandstone Group in the Bowland Basin comprises of the stratigraphically lower and less-permeable St. Bees Sandstone Formation and the

31

stratigraphically higher and more-permeable Sherwood Sandstone Formation [*Cai & Ofterdinger*, 2014]. The St. Bees Sandstone is a fluvially dominated sandstone formed by a long-lived braided fluvial system transporting sediment northward [*Medici et al.*, 2019]. The frequent occurrence of fine-grained floodplain deposits likely accounts for the lower permeabilities of the St. Bees Sandstone compared to the overlying Sherwood Sandstone Formation, which is more sand-prone and considered to be of more aeolian origin due to a reduction in fluvial discharge [*Medici et al.*, 2019]. The Mercia Mudstone Group, consisting of salt-rich mudstone formations, was deposited following further retreat of the fluvial environments and the establishment of marine-sourced hypersaline water bodies and mudflats, to which flash floods and wind-blown dust added silts and fine sands [*Howard et al.*, 2008].

Jurassic and Cretaceous sediments are mostly absent from the Bowland Basin, most likely due to uplift and subsequent erosion in the Palaeogene followed by Alpine Orogeny-related inversion in the Neogene [*Lewis et al.*, 1992; *Kirby et al.*, 2000]. The uplift also eroded the Mercia Mudstone Group in the eastern Fylde. Consequently, the Sherwood Sandstone Group directly underlies the superficial deposits in the eastern Fylde but is confined by the Mercia Mudstone Group in the western Fylde (Figure 1.13). The boundary between the Mercia Mudstone Group in the western Fylde and the Sherwood Sandstone Group in the eastern Fylde is fault-bounded by the Woodsfold fault, which has a maximum vertical displacement of ~600 m (Figure 1.13).

Regional uplift continued into the Quaternary along with eastward tilting of the Bowland Basin [*Kirby et al.*, 2000]. Quaternary glaciation led to the widespread deposition of superficial glaciofluvial sands and gravels, and clay-dominated tills across the basin. The glacial deposits have been further added to by blown sands, peat and tidal alluvium (Figure 1.14) [*BGS*, 1975; 1989; 1990; 2012]. The Superficial Deposits are near-ubiquitous across the Fylde and form a complex distribution averaging 30 to 40 m in

thickness [*Cripps et al.*, 2016]. As a result, the Mercia Mudstone Group does not outcrop in the Fylde and the Sherwood Sandstone Group very rarely outcrops. Across the Forest of Bowland, superficial deposits consisting of till, peat and alluvium overlay the Millstone Grit and Bowland High and Craven Groups, although bedrock outcrops do exist (Figure 1.14).
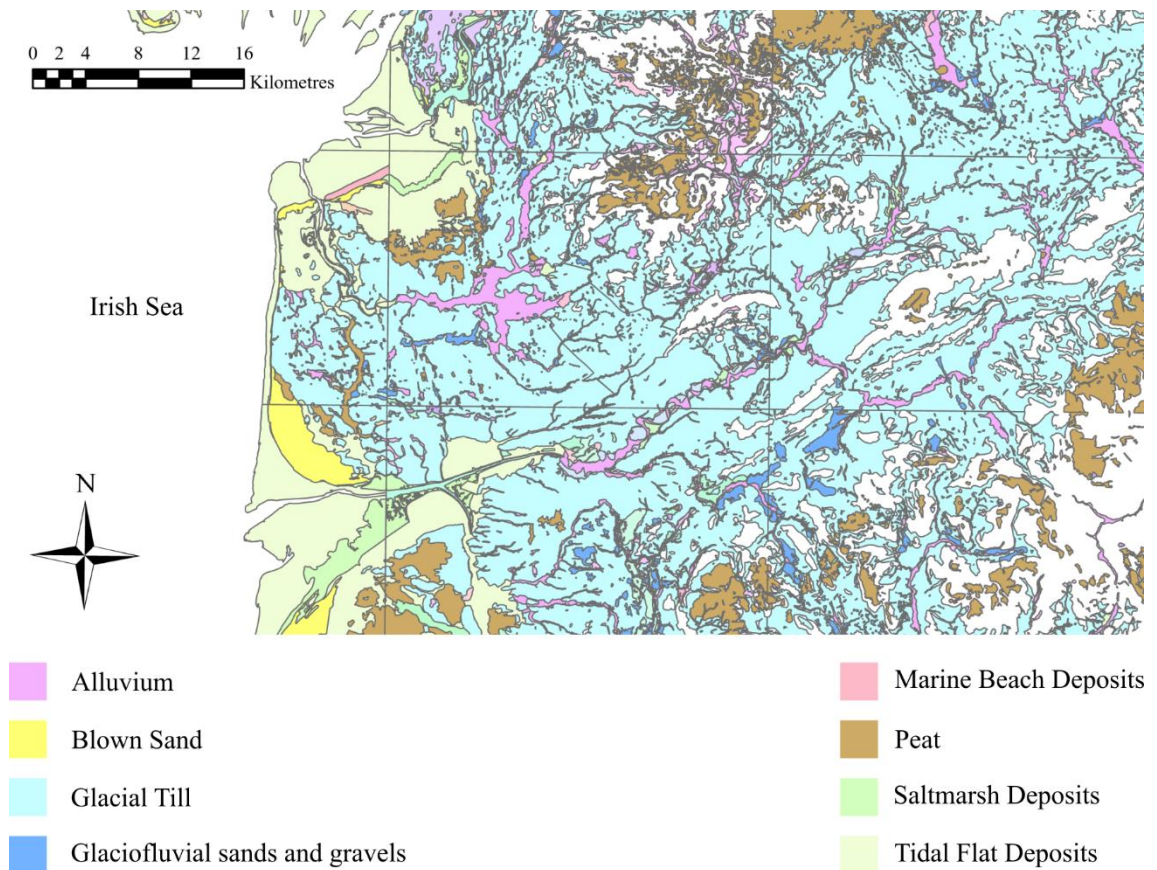
Figure 1.14
Map of superficial deposits across the Bowland Basin as mapped by the BGS. Only the main deposits are included in the legend. Contains British Geological Survey data © Crown copyright and database right (2018). A British Geological Survey/EDINA supplied service.

1.7.2   Hydrology

Rainfall over the Bowland Basin can be split into two areas corresponding to both elevation and bedrock geology. Over the low-lying Fylde, which is predominantly arable land, average rainfall is <1000 mm/year. Further east at the higher elevations of the Forest

of Bowland, where land is moorland or rough pastures, average rainfall is greater at ~1800 mm/year [*Mott MacDonald*, 1997]. The Bowland Basin is also split in two by the two major river catchments present: the River Wyre and the River Ribble catchments. In the north of the basin the River Wyre originates in the Forest of Bowland before running onto the Fylde, through Garstang, and eventually ending in the south of Morecambe Bay (Figure 1.2). The River Ribble is located in the south of the Bowland Basin and originates further inland than the River Wyre; starting in the Yorkshire Dales. From the Yorkshire Dales the River Ribble runs south then south-westwards, skirting the southern edge of the Forest of Bowland before running through Preston and into the Irish Sea (Figure 1.2). A major tributary of the River Ribble is the River Hodder which originates in the Forest of Bowland. The watershed divide between the Wyre and Ribble catchments in the Fylde approximately follows the east-west M55 motorway between Preston and Blackpool.

The Sherwood Sandstone Group forms the principal aquifer in the eastern Fylde and the Millstone Grit Group forms the main aquifer unit across the Forest of Bowland. The contact between these two formations is at the eastern edge of the Fylde and is unconformable or faulted [*Mott MacDonald*, 1997]. Initial groundwater models of the Fylde considered recharge of the Sherwood Sandstone Group from good hydraulic continuity between the Sherwood Sandstone Group and the adjacent Millstone Grit Group [*WRC*, 1972]. However, abstraction data indicates that recharge from the Millstone Grit Group is relatively minor in the northern Fylde and absent in the central Fylde. It was alternatively suggested that the majority of recharge occurs as vertical leakage through the overlying superficial deposits where low-permeability glacial till is absent [*Sage & Lloyd*, 1978; *Mott MacDonald*, 1997]. In the southern Fylde near the River Ribble, inflow from the Carboniferous strata is considered more significant, although north-south trending horst and graben faults reduce horizontal flow [*Seymour et al.*, 2006]. Recharge of the Millstone Grit Group occurs from direct precipitation and infiltration through the

overlying superficial deposits. Groundwater flow across the Fylde is towards Morecambe Bay in the north and the Ribble Estuary in the south.

Public and private groundwater abstractions in the Bowland Basin are focussed on the Sherwood Sandstone Group in the eastern Fylde, with few boreholes penetrating the Sherwood Sandstone Group in the western Fylde and no current abstractions from it [*Mott MacDonald*, 1997; 2010]. Consequently, little is known about groundwater in the Sherwood Sandstone Group across the western Fylde where fracking operations are currently focussed. However, one recent borehole at Rose Acre Wood has confirmed brine at depths of 360 to 500 m (Figure 1.11) [*BGS*, 2018]. Groundwater quality in the Sherwood Sandstone Group across the remainder of the western Fylde is hypothesised to be of poorer quality than in the east because the Sherwood Sandstone Group lies at greater depths (due to its south-westerly dip) and is confined by the overlying Mercia Mudstone Group (Figure 1.13) [*Ove Arup and Partners Ltd.*, 2014a]. Minor private water abstractions occur from superficial deposits (most likely from the glaciofluvial sands and gravels) across the Bowland Basin, including west of the Woodsfold fault. The superficial deposits are predominantly classified as secondary (undifferentiated) aquifers by the EA, meaning that they have been considered both minor aquifers and non-aquifer because of their complex characteristics [*DEFRA*, 2020].

2 Fracking: How far from faults?

The contents of this chapter contributed to the published comment on Westwood et al. [2017a] by Wilson et al. [2018] and an unpublished response to Verdon [2018]. The concept, microseismic literature collection and analysis, and production of the manuscript were done by M. P. Wilson. M. P. Wilson would like to thank F. Worrall for undertaking the statistical analyses and the useful discussions provided by all co-authors.

2.1 Introduction

Natural geological faults can play a critical role in the movement of fluids from kilometre-scale depths to the surface (see Section 1.4). It has been proposed that geological faults may also act as fluid pathways between unconventional shale reservoirs and shallow groundwater resources [*Kissinger et al.*, 2013; *Birdsell et al.*, 2015]. To reduce the risk of fracking-related fluids entering faults and potentially migrating upwards to shallow groundwater resources, the simplest solution is to prevent stimulated hydraulic fractures interacting with known faults, i.e. those observable on seismic reflection data. In addition, avoiding known faults is important for reducing the risk of induced seismicity that may damage infrastructure or pose a nuisance to the local population. Fracking-induced earthquakes have been documented in Canada, China, Poland, the UK and the USA [*Wilson et al.*, 2017a], with magnitudes up to M_L 5.7 in China [*Lei et al.*, 2019] and felt events down to M_L 0.5 in the UK [*BGS*, 2019c].

Using numerical modelling *Westwood et al.* [2017a] provided the first analysis of its kind to investigate how far from faults fluid injection for fracking should be carried out to avoid felt, induced seismicity. *Westwood et al.* [2017a] concluded that the maximum horizontal respect distance from faults varies from 63 to 433 m, depending on fracture intensity and failure threshold value. However, although a sensitivity analysis was carried

out on injection rate, fluid pumping time and differential pressure [*Westwood et al.*, 2017b], a number of factors were kept constant in the modelling scenarios and no uncertainty estimates or sensitivity analyses were carried out on: injection volume, Young's modulus, shear modulus, bulk modulus, Poisson's ratio, coefficient of friction, friction angle, cohesion, fracture aperture, permeability, compressibility, fracture orientation or depth. Furthermore, the modelling did not include poroelastic effects which can play an important role in stress changes and triggering earthquakes [e.g. *Deng et al.*, 2016; *Skoumal et al.*, 2018]. Changes in the model parameters and the inclusion of poroelasticity may therefore lead to different horizontal respect distances.

An alternative approach to numerical modelling is to use microseismic data from previous fracking operations to empirically determine a horizontal respect distance to faults. Microseismic events are weak earthquakes (the BGS classify microseismic events as those with $M_L <2.0$) of natural or anthropogenic origin. Microseismic monitoring is routinely carried out during fracking operations to track fracture propagation and infer the extent of stimulated fractures, and thus the SRV [*Mayerhofer et al.*, 2010]. Microseismicity associated with fracture stimulation is usually too small to be felt by humans at the surface. Monitoring may also detect seismicity related to the reactivation of geological faults [e.g. *Kratz et al.*, 2012], which can be identified by spatial trends in microseismic events or from the occurrence of larger macroseismic events [*Davies et al.*, 2013a]. Macroseismic events are more likely to be felt by humans at the surface. The reactivation of faults indicates that injected fluid has reached the fault plane or has perturbed the stress state of the fault without reaching it itself. Microseismic monitoring can therefore provide a measure of fracture propagation length and the extent of stress changes beyond the SRV.

As mentioned in Section 1.3.3 microseismic data have previously been used to suggest a vertical respect distance of 600 m between unconventional shale reservoirs requiring fracking and overlying aquifers [*Davies et al.*, 2012; 2013b]. This 600 m vertical respect distance now forms the basis of UK legislation for onshore fracking operations [*Infrastructure Act*, 2015]. In this study microseismic data were used to empirically determine a horizontal respect distance to faults, and thereby augment the study by *Westwood et al.* [2017a]. The presented method and results of this chapter are those of the original study by *Wilson et al.* [2018]. Discussion and further results in response to the comments made by *Verdon* [2018] have been incorporated into the presented discussion (Section 2.4.3).

2.2   Approach and methodology

The vast majority of microseismic data are privately owned by operators and contractors. Therefore, peer-reviewed literature and conference papers with plan-view maps or cross-sections of fracked boreholes with microseismic data were searched for on Google Scholar using keyword and phrase searches, for example "hydraulic fracturing microseismicity". The microseismic maps and cross-sections were used to infer the extent of fracture stimulation and stress changes by measuring distances to microseismic events. The results were collated and statistically analysed to empirically determine a horizontal respect distance. The statistical approach described below recognises that the collated microseismic maps and cross-sections are a small subset of all fracking microseismic datasets ever recorded.

2.2.1   Measuring the extent of stimulation and stress changes

The extent of fracture stimulation and stress changes was assumed to extend as far as the furthest detected microseismic event. Therefore, for each microseismic map and cross-

section the horizontal distance between the furthest detected microseismic event and the associated fluid injection stage was measured. Microseismic maps and cross-sections without borehole geometries or scale bars were excluded from the study. Where horizontal scales in map view were different within a map, the map was adjusted so that horizontal scales were equal. When no injection stage intervals were shown or it was unclear which stage related to which cluster of microseismic events, the perpendicular distance between the furthest detected microseismic event and the borehole was measured. Where the distance between the furthest detected microseismic event and the borehole was ambiguous because microseismic data from adjacent boreholes overlapped, the distance between the outermost borehole and the furthest outer microseismic event was measured. Microseismic event location errors were ignored because most sources did not provide error values. All distances were converted to SI units and the injection volumes, injection rates and reservoir lithologies were noted where possible.

2.2.2 *Statistical analyses*

Analysis of variance (ANOVA) and multiple and partial regression in Minitab (v.17) were used to determine statistically significant factors and covariates that controlled the extent of fracture stimulation and stress changes. Lithology was taken as a factor with three levels (coal, sandstone or shale) and the covariates were injection volume and injection rate. The Anderson-Darling test [*Anderson & Darling*, 1952] was used to assess the normality of the data prior to analysis and, if necessary, the data were transformed. The ANOVA was performed with and without the covariates, but inclusion of the covariates severely limited the size of the dataset. Therefore, multiple regression was used to understand the role of injection volume and rate, and partial regression was used to estimate the relative importance of these covariates in explaining microseismic distance variation. All statistical significance was judged at the 95% probability of being greater

than zero. Results are presented as least squares means (otherwise known as marginal means) where the range is the standard error in the least squares mean.

2.3   Results

One hundred and nine examples of fracking operations with suitable microseismic maps or cross-sections were collated from peer-reviewed literature and conference papers. Distances between injection stages or boreholes and the furthest detected microseismic events ranged from ~59 to 720 m (Table B1); up to ~287 m more than the maximum horizontal respect distance of *Westwood et al.* [2017a]. In general, fracking operations in coal had their furthest detected microseismic events nearer than those in sandstones, and those in sandstones were nearer than in shales (Figure 2.1). A cumulative distribution function of the dataset implied that the probability of observing a microseismic event at a distance >433 m was ~12% and observing one at >720 m was ~1% (Figure 2.2). However, the sample size was an extremely small proportion of the total number of fracking operations carried out globally. Consequently, probabilities calculated using the cumulative distribution function were not representative of the total population of global fracking operations.
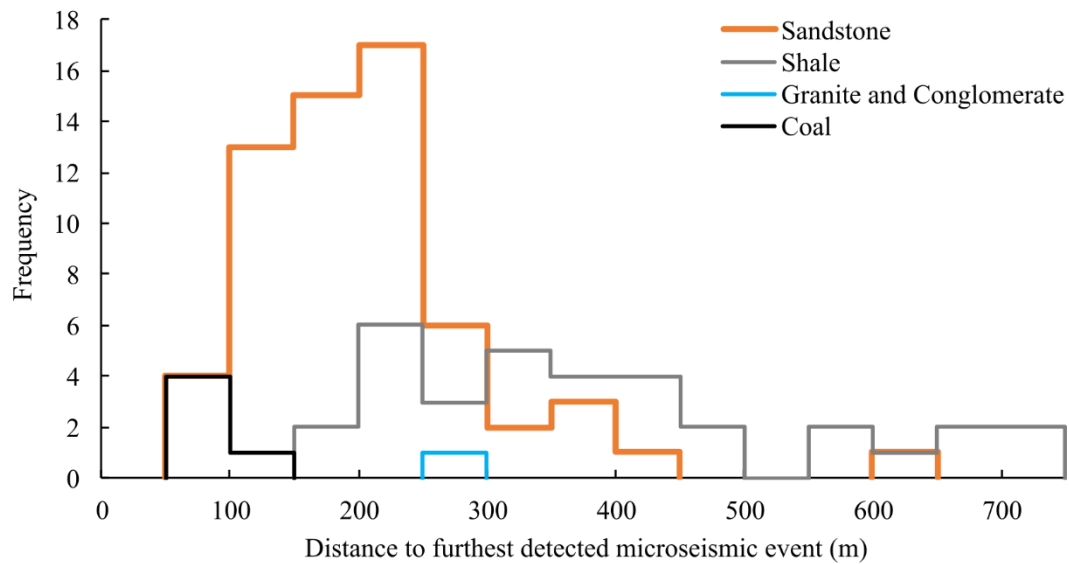
Figure 2.1
Graph of frequency against distance to furthest detected microseismic event for sandstone, shale, coal, and granite and conglomerate lithologies.
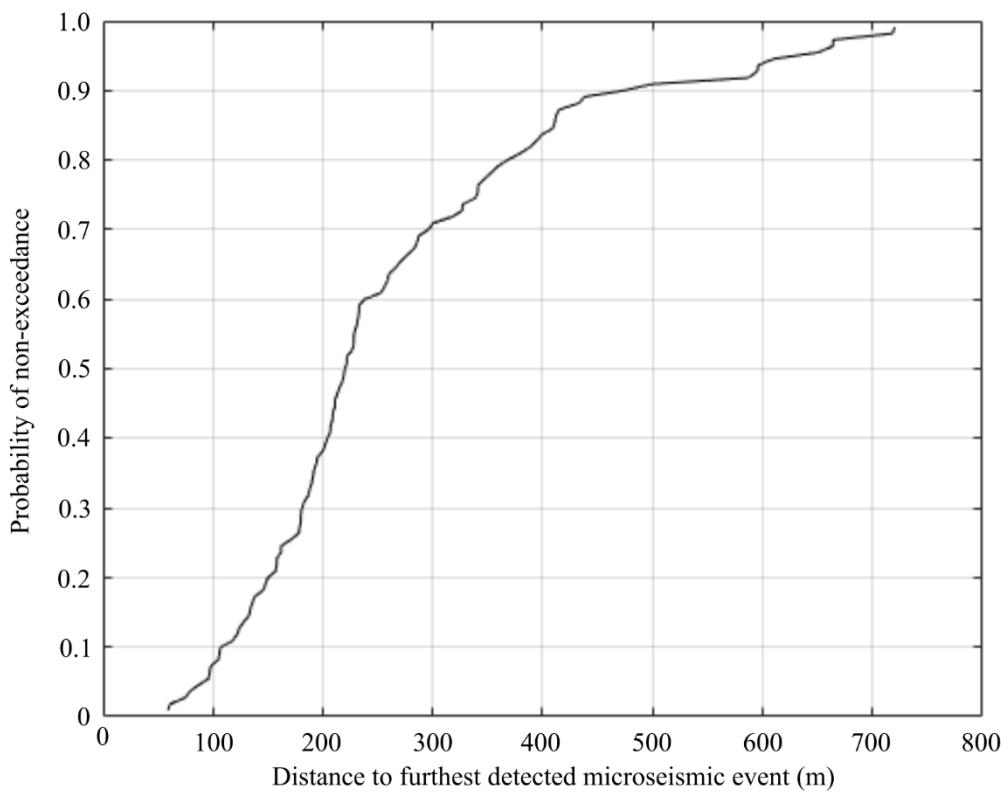
Figure 2.2
Graph of probability of non-exceedance against distance to furthest detected microseismic event based on the 109 cases in this study.

2.3.1 ANOVA

Normality tests on the lithology distributions showed them to be log-normal and so all data were log-transformed prior to the ANOVA. The ANOVA showed that there was a statistically significant difference between coal, sandstone and shale lithologies for the distance to the furthest detected microseismic event. The least squares means for coal, sandstone and shale were 91 m (75 to 109 m), 190 m (182 to 200 m) and 363 m (338 to 389 m), respectively. Given this ANOVA the probability of exceeding 433 m (the maximum horizontal respect distance of *Westwood et al.* [2017a]) was 0.1% in coal, 2% in sandstone and 32% in shale. There was a 1% chance of exceeding 228 m in coal, 494 m in sandstone and 895 m in shale.

2.3.2 Multiple and partial regression

Of the 109 cases, 16 had both injection volume and rate data. A further nine examples had just injection rate data. A statistically significant empirical relationship existed between injection volume and distance to the furthest detected microseismic event (Figure 2.3a). The relationship between injection rate and distance to the furthest detected microseismic event had a smaller Pearson product-moment correlation coefficient, but was still statistically significant (Figure 2.3b). The best-fit multiple regression model (Equation 2.1) explained 91% of the variation in distance to the furthest detected microseismic event:

$$log\ D = -0.277 - 0.000055V - 0.708\ log\ r + 1.139\ log\ V \qquad \textit{Equation 2.1}$$
$$\qquad (0.281)\quad (0.000012)\quad (0.149)\qquad (0.14)\qquad n = 16,\qquad R^2 = 91\%$$

where D is the distance to the furthest detected microseismic event (m), V is the injection volume (m^3) and r is the injection rate (m^3/min). Only those covariates found to be statistically significant were included in Equation 2.1 and the values in brackets below Equation 2.1 represent the standard errors in the coefficient. On application of partial regression analysis, the terms in volume (V and $log\ V$) in Equation 2.1 were found to be more important than the term in rate ($log\ r$). When those cases with both injection volume and rate data available were considered in the ANOVA, there was no significant difference between lithologies, with or without including covariates, indicating there was no evidence that fluid injection parameters explained the difference between lithologies.
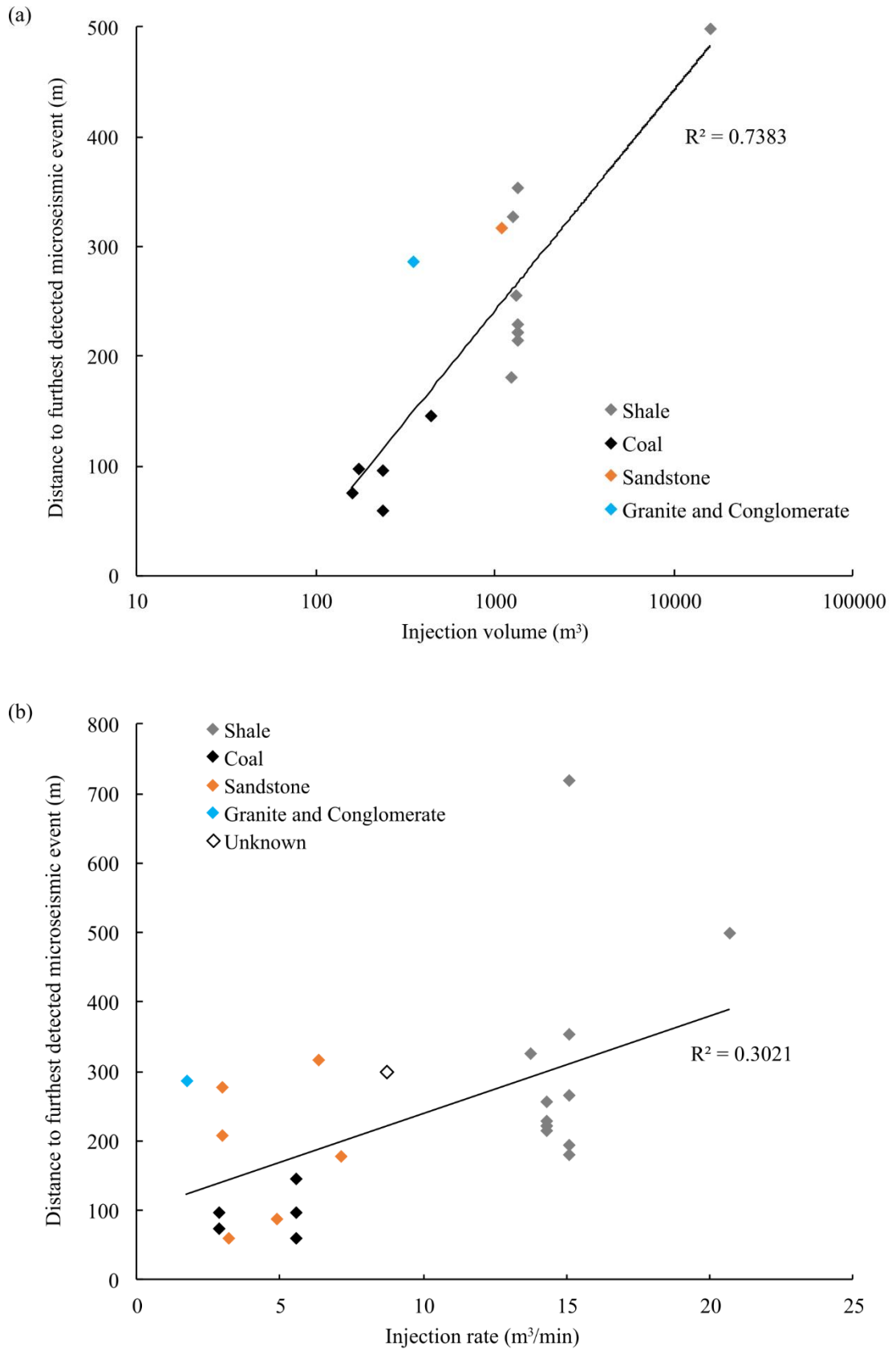
Figure 2.3
(a) Graph of distance to furthest detected microseismic event against injected fluid volume. (b) Graph of distance to furthest detected microseismic event against fluid injection rate. R^2 in graphs refers to the Pearson product-moment correlation coefficient.

2.4 Discussion

2.4.1 Limitations of microseismic data

All determined microseismic locations have an error associated with them, which may increase or decrease the inferred extent of fracture stimulation and stress changes. Additionally, detection will only be complete (i.e. all seismic events detected) above a particular magnitude. This magnitude can be calculated from a Gutenberg-Richter plot and is dependent on the sensitivity, location and type of monitoring equipment [*Johnston & Shrallow*, 2011; *Warpinski*, 2014]. Biased detection can lead to misleading microseismic maps [*Warpinski*, 2014] and, if the array is particularly poorly designed, the reactivation of faults could be missed and the inferred extent of fracture stimulation could be entirely controlled by the detection limit. Even for well-designed arrays stress changes may occur beyond recorded microseismic event clouds [*Lacazette & Geiser*, 2013].

2.4.2 Orientation of horizontal boreholes, maximum horizontal stress and faults

Fracking-induced fault reactivation is most likely to occur when faults are optimally orientated relative to the regional stress state. For example, the fracking-induced earthquakes at Preese Hall in 2011 are hypothesised to have occurred from left-lateral shear along an optimally orientated fault striking at 47° to the maximum horizontal stress (S_{Hmax}) (Figure 2.4) [*Clarke et al.*, 2014a]. Horizontal fracking boreholes are normally drilled perpendicular to S_{Hmax} to maximise the extent of fracture stimulation, thereby maximising oil and gas recovery. The orientation of pre-existing natural fractures is also an important consideration in borehole placement [*Gale et al.*, 2007]. When boreholes are drilled non-perpendicular to S_{Hmax} and then fracked, the extent of fracture stimulation from the borehole may be less than the actual fracture propagation length, and thus

smaller than a horizontal respect distance based on perpendicular fracture growth (Figure 2.5). Because of these directional effects, the orientation of horizontal boreholes, maximum horizontal stress and faults are important considerations for determining any site-specific horizontal respect distances.
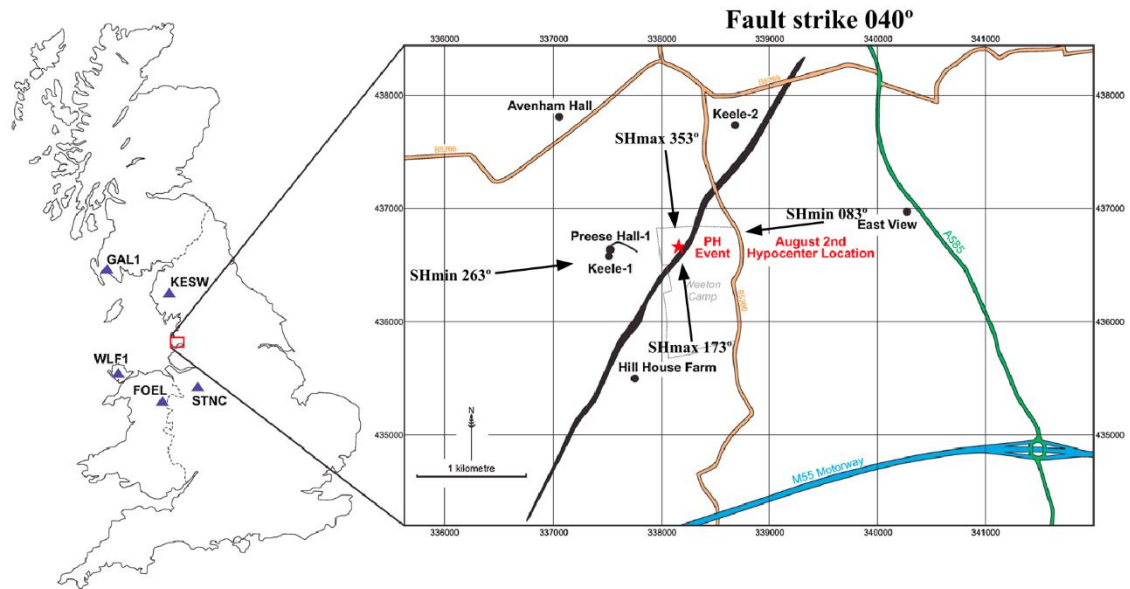
Figure 2.4
Map showing the epicentre of the fracking-induced earthquake of the 2ⁿᵈ August 2011 (PH Event) in relation to the hypothesised fault which slipped and the orientations of the maximum (S_{Hmax}) and minimum (S_{Hmin}) horizontal stress directions. Image adapted from Clarke et al. [2014a].
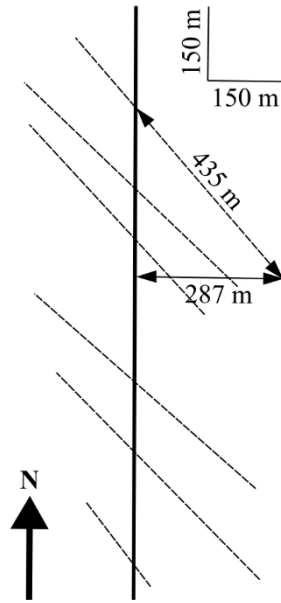
Figure 2.5
Schematic diagram of the plan-view microseismic map shown by Kilpatrick et al. [2010].
The solid line shows the approximate horizontal borehole orientation. The dashed lines
show the approximate orientation and extent of fracture propagation inferred from
microseismic data. The maximum extent of fracture stimulation from the borehole
(287 m) and the length of the longest fracture (435 m) are marked with labelled arrows.

2.4.3   Interaction of hydraulic fractures with faults and previously stimulated zones

In this section the comments made by *Verdon* [2018] are discussed and further results are

presented in response to the comments made. *Verdon* [2018] made two reasonable

critiques of the method for determining the extent of horizontal fracture stimulation by

measuring the furthest microseismic event. Firstly, microseismic events propagating

along a fault may lead to an overestimation of the distance measured for stimulated

fracture extent. Secondly, when boreholes are fracked adjacent to previously fracked

boreholes, microseismic events may occur on the previously stimulated fractures, thereby

also leading to an overestimation of the stimulated fracture extent.

    Nevertheless, these issues only apply to a handful of cases from the dataset collated

in this study. *Verdon* [2018] correctly identified interference in microseismic maps by

Malone et al. [2009] and *Mayerhofer et al.* [2011]. However, the interference shown by

Wolhart et al. [2006] did not extend further than the inferred fracture extent in the opposite direction into the previously non-stimulated area. Furthermore, in microseismic maps presented by *Neuhaus et al.* [2013], microseismic events were measured outside of the interference zones (i.e. the outer edge of outer boreholes only) because the spatial density and colour of microseismic events made measurements between adjacent boreholes ambiguous. Moreover, *Verdon* [2018] incorrectly used a microseismic map from *Warpinksi* [2014] as a further case of interference, which is actually the same microseismic map produced by *Mayerhofer et al.* [2011]. Five of the 109 examples may exhibit where fault interaction influenced the measurement of horizontal fracture extent (Table 2.1). The faults mentioned by *Maxwell et al.* [2008], *Neuhaus et al.* [2013] and *Warpinkski* [2014] were either not included in this analysis or did not affect the analysis. Furthermore, it is unclear from *Warpinksi and Du* [2010] if the analysed fault planes refer to distinct larger-scale faults or typical fracture stimulation within the SRV.

Table 2.1
Examples where fault interaction may have influenced the measurement of horizontal fracture extent.

Study	Borehole and/or stage
Neuhaus and Miskimins [2012]	Stage V
Wolhart et al. [2006]	EAST 3 Stage 3
Wolhart et al. [2006]	EAST 3 Stage 6
Wolhart et al. [2006]	EAST 4 Stage 3
Wolhart et al. [2006]	EAST 6 Stage 3

The effect of these examples on the results was investigated by re-running the ANOVA with them removed from the analysis. Furthermore, the second ANOVA was performed within a Bayesian framework so that the statistical distributions fitted and modelled in the ANOVA could be used as prior information for future analysis. The Bayesian ANOVA was performed using WinBUGS (v.1.4) [*Lunn et al.*, 2000] and Markov Chain Monte Carlo (MCMC) simulation to estimate the posterior distribution of

the fracture length. The length of the MCMC chain was 30000 cycles after 10000 burn in cycles, with samples saved every 10 cycles and with one chain. Statistical significance was judged as the 95% credible interval (CI) for any factor not including zero. In the Bayesian analysis a weak uninformative Jeffrey prior distribution was used whereby the expected value was set as the mean of the fracture length and the standard deviation was set as 100 times the coefficient of variation of the dataset, i.e. the prior was centred on the expected value of the data and was almost uniform in distribution.

Despite the correction of the dataset the ANOVA results were the same as the original analysis, i.e. there were significant differences at the 95% probability between the lithologies. There also remained a 1% chance of detecting microseismicity beyond a horizontal distance of 895 m in shale. The current best estimate of the statistical distribution from the Bayesian framework was log-normal ($\bar{x} = 4.48$, $\sigma = 0.19$).

2.4.4 Horizontal respect distance to known faults

Verdon [2018] argued that the application of a single respect distance is not an appropriate regulatory mechanism and instead that a site-specific numerical modelling approach for predicting the extent of fracture stimulation, as currently used in the UK [*OGA*, 2017], is adequate prior to fracking. Aside from the fact that current UK regulation for the vertical extent of hydraulic fractures uses a single respect distance [*Infrastructure Act*, 2015] based on the same empirical approach used in this study, only two fracking operations with microseismic monitoring have taken place in the UK to date (PNR-1z and -2). Therefore, there exist very few data on which to ground-truth numerical models of fracture propagation in UK geological settings. This problem is highlighted when comparing the predicted fracture heights and half lengths for PNR-1z with recorded microseismic data. Using 765 m^3 stage injection volumes, numerical models predicted average fracture heights and half lengths of 25 to 154 m and 64 to 313 m, respectively

[*Cuadrilla Resources Ltd.*, 2018b]. Recorded microseismic events for PNR-1z extended ~150 m above and below the borehole and ~200 m horizontally from the borehole [*Clarke et al.*, 2019]. Although these distances initially appear comparable to the predictions, only 17 of the 41 stages were injected and only two of these were injected with the planned 50 tons of proppant and injection volumes of 400 m^3 [*Clarke et al.*, 2019]. It therefore appears that for PNR-1z fewer and smaller injection volumes were capable of producing the stimulated fracture extents predicted for larger injection volumes.

Numerical modelling is a powerful tool for predicting the extent of fracture stimulation and stress changes, and improvements in the predictive capabilities of models will likely occur as more microseismic data are collected and used to ground-truth models. However, until numerical models can accurately predict the extent of fracture propagation and stress changes, a cautionary regulatory approach in nations with limited fracking experience would be to use an empirical horizontal respect distance to known faults. The microseismic data compiled in this study suggest that fracture propagation and stress changes can occur beyond the maximum 433 m horizontal respect distance proposed by *Westwood et al.* [2017a]. The empirical risk of microseismicity in shale beyond 433 and 895 m is 32 and 1%, respectively. The distance of 895 m is also similar in scale to a fracking operation at the Poland Township, Ohio, USA, which is hypothesised to have reactivated a fault/fracture zone up to 850 m away from the borehole [*Skoumal et al.*, 2015]. The extent of fracture propagation and stress changes is likely to be a combined result of operational parameters, borehole orientation, local geological factors and the regional stress state. Therefore, applying a horizontal respect distance of 895 m between horizontal boreholes orientated perpendicular to S_{Hmax} and known faults optimally orientated for failure in their regional stress state (Figure 2.6), could be a cautionary approach to reduce the risk of fracking-related fluids interacting with known faults. A more extensive study using a much larger compilation of microseismic datasets

with known operational parameters and regional stress settings may be able to provide a series of revised empirical horizontal respect distances to faults which are more site specific.
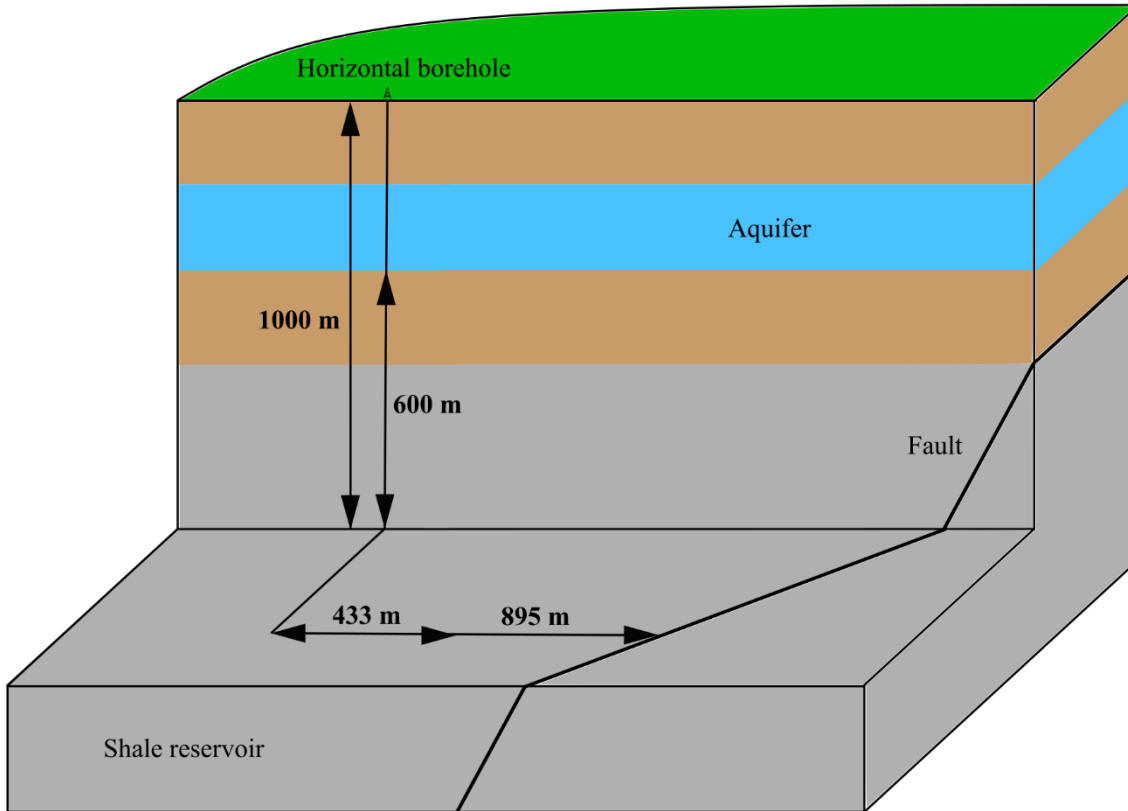
Figure 2.6
Schematic diagram illustrating: the 1000 m below surface regulation of the Infrastructure Act [2015]; the 600 m vertical respect distance of Davies et al. [2012; 2013b]; the 433 m horizontal respect distance of Westwood et al. [2017a]; and the 895 m horizontal respect distance of this study. The horizontal borehole is orientated perpendicular to the maximum horizontal stress and the fault is optimally orientated for failure.

2.5   Conclusions

Avoiding fluid injection into faults is important in fracking operations to reduce the risk of induced seismicity and potential fluid migration towards the surface. *Westwood et al.* [2017a] used numerical modelling to provide a maximum horizontal respect distance of 433 m between fracking fluid injection and faults. However, the numerical modelling may have been limited by the selected model parameters. An alternative approach to numerical modelling is to use microseismic data from previous fracking operations to

empirically determine a horizontal respect distance to faults. Using a sample set of 109 fracking operations with published microseismic data, it was found that the empirical risk of detecting microseismicity in shale beyond a horizontal distance of 433 m was 32% and beyond 895 m was 1%. Fracking operations in shales generally had their furthest detected microseismic events at greater distances than those in coals and sandstones. Injection volume and rate both showed statistically significant relationships with the distance to the furthest detected microseismic event. However, there was no evidence that fluid injection parameters explained the microseismic distance differences between lithologies. The extent of fracture propagation and stress changes is likely a result of operational parameters, borehole orientation, local geological factors and the regional stress state. For nations with limited fracking experience, and therefore with numerical models that are not ground-truthed, applying a horizontal respect distance of 895 m between horizontal boreholes orientated perpendicular to the maximum horizontal stress direction and faults optimally orientated for failure in their regional stress state, could be a cautionary approach to reduce the risk of fracking-related fluids interacting with known faults.

3 Shallow aquifer vulnerability from subsurface fluid injection at a proposed shale gas hydraulic fracturing site

The contents of this chapter contributed to the published manuscript by Wilson et al. [2017b]. The concept, model construction, simulations and production of the manuscript were done by M. P. Wilson. M. P. Wilson would like to thank F. Worrall for running the statistical analyses and the useful discussions provided by all co-authors.

3.1 Introduction

As discussed in Section 1.5 a number of approaches exist to assess the potential migration of fracking-related fluids from the deep to shallow subsurface along natural geological pathways. However, numerical modelling offers a more practical and predictive approach than field-based groundwater monitoring. Since *Myers* [2012] produced the first numerical model to assess upward fluid migration from fracking, the complexity of numerical models investigating upward fluid migration has increased. However, one aspect that has remained relatively untouched is the inclusion of more complex geological structure; models to date have tended to use horizontal geological strata and homogenous overburdens to the shale reservoir. This approach may be appropriate for some sedimentary basins, but may not be appropriate for more complex prospective basins such as the Bowland Basin. Furthermore, previous models have focussed on worst-case scenarios of fluid injection directly into high-permeability fault or fracture structures. Conversely, Chapter 2 highlighted the deliberate avoidance of known faults to reduce the risks of groundwater contamination and induced seismicity. Consequently, real-life fracking operations are planned to inject into strata situated between any known faults, i.e. geological compartments.

The aim of this study was to numerically model a real-life fracking operation (which was planned to avoid known faults) in a complex sedimentary basin to consider the hydrogeological factors that would affect the travel time for fracking fluids injected at ~2000 m depth to reach a shallow aquifer at ~300 to 500 m depth. These hydrogeological factors may increase or decrease how vulnerable the aquifer is to any type of contaminant at a particular locality [*Palmer & Lewis*, 1998; *Worrall & Kolpin*, 2004]. This study was the first to use ANOVA to identify hydrogeological factors which play a statistically significant role in decreasing the fluid travel time between a fracked shale reservoir and shallow groundwater resources.

3.2 Approach and methodology

In this study the Preston New Road fracking operation in the Bowland Basin was numerically modelled prior to any fluid injection (Figure 3.1) (note that this operation has since been completed and thus information used in this study has subsequently been modified or changed by the operator). The fracking operation targeted the Bowland Shale, an organic-rich shale deposited during the mid-Carboniferous across northern England [*Andrews*, 2013], and was the first fracking operation in England to target shale gas using a horizontal borehole.

Numerical modelling was performed using the MODFLOW groundwater code and its associated graphical user interface (GUI); ModelMuse. The model scenarios were selected to be a factorial combination of the hydrogeological factors of interest. The factors considered were: the presence of faults acting as fluid conduits; the vertical extent of stimulated fractures; the presence of deep low hydraulic conductivity (i.e. low-permeability) strata above the target shale formation; the presence of deep high hydraulic conductivity (i.e. high-permeability) strata above the shale formation; cross-basin

groundwater flow; and overpressure. Particle tracking was used to provide a measure of the fracking fluid travel time to the regional shallow aquifer. ANOVA was used to analyse the results.
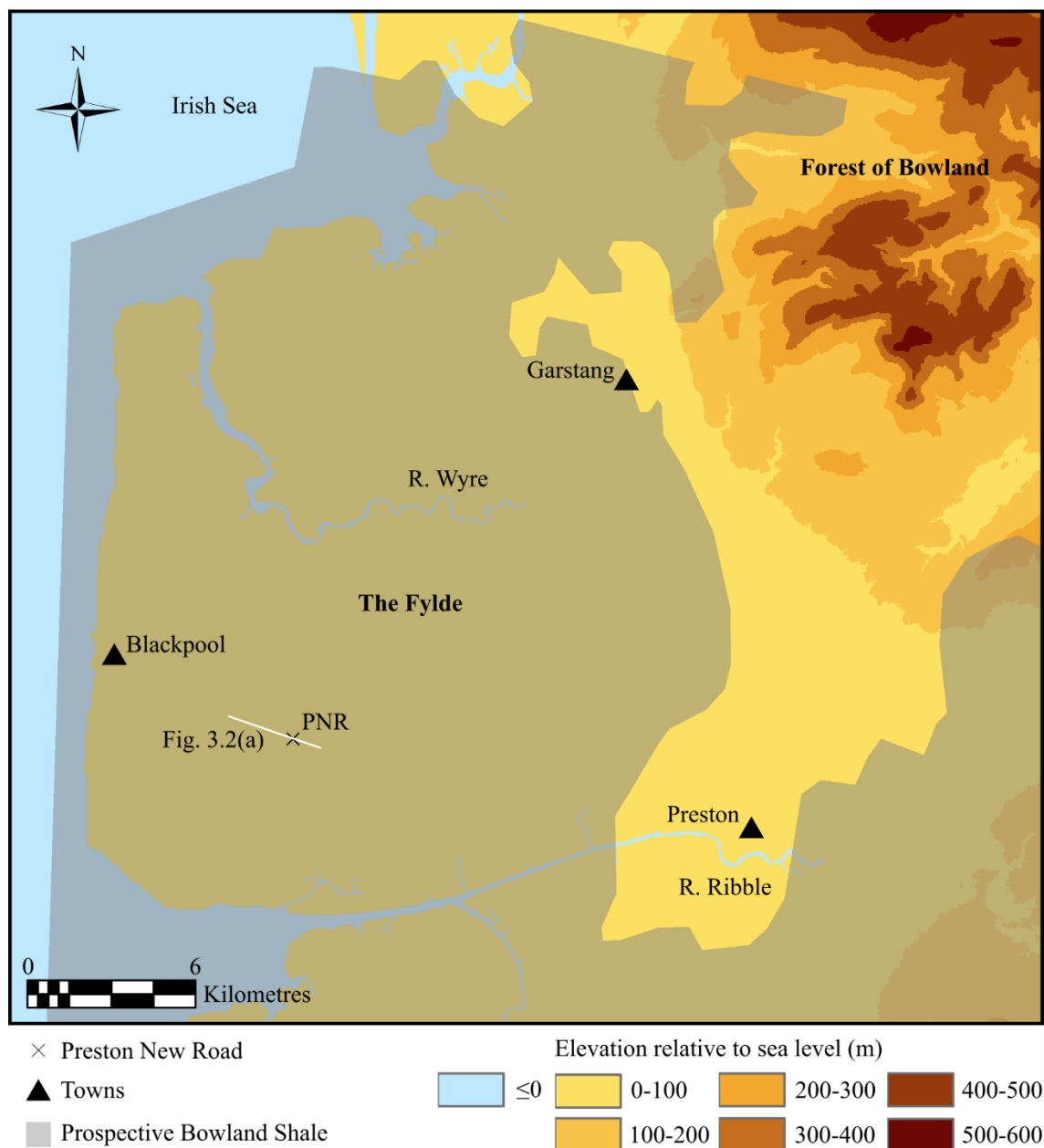
Figure 3.1
Map of the Fylde showing the location of Preston New Road (PNR) and cross-section of Figure 3.2.

The effects of faulting were a particular focus because faults can act as conduits and barriers to regional groundwater flow. It is already known that faults influence shallow

groundwater flow in the Bowland Basin [*Seymour et al.*, 2006; *Mott MacDonald*, 2010]. The effects of low and high hydraulic conductivity strata above the shale formation were also considered because both have been suggested to act as barriers to vertical fluid migration [*Ove Arup and Partners Ltd.*, 2014a; *Cai & Ofterdinger*, 2014]. Although the analysis was undertaken on a specific site, hydrogeological factors were identified that could increase or decrease aquifer vulnerability across global shale basins.

3.2.1 MODFLOW, ModelMuse and MODPATH

MODFLOW is an open-access finite-difference groundwater code created by the United States Geological Survey (USGS) [*McDonald & Harbaugh*, 1984]. This study used the latest version available at the time; MODFLOW-2005. MODFLOW simulates steady and transient groundwater flow in irregularly shaped flow systems subject to external stresses such as wells, areal recharge, evapotranspiration, drains and rivers [*Harbaugh*, 2005]. MODFLOW has been used to model groundwater scenarios from small-scale localised fracking [e.g. *Myers*, 2012] to large-scale regional studies [e.g. *Belcher & Sweetkind*, 2010].

To build a numerical hydrogeological model to run using MODFLOW, the USGS GUI ModelMuse was used. ModelMuse enables the user to create a model grid and input spatial and temporal data such as hydrogeological parameters and boundary conditions [*Winston*, 2009]. MODFLOW can be executed from ModelMuse and the results also displayed through ModelMuse. Within ModelMuse, the MODPATH Version 6 package was used to undertake particle tracking. MODPATH is a post-processing particle tracking code which computes 3D groundwater flow paths using the output from MODFLOW groundwater flow simulations [*Pollock*, 2012]. Particle tracking provided a quantitative

prediction of the long-term migration route of injected fracking fluid and travel time to the shallow aquifer.

3.2.2 *Geological model*

The geological model for the fracking site was based on a schematic geological cross-section provided in the submitted Environmental Statement required for the development [*Ove Arup and Partners Ltd.*, 2014a]. The expected geology at the site included folded and dipping strata, strata thickness variations, erosional truncation geometries and faulting. The cross-section was orientated approximately west-northwest to east-southeast and had approximate dimensions of 3.5 by 3.7 km^2 (Figure 3.2a). A single borehole trajectory was shown contained within the Upper Bowland Shale. The expected strata were modified to account for the commonly observed two-layer stratification of the Sherwood Sandstone Group; the upper, more hydraulically conductive Sherwood Sandstone and the lower, less hydraulically conductive St. Bees Sandstone [*Allen et al.*, 1997; *Ambrose et al.*, 2014]. The Sherwood Sandstone is the primary regional aquifer in the Bowland Basin [*Allen et al.*, 1997].

The Haves Ho fault was interpreted by the operator to extend from the Hodder Mudstone (the underlying formation to the Bowland Shale) to the surface (Figure 3.2) [*Ove Arup and Partners Ltd.*, 2014b]. Due to this possible direct conduit to the surface, the study cross-section and modelled area were extended westwards (6.0 by 3.5 km^2, with grid spacing of 50 by 50 m^2 as shown in Figure 3.3), ensuring the geological model was consistent with the seismic reflection interpretations of the Haves Ho fault shown by *Ove Arup and Partners Ltd.* [2014b] (Figure 3.2b). A result of this was the lithological change in the bottom left corner of the cross-section.
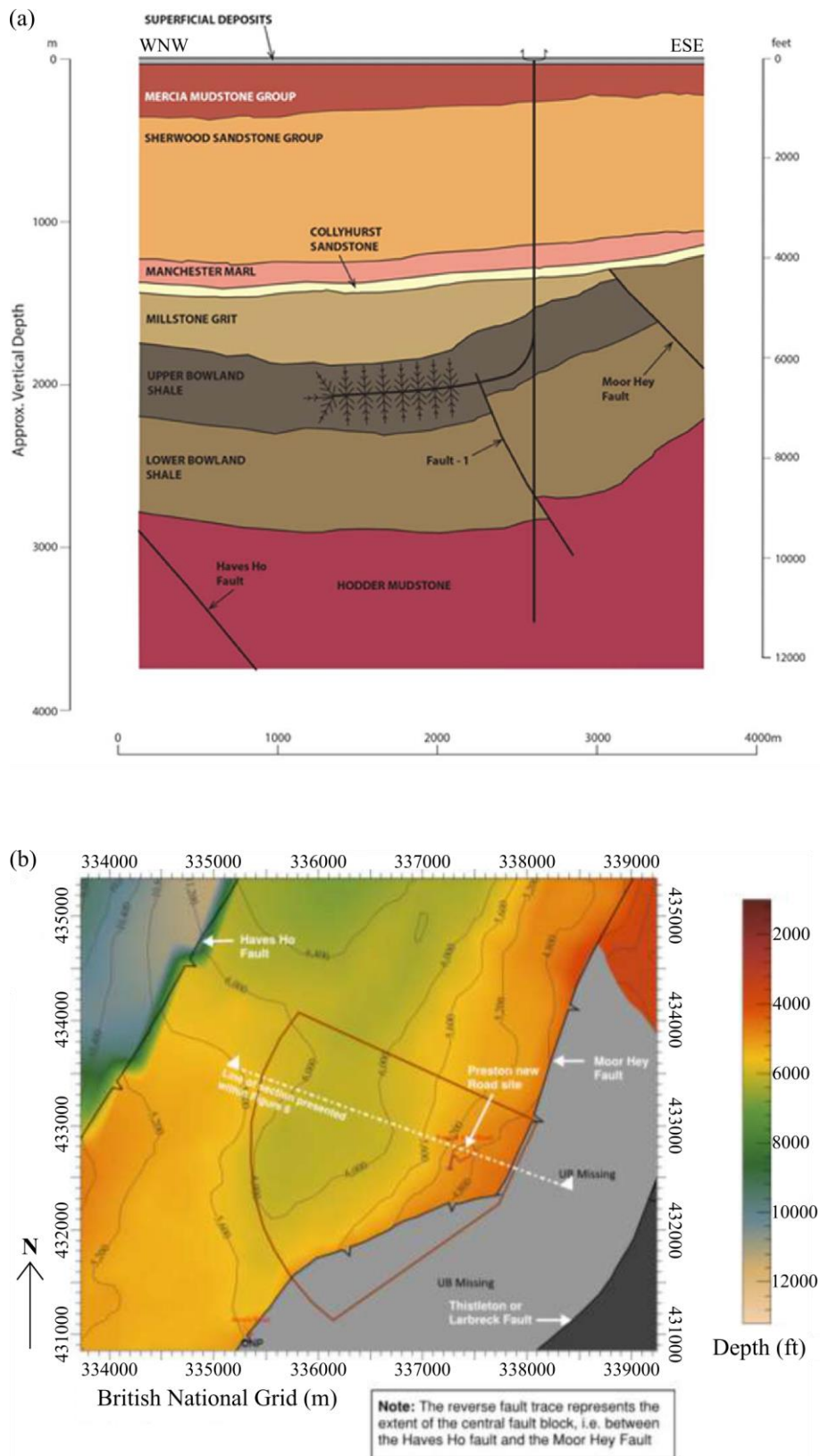
Figure 3.2
(a) Geological cross-section of the expected pre-drill geology and structure at Preston New Road. (b) Depth structure map illustrating the depth below ground level of the interpreted top of the Upper Bowland Shale. The locations of interpreted faults and the cross-section of (a) (dashed white line) are also shown. Images adapted from Ove Arup and Partners Ltd. [2014b].

60
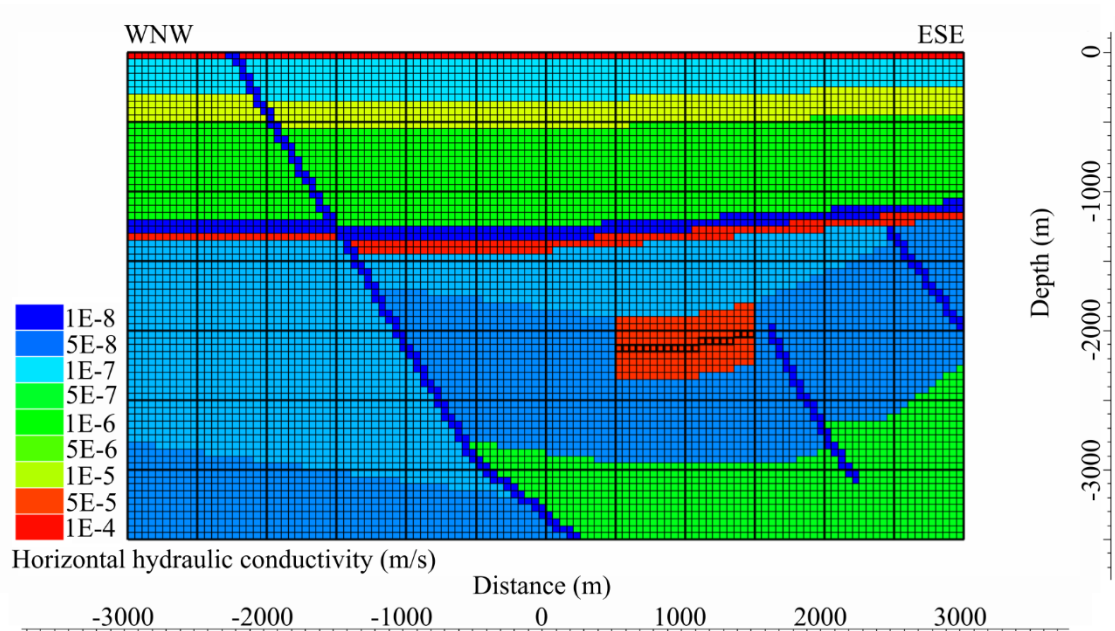
Figure 3.3

Hydrogeological model of Figure 3.2a, including predicted extension to the west-northwest. The finer grid spacing is 50 by 50 m². Fracking stages are shown as bold black outlined squares contained within a stimulated vertical fracture extent of 200 m above and below the stages (red).

3.2.3 Hydrogeological model

The typical strata hydraulic parameters identified by *Cai and Ofterdinger* [2014] were used to populate the geological model (Table 3.1). *Cai and Ofterdinger* [2014] primarily selected hydraulic parameter values considered most appropriate to the Bowland Basin from two aquifer reports by the BGS [*Allen et al.*, 1997; *Jones et al.*, 2000]. Hydraulic conductivity and storage coefficient values come from field-scale measurements, for example pumping tests, whereas porosity values appear to come from core measurements, although it is unknown whether these measurements refer to total porosities or effective porosities. As *Cai and Ofterdinger* [2014] explained, the lack of fracture data available justifies the use of representing each stratigraphic unit with an equivalent porous medium. However, it is appreciated that fractures likely play a major role in fluid flow through some of the modelled units, for example the Sherwood Sandstone Group [*Allen et al.*, 1997], and thus the effect of fracture porosity is discussed in Section 3.4.6.2.

61

The hydraulic properties of the Bowland Shale and Hodder Mudstone were based on the Marcellus Shale because few, if any, field-scale observations of hydraulic conductivity, porosity, and storage coefficient were available [*Cai & Ofterdinger*, 2014]. No hydraulic distinction was made between the Upper and Lower Bowland Shale Formations because one-way ANOVA of core plug permeability data (restricted access so not shown) from PH-1 [*Hird & Clarke*, 2012] showed that measured values were not statistically different between the stratigraphically defined Upper and Lower Bowland Shale. The numbers of measured core plug samples were: 13 horizontal and five vertical permeabilities from the Upper Bowland Shale and eight horizontal and two vertical permeabilities from the Lower Bowland Shale. The formation (Upper or Lower) and permeability direction (Horizontal or Vertical) factors had probabilities of having zero effect of 0.756 and 0.659, respectively.

Above the Bowland Shale there were two formations of particular interest. Firstly, the Manchester Marl (Figure 3.2a) is a low hydraulic conductivity formation that has been proposed as protecting the overlying aquifer from ingress of fracking fluids [*Ove Arup and Partners Ltd.*, 2014a]. Secondly, the Collyhurst Sandstone (Figure 3.2a) is a relatively high hydraulic conductivity layer at the base of the Permian sequence, which has also been proposed to protect the overlying aquifer from the ingress of any fracking fluids [*Cai & Ofterdinger*, 2014]. In some modelled scenarios, the low hydraulic conductivity Manchester Marl, the high hydraulic conductivity Collyhurst Sandstone, or both formations were removed. The removal of the Manchester Marl was achieved by assigning this model layer the same hydraulic properties as the overlying St. Bees Sandstone. This approach was also taken when both formations were removed. The removal of the Collyhurst Sandstone was achieved by assigning this model layer the same hydraulic properties as the Manchester Marl. The removal of these formations was undertaken to investigate how potential fluid migration changes with their absence

because their occurrence at the site had yet to be proven with drilling. Seismic interpretation in the Bowland Basin suggests that in some locations the Collyhurst Sandstone was not deposited [*Clarke et al.*, 2014b].

The hydraulic properties of the faults at the proposed site (Moor Hey Fault, Fault-1 and Haves Ho Fault; Figure 3.2) are highly uncertain. These faults were therefore modelled with low, medium and high estimates for hydraulic conductivity (Table 3.1). The low hydraulic conductivity case was taken as a fault permeability of 10^{-19} m^2 [*Rutqvist et al.*, 2013; 2015] and converted to hydraulic conductivity by assuming gravitational acceleration of 10 m/s^2 and fluid density and viscosity of 1000 kg/m^3 and 0.001 kg/m/s, respectively. The allocation of bulk hydraulic conductivity values to the fault zone grid blocks followed a similar approach to *Gassiat et al.* [2013], where a bulk permeability value was applied to the fault zone without considering fracture apertures and grid block size. More complex approaches do exist, such as the dual porosity and cubic law approach by *Birdsell et al.* [2015], but application to models with complex geological structure is much more difficult; fault zones in this study are inclined relative to the model grid and the shale overburden is inhomogeneous. The three fault scenarios represent cases where the faults have lower, similar or higher hydraulic conductivities relative to the surrounding strata. Each scenario assumes that all faults have the same hydraulic properties as each other and that these properties do not vary along the fault length. This assumption is a simplification of reality but is a practical approach when further information does not yet exist for these faults.

All model scenarios included three stress periods: an initial steady-state period, a two hour transient fluid-injection period (no fluid injected in scenarios with no fracture propagation) and a 10000 year transient-state period. To model an SRV, the hydraulic conductivities of the strata immediately overlying and underlying the horizontal borehole

were increased by a factor of 1000 to represent the increase in hydraulic conductivity caused by stable induced fractures [*Gaskari & Mohaghegh*, 2006]. The fractured areas in the models can be thought of as 2D representations of an SRV [*Mayerhofer et al.*, 2010]. These hydraulic conductivity changes were made after the initial steady-state period but prior to fluid injection. Due to software limitations, this approach required the initial steady-state periods to be modelled as separate simulations and their outputs used as the starting conditions for the transient periods.

The vertical extents of the modelled SRVs were 0 (no SRV and fluid injection represents a natural groundwater flow scenario), 200 and 600 m above and below the horizontal borehole. The horizontal portion of the borehole was situated at ~2000 m depth. An upper limit of 600 m was chosen because the largest reported vertically stimulated fracture in the Barnett Shale was found to be ~588 m [*Davies et al.*, 2012]. A 600 m extent results in fracture propagation into the overlying Millstone Grit. A 200 m fracture extent was also modelled because this extent reaches the upper boundary of the Bowland Shale at the site, but does not penetrate the overlying Millstone Grit (Figure 3.3). It was hypothesised that the vertical extent of the SRV would be ~50 to 150 m from the borehole [*Ove Arup and Partners Ltd.*, 2014b]. Due to the 2D nature of the model, the lateral extent of the SRV was not considered.

Table 3.1

Hydraulic parameters for model scenarios. Data from Cai and Ofterdinger [2014] unless stated. "n/a" indicates not applicable.

Unit	Horizontal hydraulic conductivity (K_h) (m/s)	K_h/K_v	Fracked hydraulic conductivity (m/s)	Porosity (fraction)	Storage Coefficient (S_c)
Superficial Deposits	$1.7{\times}10^{-4}$ [a]	100000 [a]	n/a	0.30 [b]	$1.0{\times}10^{-3}$ [b]
Mercia Mudstone Group	$1.0{\times}10^{-7}$	100	n/a	0.10	$1.0{\times}10^{-3}$
Sherwood Sandstone	$1.2{\times}10^{-5}$	10	n/a	0.23	$2.0{\times}10^{-3}$
St. Bees Sandstone	$8.1{\times}10^{-7}$	10	n/a	0.15	$8.6{\times}10^{-5}$
Manchester Marl	$1.0{\times}10^{-8}$	10	n/a	0.15	$2.0{\times}10^{-5}$
Collyhurst Sandstone	$7.9{\times}10^{-5}$	10	n/a	0.26	$5.0{\times}10^{-4}$
Millstone Grit	$7.9{\times}10^{-8}$	10	$7.9{\times}10^{-5}$	0.08	$1.0{\times}10^{-4}$
Bowland Shale (Upper and Lower)	$6.0{\times}10^{-8}$	10	$6.0{\times}10^{-5}$	0.03	$1.0{\times}10^{-4}$
Hodder Mudstone (formerly called Worston Shales)	$6.0{\times}10^{-7}$	10	n/a	0.03	$1.0{\times}10^{-4}$
Faults (*Moor Hey Fault, Fault-1, Haves Ho Fault*)	$1.0{\times}10^{-12}$ (low) [c] $1.0{\times}10^{-8}$ (medium) $1.0{\times}10^{-4}$ (high)	1	n/a	0.25 (Default)	$1.0{\times}10^{-5}$ (Default)

[a] Based on Mott MacDonald's and the Environment Agency's conceptual model for the Fylde Aquifer.

[b] Assumed. Other values make negligible difference to simulation and particle tracking results.

[c] Low fault hydraulic conductivity is from a permeability of 10^{-19} m^2 [Rutqvist et al., 2013; 2015].

3.2.4   Boundary conditions

Both the presence of a horizontal hydraulic head gradient (resulting in cross-basin groundwater flow) and the magnitude of overpressure were considered important factors in the study design. Two levels of horizontal hydraulic head gradient were considered. Firstly, the same horizontal hydraulic head boundary condition as applied by *Cai and Ofterdinger* [2014] was applied to the model. A horizontal hydraulic head gradient of 0.5% was applied with flow from east-southeast to west-northwest (i.e. east-southeast boundary had a hydraulic head value of 3530 m and the west-northwest boundary 6000 m away had a hydraulic head value of 3500 m). Groundwater is expected to flow from northeast/east to southwest/west [*Mott MacDonald*, 1997] but due to the 2D nature of the model domain the horizontal gradient was assigned as stated. Secondly, the horizontal hydraulic head gradient was removed by applying a hydraulic head value of 3500 m to the east-southeast boundary. The datum for hydraulic head was the base of the model domain, i.e. for a head boundary of 3500 m the hydraulic heads at the top and base of the model were the result of the elevation and pressure heads, respectively.

Hydraulic head values of either 3850 or 4900 m were applied to the entire lower boundary of the model. The hydraulic head value of 4900 m corresponds to ~40% overpressure above hydrostatic pressure; the overpressure as measured at PH-1 [*Cai & Ofterdinger*, 2014]. The hydraulic head value of 3850 m corresponds to a lower overpressure of 10%. Rainfall recharge was not assigned to the upper boundary of the model domain based on the assumption that little rainfall recharge reaches deeper than the Mercia Mudstone Group. This assumption of no rainfall recharge at depth infers that the horizontal head gradient is the result of recharge from the upland topography of the Forest of Bowland (Figure 3.1). All head boundaries were implemented as constant head boundaries to ensure that the cross-basin flow and overpressure conditions remained

constant for the duration of the 10000 year simulations (constant head boundaries have an infinite capacity to supply and remove water from the model). Constant head boundaries provided the simplest boundary conditions to observe the effects of the considered hydrogeological factors. However, constant head boundaries are not affected by transient stresses such as fluid injection volumes. Nevertheless, constant head boundaries were considered appropriate because the stress effects of the modelled fluid injection were likely to be negligible and short-lived; assuming an average model porosity of 10%, the volume of groundwater in the model was 1.05×10^8 m^3 whereas the injection volume was 5×10^4 m^3, i.e. injection volume was <0.05% of the groundwater volume.

3.2.5   *Fluid injection and particle tracking*

At the time of this study details of the fluid injection were yet to be confirmed. This study considered a single 1000 m long, strata-parallel borehole with injection stages at 50 m intervals (i.e. 20 stages) (Figure 3.3). Each stage within the model was represented as a point source using the Well package (WEL) within ModelMuse and MODFLOW. For simplification and consistent with *Cai and Ofterdinger* [2014], all stages were injected simultaneously at a rate of ~0.35 m^3/s for two hours, equivalent to stage injection volumes of 2500 m^3. Flowback and production volumes were not accounted for. Simultaneous injection without flowback and production can be thought of as a worst-case situation. In reality, flowback and production operations would occur between each stage, reducing the volume of fracking fluid left in the subsurface and also reducing the pore fluid pressure. Flowback and production may reduce the risk of injected fluid migrating beyond the SRV. The neglect of flowback and production is discussed in Section 3.4.6.3.

Particle tracking was used to investigate potential migration routes and travel times to the base of the Sherwood Sandstone (the primary regional aquifer). Because fracture

propagation was not modelled explicitly, particle tracking was initiated at the furthest extent of the SRV and at the end of the two hour injection period. This approach assumes that injected fluid reaches the edges of the SRV, although it is unclear if this always occurs in practice. Again, this is a worst-case assumption and is further discussed in Section 3.4.6.2. Particles were tracked for 10000 years after the termination of injection.

3.2.6   *Scenario design and statistical analysis*

The scenario design used in this study was a factorial design with respect to: the Manchester Marl; the Collyhurst Sandstone; cross-basin flow (generated by the horizontal hydraulic head gradient); stimulated fracture extent; fault hydraulic conductivity; and overpressure. For the Manchester Marl, the Collyhurst Sandstone and the cross-basin flow, only two levels were considered for each factor. These levels were the presence or absence of that stratum or phenomenon. For the stimulated fracture extent three levels (0, 200 and 600 m) were considered. Fault hydraulic conductivity also considered three levels (1.0×10^{-12}, 1.0×10^{-8} and 1.0×10^{-4} m/s). The factorial combination resulted in 72 scenarios. A second factorial analysis was then used to investigate the influence of overpressure; two levels (10 and 40% above hydrostatic pressure) were used in conjunction with statistically significant factors from the previous 72 scenarios. Overall 91 scenarios were modelled.

ANOVA in Minitab (v.17) was used to assess the significance of individual factors and the two-way interactions between them, with significance judged at the 95% probability of the factor or interaction not having zero effect. Scenarios where particles did not reach the Sherwood Sandstone within 10000 years were assigned an arbitrary travel time of 15000 years. The Tukey test was used *post hoc* to assess where significance lay within those factors with three levels. The factor and level effects were reported as

least squares means (marginal means) because these are the best measure of the average after allowing for the influence of the other factors and interactions. The proportion of the variance explained by each factor and interaction was estimated using the ω^2 method of *Olejnik and Algina* [2003].

The hydraulic properties of the deep strata in the Bowland Basin are uncertain. The factorial analysis did not consider the potential range of hydraulic conductivities for strata due to the large number of scenarios and time this would require. Instead, a single worst-case scenario was modelled. This worst-case scenario was achieved by using the maximum values for strata hydraulic conductivity used by *Cai and Ofterdinger* [2014] (see their table 1) in the factorial scenario which resulted in the shortest particle travel time to the Sherwood Sandstone. The minimum, typical and maximum hydraulic conductivity values used by *Cai and Ofterdinger* [2014] covered three orders of magnitude.

3.3 Results

Of the 72 scenarios modelled in the initial factorial analysis, 16 of these resulted in particles reaching the base of the Sherwood Sandstone within 10000 years (Table 3.2). All of these 16 scenarios had the Collyhurst Sandstone absent. The shortest particle travel time to the Sherwood Sandstone was 560 years (expressed to the nearest 10 years), which occurred when the stimulated fracture extent was 600 m and the Manchester Marl, Collyhurst Sandstone and cross-basin flow were absent. None of the scenarios without fracking and fluid injection resulted in particles reaching the Sherwood Sandstone within 10000 years.

Table 3.2
Factorial scenarios that resulted in particle travel times under 10000 years to the base
of the Sherwood Sandstone.

Stimulated fracture extent (m)	Fault hydraulic conductivity (m/s)	Manchester Marl present?	Collyhurst Sandstone present?	Cross-basin flow present?	Travel time to nearest 10 years
200	1.0×10^{-8}	Yes	No	Yes	9390
200	1.0×10^{-8}	Yes	No	No	7430
200	1.0×10^{-8}	No	No	Yes	3660
200	1.0×10^{-8}	No	No	No	3200
600	1.0×10^{-8}	Yes	No	Yes	3140
200	1.0×10^{-12}	Yes	No	Yes	3050
200	1.0×10^{-12}	Yes	No	No	2990
600	1.0×10^{-8}	Yes	No	No	2900
200	1.0×10^{-12}	No	No	No	1760
200	1.0×10^{-12}	No	No	Yes	1720
600	1.0×10^{-12}	Yes	No	No	1490
600	1.0×10^{-12}	Yes	No	Yes	1460
600	1.0×10^{-8}	No	No	Yes	790
600	1.0×10^{-8}	No	No	No	790
600	1.0×10^{-12}	No	No	Yes	580
600	1.0×10^{-12}	No	No	No	560

3.3.1   Factors

The factors of Collyhurst Sandstone, stimulated fracture extent and fault hydraulic conductivity were found to have a statistically significant impact on particle travel times, all with probabilities of not having zero effect of >0.9995. The most important of these three significant factors (as measured by ω^2) was the Collyhurst Sandstone. The Collyhurst Sandstone factor explained 14% of the original variance while the stimulated fracture extent and fault hydraulic conductivity factors each explained no more than 7% of the original variance. The presence of the Collyhurst Sandstone encouraged the horizontal movement of particles within itself, rather than the vertical passage of particles through it and towards the shallower aquifer. The mean particle travel time for models with the Collyhurst Sandstone absent was 9581 years (Table 3.3). No particles reached

the Sherwood Sandstone in any scenarios where the Collyhurst Sandstone was present, hence the mean travel time of 15000 years (the arbitrary limit chosen for ANOVA).

As for the fault hydraulic conductivity factor, no scenarios with the high value for fault hydraulic conductivity (1.0×10^{-4} m/s) resulted in particles reaching the Sherwood Sandstone (mean travel time of 15000 years). The scenarios with medium (1.0×10^{-8} m/s) and low (1.0×10^{-12} m/s) fault hydraulic conductivities had mean travel times of 11304 and 10567 years, respectively. The *post hoc* Tukey tests on the levels of this factor showed that the significant difference lay between the highest value of the fault hydraulic conductivity and the other two levels but not between the medium and lower levels, i.e. it was when the fault was more conductive than the surrounding strata that it prevented upward particle travel. Less conductive faults led to the compartmentalisation of hydraulic head and consequently encouraged the movement of particles vertically.

None of the scenarios without fracking or fluid injection resulted in particles reaching the Sherwood Sandstone, resulting in mean travel times of 15000 years. The scenarios with stimulated fracture extents of 200 and 600 m had mean travel times of 11381 and 10490 years, respectively. That a greater stimulated fracture extent results in a shorter mean travel time to the Sherwood Sandstone was an intuitive result, but it should be emphasised that *Davies et al.* [2012] only reported a ~5% chance of stimulated fractures propagating vertically more than 200 m. *Post hoc* analysis of the stimulated fracture extent factor showed that the significant differences between levels of the factor were between the 0 m and both the 200 and 600 m stimulated fracture extents, but not between fracture extents of 200 and 600 m.

The cross-basin flow and Manchester Marl were statistically insignificant factors, with probabilities of the factors having zero effect on the particle travel times of 0.855 and 0.243, respectively. That is, this study could find no statistical evidence that the low

hydraulic conductivity Manchester Marl provided protection for the overlying aquifer. Rather it was the presence of higher hydraulic conductivity strata (i.e. the Collyhurst Sandstone) that led to greater fluid dispersion, and therefore afforded a degree of protection to overlying layers. Mean travel times for all factors are shown in Table 3.3.

Table 3.3

Mean travel times with standard error for factors and statistically significant factor interactions in the initial factorial analysis. P-Value is the probability of a factor or interaction not having zero effect, judged at 95% confidence.

Factor or factor interaction	P-Value	Factor options		Mean (years)	Standard error of mean (years)
Collyhurst Sandstone	>0.9995	No		9581	292
		Yes		15000	292
Stimulated fracture extent	>0.9995	0 m		15000	358
		200 m		11381	358
		600 m		10490	358
Fault hydraulic conductivity	>0.9995	1.0×10^{-4} m/s		15000	358
		1.0×10^{-8} m/s		11304	358
		1.0×10^{-12} m/s		10567	358
Cross-basin flow	0.145	No		12250	314
		Yes		12331	314
Manchester Marl	0.757	No		12028	314
		Yes		12553	314
Stimulated fracture extent *Fault hydraulic conductivity	>0.9995	0 m	1.0×10^{-4} m/s	15000	620
		0 m	1.0×10^{-8} m/s	15000	620
		0 m	1.0×10^{-12} m/s	15000	620
		200 m	1.0×10^{-4} m/s	15000	620
		200 m	1.0×10^{-8} m/s	10453	620
		200 m	1.0×10^{-12} m/s	8690	620
		600 m	1.0×10^{-4} m/s	15000	620
		600 m	1.0×10^{-8} m/s	8460	620
		600 m	1.0×10^{-12} m/s	8011	620
Stimulated fracture extent *Collyhurst Sandstone	>0.9995	0 m	No	15000	506
		0 m	Yes	15000	506
		200 m	No	7762	506
		200 m	Yes	15000	506
		600 m	No	5981	506
		600 m	Yes	15000	506
Collyhurst Sandstone *Fault hydraulic conductivity	>0.9995	No	1.0×10^{-4} m/s	15000	506
		Yes	1.0×10^{-4} m/s	15000	506
		No	1.0×10^{-8} m/s	7608	506
		Yes	1.0×10^{-8} m/s	15000	506
		No	1.0×10^{-12} m/s	6134	506
		Yes	1.0×10^{-12} m/s	15000	506

3.3.2 Factor interactions

The following factor interactions were all statistically significant (all with probabilities of not having zero effect of >0.9995): stimulated fracture extent with fault hydraulic conductivity; stimulated fracture extent with Collyhurst Sandstone; and fault hydraulic conductivity with Collyhurst Sandstone. The most important of the significant interactions (as measured by ω^2) was the interaction of the stimulated fracture extent with fault hydraulic conductivity. This interaction explained 42% of the original variance. The other significant interaction terms explained no more than 7% of the original variance. The shortest mean travel time for stimulated fracture extent with fault hydraulic conductivity interactions was 8011 years, which occurred for scenarios with 600 m fractures and a fault hydraulic conductivity of 1.0×10^{-12} m/s. The shortest mean travel time for stimulated fracture extent with Collyhurst Sandstone interactions was 5981 years, which occurred for scenarios with 600 m fractures and no Collyhurst Sandstone present. The shortest mean travel time for fault hydraulic conductivity with Collyhurst Sandstone interactions was 6134 years, which occurred for scenarios with a fault hydraulic conductivity of 1.0×10^{-12} m/s and no Collyhurst Sandstone present. Mean travel times for all the statistically significant interactions are shown in Table 3.3. Seven of the possible ten factor interactions were statistically insignificant (Table 3.4). The cross-basin flow and Manchester Marl did not interact with other factors in a statistically significant way, further supporting the single factor results that they did not influence particle travel times to the Sherwood Sandstone.

To test the effect of allocating an arbitrary 15000 year travel time to scenarios where particles did not reach the Sherwood Sandstone within 10000 years, the arbitrary travel time was changed to 10000 years and the ANOVA re-run with all the same factors and interactions as before. The change in the default travel time made no difference to which

factors and interactions were and were not significant at probability of 95% difference from zero. The proportion of the overall variance explained did shift marginally from 91.8% when 15000 years was used compared to 89.9% when 10000 years was used.

Table 3.4
Insignificant factor interactions with probabilities (P-Value) of not having zero effect, judged at 95% confidence.

Factor interaction	P-Value
Stimulated fracture extent*Manchester Marl	0.368
Stimulated fracture extent*Cross-basin flow	0.023
Fault hydraulic conductivity*Manchester Marl	0.475
Fault hydraulic conductivity*Cross-basin flow	0.028
Manchester Marl*Collyhurst Sandstone	0.757
Manchester Marl*Cross-basin flow	0.088
Collyhurst Sandstone*Cross-basin flow	0.145
Overpressure*Stimulated fracture extent	0.720
Overpressure*Fault hydraulic conductivity	0.721

3.3.3 Overpressure

The significance of overpressure as a vulnerability factor was assessed using a further factorial analysis based on the results of the previous factorial analysis. Overpressure was a statistically significant factor with a probability of not having zero effect on particle travel times of 0.966. The overpressure factor explained 8% of the original variance in the second factorial analysis, which was less important than the Collyhurst Sandstone factor (21% of the original variance in the second factorial analysis) and both the stimulated fracture extent and the fault hydraulic conductivity factors (both explained 10% of the original variance in the second factorial analysis). The interaction between overpressure with the Collyhurst Sandstone was also statistically significant (probability of not having zero effect of 0.966). This interaction explained 8% of the original variance in the second factorial analysis. Scenarios with no Collyhurst Sandstone and 40% overpressure were more likely to result in particles reaching the Sherwood Sandstone than scenarios with 10% overpressure (four of nine scenarios compared to one of nine). The

interactions of overpressure with stimulated fracture extent and overpressure with fault hydraulic conductivity were statistically insignificant (Table 3.4).

3.3.4   Worst-case scenario

The worst-case scenario used the maximum strata hydraulic conductivity values of *Cai and Ofterdinger* [2014] and the factor combination that produced the shortest travel time scenario (560 years) in the initial factorial analysis (600 m stimulated fracture extent, fault hydraulic conductivity of 1.0×10^{-12} m/s, no Manchester Marl present, no Collyhurst Sandstone present, and no cross-basin flow present). The particle travel time to the base of the Sherwood Sandstone for the worst-case scenario was 130 years (Figure 3.4). This result was 430 years earlier than the equivalent scenario using typical strata hydraulic conductivity values.
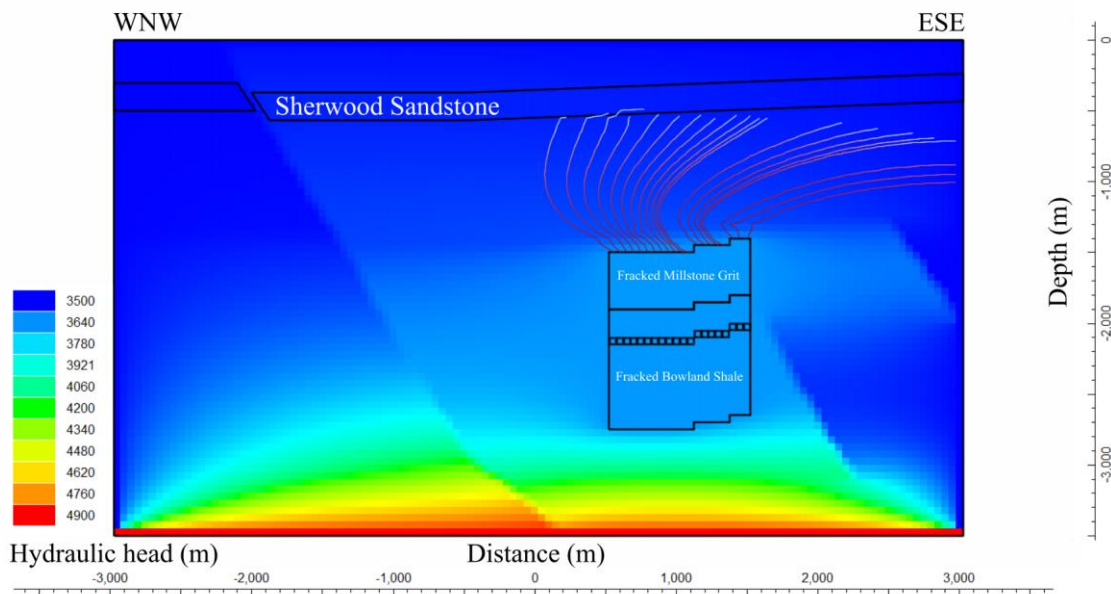
Figure 3.4
Simulated hydraulic head 10000 years after the termination of fracking fluid injection in the worst-case scenario. Also shown are 130 year particle tracks (red to white graded curves), the Sherwood Sandstone, the SRV (split by strata type), and injection stage locations.

3.4 Discussion

3.4.1 Stimulated fracture extent

No scenarios without fluid injection and a SRV resulted in particles reaching the base of the Sherwood Sandstone within 10000 years but eight scenarios with a stimulated fracture extent of 200 m and eight scenarios with a fracture extent of 600 m did (Table 3.2). The majority of scenarios with 600 m fracture extent (six of eight) resulted in quicker travel times to the Sherwood Sandstone than the 200 m fracture extent scenarios (Table 3.2). These results suggest that given certain hydrogeological configurations, the propagation of vertical fractures at the proposed site would increase the chance of fluid migration from the Bowland Shale to the Sherwood Sandstone. It also suggests that a greater stimulated fracture extent further increases the chance of fluid migration to the Sherwood Sandstone. The difference in mean travel times for scenarios with 200 and 600 m stimulated fracture extents was 891 years, with both means being of the order of 10000 years (Table 3.3). However, the *post hoc* analysis showed no significant difference between fracture extents of 200 and 600 m. Furthermore, 600 m stimulated vertical fractures are greater than any observed using microseismic data (~588 m) and the probability that an upward propagating fracture extends further than 200 m is ~5% [*Davies et al.*, 2012, see their figure 6b].

3.4.2 Faulting and fault hydraulic conductivity

Environmental concerns related to faults and the migration of fracking fluids are generally focussed on faults acting as fluid conduits to shallow aquifers [e.g. *Myers*, 2012; *Gassiat et al.*, 2013]. The results here suggest that the Haves Ho fault, which is considered to reach the surface near Preston New Road, will not act as a direct conduit for fracking fluid between the Bowland Shale and the Sherwood Sandstone, even when assigned a

hydraulic conductivity higher than the most hydraulically conductive strata in the model. An explanation of this result is due to the interaction between the Haves Ho fault and the modelled overpressure. In the high hydraulic conductivity fault scenarios the Haves Ho fault acted to increase hydraulic head values along its length to values higher than those at similar depths in the surrounding strata. This interaction resulted in a horizontal head gradient opposite to and larger than the assigned regional horizontal head gradient, resulting in particles moving horizontally away from the fault in an east-southeast direction. When the modelled faults were assigned low values for hydraulic conductivity, the scenarios displayed hydraulic head compartmentalisation (hydraulic heads increased in the area between the Haves Ho fault and Fault-1, see Figure 3.4 for an example). Compartmentalisation discouraged horizontal fluid migration (the faults acted as barriers to horizontal groundwater flow) and encouraged vertical fluid migration, resulting in scenarios with upward particle migration to the Sherwood Sandstone. Because faults are a common feature of sedimentary basins, this modelling result is important in environmental risk assessments for aquifer vulnerability. The compartmentalising effects of low-permeability faults mean that low-permeability faults may, in some hydrogeological scenarios, lead to greater shallow aquifer vulnerability than the presence of high-permeability faults.

3.4.3   *Low and high hydraulic conductivity stratigraphic barriers*

The low hydraulic conductivity Manchester Marl, which was expected to act as the key vertical migration barrier [*Ove Arup and Partners Ltd.*, 2014a], was not a statistically significant factor (probability of having zero effect of 0.243). *Cai and Ofterdinger* [2014] concluded that the high hydraulic conductivity Collyhurst Sandstone acts as a barrier to upward fluid migration by increasing horizontal fluid flow. Our results supported this conclusion. All 16 scenarios where particles reached the Sherwood Sandstone within

10000 years had the Collyhurst Sandstone absent. Additionally, no scenarios where the Collyhurst Sandstone was present resulted in vertical migration to the Sherwood Sandstone within 10000 years. In contrast to *Cai and Ofterdinger* [2014], horizontal flow in the modelled Collyhurst Sandstone was reversed to the regional horizontal head gradient because of its interaction with the Haves Ho fault and overpressure. These results indicate that high hydraulic conductivity formations in the deep subsurface, but beyond the stimulated fracture extent, can be more effective barriers to upward fluid migration than low hydraulic conductivity formations. Numerical modelling of the North German Basin has also shown horizontal fluid transport in more hydraulically conductive formations above the modelled fluid injection [*Pfunt et al.*, 2016], suggesting that this protective mechanism is not unique to the site in this study.

3.4.4   Overpressure

An overpressured formation is one in which the pore fluids contained within it are at a higher pressure than the hydrostatic pressure for that depth. One mechanism of overpressure formation is disequilibrium compaction; sediment is buried quicker than its pore water can escape. The conditions that favour disequilibrium compaction are rapid burial and low permeability, thus many shale successions with their low permeability and often rapid burial are commonly overpressured. Furthermore, the conversion of kerogen to oil and gas may be accompanied by volume expansion. Within a closed or low permeability system this can also contribute to overpressure [*Osborne & Swarbrick*, 1997]. Various shale resources around the globe are overpressured [*Advanced Resources International Inc.*, 2011; *Gassiat et al.*, 2013 and references therein]. Overpressure was found to be a statistically significant factor in this study. Furthermore, the interaction of overpressure with the Collyhurst Sandstone was also statistically significant. When the Collyhurst Sandstone was not present, the scenarios with 40% overpressure were more

likely to result in particles reaching the Sherwood Sandstone within 10000 years than scenarios with 10% overpressure, i.e. a greater upward driving force resulted in a quicker travel time. When the Collyhurst Sandstone was present, the magnitude of the overpressure made no difference to the travel time to the Sherwood Sandstone (particles did not reach the Sherwood Sandstone within 10000 years). This result occurred because particles were transported horizontally within the Collyhurst Sandstone as a result of generated horizontal head gradients being greater than the modelled regional horizontal head gradient. Given the common occurrence of overpressure in shale formations, its possible presence and magnitude should be considered along with overlying stratigraphy and geological structure when assessing shallow aquifer vulnerability.

3.4.5   *Shallow aquifer vulnerability*

The vulnerability of shallow aquifers to anthropogenically introduced fluids has generally concentrated on fluids introduced at the surface, for example pollution by agricultural pesticides [e.g. *Worrall & Kolpin*, 2004] or chemical spills [e.g. *Gross et al.*, 2013]. Subsurface fracking operations introduce a new potential source of aquifer contamination. Because such operations in England would inject fluids into shales at a minimum depth of 1000 m by law [*Infrastructure Act*, 2015], shallow aquifer vulnerability must now also be considered from a bottom-up perspective. This study has identified important hydrogeological factors to consider in a bottom-up approach to shallow aquifer vulnerability at proposed fracking sites: the vertical extent of induced fractures; the magnitude of overpressure; the presence of high-permeability formations acting as vertical fluid barriers; and low-permeability faults leading to compartmentalisation. The latter two factors are not normally considered [e.g. *Ove Arup and Partners Ltd.*, 2014a], but the results of this study suggest that they are important factors to consider in shallow aquifer vulnerability at proposed fracking sites.

3.4.6 Model limitations

3.4.6.1 2D vs. 3D models

The modelled scenarios in this study were all 2D because of the single geological cross-section available. This approach restricted the flow directions within the model to the 2D plane. This necessary restriction may have influenced particle travel times by not allowing any lateral movement of the particles. To investigate any lateral flow effects on travel times the model domain was extended by 1000 m to the north-northeast and south-southwest (Figure 3.5), i.e. the 3D model had a width of 2050 m (note that the original 2D model had a width of 50 m but was essentially 2D in comparison to the length and depth scales). The 3D SRV was modelled with equal horizontal and vertical extents. The 3D model was not made any wider than 2050 m because the 3D geology in the area was not constrained at the time of this study. However, it was wide enough to accommodate 600 m stimulated fractures and exclude edge effects. Scenarios were not run in 3D for every 2D scenario because of time constraints setting up the 3D versions. Instead, five 3D simulations were chosen based on their factor combinations (Table 3.5).

The extension to 3D had no effect on the particle travel time in the worst-case scenario, although ~75 m of lateral movement was observed by the time the particles reached the base of the Sherwood Sandstone (Table 3.5). Lateral particle movement was also observed for three other scenarios. Two of these had the Collyhurst Sandstone absent. In these scenarios travel times increased by 70 and 280 years, equating to ~13% and ~16% increases in respective travel times (Table 3.5). When the Collyhurst Sandstone was present extensive lateral movement was observed and particles reached the eastern corner of the 3D model domain. Nevertheless, particles remained within the Collyhurst Sandstone and did not reach the Sherwood Sandstone aquifer, supporting the 2D scenario results that the Collyhurst Sandstone acts as an effective barrier to upward flow. The

81

remaining scenario, with high fault hydraulic conductivity (1.0×10^{-4} m/s), showed no lateral movement in the 3D scenario and particles did not reach the Sherwood Sandstone (Table 3.5).
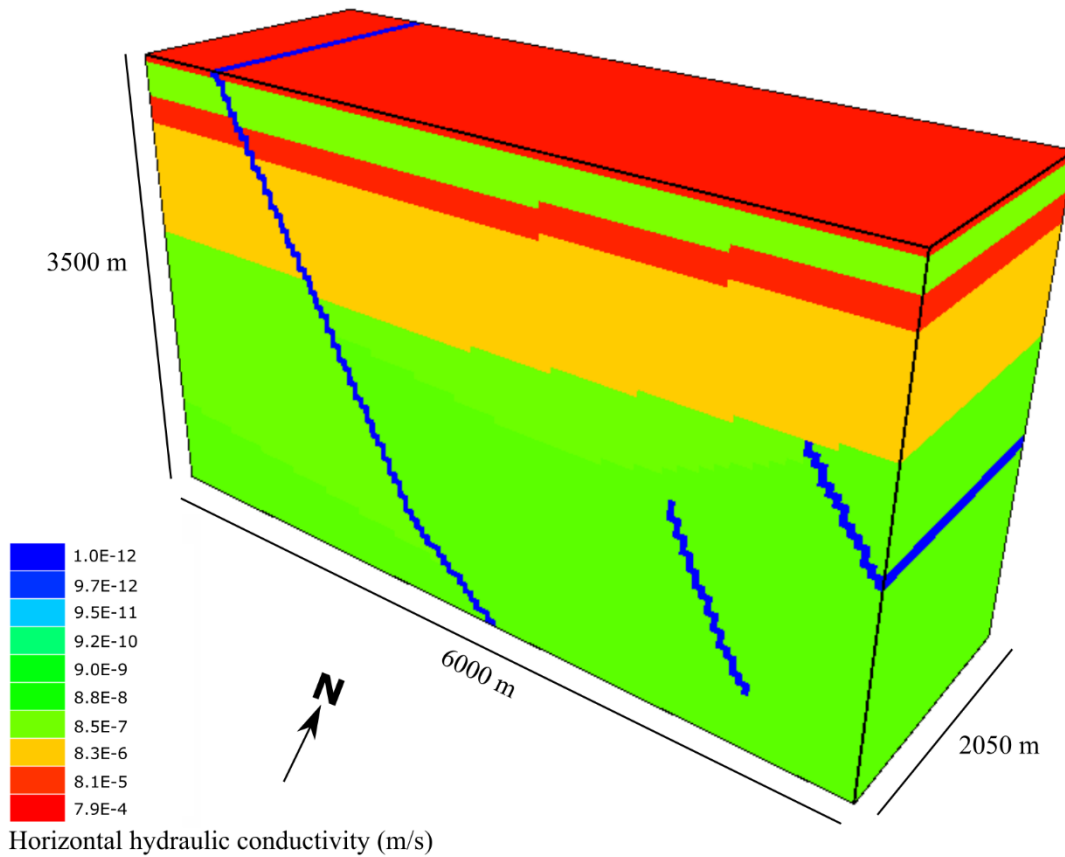
Figure 3.5
3D model domain using strata hydraulic conductivities from the worst-case scenario. The SRV is situated in the middle of the model and is therefore hidden from view.

Although lateral movement of particles was sometimes observed when the 2D scenarios were run in 3D, the travel time results still supported the 2D results that the Collyhurst Sandstone acts as an upward flow barrier and low-permeability faults encourage vertical fluid flow through compartmentalisation. Furthermore, the extension to 3D can increase travel times to aquifers, thereby reducing aquifer contamination risk. As more information and data are released for the study area, the development of more

informed, more extensive, and more sophisticated 3D models will be possible to further investigate these results (see Chapter 6).

Table 3.5
Particle travel times and extent of lateral movement for 3D scenarios. The Manchester Marl and cross-basin flow were absent in all scenarios. "+" indicates an increase in particle travel time compared to the equivalent 2D scenario.

Stimulated fracture extent (m)	Fault hydraulic conductivity (m/s)	Collyhurst Sandstone present?	Travel time to nearest 10 years	Travel time difference compared to 2D scenario (years)	Approximate extent of lateral movement (m)
600	1.0×10^{-12}	No	130*	0	75
600	1.0×10^{-12}	No	630	+70	50
600	1.0×10^{-4}	No	10000	0	0
600	1.0×10^{-12}	Yes	10000	0	1000
200	1.0×10^{-12}	No	2040	+280	175

* The worst-case scenario of Section 3.3.4.

3.4.6.2   Particle use and assumption

The study used the travel times of the first particles to reach the base of the Sherwood Sandstone as a measure of aquifer contamination risk. Chemical concentrations, which would be the common measure for comparison with environmental standards in aquifers and surface waters, were not considered. In reality, fracking fluids passing through geological strata would be subject to a number of natural attenuation processes, which could include non-conservative processes such as dilution, dispersion, degradation, adsorption and precipitation. Such processes would decrease, remove, and/or retard the fracking fluid constituents and contribute to increasing the travel time to shallow aquifers. In addition, all the constituents of a fracking fluid are subject to chemical risk assessments. In England only substances determined as "non-hazardous" by the Environment Agency have been identified suitable for permits. However, a major water quality concern from shale exploitation is the highly saline nature of fracking and

flowback fluids, and salinity is generally a conservative property in water bodies. Nevertheless, at the proposed site in this study the overlying shallow regional aquifer is expected to be saline and is not currently used as a groundwater resource [*Sage & Lloyd*, 1978; *Griffiths et al.*, 2003].

In addition to non-conservative attenuation processes that might increase travel times to shallow aquifers, this study also neglected the effect of fractures on particle travel time. Particle travel time is dependent on groundwater flow velocity, which is inversely proportional to the effective porosity (i.e. a decrease in effective porosity increases flow velocity and thus decreases particle travel time). Preferential fracture flow at field-scale can mean the effective porosity of a stratigraphic unit is much lower than porosities measured from core samples. Consequently, although this study took an equivalent porous medium approach consistent with *Cai and Ofterdinger* [2014], the particle travel times in this study may be too long because of the core porosities used and the neglect of fracture flow in the stratigraphic units of the Fylde [*Allen et al.*, 1997]. Considering the St. Bees Sandstone makes up approximately half of the thickness between the borehole and the Sherwood Sandstone aquifer, a decrease in effective porosity from 0.15 to 0.07 would halve the travel time through the St. Bees Sandstone, and thus may decrease particle travel times below those reported in Section 3.3. Nevertheless, such decreases in particle travel times would be unlikely to change the relative travel times between the different scenarios and therefore would be unlikely to affect which hydrogeological factors were, or were not, significant.

In each scenario particles were released at the edge of the SRV because fracture propagation was not modelled explicitly. However, it is unclear in practice if injected fluid always reaches the edge of the SRV. To investigate the travel time sensitivity to initial particle placement, six further 2D models were run under the same hydraulic

conditions as the worst-case scenario. These six scenarios decreased the distance between the injection cells and the particle release point at intervals of 100 m (the SRV remained at 600 m extent). Travel times for distances ≥300 m were the same as the original worst-case scenario and 10 years greater for distances ≤200 m (Table 3.6). Although the travel times were 10 years greater for release points ≤200 m to the injection cells, the effect does not substantially increase travel times, suggesting that the model results were not particularly sensitive to initial particle placement within the SRV.

Table 3.6
Particle travel times to the Sherwood Sandstone for the worst-case scenario with particles released at different distances from the fluid injection cells.

Distance between injection cells and particle release point (m)	Travel time to nearest 10 years
600*	130
500	130
400	130
300	130
200	140
100	140
0	140

* The worst-case scenario of Section 3.3.4.

3.4.6.3   Operational effects

Variations in the fracking operation parameters were not considered in the model scenarios. A single injection rate and a consistent number of fracking stages were used in all scenarios. Furthermore, modelled fluid injection was run simultaneously for all stages without flowback. A real-life fracking operation would inject stage fluids sequentially, flow back fluids between each stage, and then ideally produce hydrocarbons for a number of years. Flowback and production decrease the pressure and volume of fluid in the subsurface, reducing the chances of fluid migration into the overburden. *Birdsell et al.* [2015] included flowback and production in their numerical model and found that, in scenarios with a permeable pathway to the shallow aquifer, the combined effect of

production and capillary imbibition reduced the amount of fracking fluid reaching the aquifer by a factor of ten. *Brownlow et al.* [2016] also studied the effect of flowback and production as part of a numerical model investigating the influence of fracking operations on abandoned or converted boreholes. The flowback of 8% of the injected fluid volume had negligible effect to hydraulic head values. However, production over 15 years reduced hydraulic head values to nominal values up to 200 m from the fracked borehole [*Brownlow et al.*, 2016].

To investigate particle travel time sensitivity to flowback and production in the 2D model of this study the same 15 year flowback and production scenario of *Brownlow et al.* [2016] was employed to our worst-case scenario (Table 3.7). Particles were released at the upper edge of the SRV on the termination of injection. Each fracking injection stage of the model commenced flowback and production following the termination of injection using the Well package (WEL) within ModelMuse and MODFLOW. Despite the inclusion of flowback and production, particles reached the base of the Sherwood Sandstone in 130 years; the same as the original worst-case scenario. A key difference between this scenario and that by *Brownlow et al.* [2016] was the simulation time. Our scenario had a simulation time 10000 years beyond the 15 year production phase, whereas *Brownlow et al.* [2016] ended their simulation after 15 years of production. Consequently, the 130 year travel time was the result of the long-term interaction of the SRV and the model boundary conditions, which dominated over the shorter production phase. However, it is recognised that the scenarios in this study do not account for fracture aperture reduction and subsequent hydraulic conductivity reduction associated with production from a SRV [*Birdsell et al.*, 2015].

Table 3.7
Time phases for the flowback and production scenario. + and - indicate fluid injection and extraction, respectively.

Time phase	Time interval	Approximate fluid injection or extraction rate (m³/s)
Steady state	-	0
Fluid injection	2 hours	+0.35
Flowback	7 days	-0.00033
Early production	2 years	-0.00019
Main production	13 years	-0.00004
Post production	10000 years	0

3.4.6.4 Boundary conditions

Section 3.4.2 noted the interaction of the overpressure boundary and high hydraulic conductivity fault influencing particle movement within the Collyhurst Sandstone. Such an interaction between the overpressure boundary and the high hydraulic conductivity fault may not be entirely realistic; the constant head boundary provided a constant fluid flux along the fault whereas in reality a high hydraulic conductivity fault might have led to the dissipation of overpressure. Consequently, groundwater flow and particle movement away from the fault within the Collyhurst Sandstone may be a model effect and geologically unrealistic.

3.4.6.5 Other effects

The cross-section used in this study was based on confidential seismic interpretation, which inherently introduces errors. For example, the formation tops may have been interpreted at the wrong two-way-time (TWT), time to depth conversion may have been inaccurate and faults may have been incorrectly interpreted or missed due to the seismic resolution. Another model limitation was the availability of hydraulic data. Although shallow groundwater flow has been modelled effectively to the east of the proposed site [*Mott MacDonald*, 1997; 2010], little is known about the hydraulic properties and

gradients of the deep strata in the Bowland Basin. Future data from deep borehole core samples and pumping tests would help constrain the model parameters.

The effects of heat, variable-density flow and multiphase flow were not modelled. Thermal and density gradients in the subsurface can lead to the advection of groundwater. These effects could enhance or inhibit the migration of fracking-related fluids depending on the particular hydrogeological scenario. Multiphase flow could also be an important factor to model in future studies because fracking fluid injection leads to at least two-phase flow within a shale gas reservoir (injected liquid water and chemicals, injected solid proppants, and *in situ* natural gas – phase dependant on subsurface pressure). With the introduction of multiple phases, the absolute permeability of a single phase is reduced to the effective permeability. This decrease in permeability would reduce the ability of fracking fluid to flow through, and potentially out of, the shale reservoir.

A final remark is that *Davies et al.* [2012] based their stimulated fracture extents on microseismic data, which may not record the full extent of stimulated fractures [*Lacazette & Geiser*, 2013]. Stimulated fractures beyond the considered maximum limit of 600 m would be expected to further reduce particle travel times.

3.5   Conclusions

Under certain hydrogeological modelling configurations, fracking of a shale resource at ~2000 m below the surface decreased the travel time of fluid migration between the shale formation and the shallow regional aquifer at ~300 to 500 m below the surface. Of the 91 modelled hydrogeological scenarios, 18 scenarios resulted in particle travel times to the shallow aquifer within 10000 years. The study found that four subsurface factors acted to decrease particle travel times to the shallow aquifer and, as a result, increased the vulnerability of that groundwater resource:

1)   increased stimulated fracture extent;

2)   low-permeability faults, which result in compartmentalisation and encourage vertical fluid migration;

3)   the absence of deep high-permeability formations above the greatest stimulated fracture extent;

4)   and greater amounts of overpressure.

These factors in prospective shale basins could lead to increased vulnerability of shallow aquifers from fracking fluids injected at several kilometres depth. Two factors are not typically considered in hydraulic fracturing environmental risk assessments: deep high-permeability formations above the greatest stimulated fracture extent can be more effective barriers to vertical fluid flow than low-permeability formations; and low-permeability faults can result in compartmentalisation which can encourage vertical fluid migration more than high-permeability faults. The worst-case scenario modelled, which used an unlikely hydrogeological configuration at the modelled fracking site and stimulated vertical fractures greater than ever observed using microseismic data, resulted in a travel time to the shallow aquifer of 130 years. This result did not account for dilution, dispersion, degradation, adsorption or precipitation of the fracking fluid constituents, which would all act to further increase the travel time. On the other hand, the inclusion of fracture porosity and subsequent preferential flow effects in the scenarios may act to decrease travel times to the shallow aquifer.

4 Identifying groundwater compartmentalisation for hydraulic fracturing risk assessments

This chapter contributed to the published manuscript by Wilson et al. [2019]. The concept, analysis and production of the manuscript were done by M. P. Wilson. M. P. Wilson would like to thank the co-authors for their useful guidance and discussions, as well as Ian Boothroyd for his help with kriging and principal component analysis.

4.1 Introduction

Chapter 3 numerically modelled a real-life fracking operation in a structurally complex geological basin to investigate hydrogeological factors which increased the vulnerability of shallow groundwater resources. It was found that for fluid injection situated between faults (a more likely development scenario because operators aim to avoid fluid injection into faults), it was the scenarios with low-permeability faults that resulted in the highest risk to the shallow aquifer. This result occurred because the modelled low-permeability faults acted to compartmentalise groundwater in the basin, thereby discouraging lateral flow and encouraging upward flow through strata in the presence of a vertical hydraulic head gradient [*Wilson et al.*, 2017b].

Compartmentalisation can also be caused by stratigraphic changes, for example aquifers vertically separated by low-permeability formations or the lateral pinch-out of the aquifer bodies. Both structural and stratigraphic groundwater compartmentalisation are analogous to the compartmentalisation of petroleum reservoirs. In simple geological basins where stratigraphic units extend undisturbed for 100s to 1000s km and faulting is of minor importance for basin structure, compartmentalisation of petroleum resources and groundwater is unlikely to be an important hydraulic effect. However, for basins where stratigraphic changes and faults are common, for example offshore and onshore basins of

the UK, compartmentalisation can be an important effect [*Smalley et al.*, 1996; *Leveille et al.*, 1997; *Mohamed & Worden*, 2006; *McKie et al.*, 2010; *Medici et al.*, 2019].

Groundwater compartmentalisation can be identified from observations of hydraulic head, water table height and groundwater geochemistry, temperature and age [*Mohamed & Worden*, 2006; *Bense et al.*, 2013], although very different hydrodynamic interpretations can be made from the same data [*Bredehoeft et al.*, 1992]. Whereas the identification of compartmentalisation in petroleum reservoirs is normally driven by economic reasons [*Smalley et al.*, 1996], the main driver for identifying groundwater compartmentalisation is the environmental protection of water resources [*Mohamed & Worden*, 2006]. Compartmentalisation can generate flow directions different to regional trends, create areas of no flow or reduced flow and produce large variations in groundwater levels, temperatures and compositions [*Hamaker & Harris*, 2007; *Hortle et al.*, 2009; *Smerdon & Turnadge*, 2015]. All these effects have implications for groundwater abstractions, fluid injection and the potential subsurface movement of contaminants. Consequently, there is a need to be able to adequately identify groundwater compartmentalisation for environmental risk assessments of fracking operations.

Section 1.5 demonstrated that high-permeability fault and fracture structures are generally considered higher risk basin features than compartmentalisation by low-permeability faults. As a result, compartmentalisation is not necessarily a focus in environmental risk assessments for fracking operations. In this study an approach for identifying groundwater compartmentalisation in prospective shale basins is proposed. Historical data (groundwater quality data and seismic reflection surveys) from the Bowland Basin, where the mid-Carboniferous Bowland Shale is hypothesised to be prospective for shale gas (Figure 4.1) [*Andrews*, 2013], were combined to identify compartmentalisation and consider if current data enable adequate identification across

the basin. Groundwater quality data were analysed using spatial statistics, interpolation, standard groundwater plots and principal component analysis (PCA). These results were then directly related to subsurface basin geology interpreted from seismic reflection data. This study was the first to integrate groundwater quality data with seismic reflection data to specifically identify groundwater compartmentalisation prior to the widespread development of a prospective shale gas basin.
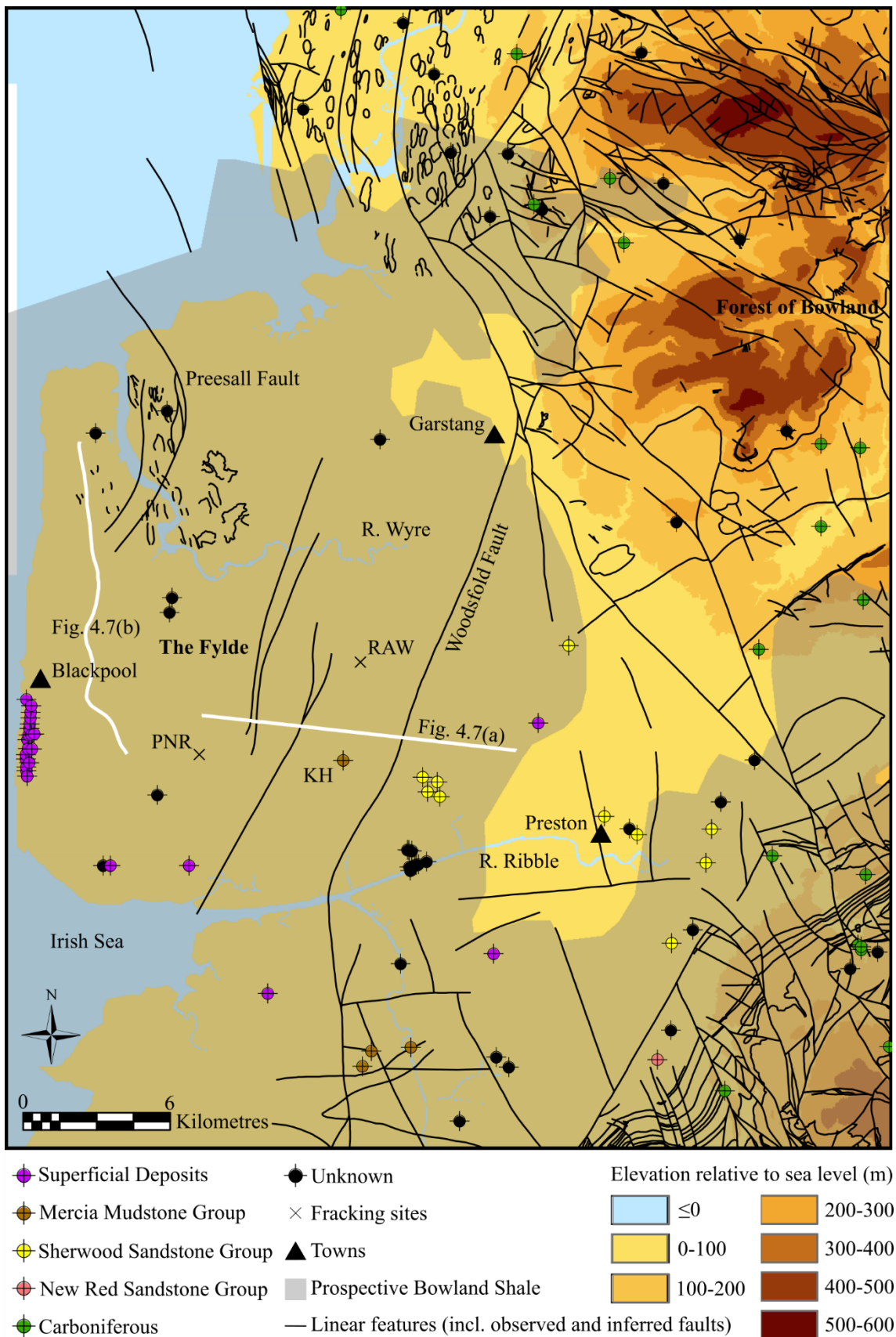
Figure 4.1
Map showing the study region with the locations of sampled groundwater boreholes, the
fracking site Preston New Road (PNR), the previously proposed fracking site Rose Acre

Wood (RAW), the Kirkham Borehole SD43/20 (KH), the 2D seismic lines from Figure 4.7, BGS mapped linear features and the prospective area of the Bowland Shale from Andrews [2013]. Contains OS and BGS data © Crown copyright and database right (2018). A BGS/EDINA supplied service.

4.2 Approach and methodology

The approach taken was to integrate environmental groundwater quality data with subsurface geology, interpreted using 2D seismic reflection data, from the Bowland Basin. The data were collected prior to widespread shale exploitation (only two boreholes targeting shale gas had been fracked in the Bowland Shale at the time of writing) and were unrelated to shale exploration. The data were therefore opportunistic in terms of environmental risk assessment needs. The approach of combining groundwater and seismic reflection data could be used in other prospective basins to identify groundwater compartmentalisation as part of the exploration stage prior to fracking. By adequately identifying groundwater compartmentalisation, operators and regulatory bodies may be better able to assess areas where shallow groundwater resources are more, or less, vulnerable to contamination from the potential upward migration of fracking-related fluids. This approach could lead to improved vulnerability maps and consequently help guide the drilling locations of boreholes from an environmental perspective.

4.2.1 Groundwater quality data

Water quality data for Lancashire and Cumbria, northwest England, were downloaded from the EA's Water Quality Archive [*EA*, 2017] for the years 2000 to 2016, inclusive. Groundwater samples within a rectangular area of interest were extracted (Figure 4.1). This area of interest covered the Fylde where the Bowland Shale is prospective and fracking operations are focussed, for example the Preston New Road and Rose Acre Wood (has since been refused planning permission) sites (Figure 4.1). Only those

groundwater samples collected as part of routine monitoring were considered and no samples noted as coming from pollution incidents or collected as part of specific investigations were included so as not to bias the dataset in favour of specific sites or specific groundwater properties. Entries located offshore or with miscellaneous names and arbitrary grid references were also removed. Fourteen common groundwater properties (herein termed determinands) were extracted: alkalinity to pH 4.5 as $CaCO_3$; barium concentration; calcium concentration; chloride concentration; conductivity at 20°C; conductivity at 25°C (specific conductance); iron concentration; magnesium concentration; manganese concentration; pH; potassium concentration; sodium concentration; strontium concentration; and sulfate concentration as SO_4. These groundwater determinands were sampled across 96 unique locations. To average out irregular timings between groundwater samples and seasonal variations in groundwater chemistry, groundwater determinands at each unique location were mean-averaged for the time period 2000 to 2016, inclusive. This approach was considered appropriate because the size and distribution (both spatially and temporally) of the dataset meant that the variability or effect of individual measurements was limited. Measurement errors are not included in the EA Water Quality Archive. Therefore, within this study and unless otherwise stated, measurement error was assumed to be ± half the smallest division stated in the EA archive.

The Global Moran's I test in ArcMap 10.3 (see Appendix C for a description) was used to investigate if any groundwater determinands were significantly spatially autocorrelated. The influence of data at a sample location was assumed to be inversely related to distance from the location. Distances between sample locations were calculated using the Euclidean distance, with the threshold distance set so that every sample location had at least one neighbouring sample location. Statistical significance was judged at the 95% probability (P-values ≤0.05) of the spatial distribution not being the result of random

chance. This approach further mitigated against temporal variations in the groundwater samples because if differences in sampling date were causing a comparatively high degree of variability between locations then the data would fail the Global Moran's I test at the defined probability. Groundwater determinands showing statistically significant spatial autocorrelation were interpolated using kriging. Prior to kriging the numerical distributions of the groundwater determinands were qualitatively assessed using histograms and normal quantile-quantile (Q-Q) plots. Groundwater determinands that were not normally distributed were log-transformed prior to interpolation and re-examined to test for normality – no further transformations were found necessary. The automated iterative cross validation technique in ArcMap 10.3 was used to maximise the model fits of the semivariograms for each statistically significant groundwater determined. Interpolation without predefined barrier features was chosen to prevent biasing the results by pre-defining compartmentalisation.

An additional Global Moran's I test was run under the same parameters as above to investigate if groundwater total dissolved solids (TDS) were spatially autocorrelated across the Bowland Basin. TDS values were estimated by summing the concentration of the major cations (Na^+, K^+, Ca^{2+}, Mg^{2+}) and anions (Cl^-, SO_4^{2-}, HCO_3^-) at each location. Because the EA data contained only two HCO_3^- measurements across the study area and timespan, HCO_3^- concentrations were approximated using the atomic mass ratio (0.61) of HCO_3 to $CaCO_3$ and the alkalinity to pH 4.5 as $CaCO_3$ measurements. Where one or more cation or anion measurement was missing at a location, the location was ignored for TDS estimation; only 90 of the 96 unique locations had the complete suite of major cation and anion data for TDS estimation. Error in TDS was calculated from the square root of the summed squares of the major cation and anion measurement errors. The cation and anion data were also plotted on Piper and Gibbs plots [*Piper*, 1944; *Gibbs*, 1970], and used to

calculate sodium to chloride ratios (Na:Cl) to further characterise groundwater chemistry. The Piper plot was created using GW_Chart (v.1.29.0.0) [*Winston*, 2000].

Principal component analysis (PCA) (see Appendix C for a description) was performed on 56 unique sample locations where all spatially autocorrelated groundwater determinands were present and TDS could also be estimated. A PCA was chosen because it is a multivariate statistical technique which can be used to reduce large numbers of observations while still maintaining the majority of information. Prior to the PCA, the groundwater determinands were z-transformed to normalise each determinand. This transformation allowed the comparison of determinands with different units, for example conductivity was measured in microsiemens/centimetre (μS/cm) whereas ion concentrations were measured in milligrams/litre (mg/l) or micrograms/litre (μg/l). Principal components (PCs) in the analysis were chosen based on selecting all PCs with an eigenvalue >1 and the first PC with an eigenvalue <1 [*Chatfield & Collins*, 1980]. Principal components with an eigenvalue >1 represent components that explain more of the underlying variation than any of the original variables. The PCA was performed in Minitab (v.18). Interpretation of groundwater end-members, trends and outliers in the PCA results was undertaken using scatter plots of PC values. No end-members, trends or outliers were known or assumed prior to this interpretation.

A limiting factor of the EA Water Quality Archive is that it does not contain the depths or geological formations groundwater samples were taken from. To provide some depth constraint on the groundwater samples, information on the groundwater boreholes across the area of interest was extracted from the BGS Onshore GeoIndex [*BGS*, 2019d]. Sample locations from the EA Water Quality Archive were manually matched with groundwater borehole locations from the BGS Onshore GeoIndex using geographic coordinates and

location names. BGS borehole depth and aquifer designation were taken as proxies for which geological formation EA groundwater samples were taken from.

4.2.2 *Geological and geophysical data*

Geological and geophysical data for the Bowland Basin were collated from the UK Onshore Geophysical Library [*UKOGL*, 2019] to interpret and discuss the groundwater analysis results in terms of subsurface geology. These data included post-stack 2D seismic reflection data and well header, formation top and deviation data from petroleum boreholes. Well header and formation top files were created manually from the collated data before all seismic reflection and well data were imported to Schlumberger's Petrel E&P Software Platform Version 2015.4. Additional spatial data that were imported to Petrel included the UK coastline, bedrock geology and faults interpreted by the BGS. Prior to any interpretation the seismic reflection line GC83-352_RM was tied to the formation tops of Thistleton-1 and Elswick-1 using the interpretation of *Clarke et al.* [2014] as a guide. All other seismic reflection lines were time-shifted where necessary to tie to GC83-352_RM.

Horizons and faults were interpreted in the time domain across the 2D seismic reflection lines covering the study area. The six horizons interpreted were: Top Sherwood Sandstone; Top St. Bees Sandstone; Top Manchester Marl; Top Collyhurst Sandstone; Base Permo-Triassic (an erosional surface); and Top Bowland Shale (Figure 1.11). Interpretation of the seismic reflection data was guided by the formation top data, BGS mapping [*BGS*, 1975; 1989; 1990; 2012] and previously published interpreted seismic lines: GC83-352 [*de Pater & Baisch*, 2011; *Clarke et al.*, 2014]; GC87-372 [*Cuadrilla Resources Ltd. & A. J. Lucas Group*, 2008]; GCE-86-DV37 [*Hough et al.*, 2011]; and the regional lines of *Andrews* [2013] and UKOGL-RG-006 [*UKOGL*, 2012].

4.2.3 Interpreting compartmentalisation

The interpretation of compartmentalisation draws from both the seismic reflection and groundwater quality data. In the seismic reflection data faults may be observable and the interpretation of horizons across the study area will indicate any juxtaposition of geological formations across the faults. Where low-permeability formations lie juxtaposed against high-permeability formations, a barrier (no flow) or baffle (reduced flow) to groundwater flow may be formed. Even when high-permeability formations are juxtaposed the fault core may act as a barrier or baffle due to clay smearing, cataclasis, compaction, and cementation [*Bense et al.*, 2013]. Large contrasts in groundwater quality either side of the fault may then support the barrier or baffle hypothesis. Conversely, exceptions to any regional trends in groundwater quality data or the presence of different groundwater types may indicate the presence of compartmentalisation. Seismic reflection data can then be used to see if there are any geological structures or stratigraphic features that may account for the difference in groundwater.

4.3   Results

4.3.1 Depth control on groundwater sample locations

Of the 96 unique groundwater sampling locations, coordinates and names of 71 boreholes in the EA Water Quality Archive were matched with the BGS Onshore GeoIndex (Table C1); 50 with exact coordinates and names and 21 with similar coordinates and names. It was not possible to match 25 locations with boreholes in the BGS Onshore GeoIndex. The sampling frequency for different geological formations is given in Table 4.1 and the spatial distribution of sampled geological formations can be seen in Figure 4.1. Two of the 71 matched sample locations had the aquifer classification "No Aquifer". One of these locations is the Kirkham Borehole (SD43/20), in which

groundwater in the Mercia Mudstone Group was sampled (Figure 4.1) [*Ove Arup and Partners Ltd.*, 2014c], and the other sample was taken at a depth of 23.6 m, suggesting it was located in superficial deposits. These two samples were re-classified based on this information. The Kirkham Borehole is the deepest borehole in the dataset (depth of 445 m) and therefore all boreholes can be considered to sample shallow groundwater.

Table 4.1
Groundwater borehole frequency of different geological formations in the study area.

Geological formation	Number of boreholes
Superficial Deposits	23
Mercia Mudstone Group	4
Sherwood Sandstone Group	10
New Red Sandstone Group	1
Carboniferous (Limestone, Shale, Coal, Gritstone, Undifferentiated)	17
Unknown	41

4.3.2   Spatial autocorrelation and interpolation

The EA groundwater data used consisted of 4865 samples across 96 unique locations (Table C2). Mean-averaged values of the 14 groundwater determinands at each location are presented in Table C1. Of the 14 groundwater determinands tested for spatial autocorrelation using the Global Moran's I test, alkalinity to pH 4.5 as $CaCO_3$, calcium, specific conductance, magnesium and potassium showed statistically significant spatial autocorrelation (Table 4.2). For the remaining nine determinands it could not be statistically ruled out that their spatial distribution was due to random chance. The five groundwater determinands showing statistically significant spatial autocorrelation were log-transformed prior to interpolation because they were not normally distributed. All five groundwater determinands that showed spatial autocorrelation, generally showed increases from northeast to southwest across the study area, with the concentrations of calcium, magnesium and potassium increasing by factors of 10 to 1000 towards the Fylde coastline (Figure 4.2). An obvious exception to this trend was the Kirkham Borehole,

which showed reduced alkalinity at pH 4.5 as CaCO$_3$ (Figure 4.2a). A comparison of

Table 4.2 with Table C1 confirmed the unusual nature of groundwater in the Kirkham

Borehole; the borehole had the highest values in the dataset for calcium, chloride,

conductivity at 20°C, magnesium, sodium, strontium and sulfate as SO$_4$. Specific

conductance was not measured in the Kirkham Borehole but would be expected to be

elevated because of the elevated ion concentrations.

Table 4.2
Descriptive statistics of groundwater determinands extracted from the EA Water Quality Archive for the area of interest, along with P-value results from the Global Moran's I test.

Groundwater determinand	Number of locations	Units	Assumed measurement error	Minimum value	Maximum value	Mean value	Standard deviation (±1σ)	P-value
Alkalinity to pH 4.5 as CaCO$_3$	96	mg/l	0.5	5.0	1263.1	346.6	237.3	0.000
Barium	46	µg/l	0.5	10.0	2830.0	196.3	415.3	0.195
Calcium	92	mg/l	0.5	1.2	1285.0	176.9	204.9	0.001
Chloride	95	mg/l	0.5	8.4	77000.0	1282.0	7969.7	0.485
Conductivity at 20°C	65	µS/cm	0.5	85.6	251500.0	5379.4	31095.4	0.749
Conductivity at 25°C (Specific conductance)	62	µS/cm	0.5	107.0	22300.0	2331.5	3565.1	0.002
Iron	91	µg/l	0.5	30.0	329871.4	22942.7	49983.0	0.071
Magnesium	92	mg/l	0.5	0.3	502.5	54.5	74.3	0.000
Manganese	91	µg/l	0.5	10.0	12943.3	1242.8	2373.6	0.275
pH	95	pH units	0.5	6.0	9.1	7.3	0.5	0.087
Potassium	91	mg/l	0.5	0.6	104.7	17.5	23.3	0.000
Sodium	91	mg/l	0.5	5.8	51550.0	819.8	5403.0	0.540
Strontium	71	µg/l	0.5	15.6	19050.0	1081.8	2347.8	0.513
Sulfate as SO$_4$	94	mg/l	0.5	1.0	6085.0	202.3	648.2	0.545
TDS*	90	mg/l	1	47	136487	2823	14406	0.477

* Calculated (see Section 4.2.1).
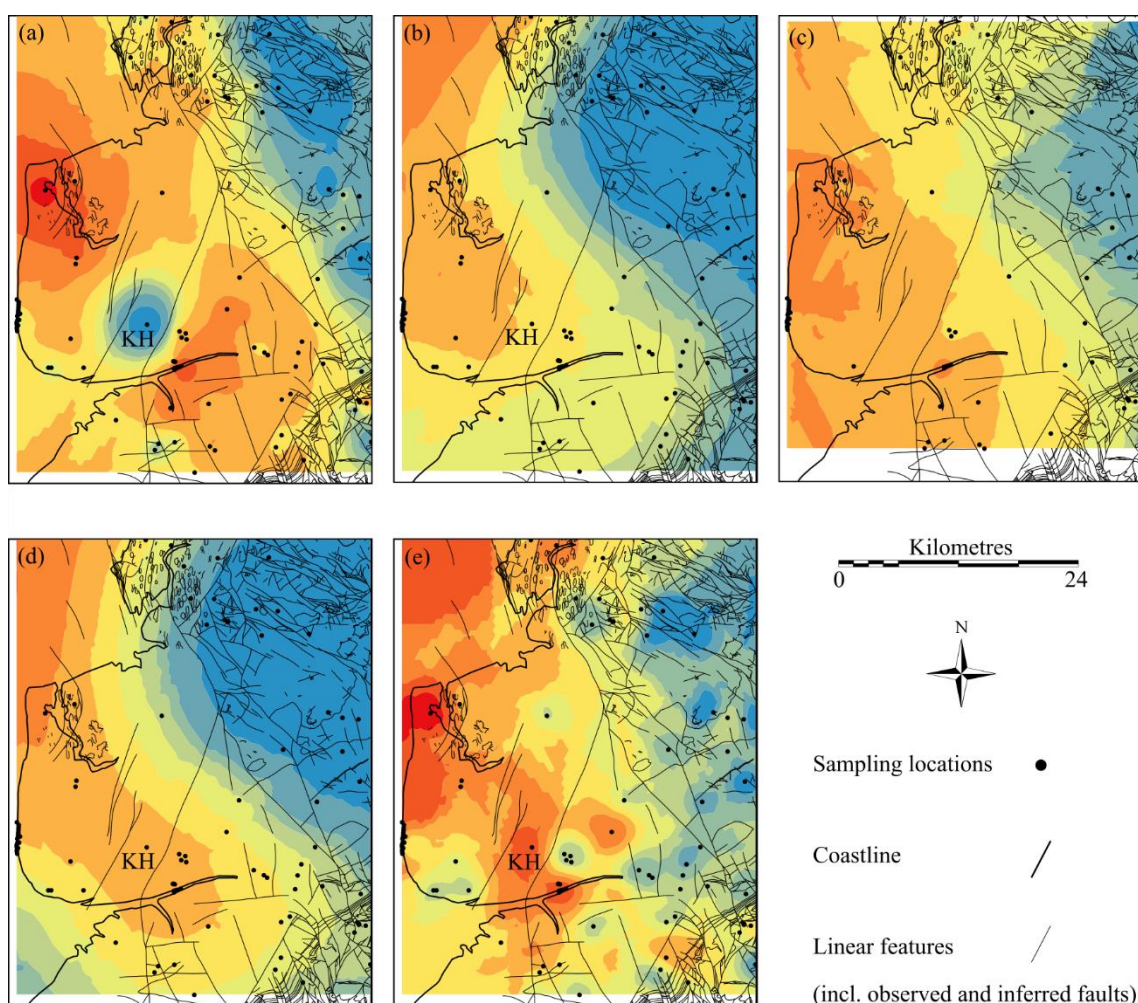
Alkalinity to pH 4.5 as CaCO₃ (mg/l)	Calcium (mg/l)	Conductivity at 25°C (µS/cm)	Magnesium (mg/l)	Potassium (mg/l)
5.0-109.1	1.2-41.4	107.0-438.6	0.3-9.8	0.6-1.6
109.1-176.1	41.4-65.8	438.6-603.4	9.8-14.8	1.6-2.2
176.1-219.3	65.8-80.5	603.4-685.2	14.8-17.4	2.2-3.1
219.3-247.2	80.5-104.9	685.2-850.0	17.4-22.4	3.1-4.8
247.2-290.3	104.9-145.1	850.0-1181.6	22.4-31.9	4.8-7.8
290.3-357.4	145.1-211.3	1181.6-1849.1	31.9-49.8	7.8-12.8
357.4-461-5	211.3-320.4	1849.1-3192.8	49.8-83.8	12.8-21.4
461.5-623.0	320.4-500.2	3192.8-5897.4	83.8-148.4	21.4-36.1
623.0-873.8	500.2-796.5	5897.4-11341.6	148.4-270.7	36.1-61.3
873.8-1263.1	796.5-1285.0	11341.6-22300.0	270.7-502.5	61.3-104.7

Figure 4.2

Interpolated groundwater maps of: (a) alkalinity to pH 4.5 as CaCO₃; (b) calcium concentration; (c) conductivity at 25ºC (specific conductance); (d) magnesium concentration; and (e) potassium concentration in the study area. Also shown are BGS mapped linear features. KH is the Kirkham Borehole SD43/20. Contains BGS © Crown copyright and database right (2018). A BGS/EDINA supplied service.

4.3.3   TDS

Estimated TDS concentrations for the 90 locations ranged over four orders of magnitude; from 47 ±1 mg/l to 136487 ±1 mg/l. A Global Moran's I test on the TDS data could not rule out that the spatial distribution was the result of random chance (Table 4.2). The TDS data were therefore not interpolated. Nevertheless, the TDS data were discretely mapped using a standard TDS classification [*Davis*, 1964] and a drinking water classification of TDS ≤250 mg/l (Table 4.3). The categorisation indicated that drinking type groundwater was related to higher elevations (Figure 4.3). The low lying Fylde had both fresh and brackish groundwater present (Figure 4.3), although one location was classified as saline groundwater (G&G 92 at Clifton Marsh Landfill near the River Ribble mouth) and one location was classified as brine (Kirkham Borehole) (Table C1).

Table 4.3
Groundwater type classification of samples based on total dissolved solids (TDS). Note that drinking type groundwater is also taken into account as part of fresh groundwater.

Groundwater type	TDS (mg/l)	Number of locations	Mean TDS (mg/l)	Standard deviation in TDS (±1σ) (mg/l)
Drinking	TDS ≤ 250	10	116	74
Fresh	TDS ≤ 1000	55	410	212
Brackish	1000 < TDS ≤ 10000	33	2418	1943
Saline	10000 < TDS ≤ 100000	1	15273	-
Brine	100000 < TDS	1	136487	-
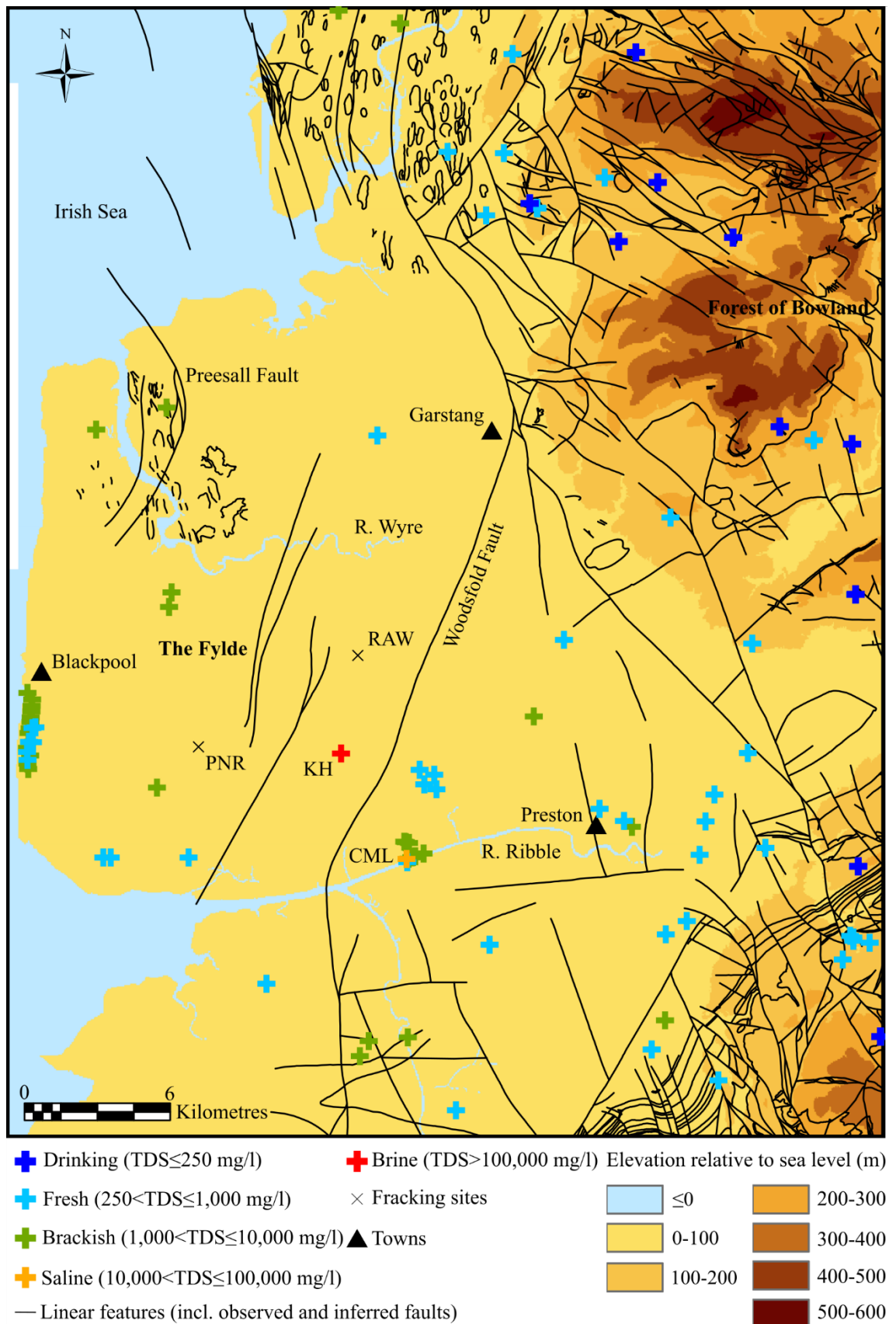
Figure 4.3

Map showing the 90 locations where groundwater TDS was estimated. Also shown are BGS mapped linear features, the fracking site Preston New Road (PNR) and the

previously proposed fracking site Rose Acre Wood (RAW). KH is the Kirkham Borehole SD43/20 and CML is Clifton Marsh Landfill. Contains OS and BGS data © Crown copyright and database right (2018). A BGS/EDINA supplied service.

4.3.4   Piper and Gibbs plots

Figure 4.4a shows a Piper plot for the 90 locations where all major cations and anions were sampled. Groundwater samples from the Sherwood Sandstone Group and Carboniferous were predominantly Ca-HCO$_3$ type and categorised as drinking or fresh groundwater. Such samples likely occur due to calcite cement dissolution (Equation 4.1) [*Abesser et al.*, 2005]. Groundwater samples from the Mercia Mudstone Group classified as mixed-SO$_4$ type or Na-Cl type. These samples were either brackish groundwater or brine, respectively. Groundwater samples from superficial deposits were generally mixed or Na-Cl type, and included both fresh and brackish groundwater types. However, the Na-Cl type groundwater samples were predominantly brackish groundwater samples.

$$CaCO_{3\,(s)} + H_2CO_{3\,(aq)} \leftrightarrow Ca^{2+}{}_{(aq)} + 2HCO_3{}^-{}_{(aq)} \qquad Equation\ 4.1$$
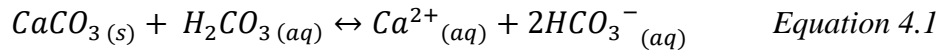
A Gibbs plot of the same 90 locations suggested that groundwater quality across the Bowland Basin is influenced by the three major processes (Figure 4.4b): atmospheric precipitation (precipitation dominance); water-rock interaction (rock dominance); and evaporation-crystallisation (sea water dominance). Drinking groundwater samples from the Carboniferous plotted towards the precipitation trend because meteoric water has had limited time to chemically interact with the local geology. The remaining Carboniferous samples and the Sherwood Sandstone Group samples plotted towards rock dominance, showing increased TDS because of increased chemical interaction time with rocks in the Bowland Basin. Samples from superficial deposits also plotted in the area of rock dominance but also extended out towards sea water dominance, as did samples from the Mercia Mudstone Group.

(a)

● Unknown

● Superficial Deposits

● Carboniferous

● Mercia Mudstone Group

○ Sherwood Sandstone Group

● New Red Sandstone Group

(b)
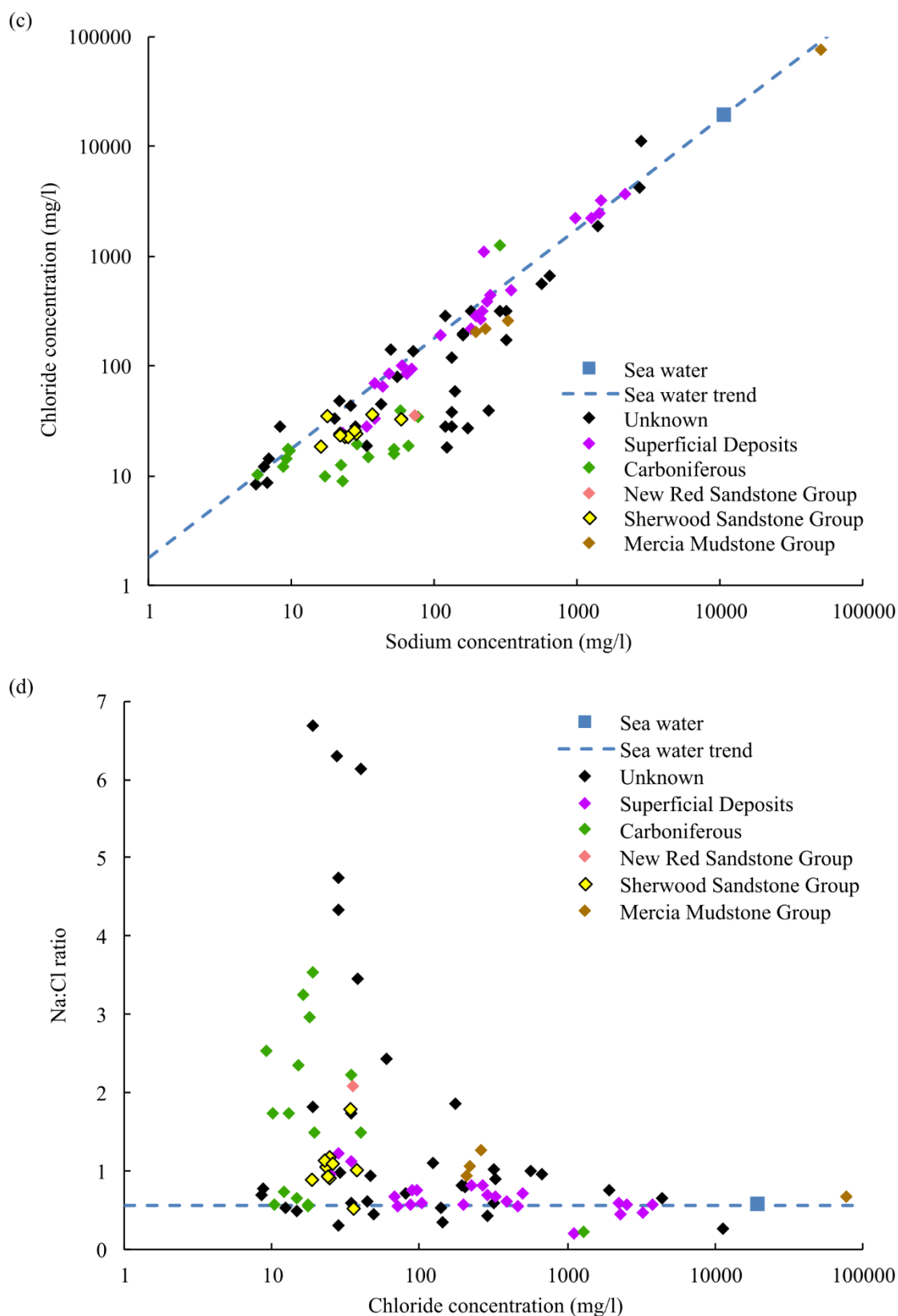
Figure 4.4
(a) Piper plot; (b) Gibbs plot; (c) chloride versus sodium concentration plot; and (d)
Na:Cl ratio versus chloride concentration plot of 90 locations where major cations and
anions were measured. A sea water chloride concentration of 19300 mg/l and a Na:Cl
ratio of 0.5567 are shown for reference [Riley & Tongudai, 1967; Edmunds, 1996].

108

4.3.5 Sodium and chloride data

Sodium and chloride concentrations and their ratios from the 90 locations with measurements were compared to a modern day sea water composition in Figure 4.4c and d. The brine sample from the Mercia Mudstone Group in the Kirkham Borehole was the only sample in the dataset more concentrated than sea water. This sample lay along the sea water trend, as did the majority of other samples. A separate trend consisting of Carboniferous and Unknown samples were enriched in sodium with respect to chloride. These samples generally had chloride concentrations from 10 to 100 mg/l, TDS from 250 to 1000 mg/l (fresh groundwater) and Na:Cl ratios up to ~12 times that of sea water. These samples may be enriched in sodium as a result of ion exchange processes (Equation 4.2) or albite weathering to kaolinite (Equation 4.3) [*Abesser et al.*, 2005]:

$$Ca^{2+}{}_{(aq)} + 2Na \cdots X_{(s)} \leftrightarrow Ca \cdots X_{(s)} + 2Na^{+}{}_{(aq)} \qquad \textit{Equation 4.2}$$
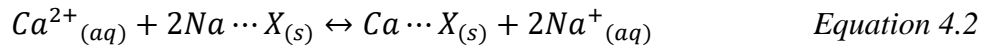
where *X* is a mineral.

Equation 4.3

$$2NaAlSi_3O_{8\,(s)} + 2H^{+}{}_{(aq)} + 9H_2O_{(l)} \leftrightarrow Al_2Si_5O_5(OH)_{4\,(s)} + 2Na^{+}{}_{(aq)} + 4H_4SiO_{4\,(aq)}$$
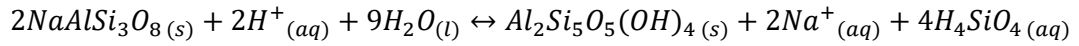
4.3.6 PCA

The PCA reduced the five spatially autocorrelated groundwater determinands to three PCs based on their eigenvalues. These three PCs explained 93.1% of the variance in the data (Table 4.4). The first two PCs (PC1 and PC2) accounted for 79.0% of the variance (Table 4.4), but it was considered appropriate to include PC3 because the eigenvalue of PC2 was approximately one. All determinands had positive loadings in PC1 (Table 4.4), indicating PC1 was a general concentration component and facilitated normalisation of the data for concentration variations. Potassium and magnesium had the highest loadings on PC1 and calcium had the lowest loading. Loading on PC2 was dominated by calcium

(Table 4.4). Alkalinity to pH 4.5 as $CaCO_3$ was strongly negatively loaded in PC2 whereas potassium showed a much weaker negative loading. In PC3, alkalinity to pH 4.5 as $CaCO_3$ and calcium had strong negative loadings whereas specific conductance had a strong positive loading (Table 4.4).

Table 4.4
Results of principal component analysis for the groundwater determinands which showed statistically significant spatial autocorrelation.

Groundwater determinand	Principal Components				
	PC1	PC2	PC3	PC4	PC5
Alkalinity to pH 4.5 as $CaCO_3$	0.362	-0.506	-0.686	0.269	-0.263
Calcium	0.209	0.842	-0.479	0.126	0.047
Conductivity at 25°C (specific conductance)	0.482	0.069	0.509	0.706	-0.073
Magnesium	0.535	0.100	0.201	-0.579	-0.572
Potassium	0.553	-0.144	-0.007	-0.279	0.772
Eigenvalue	2.9542	0.9940	0.7070	0.2509	0.0939
Proportion (%)	59.1	19.9	14.1	5.0	1.9
Cumulative (%)	59.1	79.0	93.1	98.1	100.0

Further interpretation of the PCA results was achieved through plots of PC2 versus PC1, PC3 versus PC2, and PC3 versus PC1 (Figure 4.5) – with data coloured by their TDS values. For PC2 versus PC1 three end-members (EMs), two trends, and a possible outlier group of samples were identified (Figure 4.5a). EM-A was groundwater with low TDS (i.e. drinking type groundwater) and formed the consistent EM for trends to EM-B and EM-C. The trends to EM-B and EM-C showed increasing PC1, signifying increasing elemental concentrations, alkalinity to pH 4.5 as $CaCO_3$ and specific conductance. This increase was also evident from the TDS colour coding, with a progression from drinking, to fresh, to brackish groundwater along the trends to EM-B and EM-C from EM-A. The trend to EM-B showed increasing PC2 with increasing PC1. Increasing PC2 was correlated with increasing calcium and decreasing alkalinity to pH 4.5 as $CaCO_3$. The

trend to EM-C had decreasing PC2 with increasing PC1. The samples between the trends to EM-B and EM-C may represent mixing between the two trends plus outliers.

The interpretation of PC2 versus PC1 was supported by plots of PC3 versus PC2 and PC3 versus PC1. These plots also showed the trends to EM-B and EM-C and more clearly distinguished outliers (Figure 4.5b and c). Trends to EM-B and EM-C showed decreasing PC3 with increasing or decreasing PC2, respectively. Decreasing PC3 was correlated with increasing calcium and alkalinity to pH 4.5 as $CaCO_3$, but decreasing specific conductance. However, the decreasing specific conductance was not a real effect and was probably the result of skewing by some of the outliers, which had high TDS and specific conductance. The proportions of EM-A, EM-B and EM-C in the 43 sample locations in the mixed zone between the EMs defined in Figure 4.5b was calculated using line equations and Pythagoras. Sample locations in the east of the study area were generally at higher elevations and were dominated by EM-A (Figure 4.6); of the 15 sample locations >100 m elevation above sea level, all but one had ≥64% EM-A. EM-A was jointly located at the New Drop Inn Borehole and Saddleside Springs. EM-A also dominated 21 of the 28 locations at elevations <100 m. Two locations, both located in Blackpool, were dominated by EM-B (Figure 4.6). EM-B was located at Blackpool Promenade No.9 Borehole. EM-C was located at Jameson Road Landfill Site in the northwest of the Fylde. Three other samples in the study area were also dominated by EM-C (Figure 4.6).

(a)

(b)

Drinking (TDS≤250 mg/l) Fresh (250<TDS≤1000 mg/l)
Brackish (1000<TDS≤10000 mg/l) Saline (10000<TDS≤100000 mg/l)

(c)

Drinking (TDS≤250 mg/l)   Fresh (250<TDS≤1000 mg/l)
Brackish (1000<TDS≤10000 mg/l)   Saline (10000<TDS≤100000 mg/l)
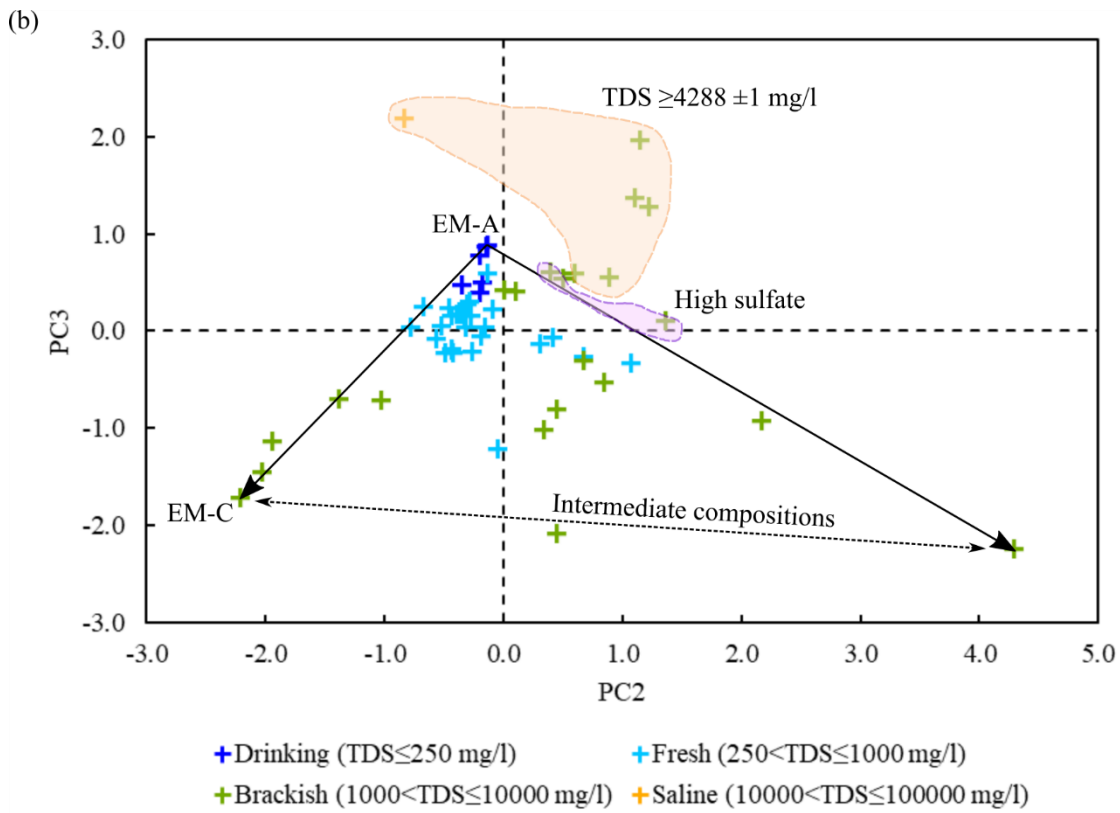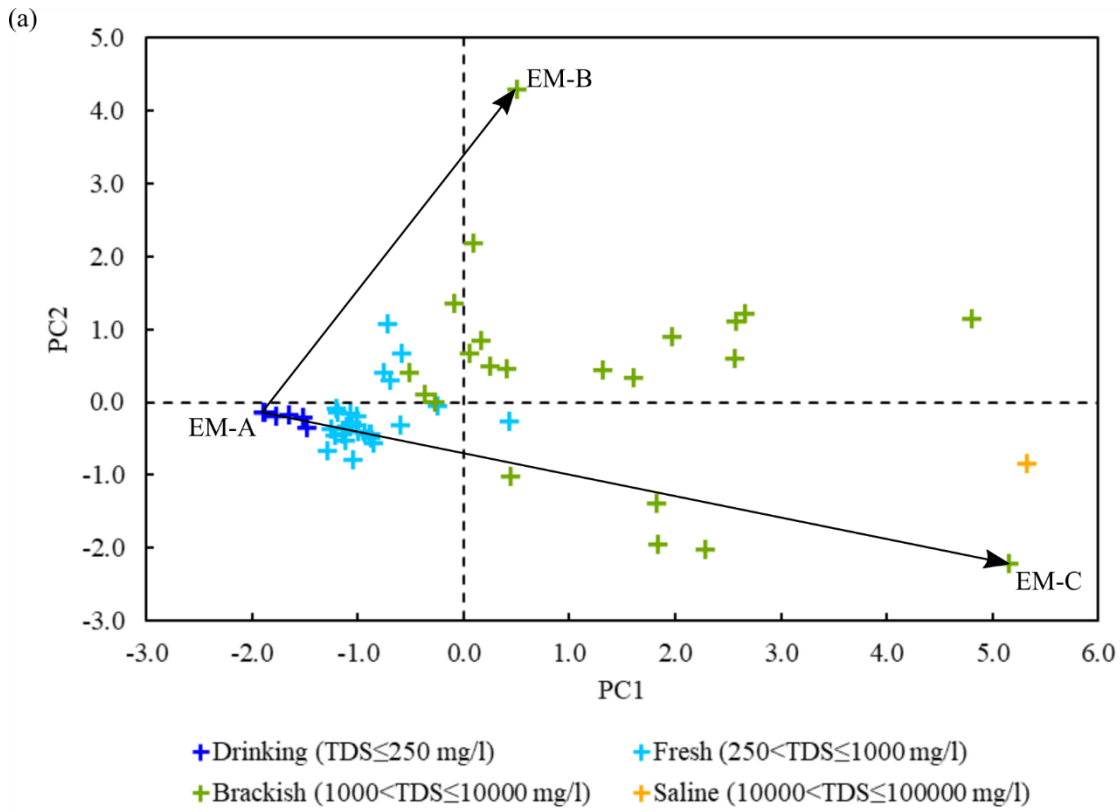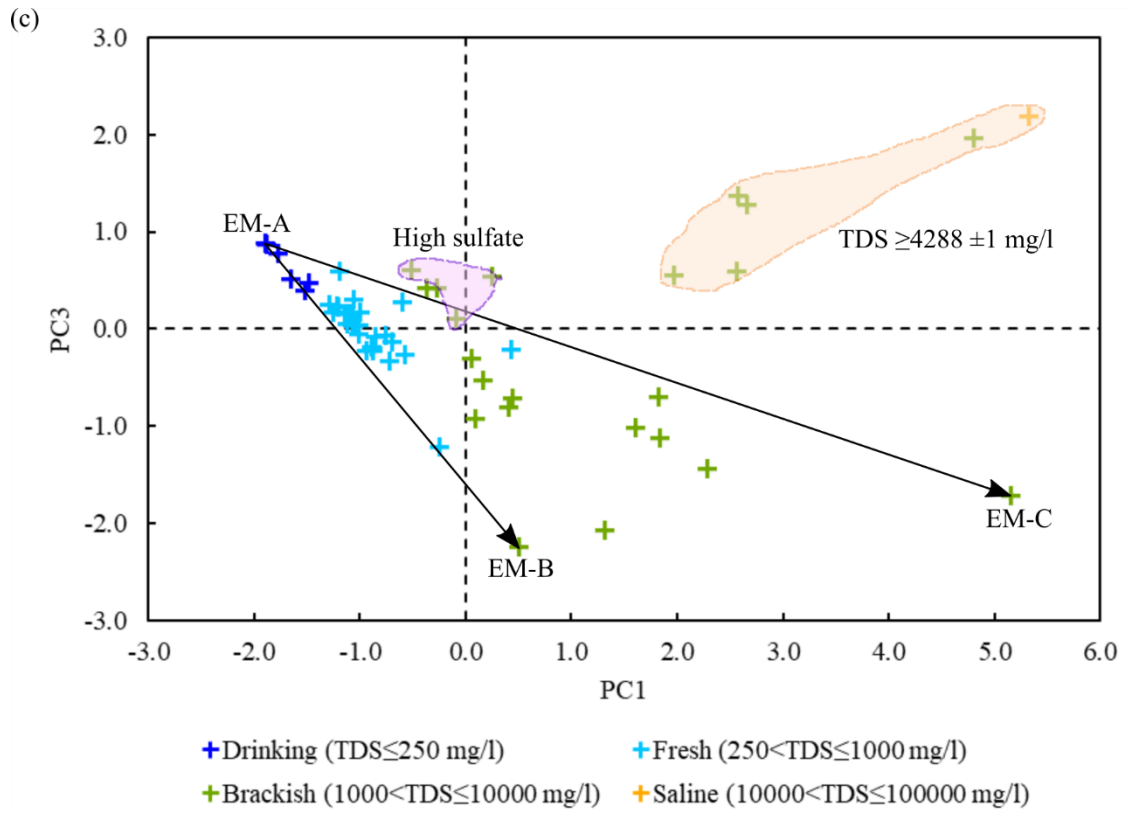
Figure 4.5
Principal components plots of: (a) PC2 versus PC1; (b) PC3 versus PC2; and (c) PC3 versus PC1 of 56 locations. Interpreted end-members (EM), trends (arrows) and outliers (shaded areas) are labelled. The minimum TDS concentration for the outlier samples with high TDS was 4288 mg/l.
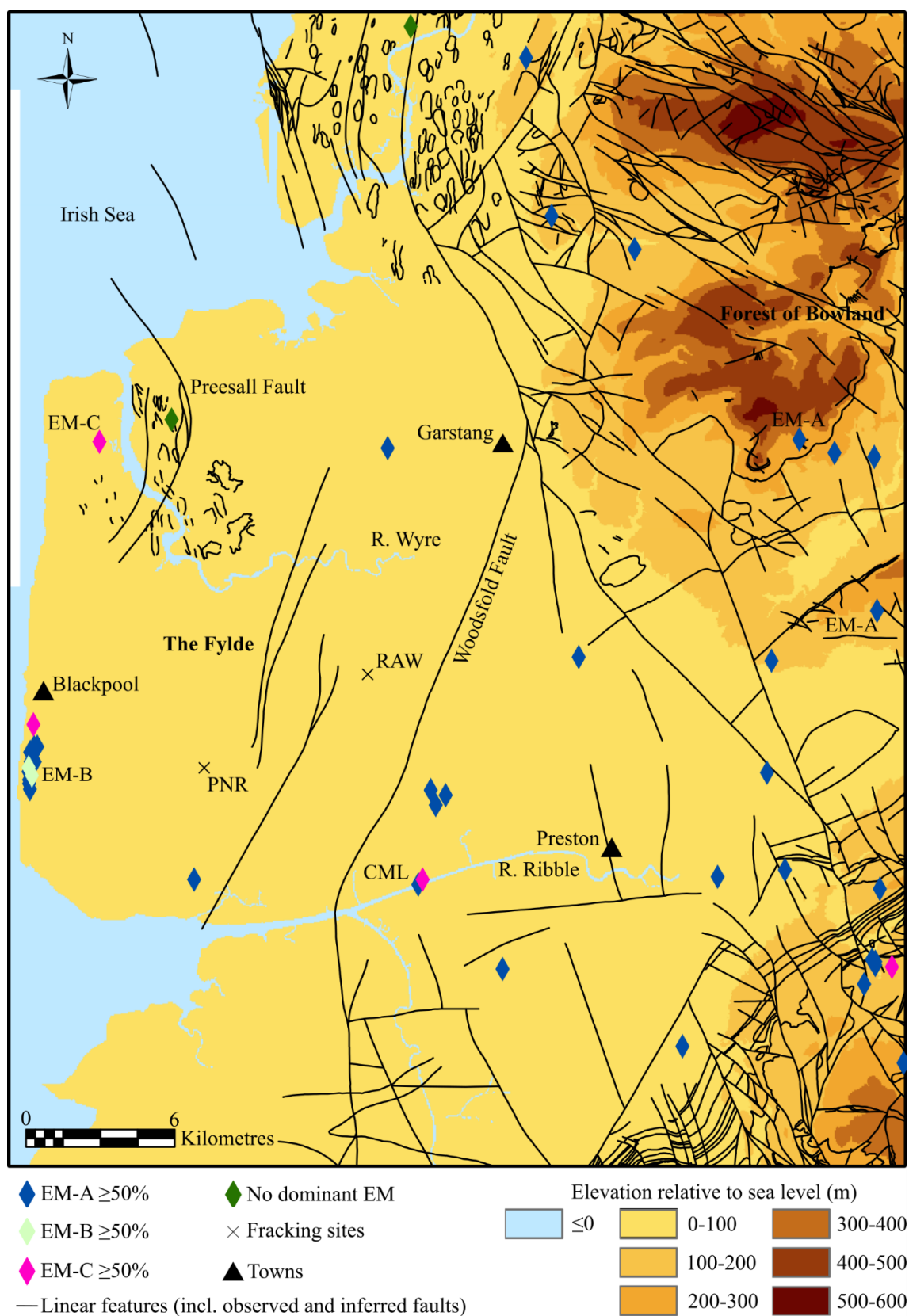
Figure 4.6
Map showing the locations of the three end-member (EM) groundwater types and their dominance (taken as ≥50%) at 40 other locations. Also shown are BGS mapped linear features. CML is Clifton Marsh Landfill. Contains OS and BGS data © Crown copyright and database right (2018). A BGS/EDINA supplied service.

A comparison of the relative chemical compositions of EM-A, EM-B and EM-C showed that although EM-A had relatively similar proportions of major cations and anions (Table 4.5), EM-B was dominated by calcium (57% compared to 13% in EM-A and 3% in EM-C) and EM-C was dominated by chloride (39%) and sodium (29%).

Table 4.5
Relative concentration proportions (to nearest whole number) of groundwater determinands for EM-A, EM-B and EM-C.

Groundwater determinand	EM-A (%)	EM-B (%)	EM-C (%)
HCO$_3$*	18	8	16
Calcium	13	57	3
Chloride	27	16	39
Iron	0	0	1
Magnesium	3	2	5
Manganese	0	0	0
Potassium	2	1	2
Sodium	17	11	29
Sulfate as SO$_4$	20	5	5

* Calculated (see Section 4.2.1).

The identified outlier sample locations were sorted into two groups (Figure 4.5b). The first group (six sample locations) had high TDS ($\geq$4288 $\pm$ 1 mg/l compared to the next highest sample location in the PCA of 2460 $\pm$ 1 mg/l) and their composition most closely resembled EM-C, i.e. enriched in chloride (49 to 73%) and sodium (18 to 29%). Five samples were located in superficial deposits in Blackpool and one of unknown geological formation at Clifton Marsh Landfill. The second group of outliers were distinguished from the first group by their high sulfate composition; 47 to 53% compared to 4 to 8%. All three outliers in the second group occurred in the Mercia Mudstone Group in an area south of the River Ribble (Figure 4.1).

4.4 Discussion

4.4.1 Evidence for groundwater compartmentalisation

4.4.1.1 Structural compartmentalisation

Regular groundwater monitoring in the Bowland Basin is focussed in the eastern Fylde on the principal aquifer for the region; the Sherwood Sandstone [*Mott MacDonald*, 1997; 2010]. Abstractions from the Sherwood Sandstone are located where it directly underlies superficial deposits. In the southern Fylde this occurs to the east of the Woodsfold fault, where groundwater is fresh or marginally brackish. To the west of the Woodsfold fault the Sherwood Sandstone is confined by the overlying Mercia Mudstone Group. The Kirkham Borehole is the only borehole in the dataset that is known to sample groundwater deeper than the superficial deposits west of the Woodsfold fault in the southern Fylde (Figure 4.1). The Kirkham Borehole is 445 m deep and penetrates the Sherwood Sandstone at a depth of 367 m [*BGS*, 2018b]. Groundwater samples from the Kirkham Borehole were taken in the Mercia Mudstone Group 240 to 260 m below the surface [*Ove Arup and Partners Ltd.*, 2014c] and indicated Na-Cl type brine (Table C1). Na-Cl type brine was also recently observed in the underlying Sherwood Sandstone at the Rose Acre Wood site ~4.1 km to the north [*BGS*, 2018a]. These brines contrast with the fresh and brackish groundwater east of the Woodsfold fault, providing strong evidence that the Woodsfold fault compartmentalises groundwater in this area of the Bowland Basin (Figure 4.7a and 4.8). Further support for this hypothesis comes from groundwater level data either side of the fault, which decreases from 5 to 10 m above Ordnance Datum (OD) east of the fault to 16.8 m below OD west of the fault [*Ove Arup and Partners Ltd.*, 2014a; 2014c]. The compartmentalisation of the Sherwood Sandstone by the Woodsfold fault in this area of the basin may be the result of the large vertical offset across the fault, which is observable on seismic reflection data (Figure 4.7a). The vertical displacement

juxtaposes the Sherwood Sandstone against the lower-permeability St. Bees Sandstone (Figure 4.7a). The movement associated with this displacement may also have formed low-permeability granulation seams, crush textures and fault smears [*Bense et al.*, 2013]. Further north where aquifer abstractions take place, the Woodsfold fault passes through the Sherwood Sandstone with less vertical displacement, meaning the Sherwood Sandstone is probably in greater hydraulic continuity across the fault and groundwater is not compartmentalised (Figure 4.8).

Another possible example of structural compartmentalisation comes from the PCA. Graphical interpretation of the PCA results suggested two groundwater trends linked by a common groundwater EM (EM-A) (Figure 4.5b). EM-B and EM-C are both located on the Fylde coastline, but are ~13.6 km apart and show distinct chemical compositions. EM-B was calcium dominated whereas EM-C was sodium and chloride dominated. The distinct compositions suggest limited groundwater mixing between the two areas, implying a baffle or barrier may be present. Interpretation of the north-south trending seismic line GC-87-382_OM, which runs approximately from EM-C to EM-B, indicates the Preesall fault offsets the Sherwood Sandstone (Figure 4.7b). This fault may be acting as a baffle or barrier between the River Wyre and Blackpool areas, thereby compartmentalising the northwest area of the Bowland Basin (Figure 4.8). However, it cannot be ruled out that the groundwater composition difference may result from stratigraphic compartmentalisation; EM-B is located in superficial deposits and EM-C is of unknown depth (Figure 4.1).

Previous studies in northwest England have identified structural compartmentalisation in the Carboniferous Millstone Grit [*Abesser et al.*, 2005] and the contact with the Sherwood Sandstone in the northern and central Fylde is considered a baffle [*Mott MacDonald*, 1997]. Furthermore, the influence of faults on groundwater flow

in the Sherwood Sandstone has been identified to the east of Preston, where north-south trending horst and graben fault structures are hypothesised as the reason for discrepancies between the original Fylde aquifer model simulations and observed groundwater levels [*Seymour et al.*, 2006]. Inclusion of the north-south trending faults as baffles by a reduction in the east-west horizontal hydraulic conductivity led to improvements in matches between model simulations and groundwater observations [*Seymour et al.*, 2006]. In addition, the most recent Fylde aquifer model contained faults in the Sherwood Sandstone with hydraulic conductivities that varied over six orders of magnitude [*Mott MacDonald*, 2010]. The range in assigned hydraulic conductivity values implies that faults are considered to have varying influence on groundwater flow in the principal aquifer for the Bowland Basin.
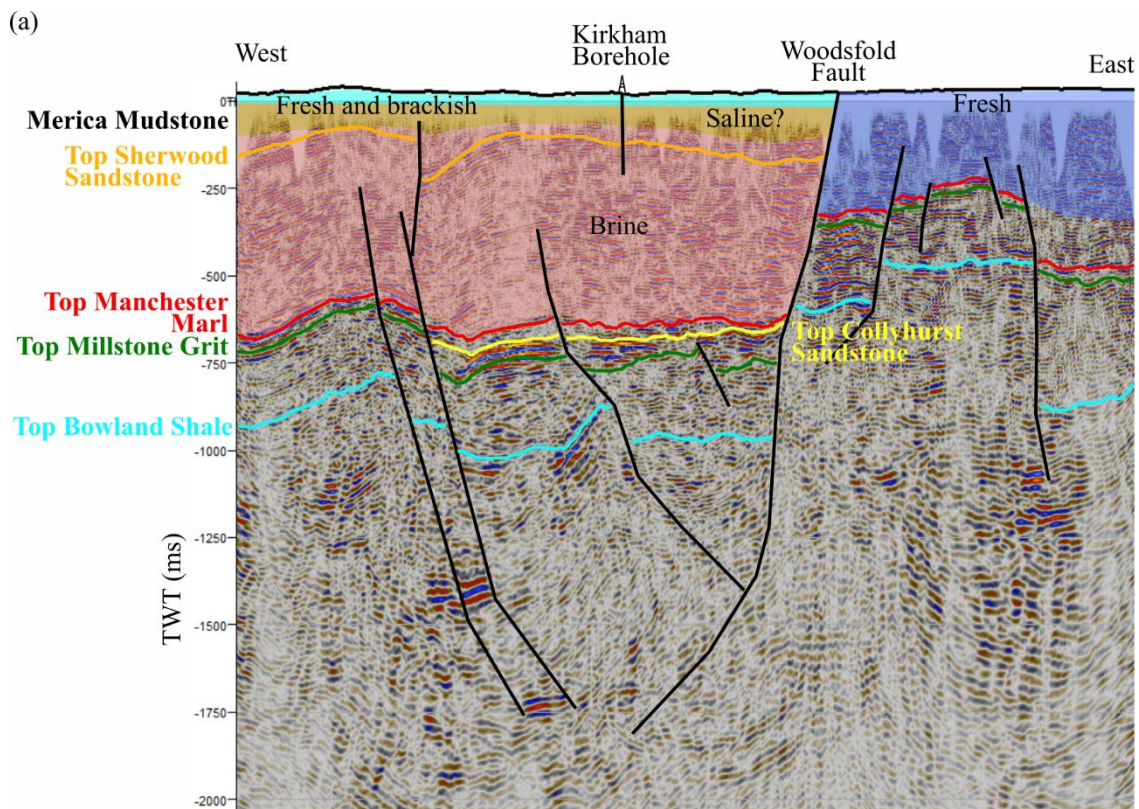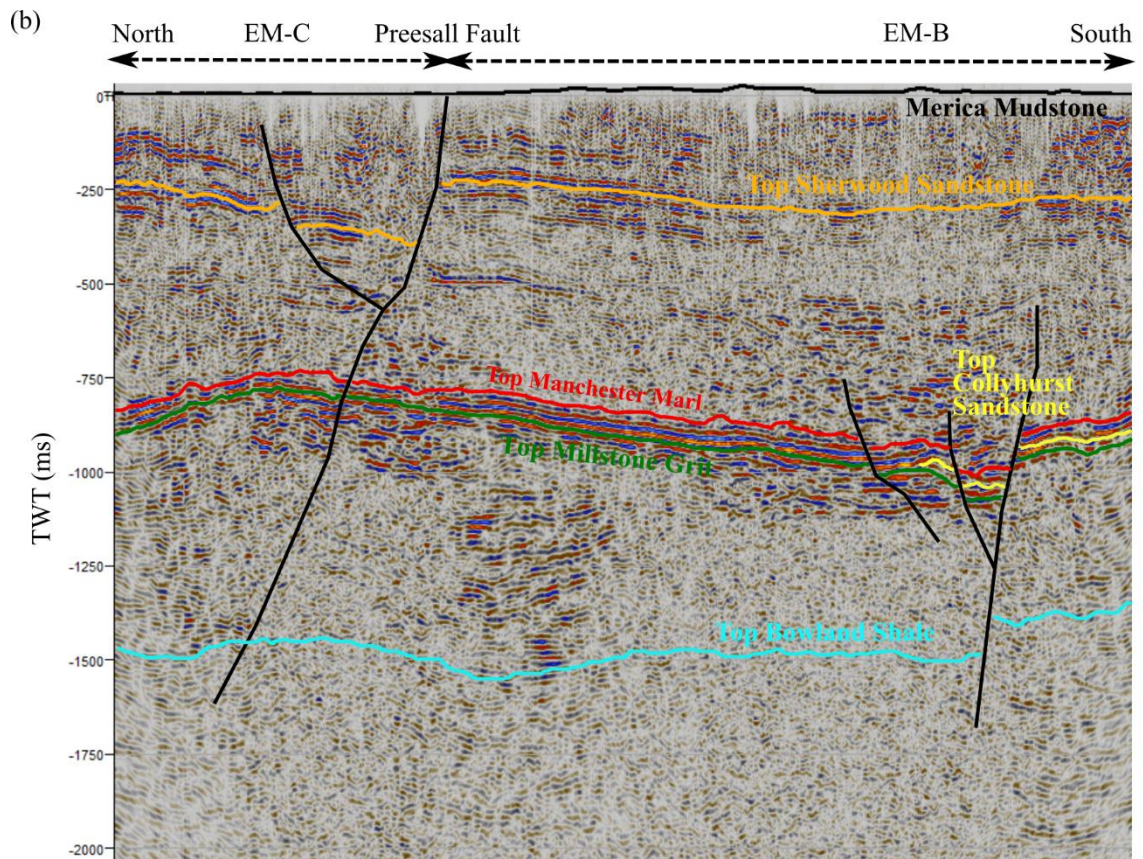
Figure 4.7
Interpreted 2D seismic reflection lines which provide evidence for fault-related groundwater compartmentalisation: (a) the east–west line GC82-342_RM and; (b) the north–south line GC87-382_OM. Line locations are shown by labelled white lines in Figure 4.1.

4.4.1.2 Stratigraphic compartmentalisation

Stratigraphic compartmentalisation by low-permeability beds has been identified in the Carboniferous Millstone Grit in northwest England [*Abesser et al.*, 2005]. However, evidence from this study for stratigraphic compartmentalisation in the Bowland Basin comes solely from the groundwater quality data of the superficial deposits. Eighteen sample locations within several hundred metres of each other in Blackpool showed a mix of fresh and brackish groundwater with various relative ion concentrations and proportions of EM groundwater types. All 18 locations sampled groundwater in

119

superficial deposits (Figure 4.1) at approximately the same depth (9.3 to 17.3 m) (Table C1), and therefore the differences are unlikely to be due to groundwater salinity increasing with sampling depth. Instead it is hypothesised that the different groundwater types occur from compartmentalisation of the superficial deposits by the variety of deposit types (tidal flats, blown sand, peat, till, alluvium and glaciofluvial deposits) which can be found across the near-surface of the Fylde near Blackpool [*BGS*, 1975; 2012].

4.4.2   Conceptual hydrogeological model for the Bowland Basin

In this section a conceptual model for groundwater flow in the Bowland Basin is proposed, focussing on the Sherwood Sandstone (Figure 4.8). This model includes the western Fylde and thus expands on the EA's numerical Fylde aquifer model which only covers the eastern Fylde [*Mott MacDonald*, 1997; 2010].

The Sherwood Sandstone aquifer is recharged from precipitation by two mechanisms. In the southern Fylde near Preston groundwater in the Sherwood Sandstone is considered to be recharged by precipitation on the higher elevation (>100 m) Carboniferous formations in the Forest of Bowland and from vertical leakage through superficial deposits (Figure 4.8). The groundwater flow from the Forest of Bowland to the Fylde is topographically driven by the ~500 m difference in elevation. In the northern and central Fylde, groundwater flow between the Carboniferous and Sherwood Sandstone is thought to be minor or absent. Instead the major recharge is considered to be vertical leakage through the overlying superficial deposits where clay-rich glacial till is absent [*Mott MacDonald*, 1997]. This mechanism also probably accounts for the freshwater recharge of superficial deposits across the western Fylde. Low TDS values (≤250 mg/l) across the Forest of Bowland (Figure 4.3) imply that groundwater has had limited chemical interaction time with rocks, although ion exchange processes and albite weathering

(Equations 4.2 and 4.3) may be responsible for the high Na-Cl ratios found in many of the Carboniferous groundwater samples [*Abesser et al.*, 2005]. Stable isotopes of δ^2H and δ^{18}O from the Millstone Grit in Lancashire indicate that groundwater is younger than 10000 years old [*Abesser et al.*, 2005]. Likewise, isotope data from fresh groundwater in the coastal plain of the Sellafield region, ~70 km northwest of the Fylde, indicate that groundwater is younger than ~11700 years old [*Bath et al.*, 2006]. Groundwater flow through the Sherwood Sandstone aquifer is hypothesised to be directed towards the Wyre and Ribble estuaries (Figure 4.8) [*Mott MacDonald*, 2010], with horst and graben fault structures reducing east-west horizontal hydraulic conductivity of the aquifer near Preston [*Seymour et al.*, 2006].

In the northern Fylde the Woodsfold fault is not considered to form a barrier to groundwater flow in the Sherwood Sandstone aquifer because of the smaller fault throw compared to further south, and thus the continuity of the Sherwood Sandstone across the fault (Figure 4.8). However, it could be argued that the fault is a flow barrier but groundwater quality either side of the fault is similar due to separate circulation cells through the same aquifer formation. Water level and pumping data would provide more insight into the effects of the Woodsfold fault on groundwater flow in the northern Fylde. Further south, near Kirkham and Rose Acre Wood, the Woodsfold fault is considered to form a barrier to east-west groundwater flow based on the presence of Na-Cl type brine west of the fault (Figure 4.8). The mean concentrations of sodium (51500 ± 4000 (1σ) mg/l) and chloride (77000 ± 19800 (1σ) mg/l) in the Kirkham Borehole are substantially higher than sea water (sodium ~15400 mg/l and chloride ~19300 mg/l), requiring concentration by the dissolution of halite or evaporation of sea water [*Hanor*, 1994]. Although parts of the Mercia Mudstone Group may have formed on near-coastal plains and sabkhas [*Wilson*, 1990], the continental depositional setting of the Sherwood Sandstone Group and Mercia Mudstone Group suggests that the sodium

and chloride concentrations are more likely the result of post-burial halite dissolution. However, whereas the Mercia Mudstone Group has been solution mined for halite in the northwest of the Fylde [*Wilson & Evans*, 1990], the lack of halite in the Kirkham Borehole at the sample depths of 240 to 260 m [*BGS*, 2018b] suggests that the brine was not formed by *in situ* dissolution. Alternatively, it is hypothesised that halite dissolution of the Mercia Mudstone Group in the offshore East Irish Sea Basin has created brine which has migrated updip to the coastline. This process has been proposed to account for two million year old brine in the Sellafield region, which was supported by the meteoric isotope composition and the 200000 mg/l sodium chloride equivalent salinity found in the South Morecambe gas field [*Bath et al.*, 1996; 2006]. Closer to the Fylde the offshore Hamilton and Lennox fields, with Sherwood Sandstone Group reservoirs, contain formation waters with sodium chloride equivalent salinities of 300000 and 280000 mg/l, respectively [*Yaliz & Chapman*, 2003; *Yaliz & Taylor*, 2003]. Because brines are persistent in basins [*Ferguson et al.*, 2018], a driving force is required to explain brine migration to the Fylde. The most likely driving force is compaction from basin loading [*Rowe et al.*, 1993; *Black & Brightman*, 1996]. Interpretation of the onshore 2D seismic reflection data indicates that the Sherwood Sandstone continues updip north-eastwards until it lies directly below the superficial deposits and becomes part of the principal aquifer. Assuming the sample location west of Garstang is fresh groundwater in the Sherwood Sandstone (Figure 4.3), the TDS concentrations imply a lateral gradient of ~5 to 17 mg/l/m within the Sherwood Sandstone from 41341 ± 1 to 153280 ± 1 mg/l at Rose Acre Wood [*BGS*, 2018a] to 377 ± 1 mg/l near Garstang (Figure 4.8).

The saline sample at Clifton Marsh Landfill on the River Ribble estuary, EM-C at Jameson Road Landfill in the northwest Fylde, and a number of samples from Blackpool were also Na-Cl type groundwater, but with sodium and chloride concentrations less than sea water. The Clifton Marsh Landfill site has no Mercia Mudstone Group present and

lies east of the compartmentalising Woodsfold fault (Figure 4.8), suggesting that the sodium and chloride concentrations are not the result of *in situ* halite dissolution or brine mixing. Alternatively, it is hypothesised that enrichment occurs either due to landfill leachate [*Baedeker & Back*, 1979; *Hackley et al.*, 1996], or from present day sea water intrusion mixing with the terrestrial groundwater system. The driving force for this possible sea water intrusion could be groundwater abstraction from the Sherwood Sandstone by British Nuclear Fuels Limited, located ~3 km north of Clifton Marsh Landfill (Figure 4.8). In the northwest Fylde no abstractions are known to occur west of the River Wyre at EM-C, although groundwater pumping has occurred ~3 km to the east at the Preesall Salt Field [*Wilson & Evans*, 1990]. The sodium and chloride concentrations found in EM-C could also be the result of landfill leachate, saline intrusion (from sea water or Na-Cl type groundwater) driven by the nearby pumping, or *in situ* halite dissolution (Figure 4.8). Groundwater connection between west of the River Wyre and Blackpool, where the calcium dominated EM-B is located, may be restricted by the Preesall fault and/or stratigraphic changes (Figure 4.8). Samples from Blackpool show a range of TDS values, EM proportions and relative major ion concentrations, indicating stratigraphic compartmentalisation in the superficial deposits. Five samples had TDS values ≥4288 ±1 mg/l and were enriched in sodium and chloride. The source of sodium and chloride is unknown, but could be related to anthropogenic inputs from Blackpool, halite dissolution in the underlying Mercia Mudstone Group, or sea water intrusion, although no groundwater abstractions are known in this area to drive this process.
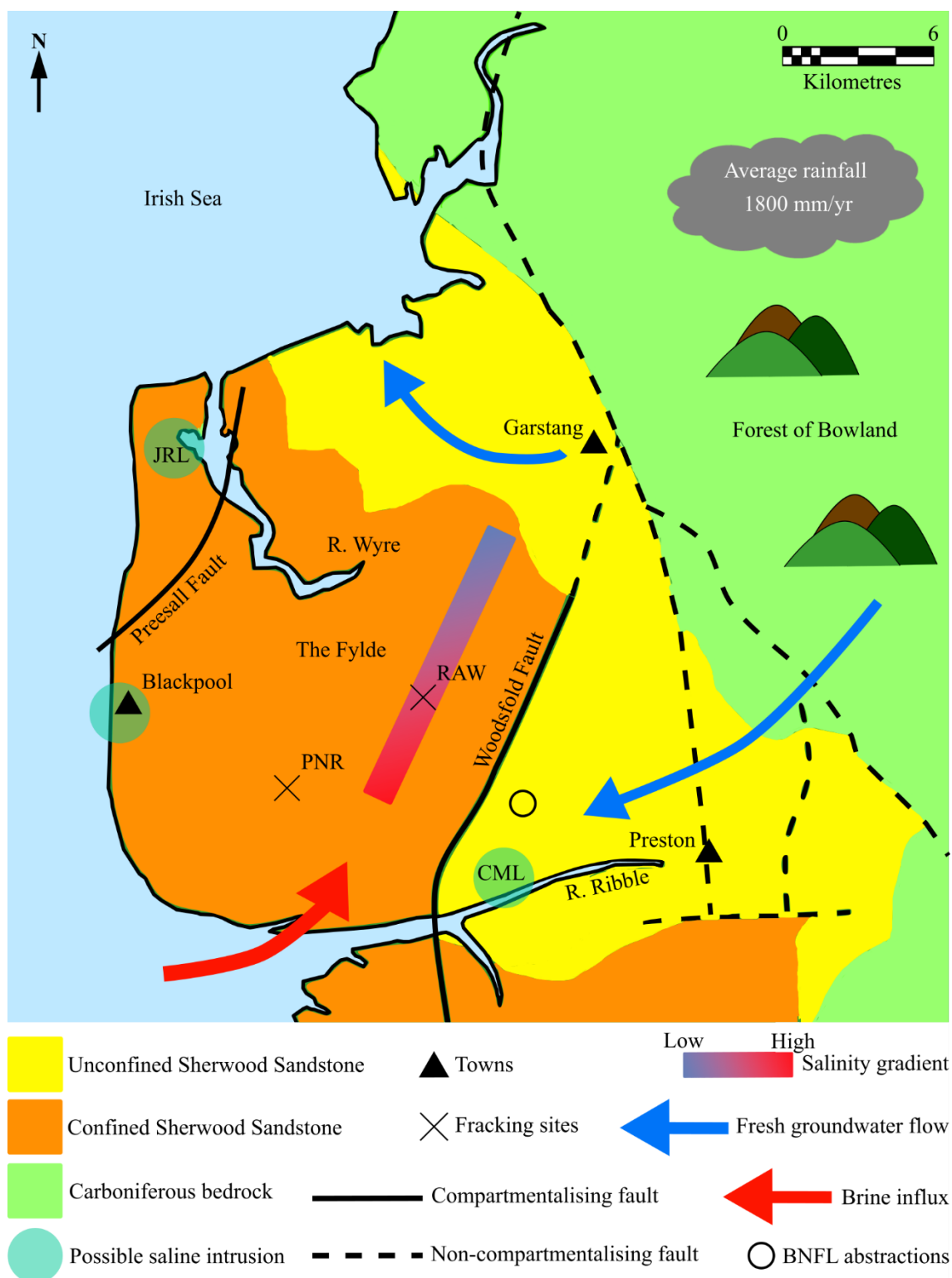
Figure 4.8
Conceptual hydrogeological model for the Bowland Basin, including the locations of Preston New Road (PNR), Rose Acre Wood (RAW), Jameson Road Landfill (JRL), Clifton Marsh Landfill (CML) and groundwater abstractions by British Nuclear Fuels Limited (BNFL). The use of confined and unconfined is with respect to the presence and absence of the Mercia Mudstone Group, respectively.

4.4.3 Study limitations

Identifying groundwater compartmentalisation across an area with no monitoring programme dedicated to its detection is dependent on the availability and quality of historical data. From the map figures in this study it can be seen that groundwater across large areas of the Bowland Basin is not sampled. Prediction of groundwater determinands away from sampled locations required extensive interpolation in some areas, which increases uncertainty in the overall groundwater system interpretation. Importantly, the lack of groundwater data in some parts of the study area also means the influence of known faults or stratigraphic changes on groundwater are unknown in these areas.

Secondly, the EA Water Quality Archive does not contain any information on the depth or aquifer that groundwater samples were taken from. To provide some depth control EA sampling locations were matched with boreholes from the BGS Onshore GeoIndex where possible. Despite matching 71 of the 96 locations, 41 of the sample locations had unknown sampling depths. Consequently, a large proportion of the groundwater samples could not be tied to specific geological formations, which in turn made it difficult to distinguish the cause of changes in groundwater quality. For example, a lateral change from fresh to brackish groundwater could be the result of structural compartmentalisation by a fault, stratigraphic compartmentalisation by a change in geological formation, or simply that the brackish sample was taken at greater depth in the same formation (assuming salinity increases with depth). Furthermore, the current groundwater monitoring is relatively shallow (the deepest borehole being 445 m) compared to shale exploration depths (~2000 m), so little is known about deep groundwater in the Bowland Basin. It may be possible to use wireline logs, pressure tests, and geochemical data from petroleum boreholes to interpret the deeper groundwater

system, for example using resistivity logs to estimate salinity. However, these data were not available for this study.

Previous studies on groundwater compartmentalisation have made use of groundwater level data [*Mohamed & Worden*, 2006]. In the Bowland Basin regular measurements of groundwater levels takes place for the Sherwood Sandstone in the eastern Fylde [*BGS*, 2019d] and these data have been used extensively for calibrating aquifer models [*Mott MacDonald*, 1997; 2010]. Regular groundwater level monitoring is rare or non-existent in the western Fylde, but some historic water levels can be obtained through the BGS Borehole record viewer. The compilation and analysis of these data is beyond the timeframe for this study. However, future work could look to compliment the current study of historic groundwater quality data with these historic groundwater level data.

The extent and quality of the seismic reflection data also limited the analysis of compartmentalisation. The 2D seismic reflection lines in the Bowland Basin generally trend north-south and east-west but the grid coverage is highly non-uniform due to surface restrictions and survey purposes. The lines also vary in acquisition age (1979 to 1999), acoustic source types (explosive charges and Vibroseis) and processing workflows. Consequently, the quality, resolution and depths of the lines vary, complicating the interpretation of horizons and faults across lines. Furthermore, petroleum boreholes across the Bowland Basin are relatively sparse, limiting the number of well ties that can be made to constrain geological interpretations.

4.4.4   *Implications for fracking*

Identifying groundwater compartmentalisation is important for determining the potential migration routes and receptors of fracking-related fluids because it can create

groundwater flow directions different to regional trends [*Hortle et al.*, 2009; *Smerdon &*
Turnadge, 2015]. Where basins and groundwater flow extend across multiple
jurisdictions, the influence of compartmentalisation on migration routes could be
important because each jurisdiction may have different groundwater management
legislation [*Smerdon & Turnadge*, 2015]. Compartmentalisation is also important
because it can discourage lateral groundwater flow and encourage upward flow in the
presence of a vertical head gradient [*Wilson et al.*, 2017b]. A compartmentalised basin
may therefore create compartments with higher vulnerabilities to contamination because
regional lateral groundwater flow cannot dilute any contaminating fluids trapped within
those compartments. This effect is hypothesised to be greatest when faults strike
perpendicular to the regional flow direction, thereby creating areas of reduced or no flow
[*Smerdon & Turnadge*, 2015]. Conversely, isolated compartments could prevent the
regional movement of contaminants; contaminants would be restricted to the
compartment they originate from, thereby protecting surrounding aquifers in
neighbouring compartments [*Mohamed & Worden*, 2006].

For the Bowland Basin a number of possible examples of compartmentalisation were
identified. Consequently, some areas within the basin may be more, or less, vulnerable to
contamination from the potential upward migration of fracking-related fluids.
Identification of compartmentalisation is not currently required under environmental
regulations for fracking in England but, because it is an important hydraulic effect, it
should be considered in environmental risk assessments for the long-term migration of
fracking-related fluids. The current data available for analysis are too spatially limited to
adequately assess compartmentalisation across the Bowland Basin and, in particular, the
influence of known faults on groundwater flow. This study therefore highlights that to
adequately identify groundwater compartmentalisation in a prospective shale basin,
historical groundwater data may need to be supplemented with a dedicated basin-wide

groundwater sampling programme. Furthermore, historical seismic reflection data may need to be complemented by dedicated seismic lines or 3D surveys to image areas of poor coverage or quality.

4.5   Conclusions

Groundwater compartmentalisation is an important hydrogeological factor to consider in the long-term migration of fracking-related fluids and can be both an advantage and disadvantage; compartmentalisation can create compartments of high vulnerability but may also prevent the regional spread of contaminants. Compartmentalisation can be caused by structural or stratigraphic changes and can be identified by integrating groundwater quality data with subsurface geological data. In the prospective Bowland Basin examples of compartmentalisation were identified using 2D seismic reflection data combined with historic groundwater quality data. However, many areas and faults in the Bowland Basin remain untested by historical groundwater sampling. Seismic reflection data are also two dimensional across much of the basin and vary in quality due to processing techniques and acquisition ages and methods. Therefore, the adequate identification of compartmentalisation in prospective shale basins may require supplementing historical data with dedicated basin-wide groundwater sampling programmes and the acquisition of new seismic data in areas of poor coverage or quality.

5 Compartmentalisation and groundwater-surface water interactions in a prospective shale gas basin: Assessment using variance analysis and multivariate statistics on water quality data

5.1 Introduction

Chapter 4 aimed to identify compartmentalisation by combining groundwater quality and 2D seismic reflection data. However, historical groundwater data can be too sparse and the drilling of new groundwater monitoring boreholes can be expensive and time-consuming. For example, when monitoring for groundwater contamination at Pavillion, Wyoming, USA, the expense of drilling boreholes was the main limiting factor in the number of monitoring boreholes installed by the Environmental Protection Agency [*DiGiulio et al.,* 2011]. Conversely, surface waters are generally more accessible and may therefore provide an alternative cost-effective and higher spatial resolution method for identifying compartmentalisation. Furthermore, in addition to groundwater, surface waters form essential resources in some nations, for example surface waters provide on average ~30% of public water supply in England [*BGS*, 2019e]. Identifying groundwater-surface water interactions, and thereby hydraulic pathways, in prospective basins is also important because contamination of either water body could result from surface activities,

for example spills and water discharge [*Gross et al.*, 2013; *Olmstead et al., 2013*], or from the subsurface migration of fracking-related fluids.

The slow development of shale gas resources in England, compared to that in the USA, has provided the opportunity to undertake environmental baselines assessments of surface waters and groundwater [e.g. *Ward et al.*, 2018]. In addition, the EA has undertaken national routine water quality monitoring since its creation in 1996. These historic data, along with data from predecessor organisations, can also be used for determining baseline conditions and identifying groundwater-surface water interactions. For example, the influence of underlying bedrock geology on surface water quality, and therefore groundwater interaction in specific river catchments [*Oguchi et al.,* 2000; *Jarvie et al.,* 2002; *Neal et al.*, 2011] or geographic regions [*Thornton & Dise*, 1998; *Rothwell et al.*, 2010a; 2010b]. Mechanisms which can link surface water quality to underlying bedrock geology include: *in situ* weathering of a bedrock channel bed; weathering of channel-based superficial deposits, which could include underlying bedrock-derived material or material brought down from upstream lithologies; or baseflow (groundwater discharge), either directly from a bedrock channel bed or indirectly through hydraulic pathways through any superficial deposits.

Statistical analyses of groundwater and surface water quality data are often employed to infer interaction (similarities indicating interaction and vice versa) [e.g. *Guggenmos et al.,* 2011]. However, links to underlying geology are not always included and, when included, geological information is not always included as an objective parameter. Likewise, groundwater-surface water interactions can be interpreted and quantified using the baseflow index method, but the inclusion of geological parameters is also subjective because it requires an initial "expert judgement" [*Bloomfield et al.*, 2009]. Additionally, the baseflow index method requires hydrograph data. In the UK, hydrograph data are

generally only available on major rivers and tributaries, and are therefore not usually available in the same spatial density as water quality monitoring datasets.

This study included geological bedrock formations in the statistical analyses of surface water and groundwater quality data from the Bowland Basin to test whether groundwater-surface water interactions and compartmentalisation could be identified in surface waters as a means of assessing the vulnerability of water resources to contamination from shale gas operations. To date, no study has demonstrated if compartmentalisation increases the risk to surface waters with respect to contamination from below or whether compartmentalisation can be identified from surface water quality data alone.

5.2   Approach and methodology

5.2.1   Surface water sampling

Surface water samples were collected in two fieldwork campaigns during the 2018 UK summer, which was one of the hottest and driest summers on record in the UK [*NOAA*, 2019a; 2019b]. The Wyre and Ribble rivers, and their major tributaries, generally have a baseflow index of ~0.3 [*NRFA*, 2020], but during the 2018 summer surface waters were consistently at base flow conditions with therefore an increased chance of identifying any bedrock groundwater signatures in the surface water quality data. Sampling locations were planned in advance and were located on publicly accessible land with nearby road access (Figure 5.1). Sampling locations included both surface waters running over multiple bedrock formations and those originating and running across a single formation. The first campaign (20th to 23rd July 2018) collected samples from 128 locations in the River Wyre catchment and surrounding area. Unfiltered water samples (25.0 ml) were acidified in the field (1.0 ml of ~30% nitric acid) to fix metal ions prior to laboratory analysis. Water temperature, electrical conductivity, pH and redox potential were

131

measured in the field using electrode methods. Samples were refrigerated on the same day as returning from the field. A further 111 locations, including five locations common to the first campaign, were sampled from 10th to 14th September 2018 in the River Ribble and Hodder catchments. In total 239 surface water samples were collected from 234 unique locations (Figure 5.1).

5.2.2   *Temperature correction for electrical conductivity*

To compare electrical conductivity between sampling locations it was necessary to normalise field conductivity measurements to a standard temperature. In line with environmental water quality monitoring undertaken by the EA, field conductivity was normalised to 25°C (specific conductance) using the linear equation of *Sorensen and Glass* [1987]:

$$EC_{25} = \frac{EC_t}{1 + a(t - 25)} \qquad Equation\ 5.1$$

where EC_t is electrical conductivity measured in the field at temperature t (°C), EC_{25} is electrical conductivity at 25°C, and a is a temperature compensation factor. A standard value of $a = 0.02$ was used [*Matthess*, 1982; *Hem*, 1985].
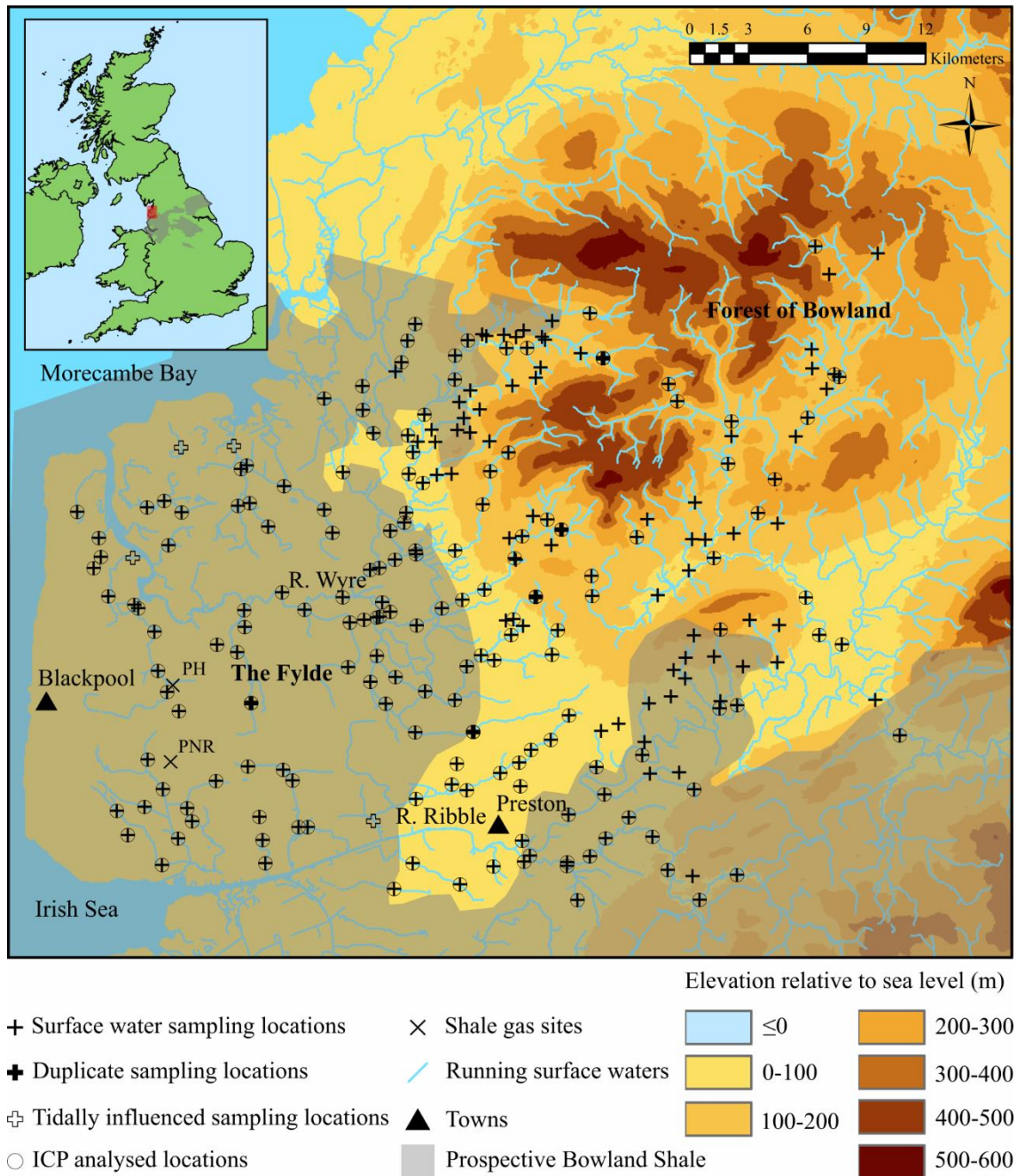
Figure 5.1
Map of the study region (red box on inset map) showing surface water sampling locations and the shale gas fracking sites of Preese Hall (PH) and Preston New Road (PNR). Prospective area of the Bowland Shale from Andrews [2013]. Contains OS data © Crown copyright and database right (2018).

5.2.3   Tidally-influenced locations

Due to the low-lying nature of the Fylde and proximity to the Irish Sea, some sampling locations were tidally influenced. Surface water samples from these locations could be

some mixture of sea and fresh water, depending on the tidal direction and river discharge. This study focussed on sources of fresh water and so samples considered to be dominated or strongly influenced by sea water were removed from the dataset (Figure 5.1). Locations to be removed were identified by abnormally elevated electrical conductivity measurements, and in some cases elevated pH and reduced redox potential compared to non-tidal water samples.

5.2.4 Duplicate sampling locations

To combine the datasets from the two fieldwork campaigns, five locations sampled during the second campaign were common to both campaigns (Figure 5.1). The five duplicate locations were chosen to cover the geographical extent and varying elevation of the study region. The two sets of results for specific conductance, pH and redox potential from these five locations were compared using one-way analysis of variance (ANOVA). The one factor considered ("Campaign") had two levels ("First" or "Second" campaign) and the ANOVA was run with and without elevation as a covariate ("Elevation"). Sample location elevations were extracted from Ordnance Survey (OS) Terrain 50 data [*OS*, 2019] using ArcMap 10.3. Statistical significance was judged at the 95% probability of the factor not having zero effect. Prior to the ANOVA, measurements were tested for normality using the Anderson-Darling test [*Anderson & Darling*, 1952] and were transformed if necessary.

5.2.5 Ion concentration analysis

Of the 239 surface water samples, 170 non-tidal samples were analysed for ion concentrations using Inductively Coupled Plasma-Optical Emission Spectrometry (ICP-OES). Samples were analysed using Thermo Scientific iCAP 6000 Series ICP-AES.

134

Calibration standards were made following serial dilution of Romil (Cambridge) 1000 mg/l reference solutions. All samples, blanks and standards had a 1.0 mg/l Yttrium (Y) spike used as an internal standard to correct for any minor ionisation or other matrix effects during the analysis. The 170 samples included all sampling locations overlying the Mercia Mudstone Group (40 samples) and Sherwood Sandstone Group (69 samples), as well as 29 samples overlying the Millstone Grit, two samples overlying the Lower Coal Measures and 30 samples overlying the Bowland High and Craven Groups (Figure 5.2). Ions measured were: calcium (Ca); iron (Fe); potassium (K); magnesium (Mg); manganese (Mn); sodium (Na); and sulfur (S). Concentrations were corrected for the dilution due to acidification. Sulfur concentrations were used to estimate sulfate (SO_4) concentrations under the assumption that all S was present as SO_4.

5.2.6   *Factorial survey design*

The study was designed to answer two questions using ANOVA: does bedrock geology influence surface water quality and can groundwater compartmentalisation affect surface water quality data?

To assess the former question three ANOVAs were run. Firstly, a one-way ANOVA was run on the surface water field measurements and ion concentrations (collectively referred to as "determinands"), with and without elevation included as a covariate ("Elevation"). Underlying bedrock geology at sampling locations, determined using British Geological Survey (BGS) 1:625000 Bedrock Geology data (Figure 5.2), was included as the one factor ("Geology") with five levels: Mercia Mudstone Group; Sherwood Sandstone Group; Lower Coal Measures; Millstone Grit; and Bowland High and Craven Groups. The second ANOVA was run on the same determinands but from mean-averaged (at each borehole location) groundwater quality data compiled in Chapter 4. The groundwater data consisted of 21 samples with specific conductance and

31 samples with pH and ion concentrations. Redox potential data were not available. The inferred aquifer sampled (Section 4.3.1) was included as the one factor ("Aquifer") with four levels: Mercia Mudstone Group; Sherwood Sandstone Group; Coal Measures; and Millstone Grit-Bowland High and Craven Group (MG-BHCG). The Millstone Grit and Bowland High and Craven Group samples were combined in one level (MG-BHCG) because the groundwater data did not allow distinction between the two. Groundwater samples from coal measures were classed as Coal Measures because no distinction was possible between the Upper, Middle or Lower Coal Measures. The third ANOVA combined both the surface water and groundwater quality data. The two factors considered were "Water body" and "Geology". The Water body factor had two levels: Surface water and Groundwater. The Geology factor had four levels: Mercia Mudstone Group; Sherwood Sandstone Group; Coal Measures; and MG-BHCG.

To assess the potential effect of groundwater compartmentalisation on surface water quality data a three-way ANOVA was conducted on the samples overlying the Mercia Mudstone and Sherwood Sandstone Groups. In Chapter 4 the Woodsfold fault (Figure 5.2) was interpreted to compartmentalise the central and southern Fylde but not the north. This contrast meant it was possible to test whether compartmentalisation could impact surface water quality. The ANOVA considered three factors, each with two levels: "Catchment" (Wyre or Ribble, i.e. north or south in the basin, respectively); "Fault" (East or West of the Woodsfold fault); and "Geology" (Mercia Mudstone or Sherwood Sandstone Group). It was necessary to investigate interactions between all three factors because the contact between the Mercia Mudstone and Sherwood Sandstone Groups in the central and southern Fylde is the Woodsfold fault. The test of our question was whether there was a significant interaction between the Catchment and Fault factors, i.e. was there a significant difference between east and west of the fault in the south and

central Fylde compared to the north of the Fylde? If yes, then it could not be ruled out that compartmentalisation was affecting surface water quality.
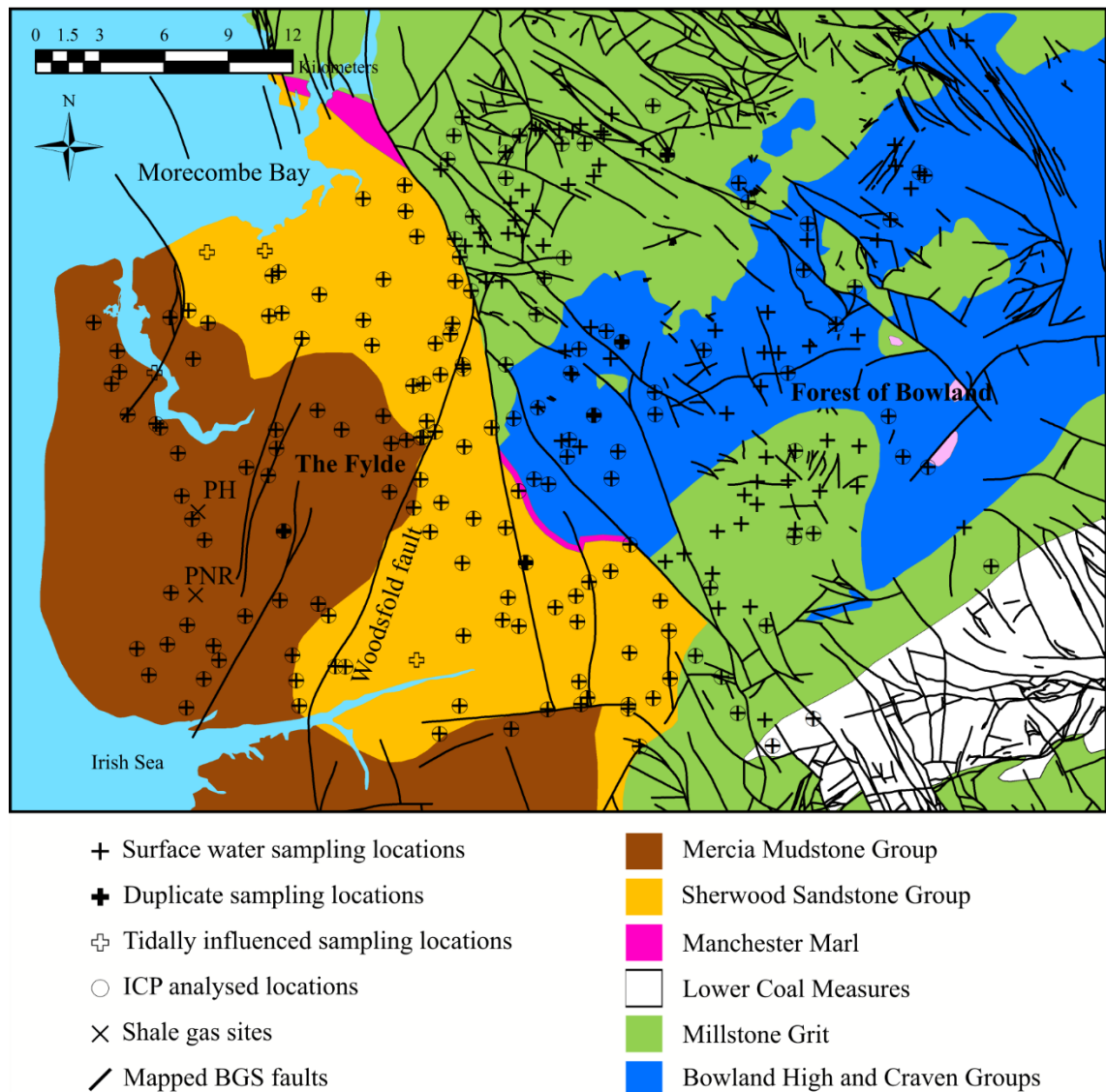
Figure 5.2
Map of the study region showing surface water sampling locations with respect to underlying bedrock geology and faults mapped by the BGS. PH and PNR are the shale gas fracking sites of Preese Hall and Preston New Road, respectively. Contains BGS data © Crown copyright and database right (2019). A BGS/EDINA supplied service.

Prior to any ANOVA, data were tested for normality using the Anderson-Darling test [*Anderson & Darling*, 1952] and transformed if necessary. Statistical significance was judged at the 95% probability of the factor or interaction not having zero effect. Results are presented as least squares means (otherwise known as marginal means). The

proportion of the variance explained by significant factors, interactions and covariates was calculated using the generalised ω^2 method [*Olejnik & Algina*, 2003]. Where factors had more than two levels, *post hoc* Tukey tests were carried out to assess where significance lay within factors.

Power analysis was also performed *post hoc* to estimate what effect size could have been detected given the sampling design used to investigate the impact of compartmentalisation, i.e. the effective detection limit for differences between bedrock formations and across the Woodsfold fault. Power analysis was performed using G*Power 3.1 software [*Faul et al.*, 2007] - *a priori* the acceptable power was set at 0.95 (a false negative probability $\beta = 0.05$). The G*Power software measures effect size (*f*) using the measured value of ω^2 as derived above from the method of *Olejnik and Algina* [2003]:

$$f = \sqrt{\frac{\omega^2}{1 - \omega^2}} \qquad\qquad Equation\ 5.2$$

5.2.7   *Principal component analysis*

Principal component analysis (PCA) is a multivariate statistical technique used to reduce large numbers of observations while still maintaining the majority of information. In Chapter 4 PCA was used to analyse groundwater quality data from the Bowland Basin. In this study PCA was firstly used to identify surface water quality trends and end-members. *A priori* measurements for specific conductance, Ca, Fe, K, Mg, Mn, Na and SO_4 were normalised using z-transformation to allow for comparison of determinands with different units. Principal components (PCs) were chosen based on eigenvalues >1, which represent components that explain more of the underlying variation than any of the original variables [*Chatfield & Collins*, 1980]. Scatter plots of PC values for each location were used to interpret trends and end-members. No trends or end-members were assumed

prior to this interpretation. A second PCA was carried out on the surface water data combined with the groundwater data used in Chapter 4. The aim of this PCA was to investigate how groundwater trends and end-members identified in Chapter 4 related to those identified for surface waters. A total of 57 groundwater locations with measurements for specific conductance and concentrations for Ca, Fe, K, Mg, Mn, Na and SO_4 were extracted from the dataset of Chapter 4.

5.3   Results

Four surface water samples were identified as being dominated or strongly influenced by sea water. These samples were removed prior to further analysis, leaving a total of 235 surface water samples from 231 unique sampling locations. All field measurements (235 samples) and ion concentrations (170 samples) are provided in Tables D1 and D2, respectively, in Appendix D.

5.3.1   Duplicate sampling locations

For field measurements at the duplicate sampling locations (Table D3), the Anderson-Darling test indicated no transformations were required prior to the ANOVA. The ANOVA showed that differences in specific conductance, pH and redox potential between the fieldwork campaigns were not significant (Table 5.1). Elevation was not a significant covariate for pH and redox potential but was significant for specific conductance, however the Campaign factor remained insignificant. The inclusion of a covariate increases the sensitivity of the analysis with respect to the difference between the campaigns, further assuring that the two campaigns could be directly compared. Given these results the data from the two campaigns were combined for further analysis without any corrections required.

Table 5.1
ANOVA results for duplicate sampling locations.

Response	Covariate	R^2 (%)	P-Value	
			Campaign	**Elevation**
Specific conductance	None	6.5	0.478	-
	Elevation	89.4	0.078	<0.0005
pH	None	29.8	0.102	-
	Elevation	39.7	0.105	0.319
Redox potential	None	17.7	0.227	-
	Elevation	42.3	0.187	0.128

5.3.2 Surface water quality and bedrock geology

Figure 5.3 shows the numerical distributions of all surface water determinands in relation to underlying bedrock geology. Specific conductance and ion concentrations appear to vary with underlying bedrock geology; samples underlain by the Mercia Mudstone and Sherwood Sandstone Groups generally have higher specific conductance and concentrations than those underlain by the Lower Coal Measures, Millstone Grit, and Bowland High and Craven Groups (Figure 5.3 and Figure 5.4). This result was not simply a consequence of increasing river length over multiple bedrock formations because the majority of surface waters sampled were restricted to a single underlying formation. However, the same numerical distribution pattern was also true for elevation (Figure 5.3d), suggesting elevation could be the dominant control or, more likely, that elevation is influenced by the different bedrock formations and their weathering rates.

Anderson-Darling tests indicated that the field measurements required no transformation prior to ANOVA. The ANOVA showed that Geology was a significant factor controlling the specific conductance, pH and redox potential of surface water samples across the basin (Table 5.2). The Geology factor explained 49.2% of the variation in specific conductance, which increased to 55.4% with the inclusion of the Elevation covariate. However, the Geology factor remained significant even after inclusion of Elevation, meaning that the difference in specific conductance between bedrock

formations was not explained away by the difference in elevation. Elevation was a significant covariate for specific conductance and pH, explaining 6.0 and 7.3%, respectively, of the variance as calculated using the generalised ω^2 method. For pH the inclusion of elevation resulted in the Geology factor becoming insignificant, meaning that the difference between bedrock formations with respect to pH was really the difference between elevations. For redox potential the Elevation covariate was insignificant and the Geology factor remained significant (Table 5.2). The best-ft model for the field measurements had an R^2 value of 55.4% (Table 5.2) which means that a minimum of 44.6% of the original variance was not explained by any of the ANOVA. Unexplained variance in ANOVA includes the measurement error and any factors, covariates and their interactions that were not considered in the original experimental design, for example changing land use. The magnitude of the unexplained variance does not negate the significance, or not, of the factors that were included.

Table 5.2

ANOVA and post hoc Tukey test results for the field measurements and ion concentrations. Groups from the Tukey tests that do not share a letter are significantly different. MMG – Mercia Mudstone Group, SSG – Sherwood Sandstone Group, LCM – Lower Coal Measures, MG – Millstone Grit, and BHCG – Bowland High and Craven Groups.

Determinand	Covariate	P-value		R^2 (%)	ω^2 (%)		Groupings from Tukey tests				
		Geology	Elevation		Geology	Elevation	MMG	SSG	LCM	MG	BHCG
Specific conductance	None	<0.0005	-	49.2	48.3	-	A	B	BC	C	C
	Elevation	<0.0005	<0.0005	55.4	11.5	6.0					
pH	None	<0.0005	-	8.8	7.2	-	-	-	-	-	-
	Elevation	0.241	<0.0005	16.5	-	7.3					
Redox potential	None	<0.0005	-	14.6	13.1	-	B	A	AB	A	A
	Elevation	<0.0005	0.208	15.2	12.2	-					
Ca	None	<0.0005	-	48.3	46.9	-	A	B	BC	C	C
	Elevation	<0.0005	<0.0005	54.6	13.1	6.0					
Log Fe	None	<0.0005	-	12.0	9.8	-	A	B	AB	B	B
	Elevation	0.003	0.689	12.1	6.7	-					
K	None	<0.0005	-	34.0	32.3	-	A	A	AB	B	B
	Elevation	0.002	0.003	37.5	5.2	3.1					
Log Mg	None	<0.0005	-	49.3	47.9	-	A	B	BC	C	C
	Elevation	<0.0005	<0.0005	57.7	7.4	8.1					
Log Mn	None	<0.0005	-	22.8	20.8	-	A	B	AB	B	B
	Elevation	<0.0005	0.034	24.9	12.8	1.6					
Log Na	None	<0.0005	-	51.2	49.9	-	A	B	ABC	C	C
	Elevation	<0.0005	<0.0005	59.5	9.1	8.0					
Log SO₄	None	<0.0005	-	35.9	34.3	-	A	B	ABC	C	C
	Elevation	<0.0005	0.002	39.6	9.5	3.3					

Post hoc Tukey tests showed that for specific conductance, significant differences lay between the Mercia Mudstone Group, the Sherwood Sandstone Group, and the Millstone Grit and Bowland High and Craven Groups (Figure 5.5; Table 5.2). Differences between the Lower Coal Measures and other bedrock formations were insignificant, which might result from the small sample size (two samples) obtained from surface waters overlying the Lower Coal Measures. For redox potential the Mercia Mudstone Group was significantly different from the Sherwood Sandstone Group, the Millstone Grit, and the

Bowland High and Craven Groups (Figure 5.5; Table 5.2). The Lower Coal Measures showed no significant difference to the other bedrock formations.

Prior to ANOVA, Fe, Mg, Mn, Na and SO_4 concentration data were log-transformed. The Anderson-Darling test suggested that no transformation was necessary for either Ca or K. The ANOVA showed that Geology was a significant factor controlling the concentrations of all seven ions (Table 5.2). The Geology factor explained from 12.0% of the variation in Fe concentrations to 51.2% of the variation in Na concentrations (Table 5.2). Elevation was a significant covariate for all ions, except Fe, and increased the overall fit of the models (i.e. R^2 values increased), but in all cases did not alter the significance of the Geology factor, i.e. there was a geological control on surface water quality over and above that due to elevation. The proportion of variance explained by the Geology factor was greater than that explained by the Elevation covariate for all ions except Mg (Table 5.2).

Post hoc Tukey tests showed that significant differences lay between the Mercia Mudstone Group, the Sherwood Sandstone Group, and the Millstone Grit and Bowland High and Craven Groups for Ca, Mg, Na and SO_4 (Figure 5.5; Table 5.2). For Fe and Mn, the Mercia Mudstone Group was the only bedrock formation that was significantly different from all other formations, excluding the Lower Coal Measures (Figure 5.5; Table 5.2). For K, the Mercia Mudstone and Sherwood Sandstone Groups were grouped together and were significantly different from the Millstone Grit and Bowland High and Craven Groups (Figure 5.5; Table 5.2). The Lower Coal Measures were only significantly different to the Mercia Mudstone Group for Ca and Mg.
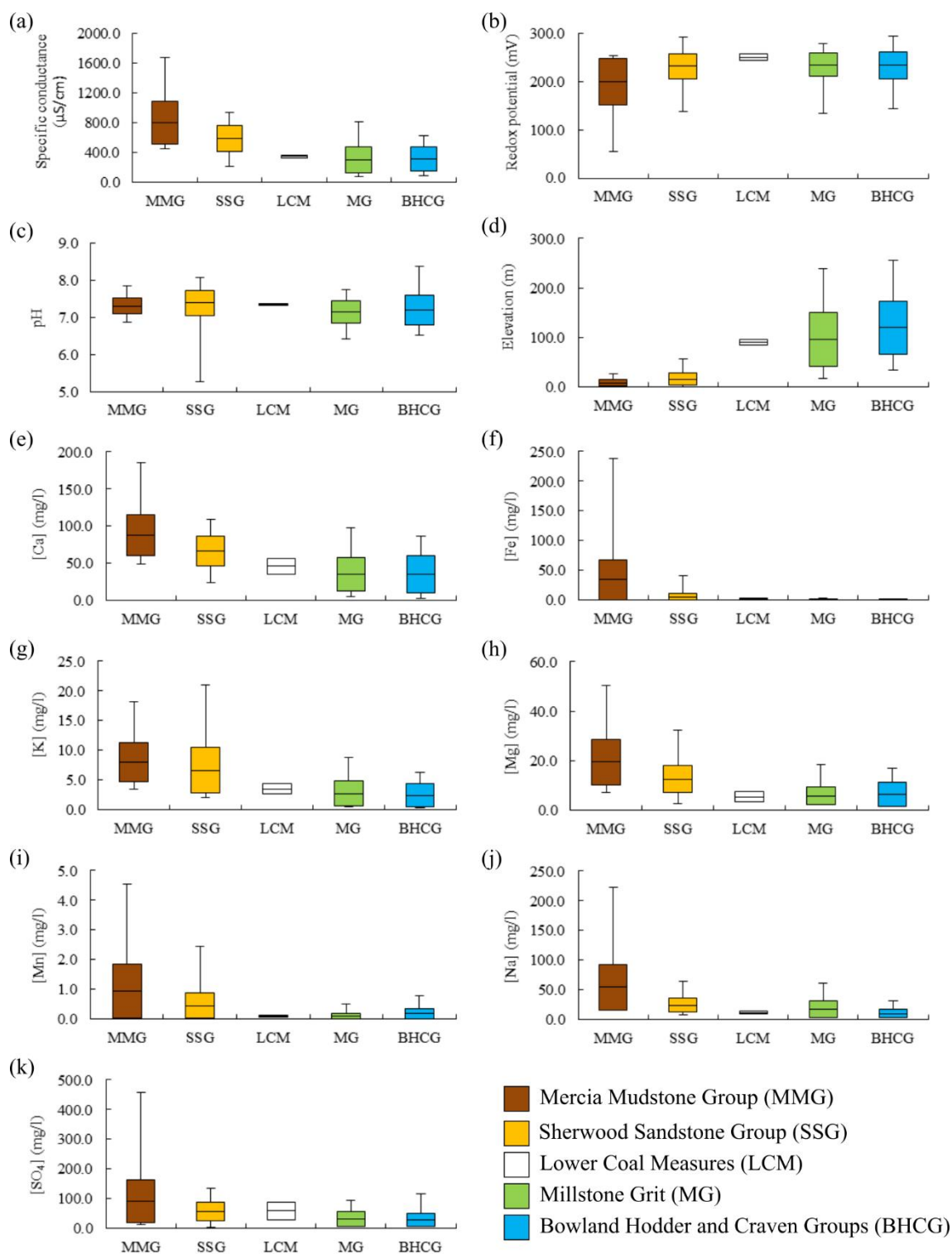
Figure 5.3

Box plots showing the maximum, minimum, mean, and first standard deviation values of field measurements, elevation and ion concentrations, split by underlying bedrock geology: (a) specific conductance; (b) redox potential; (c) pH; (d) elevation; (e) Ca concentration; (f) Fe concentration; (g) K concentration; (h) Mg concentration; (i) Mn concentration; (j) Na concentration; and (k) SO4 concentration. Where lower whiskers are not shown the standard deviation is greater than the minimum value and so the base of the box represents the minimum value.

144
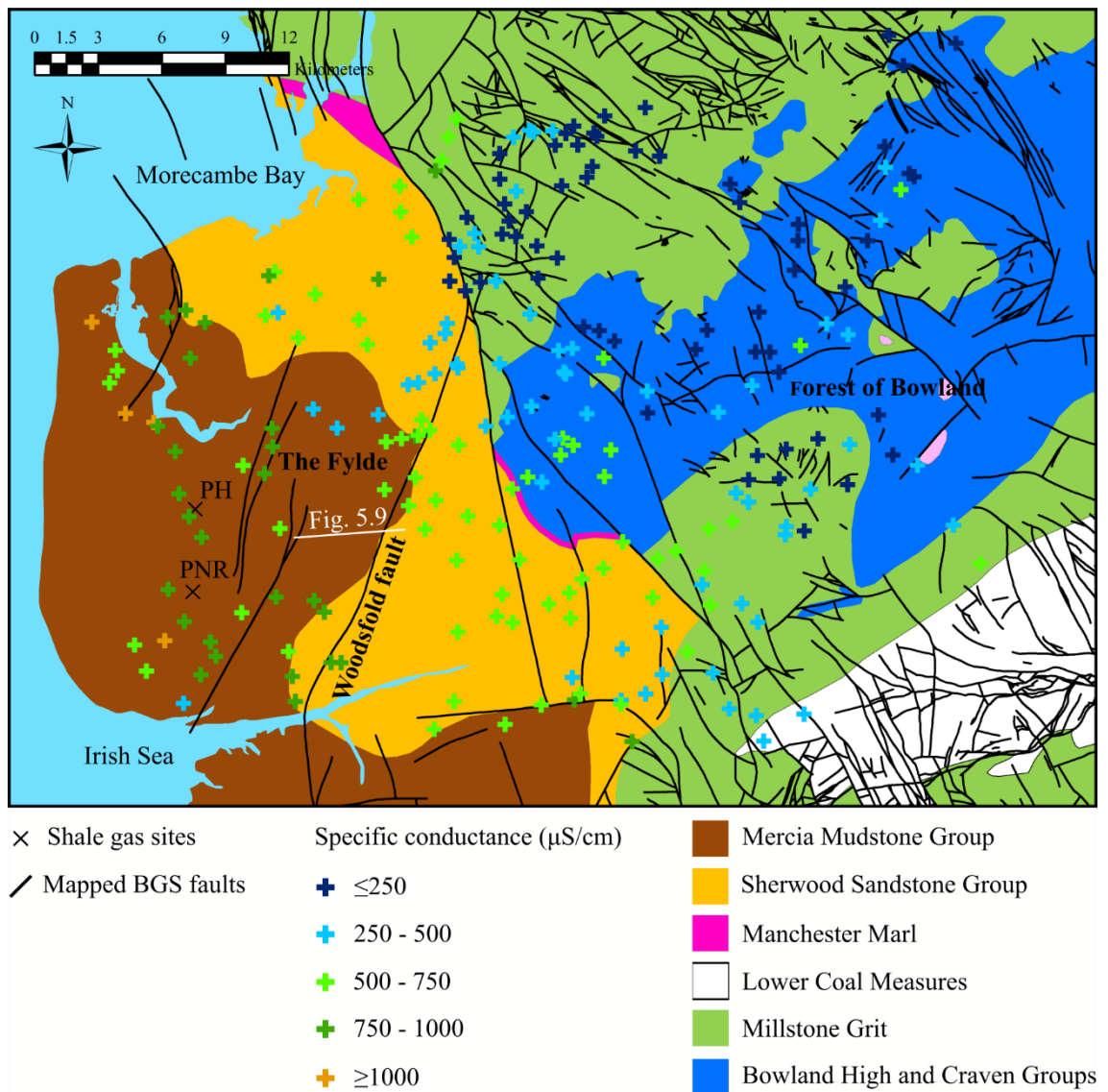
Figure 5.4
Map of study region showing specific conductance measurements and the location of the geological cross-section in Figure 5.9. PH and PNR are the shale gas fracking sites of Preese Hall and Preston New Road, respectively. Contains BGS data © Crown copyright and database right (2019). A BGS/EDINA supplied service.
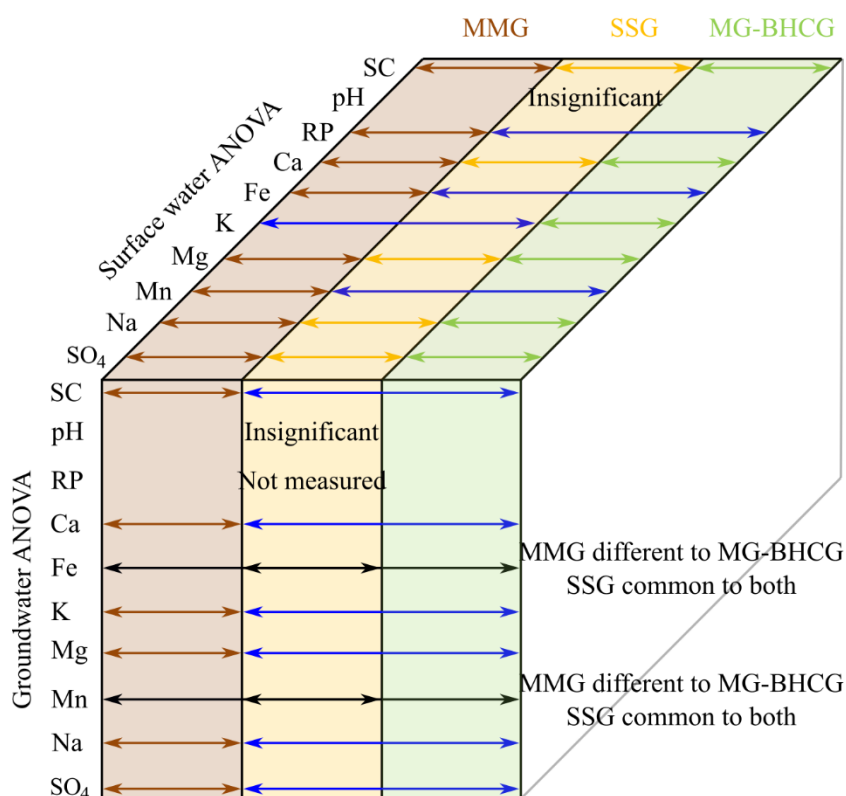
Figure 5.5

Diagram of post hoc Tukey test results for each determinand from the variance analysis on surface water (top surface) and groundwater (front surface) quality data. Double-ended arrows represent significant difference. For example, for specific conductance (SC) of surface water the Mercia Mudstone Group, Sherwood Sandstone Group and Millstone Grit-Bowland High and Craven Groups samples were all significantly different to each other. MMG – Mercia Mudstone Group, SSG – Sherwood Sandstone Group, MG-BHCG – Millstone Grit-Bowland High and Craven Groups, RP – Redox Potential. Surface water samples overlying the Lower Coal Measures and groundwater samples from the Coal Measures are not shown.

5.3.3   Groundwater quality and aquifers

All groundwater determinands, except pH, were log-transformed prior to ANOVA because of improved Anderson-Darling test values compared to the raw data. ANOVA showed that Aquifer was a significant factor in explaining differences in all determinands, bar pH, across the aquifer formations (Table 5.3). The Aquifer factor explained from 27.1% of the variation in Mn concentrations to 71.8% of the variation in SO_4 concentrations (Table 5.3). *Post hoc* Tukey tests showed that groundwater in the Mercia

146

Mudstone Group was significantly different to all other aquifer formations for specific conductance, Ca, Na and SO4 (Table 5.3), and different to the Sherwood Sandstone Group and MG-BHCG for all determinands except Fe and Mn (Figure 5.5; Table 5.3). No significant differences existed between the Sherwood Sandstone Group, Coal Measures and MG-BHCG for any determinands (Figure 5.5; Table 5.3).

Table 5.3
ANOVA and post hoc Tukey test results for the groundwater determinands with inferred aquifer as the factor. Groups from the Tukey tests that do not share a letter are significantly different. MMG – Mercia Mudstone Group, SSG – Sherwood Sandstone Group, CM – Coal Measures, MG-BHCG – Millstone Grit and Bowland High and Craven Groups.

Determinand	P-Value	R^2 (%)	Groupings from Tukey Tests			
			MMG	SSG	CM	MG-BHCG
Log Specific conductance	<0.0005	63.0	A	B	-	B
pH	0.563	7.2	-	-	-	-
Log Ca	<0.0005	47.7	A	B	B	B
Log Fe	0.003	40.5	A	AB	B	B
Log K	0.001	44.4	A	B	AB	B
Log Mg	0.001	45.8	A	B	AB	B
Log Mn	0.034	27.1	A	B	AB	AB
Log Na	<0.0005	52.9	A	B	B	B
Log SO4	<0.0005	71.8	A	B	B	B

5.3.4   Combined surface water and groundwater quality ANOVA

Prior to ANOVA all determinands, except pH, were log-transformed. ANOVA results showed that Geology was a significant factor for all determinands (Table 5.4). Within the Geology factor all determinands from the Mercia Mudstone Group, expect pH, were significantly different from the other geological formations, which was confirmed by groupings from the *post hoc* Tukey tests (Table 5.4). *Post hoc* Tukey tests also showed that the Sherwood Sandstone Group and MG-BHCG were significantly different from each other for all determinands except Fe and Mn (Table 5.4). The Coal Measures were not significantly different from any of the other geological formations as shown by the shared Tukey Test groups. The Water body factor was significant for specific

conductance, Ca, Mg and Na, but not for Fe, K, Mn, SO$_4$ and pH (Table 5.4). In other words, whereas significant differences in Fe, K, Mn, SO$_4$ and pH occurred between the different geological formations, no differences were observed between surface waters and groundwater. The generalised ω^2 method showed that the Geology factor always explained more of the variance in determinands than the Water body factor or the interaction between the two factors, ranging from 2.1% of the variance in pH to 44.8% of the variance in specific conductance (Table 5.4).

Table 5.4

ANOVA, post hoc Tukey test and power analysis results for the combined surface water and groundwater dataset. Groups from the Tukey tests that do not share a letter are significantly different. Means and standard errors are given in original determinand units. MMG – Mercia Mudstone Group, SSG – Sherwood Sandstone Group, CM – Coal Measures, MG-BHCG – Millstone Grit and Bowland High and Craven Groups, SC – Specific conductance.

Determinand	R^2 (%)	Factor and interaction P-values			Level P-values						Groupings from Tukey tests			
		Water body	Geology	Water body *Geology	Ground-water	Surface water	MMG	SSG	CM	MG-BHCG	MMG	SSG	CM	MG-BHCG
Log SC	49.5	<0.0005	<0.0005	-	<0.0005	<0.0005	<0.0005	0.036	0.311	<0.0005	A	B	ABC	C
pH	8.5	0.920	0.034	0.984	0.920	0.920	0.837	0.245	0.564	0.008	AB	A	AB	B
Log Ca	47.6	<0.0005	<0.0005	0.042	<0.0005	<0.0005	<0.0005	0.300	0.067	<0.0005	A	B	BC	C
Log Fe	19.3	0.786	<0.0005	0.016	0.786	0.786	<0.0005	0.936	0.062	0.028	A	B	B	B
Log K	44.7	0.148	<0.0005	<0.0005	0.148	0.148	<0.0005	0.187	0.800	<0.0005	A	B	ABC	C
Log Mg	56.1	<0.0005	<0.0005	0.056	<0.0005	<0.0005	<0.0005	0.184	0.021	<0.0005	A	B	BC	C
Log Mn	23.4	0.320	<0.0005	0.130	0.320	0.320	<0.0005	0.001	0.887	0.033	A	B	AB	B
Log Na	55.9	<0.0005	<0.0005	<0.0005	<0.0005	<0.0005	<0.0005	0.001	0.184	<0.0005	A	B	BC	C
Log SO₄	50.1	0.072	<0.0005	<0.0005	0.072	0.072	<0.0005	0.272	0.004	<0.0005	A	B	BC	C

Determinand	Units for mean	ω^2 (%)			Mean ± standard error in mean						Detectable difference for Water body	Detectable difference for Geology
		Water body	Geology	Water body *Geology	Ground-water	Surface water	MMG	SSG	CM	MG-BHCG		
Log SC	µs/cm	5.1	44.8	-	780±1	444±1	1050±1	721±1	454±1	347±1	142	125
pH	pH units	-	2.1	-	7.30±0.08	7.31±0.06	7.29±0.09	7.38±0.06	7.38±0.16	7.18±0.04	0.15	0.14
Log Ca	mg/l	5.5	24.3	1.4	105±1	46.7±1.1	176±1	78.5±1.1	46.6±1.3	37.1±1.1	49.5	43.4
Log Fe	mg/l	-	12.8	3.1	0.9±1.3	0.8±1.3	3.9±1.4	0.9±1.2	0.3±1.9	0.5±1.2	8.2	7.2
Log K	mg/l	-	17.3	5.6	5.3±1.2	4.0±1.1	11.4±1.2	3.9±1.1	4.3±1.4	2.3±1.1	2.8	2.5
Log Mg	mg/l	12.5	24.6	-	31.0±1.2	8.0±1.1	46.1±1.2	18.4±1.1	9.2±1.3	7.9±1.1	19.2	16.8
Log Mn	mg/l	-	9.8	-	0.2±1.3	0.1±1.2	0.4±1.4	0.1±1.2	0.1±1.8	0.1±1.2	0.3	0.2
Log Na	mg/l	9.9	33.2	11.2	72.2±1.2	18.3±1.1	184±1	23.8±1.1	25.7±1.4	15.6±1.1	1850	1630
Log SO₄	mg/l	-	39.9	14.2	65.7±1.1	44.3±1.1	332±1	46.3±1.1	23.9±1.4	23.1±1.1	226	198

The interaction between the Geology and Water body factors was significant for Ca, Fe, K, Na and SO_4. *Post hoc* Tukey tests showed that for Ca, Na and SO_4, groundwater in the Mercia Mudstone Group was significantly different to all other waters, including surface waters overlying the Mercia Mudstone Group (as shown by lines in Figure 5.6). No significant differences were observed for any determinands between groundwater and surface waters of the Coal Measures, and only K showed a significant difference between surface waters and groundwater of the Sherwood Sandstone Group (Figure 5.6). For the MG-BHCG significant differences between groundwater and surface waters occurred for Ca and Na, but not for Fe, K or SO_4. Considering interactions between groundwaters of the different geological formations, no significant differences between the Sherwood Sandstone Group, Coal Measures and MG-BHCG were observed for any determinands (as shown by the absence of lines Figure 5.6). For surface waters all five determinands were significantly different between the MG-BHCG and Mercia Mudstone Group. Surface waters overlying the MG-BHCG were also significantly different to those overlying the Sherwood Sandstone Group for Ca, K, Na and SO_4, but not for Fe. Lastly, surface waters overlying the Sherwood Sandstone Group were significantly different to those overlying the Mercia Mudstone Group for Fe, Na and SO_4.
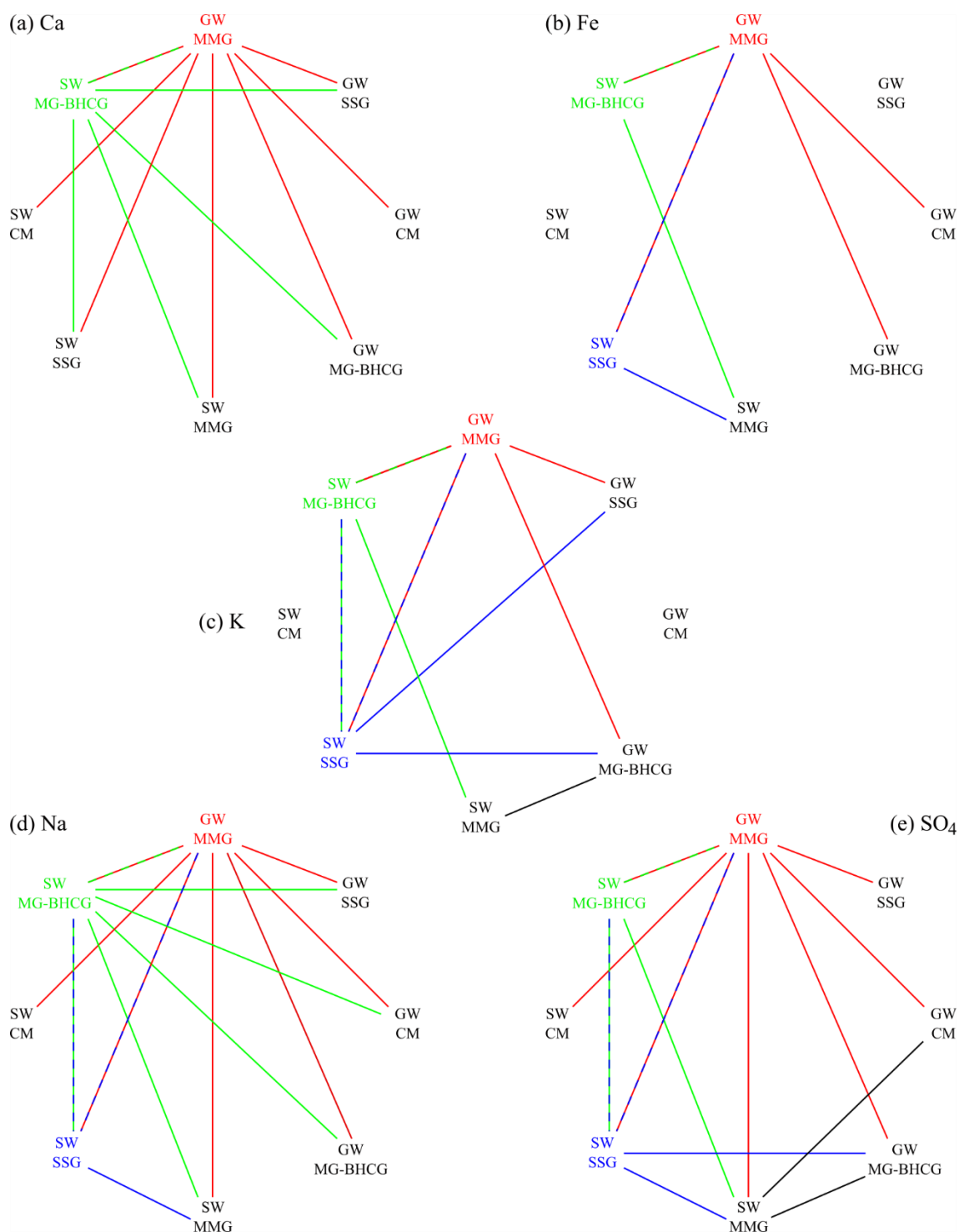
Figure 5.6

Post hoc Tukey Test results for determinands with significant interaction between the Water Body and Geology factors: (a) Ca; (b) Fe; (c) K; (d) Na; and (e) SO_4. Significant interactions between factor levels are shown by lines. Groundwater (GW) Mercia Mudstone Group (MMG), surface water (SW) Millstone Grit and Bowland High and Craven Groups (MG-BHCG), and surface water Sherwood Sandstone Group (SSG) have been coloured red, green and blue, respectively, to highlight levels with the most interactions.

The power analysis performed for the experimental design was irrelevant for the Geology factor because all determinands proved to be significant at the 95% probability. For the Water body factor the detectable difference was greater for each determinand than for the Geology factor (Table 5.4), i.e. it was easier to detect differences between the different geological formations than the difference between the water bodies. For example, for specific conductance the detectable difference between surface waters and groundwater was 142 µS/cm whereas the detectable difference between the different geological formations was lower at 125 µS/cm. However, it should be noted that while the detectable difference for Na concentration was 1850 mg/l, the detectable difference for pH was only 0.15 pH units which may not be meaningfully physical given the typical accuracy of field measurements for this determinand.

5.3.5 *Water quality trends and end-members*

The PCA reduced the eight surface water determinands from the 170 surface water samples to two PCs, which explained 79.5% of the variance in the data (Table 5.5). PC3 is not included in the results because its eigenvalue was much less than one. All determinands had positive loadings in PC1, suggesting that PC1 was a general concentration component. In PC2 the strongest positive loadings were for Fe and Mn, and the strongest negative loading was for SO_4 (Table 5.5).

A plot of PC2 versus PC1, colour-coded by underlying bedrock geology, indicated at least three end-members exist for surface waters (Figure 5.7a). Surface water end-member A (SW-A) comprised of two sampling locations (location numbers 132 and 139) in the Forest of Bowland, underlain by the Millstone Grit (Figure 5.8). These locations had low ion concentrations and specific conductance (~74 µS/cm) (Table D2) when compared to the entire dataset. The trend from SW-A to SW-B (location number 104)

showed increasing PC1, signifying increased ion concentrations and specific conductance, and increasing PC2 as a result of SW-B having the highest Fe concentration in the dataset (214 mg/l) (Table D2). SW-B is located in the northwest Fylde and is underlain by the Mercia Mudstone Group (Figure 5.8). High Fe and Mn ion concentrations can relate to bacterial reduction of metal oxides (e.g. haematite) or sulfide mineral oxidation (e.g. Equation 5.3):

$$FeS_{2\,(s)} + 7O_{2\,(aq)} + 2H_2O_{(l)} \leftrightarrow 2Fe^{2+}{}_{(aq)} + H_2SO_{4\,(aq)} + 2H^+{}_{(aq)} \qquad \textit{Equation 5.3}$$
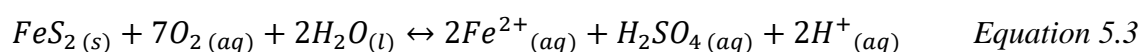
The trend from SW-A to SW-D (location number 232) showed increasing PC1 and decreasing PC2, resulting from SW-D having the highest SO_4 concentration (458 mg/l) in the dataset (Table D2). SW-D is located in the southwest Fylde and is underlain by the Mercia Mudstone Group (Figure 5.8). A fourth end-member, SW-C (location number 97) was interpreted to graphically lie between SW-B and SW-D (Figure 5.7a). SW-C had elevated Na concentrations (185 mg/l) and is located in the northwest Fylde ~1.4 km from SW-B, and is also underlain by the Mercia Mudstone Group (Figure 5.8).

The PCA on the combined surface water and groundwater data also reduced the eight determinands to two PCs, which explained 75.3% of the data variance (Table 5.5). In PC1 all determinands had positive loadings, again suggesting PC1 was a general concentration component. In PC2 the strongest loadings were for Fe and Mn, but with reversed polarity to the PCA on just the surface water data (Table 5.5). This polarity reversal occurred because a number of groundwater samples had very high values for specific conductance and Na.

Table 5.5

Results of PCA for surface water quality data and combined surface water and groundwater quality data.

Surface water	Principal Components	
	PC1	PC2
Specific conductance	0.436	-0.143
Ca	0.413	-0.074
Fe	0.206	0.653
K	0.380	-0.097
Mg	0.417	0.070
Mn	0.278	0.556
Na	0.338	-0.172
SO_4	0.296	-0.442
Eigenvalue	4.872	1.491
Proportion (%)	60.9	18.6
Cumulative (%)	60.9	79.5
Surface water and groundwater		
Specific conductance	0.416	0.235
Ca	0.292	-0.258
Fe	0.138	-0.664
K	0.427	0.049
Mg	0.451	0.050
Mn	0.240	-0.577
Na	0.432	0.231
SO_4	0.304	0.213
Eigenvalue	4.430	1.593
Proportion (%)	55.4	19.9
Cumulative (%)	55.4	75.3

A plot of PC2 versus PC1 for the combined surface water and groundwater PCA showed that the surface water data lay inside the groundwater end-members and SW-A coincided with the fresh water groundwater end-member (GW-A, previously referred to as EM-A in Chapter 4) identified in Chapter 4 (Figure 5.7b). GW-A comprised of two sampling locations in the Forest of Bowland; New Drop Inn borehole and Saddleside Springs, which sampled the Millstone Grit and an unknown aquifer, respectively (Figure 5.8). SW-B and GW-B (Blackpool Promenade Borehole no. 9) plotted towards an Fe-rich groundwater end-member at Withnell Quarry (Fe concentration 330 mg/l) (Figure 5.7b and 5.8), which was not identified as an end-member in Chapter 4 because of the different water quality determinands used. The Na-Cl groundwater end-member,

GW-C (Jameson Road Landfill Site – Figure 5.8), was clearly observed on Figure 5.7b and SW-C plotted towards it. Likewise, SW-D plotted towards the three SO_4-rich groundwater samples classified as outliers in Chapter 4 (Figure 5.7b). The other outlier samples classified in Chapter 4 (i.e. those with very high total dissolved solids) were responsible for the reversed polarity.
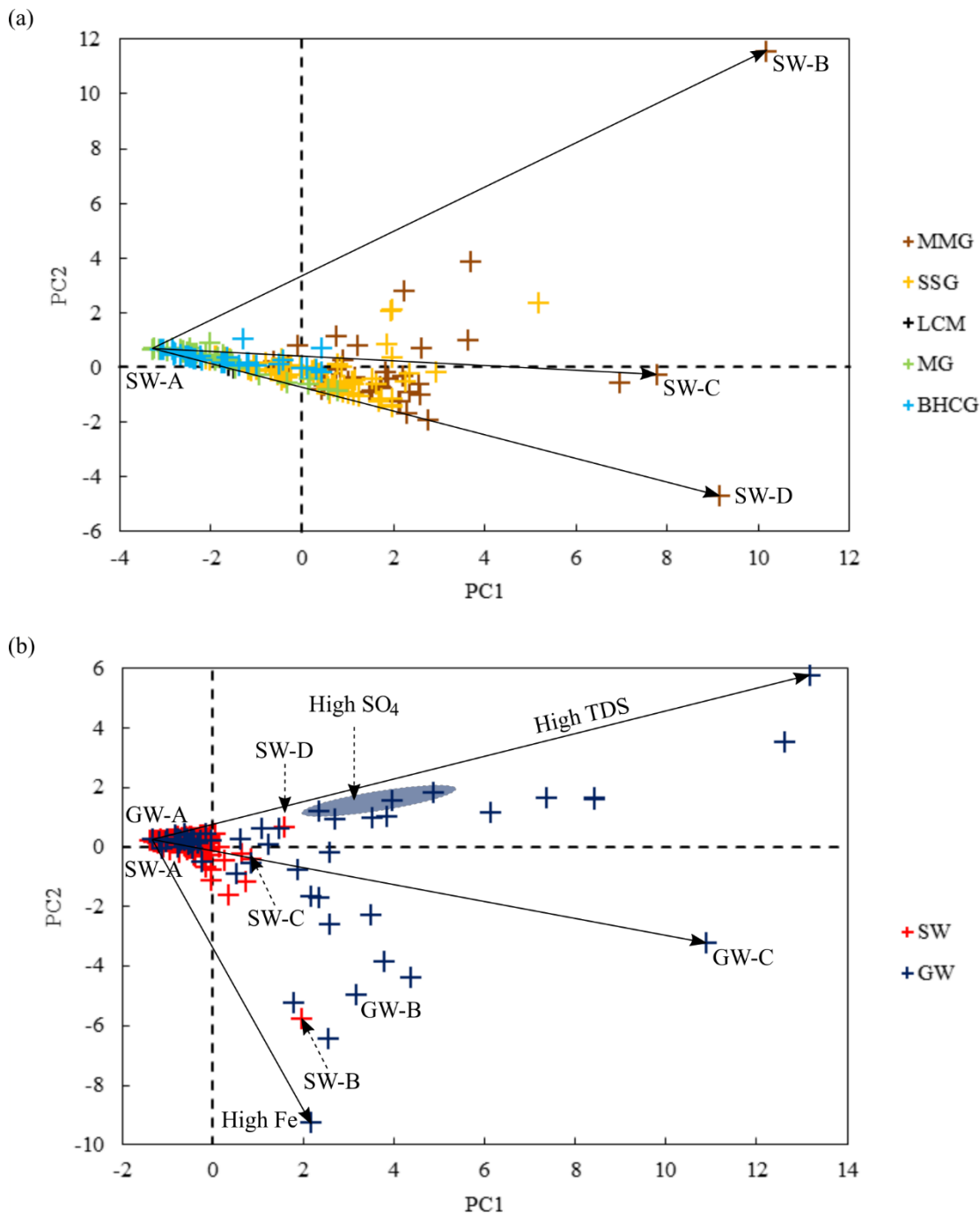
Figure 5.7

Principal components plots of PC2 versus PC1 for: (a) 170 surface water samples analysed for ion concentrations; and (b) 170 surface water samples and 57 groundwater samples analysed for ion concentrations. Interpreted surface water (SW) and groundwater (GW) end-members (from Chapter 4) are labelled, as are high SO_4 (blue ellipse), high total dissolved solids (TDS) and Fe trends. MMG – Mercia Mudstone Group, SSG – Sherwood Sandstone Group, LCM – Lower Coal Measures, MG – Millstone Grit, and BHCG – Bowland High and Craven Groups.
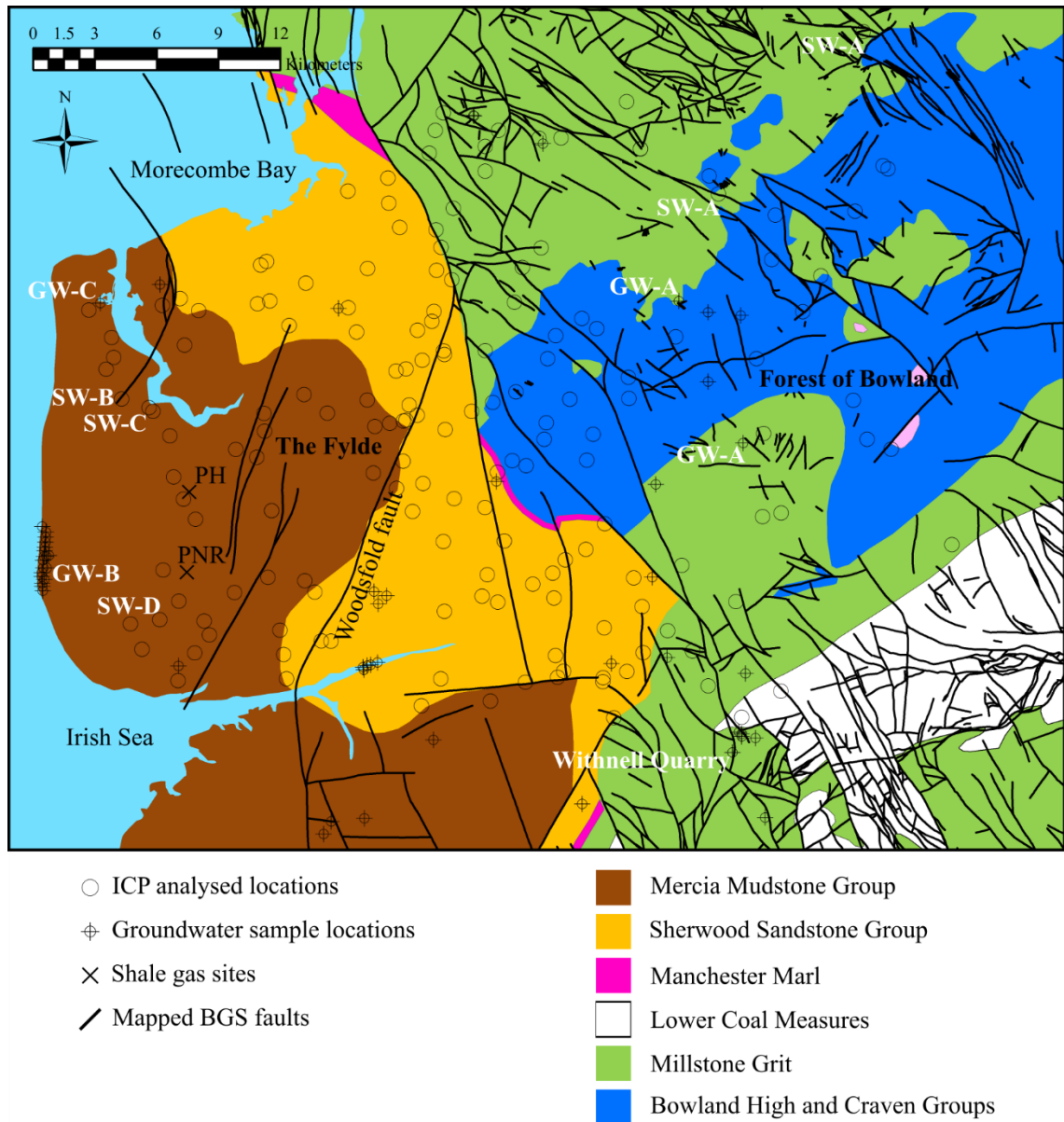
Figure 5.8
Map of the study region showing surface water and groundwater sampling locations used in the PCA. Contains BGS data © Crown copyright and database right (2019). A BGS/EDINA supplied service.

5.3.6 Identifying compartmentalisation

Prior to the three-way ANOVA all determinands, except Ca, pH and redox potential, were log-transformed because of improved normality. When single factors were considered the only significant differences observed were for SO_4 between the Wyre and Ribble catchments and Mn across the Woodsfold fault (Table 5.6). When two-way and three-

way factor interactions were considered no significant differences were observed (Table 5.6). Critically, the interaction between the Catchment and Fault factors was not significant, indicating that compartmentalisation across the Woodsfold fault did not significantly affect the surface water quality data. This result could have been due to a lack of effect of groundwater compartmentalisation on surface waters, or that the sampling design was not sufficient to detect the difference, i.e. the power of the design was not sufficient and a false negative exists. However, power analysis showed that it would have been possible at 95% significance and 95% power to detect an effect which explained 10.7% of the original variance. For specific conductance this corresponded to a detectable difference of 157 μS/cm across the Woodsfold fault (Table 5.6), which was smaller than the difference in mean specific conductance observed between the Mercia Mudstone and Sherwood Sandstone Group surface water samples (Figure 5.9). Therefore, the survey design was capable of detecting a compartmentalising effect with a difference smaller than that observed between the underlying bedrock formations.

Table 5.6
Three-way ANOVA and power analysis results for surface water quality data used to identify compartmentalisation across the Woodsfold fault. SC – Specific conductance.

Determinand	R² (%)	P-value							Detectable difference
		Geology	Catchment	Fault	Geology *Catchment	Geology *Fault	Catchment *Fault	Geology *Catchment *Fault	
Log SC	21.5	0.192	0.462	0.329	0.483	0.981	0.303	0.469	157 µS/cm
pH	8.04	0.942	0.103	0.176	0.266	0.732	0.729	0.372	0.3
Redox potential	25.6	0.237	0.175	0.193	0.928	0.341	0.571	0.944	25.5 mV
Ca	20.2	0.213	0.464	0.186	0.997	0.905	0.584	0.484	17.3 mg/l
Log Fe	18.9	0.601	0.731	0.061	0.603	0.181	0.131	1.000	22.9 mg/l
Log K	11.2	0.472	0.917	0.667	0.350	0.366	0.232	0.421	2.0 mg/l
Log Mg	29.0	0.235	0.460	0.241	0.747	0.912	0.407	0.235	5.1 mg/l
Log Mn	37.2	0.185	0.527	0.013	0.463	0.337	0.312	0.848	0.5 mg/l
Log Na	26.4	0.108	0.141	0.403	0.157	0.944	0.206	0.891	21.6 mg/l
Log SO₄	32.4	0.390	0.004	0.304	0.350	0.948	0.401	0.305	48.7 mg/l
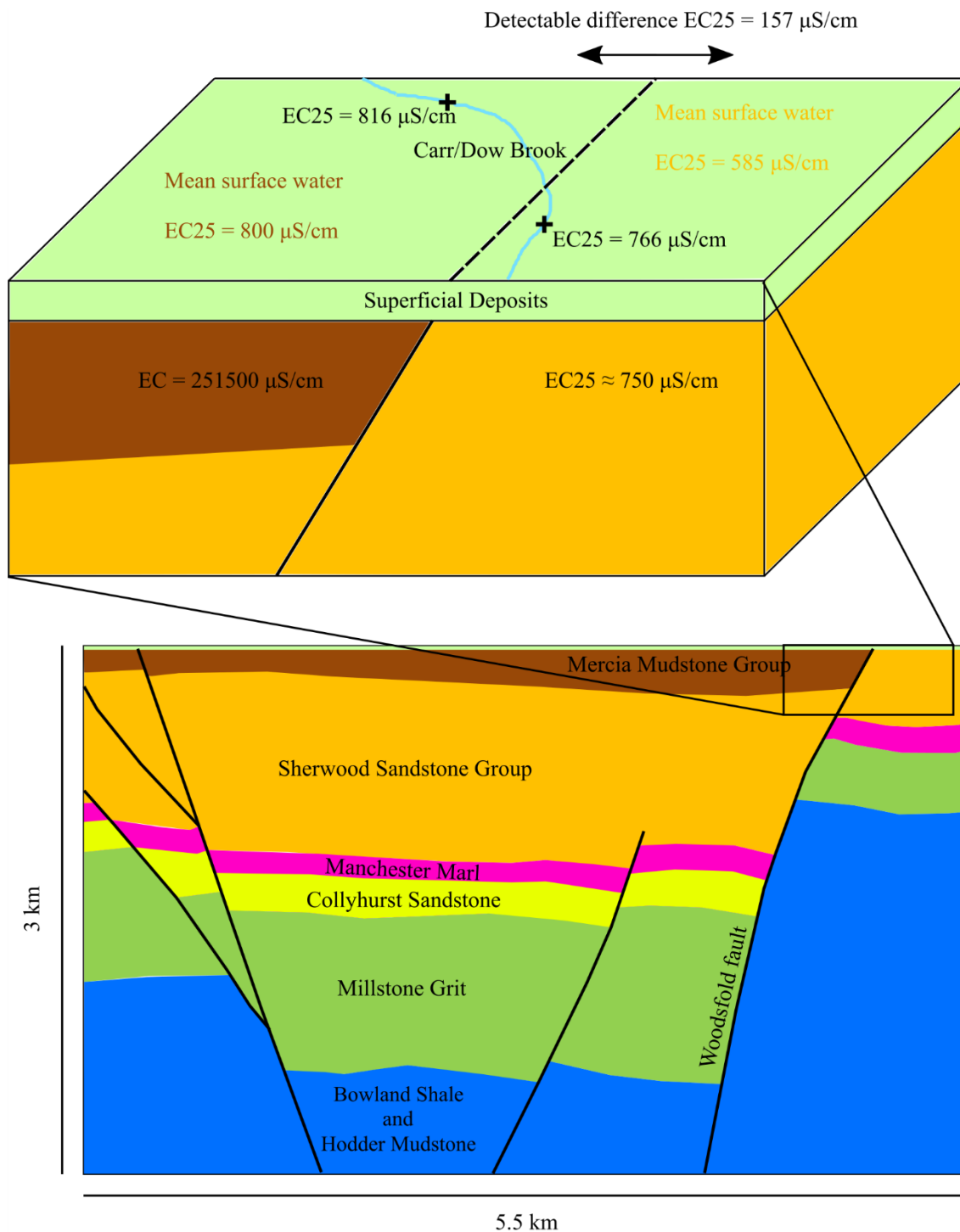
Figure 5.9

Diagram of the differences in electrical conductivity of surface waters and groundwater across the Woodsfold fault in the southern Fylde. Electrical conductivities (EC) for groundwater are from Chapter 4. Reference geological cross-section (approximate location shown in Figure 5.4) is based on BGS [1990] and Ove Arup and Partners Ltd. [2014a].

5.4 Discussion

5.4.1 Does groundwater in underlying bedrock formations affect surface water quality?

Statistical analyses of water quality data have been used in various geographical regions to investigate groundwater-surface water interactions. *Kumar et al.* [2009] used major ion chemistry and multivariate statistics to investigate the effect of monsoon rains on groundwater-surface water interactions in an urbanised section of the River Yamuna in Delhi, India. *Guggenmos et al.* [2011] also used multivariate statistics to indicate some river systems in the Wairarapa Valley, New Zealand, were recharging shallow aquifers whereas in others, groundwater was providing base flow. *Guggenmos et al.* [2011] also highlighted that differences in water quality between surface waters and groundwater can indicate disconnection. In the UK various studies have considered how bedrock geology relates to surface water quality, thereby indicating groundwater interaction [*Thornton & Dise*, 1998; *Soulsby et al.*, 2006; *Rothwell et al.*, 2010a; 2010b; *Neal et al.*, 2011]. *Rothwell et al.* [2010a] found significant relationships between bedrock geology and surface water pH, Ca, Mg and SO_4 concentrations across northwest England, although in the Bowland Basin the Mercia Mudstone and Sherwood Sandstone Groups were classified as one bedrock type. *Neal et al.* [2011] studied the Wyre and Ribble river catchments, concluding that under base flow conditions the upland rivers primarily comprise of groundwater inputs enriched in divalent base cations due to weathering of the underlying Carboniferous bedrock. Nevertheless, only 26 sites were chosen for monitoring, most of which were not located in the Fylde.

The ANOVA on surface water determinands showed that surface water quality was generally distinct across the underlying Mercia Mudstone Group, Sherwood Sandstone Group and MG-BHCG bedrocks (Figure 5.5). This result indicates that on a regional scale groundwater in underlying bedrock formations interacts with surface waters despite the widespread presence of superficial deposits which average 30 to 40 m thickness in the

Fylde [*Cripps et al.*, 2016]. The change in surface water quality is not considered to relate to changing anthropogenic land use (i.e. high-lying rough pastures or low-lying agricultural fields) because both the Mercia Mudstone and Sherwood Sandstone Groups in the Fylde are overlain by similar farming practices. Although an assessment of the physical and geochemical characteristics of the superficial deposits was beyond this study, it is likely that localised pathways between bedrock and surface waters occur in the absence of glacial till and the presence of glaciofluvial sands and gravels. These glaciofluvial pathways are considered to allow recharge of the Sherwood Sandstone aquifer in the Fylde [*Sage & Lloyd*, 1978; *Mott MacDonald*, 1997; 2010]. Alternatively, direct hydraulic connections might exist around undiscovered bedrock highs where superficial deposits are thin or absent [*Cripps et al.*, 2016].

Specific areas where there was evidence for interaction were identified through the PCA. SW-C and GW-C were Na-dominated end-members both located in the northwest Fylde (Figure 5.8), suggesting they could be related. In Chapter 4 it was suggested that the Na concentrations could be the result of landfill leachate, sea water intrusion or *in situ* dissolution of the Preesall Halite found within the Mercia Mudstone Group of the northwest Fylde [*Wilson*, 1990; *Wilson & Evans*, 1990]. Considering SW-C is ~5.6 km from GW-C (Figure 5.8), landfill leachate can likely be dismissed as the cause of the Na concentrations at SW-C and the hypotheses of *in situ* halite dissolution or sea water intrusion are preferred explanations (note that the source of Na and Cl concentrations at GW-C may be different to SW-C and could relate to landfill leachate). Evidence for interaction also occurs in the southwest Fylde (Figure 5.8). SW-D and surrounding surface water samples were Ca-rich and contained the highest concentrations of SO_4 in the study. Although the methodology assumes all S is present as SO_4, the Kirkham Mudstone Formation of the Mercia Mudstone Group, which is the bedrock in this area [*BGS*, 2019b], is rich in gypsum ($CaSO_4.2H_2O$) [*Wilson*, 1990]. Therefore, the Ca and

SO$_4$ concentrations in surface waters may relate to gypsum dissolution by groundwater in the underlying Mercia Mudstone Group (Equation 5.4).

$$CaSO_4.2H_2O_{(s)} \leftrightarrow Ca^{2+}{}_{(aq)} + SO_4{}^{2-}{}_{(aq)} + 2H_2O_{(l)}$$ *Equation 5.4*
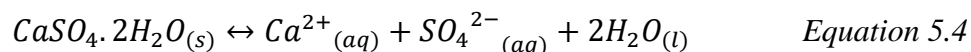
The ANOVA on groundwater determinands showed that groundwater in the Sherwood Sandstone Group and MG-BHCG could not be distinguished from each other (Figure 5.5), implying similar bedrock minerology and/or well-mixed groundwater. This result contradicts the surface water results which suggested distinct groundwater-surface water interactions across the bedrock types. The contradiction may be explained by surface waters mostly interacting with groundwater in a shallow weathered bedrock layer but not with groundwater deeper in the bedrock formations. Evidence for a weathered bedrock layer in the Fylde comes from borehole data and suggests the weathered layer may be up to 5 m thick [*Cripps et al.*, 2016].

Groundwater within the Mercia Mudstone Group was distinct from other bedrock formations (Figure 5.5) and the level interactions from ANOVA on surface water and groundwater determinands indicated that groundwater in the Mercia Mudstone Group was distinct from the overlying surface waters (Figure 5.6). This result contradicts the surface water ANOVA which indicated groundwater-surface water interaction from the significant difference in surface water quality observed between the Sherwood Sandstone and Mercia Mudstone Groups. The contradiction could be explained if groundwater within the Mercia Mudstone Group is stratified; surface waters interact with groundwater in a weathered layer of the upper Mercia Mudstone Group but groundwater in the lower Mercia Mudstone Group does not mix. Evidence for this hypothesis comes from SW-D and surrounding surface water samples. These samples were not dominated by Na like the Na-Cl dominated brine found in the lower Mercia Mudstone Group at the Kirkham Borehole (see Chapter 4) and in the underlying Sherwood Sandstone Group at Roseacre

Wood [*BGS*, 2018a]. Shallow groundwater stratification within the low-permeability Mercia Mudstone Group may be a common occurrence; in the nearby Mersey Basin Na and Cl concentrations in the Mercia Mudstone Group rapidly increase from 5950 and 9260 mg/l at 120 m depth to 123000 and 192000 mg/l at 150 m, respectively [*Tellam*, 1995].

5.4.2 *The origin of the Na-Cl brines*

Based on the absence of halite at groundwater sampling depths (240 to 260 m in the Kirkham Borehole) in the Mercia Mudstone Group, it was proposed in Chapter 4 that the origin of Na-Cl brines in the Mercia Mudstone and Sherwood Sandstone Groups was halite dissolution in the Mercia Mudstone Group in the offshore East Irish Sea Basin, with onshore emplacement driven by basin compaction; this process being analogous to that proposed to account for brines found in the Sellafield region further north [*Bath et al.*, 2006]. However, the absence of halite and previously overlooked presence of brecciation and collapse structures in the Kirkham Borehole may be explained by halite dissolution. Consequently, the origin of the Na-Cl brines might be *in situ* halite dissolution in the Mercia Mudstone Group and migration into the underlying Sherwood Sandstone Group. This process has been proposed to account for saline waters found in the Sherwood Sandstone Group in the Mersey Basin and Market Weighton Block [*Tellam*, 1995; *Bottrell et al.*, 2006].

5.4.3 *Atmospheric interactions with surface waters*

For surface water quality it was found that the Geology factor had no significant effect on pH when the Elevation covariate was included (Table 5.2). Conversely, the Geology factor was significant for redox potential and was not explained away by differences in

elevation. Redox potential values for surface waters overlying the Mercia Mudstone Group were significantly lower than those overlying the Sherwood Sandstone Group and MG-BHCG (Figure 5.5). An explanation for the lower redox potential values in surface waters overlying the Mercia Mudstone Group might be the physical nature of the surface waters at the sampling times; they were lower flow and less turbulent than surface waters overlying the Sherwood Sandstone Group and MG-BHCG, and thus oxygen diffusion was likely more limited.

The pH of surface waters is mainly controlled by acidic rainfall, anthropogenic inputs, and mineral interactions at the surface or in groundwater. Although dissolution of carbon dioxide affects water pH through the creation of carbonic acid, dissolved carbon dioxide in surface waters is not generally considered atmospheric in origin, and instead mostly originates from terrestrial ecosystem respiration, the oxidation of organic carbon, the acidification of buffered waters, the precipitation of carbonate minerals, and the direct pumping of root respiration carbon dioxide from riparian vegetation [*Butman & Raymond*, 2011]. Surface waters tend to be supersaturated in carbon dioxide compared to the atmosphere and thus the usual atmospheric interaction involves the evasion of carbon dioxide from surface waters, which forms an important part of the global carbon budget [*Cole et al.*, 2007; *Butman & Raymond*, 2011]. The significance of the Elevation covariate on pH in this study suggests that the lower pH values, which typically were associated with the higher elevations of the Millstone Grit and Bowland High and Craven Groups, may relate to the greater amounts of rainfall (presumed to be weakly acidic) across the Forest of Bowland topography.

5.4.4   Does compartmentalisation affect surface water quality?

The Woodsfold fault (Figure 5.2) is considered to form a low-permeability groundwater barrier in the central and southern Fylde [*Ove Arup and Partners Ltd.*, 2014a], compartmentalising this part of the Bowland Basin (see Chapter 4). On the west side of the fault groundwater in the Sherwood Sandstone Group is of brine nature [*BGS*, 2018a] whereas on the east side fresh water abstractions occur (Figure 5.9) [*Mott MacDonald*, 1997; 2010]. Furthermore, groundwater levels either side of the fault are different, decreasing from 5-10 m above OD east of the fault to 16.8 m below OD west of the fault [*Ove Arup and Partners Ltd.*, 2014a; 2014c]. The three-way ANOVA on surface water quality data showed no significant evidence of compartmentalisation across the Woodsfold fault, indicating no transfer of compartmentalisation to surface waters. It was not possible to support this interpretation with variance analysis that incorporated groundwater data because there is a paucity of groundwater boreholes, and hence data, in this area (see Figure 4.1).

The absence of evidence of a significant compartmentalising effect could result from a lack of data, for example not enough surface water bodies (and hence samples) cross-cut the fault in question, or the determinands measured were not sensitive enough. However, the measurements were sensitive enough to show the impact of underlying bedrock geology on surface water quality (there was a significant difference in surface water quality between the Mercia Mudstone and Sherwood Sandstone Groups) and the power analysis showed that the survey design was capable of detecting a difference smaller than that observed between the bedrock formations. Together these results indicate that the mineralogical change in geological bedrock formation affected surface water quality but not the groundwater barrier effect of the Woodsfold fault. It is proposed that although surface waters appear to interact with a weathered bedrock layer via shallow circulation through glaciofluvial sands and gravels of the superficial deposits, there is no

chemical evidence to suggest that deeper groundwater from the Mercia Mudstone Group, or below, was rising to the surface in response to the Woodsfold fault acting as a barrier.

5.4.5 Implications for shale gas exploration

Groundwater-surface water interactions may indicate potential two-way contaminant pathways exist. Identifying and understanding these pathways is therefore essential for assessing the water contamination risks posed by surface and subsurface operations related to shale gas activities, or indeed other anthropogenic activities. Although groundwater monitoring boreholes are undoubtedly useful for this purpose, there may be a lack of existing boreholes or temporal and financial constraints on drilling new boreholes [e.g. *DiGiulio et al.*, 2011]. In contrast, surface water sampling (providing a surface water system exists across the prospective basin) can be quicker, cheaper and more spatially comprehensive than groundwater samples. If the underlying bedrock geology is known, and an informed conceptual hydrological model exists, surface water samples could be used with or without groundwater samples to infer groundwater-surface water interactions. An additional issue to consider are transient hydraulic effects, for example surface waters may be gaining or losing at different points of the year in response to seasonal precipitation or human-induced effects such as abstraction [*Sophocleous*, 2002]. As a result, the receptors of potential contaminants would also change in response to directional flow changes in the pathway.

For the Bowland Basin surface water quality data indicated regional-scale groundwater-surface water interaction through the superficial deposits, highlighting the importance of localised investigations to identify specific pathways and receptors in shale gas environmental risk assessments. For sites located west of the Woodsfold fault, the thickness of the Mercia Mudstone Group appears to provide a hydraulic barrier between

groundwater in the underlying Sherwood Sandstone Group and groundwater in the overlying superficial deposits, as well as surface waters; although Ca and SO_4 signatures from proposed gypsum dissolution in the Mercia Mudstone Group were detectable in surface waters, the surface water quality data were not dominated by Na as would be expected if far more concentrated Na-Cl-rich brines in the underlying Sherwood Sandstone Group were migrating through the Mercia Mudstone Group to the surface.

Chapter 3 showed that compartmentalisation may increase the risk of injected fluids migrating to near-surface aquifers. In the Bowland Basin the Woodsfold fault is considered to compartmentalise the central and southern Fylde. Although the surface water quality sampling and study design was capable of detecting a compartmentalisation signature smaller than that between the underlying bedrock formations, the absence of any compartmentalisation signature indicated that groundwater from the lower levels of the Mercia Mudstone Group, or below, was not rising to surface in response to the Woodsfold fault acting as a barrier. Thus, whilst Chapter 3 suggested compartmentalisation may enhance upward flow to the Sherwood Sandstone, the risk of fluid migration through the overlying Mercia Mudstone Group and to the surface appears to be low in this area of the basin. There remains scope to quantify the timings of shallow groundwater circulation across the basin and investigate if compartmentalisation in other hydrogeological scenarios creates faster, shorter routes for surface discharge.

5.4.6   *Study limitations*

In the Bowland Basin the Wyre and Ribble rivers, and their major tributaries, generally have a baseflow index of ~0.3 [*NRFA*, 2020]. The hot temperatures and lack of precipitation in the 2018 UK summer provided an ideal opportunity to sample surface waters across the Bowland Basin because base flow conditions increased the probability

of detecting chemical groundwater signatures. However, in basins where surface run-off dominates and base flow is minimal, it may not be possible to detect any chemical signatures from groundwater. Conversely, in basins with no surface water system or one with very limited extent, surface sampling is possible or of extremely limited use for understanding the groundwater system and any interaction. Similarly, if bedrock geology does not vary across the basin of interest, it may not be possible to conclude from water quality data that groundwater in bedrock formations interacts with surface waters. On the other hand, differences in surface water quality over the same underlying bedrock geology may indicate localised interactions with groundwater in deeper geological formations. Alternatively, differences in surface water quality may relate to other environmental factors such as changing land use (e.g. increased agricultural and urban runoff on the Fylde leading to elevated ion concentrations) or the geochemistry of any superficial deposits (note that the omission of such factors in this study does not negate the significant effect of bedrock geology).

The chemical analyses in this study were limited to field data and ion concentrations due to financial constraints. The additional analysis of other ion concentrations and isotopes (radiogenic and stable) may improve understanding of groundwater-surface water interactions. For example, Radon-222 concentrates in subsurface waters [*Dimova, et al.*, 2013] and can therefore be used to investigate river/groundwater mixing [*Bertin & Bourg*, 1994] and groundwater discharge in coastal areas and lakes [*Cable et al.,* 1996; *Dimova et al.*, 2013]. Stable strontium isotopes (^{87}Sr/^{86}Sr) have been used effectively as groundwater tracers [e.g. *Bullen et al.,* 1996; *Gosselin et al.,* 2004; *Gunn et al.,* 2006], including in the context of unconventional hydrocarbon resources [*Frost et al.,* 2002; *Chapman et al.*, 2012]. The ratios of stable oxygen (^{18}O/^{16}O) and hydrogen (^{2}H/^{1}H) isotopes are also useful because their ratios in rainfall vary with climatic temperature, thereby providing constraints on water body ages and mixing [*Darling et al.,* 2003;

Abesser et al., 2005; *Bath et al.*, 2006]. Although it is unlikely that isotopic values would be available in sufficient numbers to enable the type of statistically rigorous analyses used in this study, isotopic analyses may provide confirmatory evidence for interpretations drawn from statistical analyses of larger water quality datasets.

Additional non-chemical analyses that could be undertaken to investigate groundwater-surface water interactions include the use of hydrograph and temperature data. Hydrograph data can be used to estimate the contribution of groundwater to river flow (or vice versa) through the calculation of baseflow indices [*Eckhardt*, 2008] and flow accretion values and indices [*Grapes et al.*, 2005]. However, the use of hydrographs in basins such as the Bowland Basin may be limited by the spatial density of gauging stations, which are often only located on major rivers and tributaries. Conversely, water temperature data can often be collected easily from a greater number of locations. Given that groundwater can be warmer or cooler than surface waters, temperature anomalies in surface waters could be used to infer groundwater-surface water interaction [*Briggs et al.*, 2016].

5.5   Conclusions

Identifying groundwater compartmentalisation and groundwater-surface water interactions in prospective shale gas basins is important for understanding potential contaminant pathways. Using surface water quality data from a prospective basin, bedrock geology was shown to be a significant factor influencing surface water quality across the prospective basin, thereby implying regional-scale groundwater-surface water interactions despite the near-ubiquitous presence superficial deposits with an average thickness of 30 to 40 m. Principal component analysis supported this conclusion by showing that surface water compositions were constrained within groundwater end-

member compositions. Surface water quality data showed no relationship with previously identified groundwater compartmentalisation, even though the statistical analysis was of sufficient power to identify the impact of different aquifer geology on the same surface waters. Therefore, although surface waters appear to interact with a weathered bedrock layer via shallow circulation through glaciofluvial sands and gravels of the superficial deposits, there is no chemical evidence to suggest that deeper groundwater in this area of the prospective basin was reaching the surface in response to compartmentalisation-enhanced flow. Consequently, compartmentalisation in this area of the prospective basin does not appear to increase the risk of fracking-related contaminants reaching surface waters.

6 Three-dimensional groundwater modelling of the Fylde

6.1 Introduction

Predicting the subsurface migration routes and timescales of fracking-related fluids ultimately requires numerical modelling because of the spatial and temporal scales involved. Section 1.5 presented an overview of previously published numerical models that investigated the potential upward migration of fracking-related fluids [e.g. *Myers*, 2012; *Birdsell et al.*, 2015]. Two limitations of these models were the use of simplistic geological structure and fluid injection directly into modelled fault or fracture zones. Consequently, in Chapter 3 a real-life fracking operation from the Bowland Basin was modelled with complex geological structure and fluid injection into a fault-bounded compartment, i.e. the strata between two faults. The model scenarios highlighted the importance of deep high-permeability formations and low-permeability faults in controlling the long-term migration of fracking-related fluids [*Wilson et al.*, 2017b]. Nevertheless, one of the main limitations of the model was that it was 2D because of the data available at the time. Since then more subsurface data have been obtained and interpreted, enabling a larger 3D model to be created.

In this chapter a 3D numerical groundwater model of the Fylde area in the Bowland Basin was created from the interpretation of historic 2D seismic reflection data, and a series of groundwater simulations were run. As in Chapter 3, the aims were to: incorporate complex geological structure; investigate how different hydrogeological factors affected the long-term migration of fracking-related fluids at the Preston New Road site; and consider if fracking-related fluids might migrate to the principal aquifer of the region (the Sherwood Sandstone [*Allen et al.*, 1997]). Although aspects of the 3D model were simple compared to previously published models such as that by *Birdsell et al.* [2015] (the 3D model did not include effects such as fluid density contrasts, buoyancy and capillary imbibition), the importance of the model developed in this chapter was to advance the

aims of Chapter 3 into three dimensions. The resulting 3D model is the first 3D basin-scale hydrogeological model used to investigate the long-term migration of fracking-related fluids in a geologically complex prospective shale gas basin. Furthermore, the model construction method is unusual for a groundwater modelling and begins to bridge the gap between groundwater and petroleum reservoir modelling. As a result, this chapter provides an initial methodology for a potential new generation of basin-scale groundwater models that could be used in environmental risk assessments for subsurface fluid-injection operations.

6.2   Approach and methodology

Petroleum borehole and 2D seismic reflection data were used to interpret the 3D subsurface geology of the Fylde area of the Bowland Basin because these data provided subsurface information beyond the depths typically considered for groundwater modelling and abstractions. The resulting geological model was then converted into a hydrogeological model and groundwater simulations of 36 different scenarios were run. The scenarios were chosen to investigate how different hydrogeological factors (cross-basin flow, overpressure, injection, SRV and low-permeability faults) might affect the long-term subsurface migration of fracking-related fluids at the Preston New Road site. Of particular interest, as in Chapter 3, was which combinations (if any) of hydrogeological factors resulted in tracked particles reaching the shallow aquifer.

6.2.1   Geological model

The 2D geological model of Preston New Road from Chapter 3 was based on a schematic geological cross-section in the Environmental Statement submitted as part of development regulations for the site [*Ove Arup and Partners Ltd.*, 2014a]. The creation of a 3D basin-scale groundwater model required the construction of a geological model

174

using the most spatially comprehensive dataset available at the time of writing; 2D seismic reflection data. A description of the seismic reflection data compilation and interpretation can be found in Section 4.2.2 and a map of interpreted lines in Figure 1.11. Unlike Chapter 3 where the presence of the Collyhurst Sandstone was still to be proved by drilling at Preston New Road, the seismic reflection interpretation and 3D geological model construction occurred post-drilling, which had proved the presence of the Collyhurst Sandstone [*Cuadrilla Resources Ltd.*, 2018a]. Horizons were interpolated between 2D seismic lines and smoothed in the time domain as continuous surfaces. Where artefact surfaces were created from the interpolation of complex horizon geometry (e.g. the interpolation of a horizon resulted in parts of its surface lying above the overlying horizon and surface), these were corrected using Petrel's in-built "Eliminate" tool which can be used to delete specified parts of surfaces. The spatial extents of all surfaces were clipped to a boundary polygon corresponding to the interpretation extent of the top of the Bowland Shale, thereby forming a 3D geological model with vertical sides.

The time domain geological model was converted to the depth domain using a velocity model of interval velocities calculated from formation top data of the PH-1 borehole (Table 6.1). This borehole was chosen because it was the most recent borehole for which two-way-times and depths for all interpreted horizons were available. The velocity model was applied to the full extent of the geological model but this simplification was considered adequate for obtaining approximate complex geological geometries for the subsequent numerical modelling.

Table 6.1

*Calculated bulk interval velocities for the major geological units in the Bowland Basin,
based on data from PH-1. Formation top data from the UKOGL [2019].*

Geological unit	Top depth relative to sea level (m)	Bottom depth relative to sea level (m)	Thickness (m)	Top TWT (s)	Bottom TWT (s)	TWT Thickness (s)	Interval velocity (m/s)
Mercia Mudstone Group	-5.1	194.4	199.5	0.000	0.144	0.144	2770
Sherwood Sandstone	194.4	410.7	216.3	0.144	0.285	0.141	3070
St Bees Sandstone	410.7	1016.9	606.2	0.285	0.58	0.295	4110
Manchester Marl	1016.9	1157.1	140.2	0.580	0.649	0.069	4060
Collyhurst Sandstone	1157.1	1233.2	76.1	0.649	0.68	0.031	4910
Millstone Grit	1233.2	1978.6	745.4	0.680	0.992	0.312	4780
Bowland Shale	1978.6			0.992			

6.2.2   Hydrogeological model

The geological model was converted to a hydrogeological model in the USGS open-access GUI "ModelMuse". As explained in Chapter 3 ModelMuse enables the user to create a model grid and input spatial and temporal data such as hydrogeological parameters and boundary conditions [*Winston*, 2009]. The spatial extent of the hydrogeological model domain was defined using the boundary polygon for the extent of the top of the Bowland Shale interpretation. The base of the model domain was set at 3500 m below sea level and the top of the model domain was defined at 0 m elevation because the Fylde is approximately flat and at sea level. Grid cell size in the horizontal directions was set at 250 by 250 m^2 and the grid angle was automatically generated at -8°. The chosen cell size was five times larger than that used in Chapter 3 but was computationally favoured because the 3D basin-scale model was considerably larger. Seven confined layers, corresponding to the interpreted horizons in Petrel, were defined in the model (Table 6.2). These layers were vertically discretised into 27 layers (Table 6.2), with equal spacing within each formation, to allow for more precise hydraulic head calculations and particle tracking.

Table 6.2
Hydraulic parameters for hydrogeological model layers. Hydraulic data from Cai and Ofterdinger [2014].

Layer group (aquifer) name	Vertical discretisation	Horizontal hydraulic conductivity (K_h) (m/s)	K_h/K_v	Porosity (fraction)	Storage Coefficient (S_c)
Mercia Mudstone Group	3	1.0×10^{-7}	100	0.10	1.0×10^{-3}
Sherwood Sandstone	3	1.2×10^{-5}	10	0.23	2.0×10^{-3}
St. Bees Sandstone	4	8.1×10^{-7}	10	0.15	8.6×10^{-5}
Manchester Marl	1	1.0×10^{-8}	10	0.15	2.0×10^{-5}
Collyhurst Sandstone	1	7.9×10^{-5}	10	0.26	5.0×10^{-4}
Millstone Grit	5	7.9×10^{-8}	10	0.08	1.0×10^{-4}
Bowland Shale	10	6.0×10^{-8}	10	0.03	1.0×10^{-4}

The seven layers in the hydrogeological model were initially defined in ModelMuse as horizontal layers but their depths were adjusted to the geological structure of the basin using the interpolated surfaces from Petrel (Figure 6.1). This process involved: exporting the surfaces as point shapefiles from Petrel to ArcScene 10.3; reformulating the shapefiles in ArcScene to include a depth attribute; importing the new shapefiles to ModelMuse as objects; creating new depth datasets using the imported shapefile attributes; and finally editing the layer definitions to the appropriate depth datasets. It was also necessary to include "If" logical functions to ensure layer surfaces did not vertically cross over. Consistent with Chapter 3 the porosities, storage coefficients and typical horizontal and vertical hydraulic conductivities defined by *Cai and Ofterdinger* [2014] were used to populate the 3D model layers (Table 6.2). Hydraulic properties were assigned to layers using the "Case" logical function, with the index set as "Layer" and hydraulic properties assigned as the results in the formula. This approach contrasted with that in Chapter 3 where objects in ModelMuse were used to assign hydraulic properties to each geological formation. This previous approach was not possible for the 3D model because of the 3D nature and geological complexity of the model.
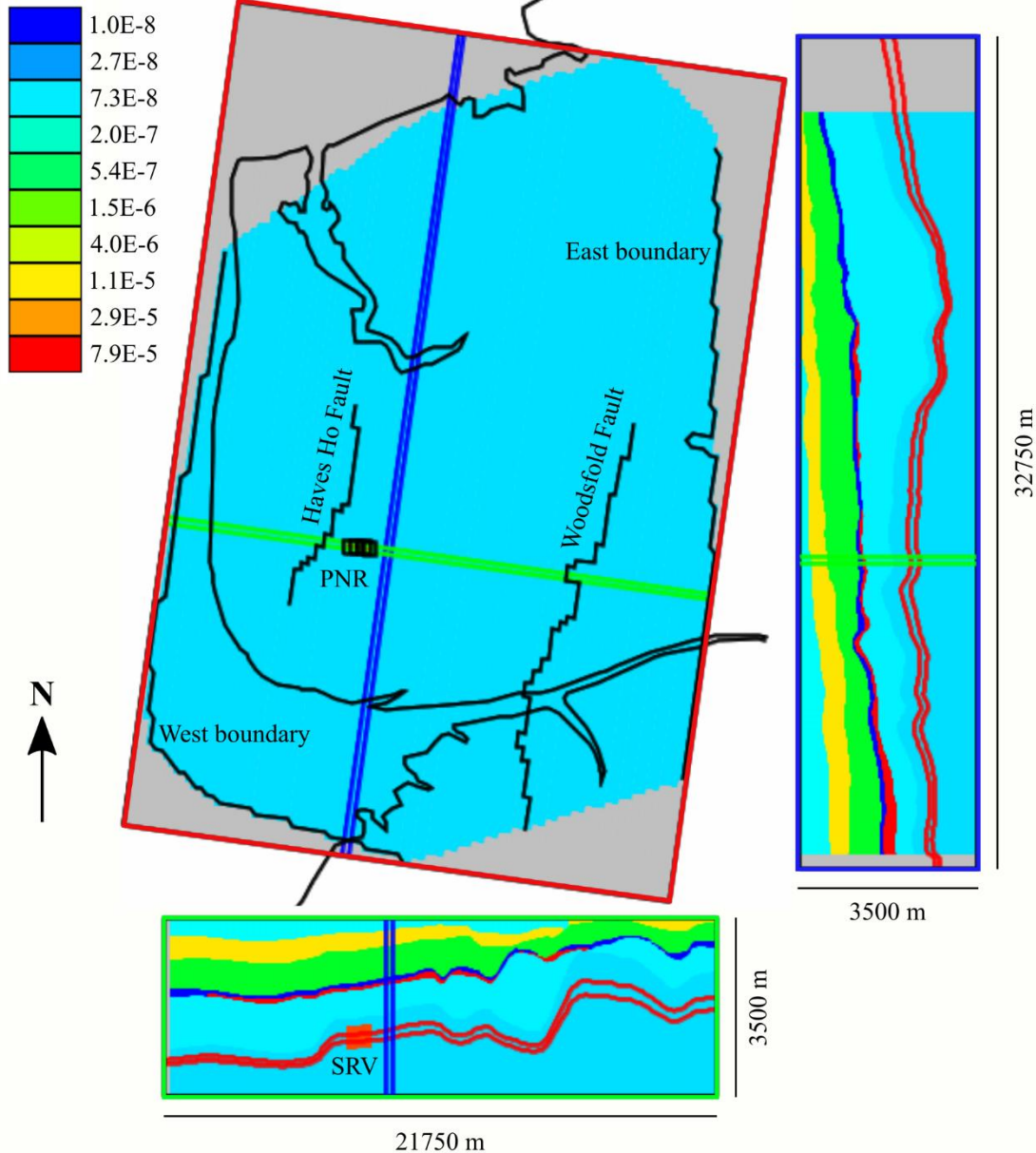
Figure 6.1

The 3D hydrogeological model in ModelMuse (red outline – map view, blue outline – west view and green outline – north view). The modelled stimulated reservoir volume (SRV) associated with the Preston New Road (PNR) site and the two low-permeability faults are also shown. Grid cells are not shown for figure clarity.

6.2.3 Boundary conditions

Models created in ModelMuse can be run using the associated MODFLOW finite-difference groundwater code, which simulates steady and transient groundwater flow in irregularly shaped flow systems subject to external stresses such as wells, areal recharge,

evapotranspiration, drains and rivers [*McDonald & Harbaugh*, 1984]. For consistency with Chapter 3 this chapter used the version MODFLOW-2005 [*Harbaugh*, 2005], despite the more recent release of MODFLOW 6 and its associated Groundwater Flow (GWF) Model [*Hughes et al.*, 2017; *Langevin et al.*, 2017].

Four boundary conditions were considered in the modelled scenarios: a horizontal hydraulic head gradient present representing topographically driven cross-basin groundwater flow; no horizontal hydraulic head gradient present; a vertical hydraulic head gradient present representing overpressure within the Bowland Shale; and no vertical hydraulic head gradient present (Table 6.3). The horizontal hydraulic head gradient was generated by applying fixed hydraulic head values of 3500 and 3600 m to the west and east model boundaries, respectively. A difference in hydraulic head of 100 m across the ~20 km wide model domain equated to a horizontal hydraulic head gradient of ~0.5%, which was consistent with previous models of the Bowland Basin [*Cai & Ofterdinger*, 2014; *Wilson et al.*, 2017b]. The horizontal hydraulic head gradient generates cross-basin groundwater flow from east to west to simulate topographically driven groundwater flow created by the ~500 m elevation difference between the upland Forest of Bowland and the low-lying Fylde coastal plain. Although this contradicted the considered lack of recharge between the Carboniferous strata and Sherwood Sandstone in the northern and central Fylde [*Mott MacDonald*, 1997], it was simplest to model cross-basin flow across the whole model domain and there is no evidence to suggest recharge does not occur across the deeper formations. The horizontal hydraulic head gradient was removed from half of the model scenarios by changing the fixed hydraulic head value at the eastern boundary to 3500 m, i.e. the difference in hydraulic head horizontally across the model domain was 0 m. The datum for hydraulic head was the base of the model domain, i.e. for a constant head boundary of 3500 m the hydraulic heads at the top and base of the model were the result of the elevation and pressure heads, respectively.

A vertical hydraulic head gradient was generated in half the modelled scenarios by applying a fixed head value of 4900 m to the entire lower boundary of the model domain. A hydraulic head value of 4900 m corresponded to ~40% overpressure in the Bowland Shale, which is what has been measured at PH-1 [*Cai & Ofterdinger*, 2014]. The vertical hydraulic head gradient was removed from the remaining scenarios by removing the fixed hydraulic head boundary at the base of the model domain. No rainfall recharge was assigned to the model top under the assumptions that little rainfall recharge reaches deeper than the Mercia Mudstone and Sherwood Sandstone Groups in the Fylde, and that any recharge would be negligible compared to the groundwater volumes involved in a model of this spatial extent and depth. All head boundaries were implemented as constant head boundaries to ensure that the cross-basin flow and overpressure conditions remained constant for the duration of the 10000 year simulations (constant head boundaries have an infinite capacity to supply and remove water from the model). Constant head boundaries provided the simplest boundary conditions to observe the effects of the considered hydrogeological factors. As explained in Section 3.2.4, the stress effects of the modelled fluid injection volumes were likely to be negligible and short-lived (even more so in the 3D model because the total injection volume was less and the groundwater volumes were substantially larger).

Table 6.3

List of modelled scenarios. Scenarios with no fluid injection are natural scenarios. "Yes" versus "No" refers to the presence or absence, respectively, of that hydrogeological factor in the scenario.

Scenario number	Cross-basin flow	Overpressure	Woodsfold fault	Fluid injection	SRV	Haves Ho fault
1	Yes	No	No	No	No	No
2	Yes	No	No	Yes	No	No
3	Yes	No	No	Yes	Yes	No
4	No	No	No	No	No	No
5	No	No	No	Yes	No	No
6	No	No	No	Yes	Yes	No
7	Yes	Yes	No	No	No	No
8	Yes	Yes	No	Yes	No	No
9	Yes	Yes	No	Yes	Yes	No
10	No	Yes	No	No	No	No
11	No	Yes	No	Yes	No	No
12	No	Yes	No	Yes	Yes	No
13	Yes	No	Yes	No	No	No
14	Yes	No	Yes	Yes	No	No
15	Yes	No	Yes	Yes	Yes	No
16	No	No	Yes	No	No	No
17	No	No	Yes	Yes	No	No
18	No	No	Yes	Yes	Yes	No
19	Yes	Yes	Yes	No	No	No
20	Yes	Yes	Yes	Yes	No	No
21	Yes	Yes	Yes	Yes	Yes	No
22	No	Yes	Yes	No	No	No
23	No	Yes	Yes	Yes	No	No
24	No	Yes	Yes	Yes	Yes	No
25	Yes	No	Yes	No	No	Yes
26	Yes	No	Yes	Yes	No	Yes
27	Yes	No	Yes	Yes	Yes	Yes
28	No	No	Yes	No	No	Yes
29	No	No	Yes	Yes	No	Yes
30	No	No	Yes	Yes	Yes	Yes
31	Yes	Yes	Yes	No	No	Yes
32	Yes	Yes	Yes	Yes	No	Yes
33	Yes	Yes	Yes	Yes	Yes	Yes
34	No	Yes	Yes	No	No	Yes
35	No	Yes	Yes	Yes	No	Yes
36	No	Yes	Yes	Yes	Yes	Yes

6.2.4 Low-permeability faults and compartmentalisation

To investigate the influence of low-permeability faults and potential compartmentalisation effects, two faults were modelled explicitly as flow barriers in some of the scenarios. These faults were the Woodsfold and Haves Ho faults (Figure 6.1). The Woodsfold fault, which lies to the east of Preston New Road is known to be a low-permeability barrier to groundwater flow in the central and southern Bowland Basin (see Chapter 4). The Woodsfold fault was included in 24 of the 36 modelled scenarios (Table 6.3). The Haves Ho fault, which lies directly to the west of Preston New Road has unknown hydraulic properties but was hypothetically included as a low-permeability barrier in 12 of the modelled scenarios where the Woodsfold fault was also included (Table 6.3). Both faults were included as vertical features extending from top to bottom of the model domain using the Horizontal Flow Barrier (HFB) package in ModelMuse and MODFLOW. Fault thickness was set at the default value of 1 m and hydraulic conductivity was set at 1.0×10^{-12} m/s, consistent with the low-permeability fault scenarios in Chapter 3.

6.2.5 Stress periods, fluid injection and stimulated reservoir volume

Scenario simulations included either two or three stress periods. All simulations included an initial steady state stress period to allow hydraulic heads to reach a steady state given the imposed boundary conditions. In scenarios with no anthropogenic fluid injection, a final transient stress period of 10000 years followed the steady state stress period. These simulations represented natural groundwater scenarios and allowed comparisons to be made to those with fluid injection. For scenarios with fluid injection, two transient stress periods followed the initial steady state period; a fluid injection period followed by a 10000 year period.

Twenty four of the modelled scenarios had water injected into the model domain to represent subsurface fluid injection at Preston New Road. The location and volume of water injected into the scenarios was based on the original hydraulic fracture plan for the PNR-2 borehole [*Cuadrilla Resources Ltd.*, 2017]. The horizontal portion of the borehole was ~1 km long and was therefore modelled across four grid cells. Using the Well package (WEL) in ModelMuse and MODFLOW, water was injected as a point source simultaneously into the four grid cells at a rate of 0.06 m^3/s for 143437.5 s, which equated to a cell injection volume of 8606.25 m^3 and a total injection volume of 34425 m^3. This total fluid volume was equal to the maximum possible injection volume from the hydraulic fracture plan (45 injection stages each with a volume of 765 m^3). Flowback and production volumes were not accounted for, thereby representing a worst-case scenario where all fluids are injected into the borehole, the borehole is shut in and then abandoned before any fluids can be recovered and pressure reduced.

Twelve of the modelled scenarios with fluid injection also had a SRV represented. Due to software limitations the fracturing process creating the SRV was not modelled explicitly. Alternatively, the hydraulic conductivities of the strata surrounding the PNR-2 borehole were increased by a factor of 1000 to represent the increase in hydraulic conductivity caused by stable induced fractures [*Gaskari & Mohaghegh*, 2006]. This change in hydraulic conductivity was applied after steady state simulation but prior to fluid injection, which required the initial steady state stress periods to be modelled as separate simulations and their outputs used as the starting conditions for the transient stress periods. The extent of the SRV was taken as the predicted vertical fracture length of 133 m from the hydraulic fracture plan [*Cuadrilla Resources Ltd.*, 2017]. This extent was applied in both the vertical and horizontal directions, meaning that the SRV remained within the Bowland Shale (Figure 6.1).

6.2.6 *Particle tracking*

Particle tracking using the MODPATH Version 6 package in ModelMuse and MODFLOW was used to investigate the potential subsurface migration of injected fluids. MODPATH is a post-processing particle tracking code which computes 3D groundwater flow paths using the output from MODFLOW groundwater flow simulations [*Pollock*, 2012]. For all modelled scenarios without a SRV, particles were initiated in the centre of each of the four grid cells corresponding to the horizontal portion of the PNR-2 borehole. For scenarios without fluid injection, particles were released and tracked for 10000 years in the transient stress period directly following the initial steady state stress period. For scenarios with fluid injection, particles were released at the start of injection and tracked until the end of the following 10000 year transient stress period. For scenarios with an SRV present, an additional set of particles were released at the upper edge of the SRV following the end of the injection period. This approach assumed that injected fluid reached the edge of the SRV, although it is unclear if this always occurs in practice. Particle tracks for each scenario were qualitatively examined and end formations were recorded.

6.2.7 *Scenario design and statistical analysis*

As in Chapter 3 the scenario design used in this study was a factorial design. Six single factors (cross-basin flow, overpressure, injection, SRV, Woodsfold fault and Haves Ho fault) were considered with each factor having two levels; these were the presence or absence of that factor in the scenario. The SRV factor was only considered in scenarios with fluid injection present. The Haves Ho fault factor was only considered in scenarios with the Woodsfold fault present. Overall this led to a total of 36 modelled scenarios

(Table 6.3). Two-way factor interactions were also considered where possible, which equated to 13 factor interactions.

Analysis of variance (ANOVA) in Minitab (v.18) was used to assess significant factors which decreased particle travel times towards the surface. As reported in the following results (Section 6.3.1), no particles reached the Sherwood Sandstone and so it was decided to consider particle travel times to the Collyhurst Sandstone in the ANOVA. Scenarios where particles did not reach the Collyhurst Sandstone within the 10000 year simulation time were assigned an arbitrary travel time of 15000 years. Statistical significance was judged at the 95% probability of the factor not having zero effect. The proportion of the variance explained by significant factors and interactions was calculated using the generalised ω^2 method [*Olejnik & Algina*, 2003]. The factor effects are reported as least squares means (marginal means) as these are the best measure of the average after allowing for the influence of the other factors.

6.3   Results

6.3.1   Overview

Of the 36 scenarios simulated no scenarios resulted in particles reaching the Sherwood Sandstone aquifer within 10000 years (Table 6.4). The shallowest formation reached by tracked particles was the Collyhurst Sandstone. Scenarios where particles reached the Collyhurst Sandstone always had the overpressure boundary present. Particles reached the Collyhurst Sandstone irrespective of the inclusion of faults, injection and a SRV (scenarios 7 to 12, 19 to 24 and 31 to 36) (Table 6.4), with travel times ranging from 280 to 390 years. Particle movement to the Collyhurst Sandstone was always essentially vertical; horizontal movement was approximately only ≤250 m. On reaching the Collyhurst Sandstone particles moved within the formation in an approximately south-westward direction, moving out under the Irish Sea until reaching the edge of the model

domain (Figure 6.2). This horizontal movement occurred for scenarios with and without

the cross-basin flow generated by the boundary conditions.

Table 6.4
Results of particle tracking. Scenarios with no fluid injection are natural scenarios.

Scenario number	Cross-basin flow	Overpressure	Woodsfold fault	Fluid injection	SRV	Haves Ho fault	Particle tracking end formation	Time to Collyhurst Sandstone to nearest 10 years
1	Yes	No	No	No	No	No	Bowland Shale	15000
2	Yes	No	No	Yes	No	No	Bowland Shale	15000
3	Yes	No	No	Yes	Yes	No	Millstone Grit	15000
4	No	No	No	No	No	No	Bowland Shale	15000
5	No	No	No	Yes	No	No	Bowland Shale	15000
6	No	No	No	Yes	Yes	No	Bowland Shale	15000
7	Yes	Yes	No	No	No	No	Collyhurst Sandstone	370
8	Yes	Yes	No	Yes	No	No	Collyhurst Sandstone	370
9	Yes	Yes	No	Yes	Yes	No	Collyhurst Sandstone	280
10	No	Yes	No	No	No	No	Collyhurst Sandstone	370
11	No	Yes	No	Yes	No	No	Collyhurst Sandstone	370
12	No	Yes	No	Yes	Yes	No	Collyhurst Sandstone	270
13	Yes	No	Yes	No	No	No	Bowland Shale	15000
14	Yes	No	Yes	Yes	No	No	Bowland Shale	15000
15	Yes	No	Yes	Yes	Yes	No	Millstone Grit	15000
16	No	No	Yes	No	No	No	Bowland Shale	15000
17	No	No	Yes	Yes	No	No	Bowland Shale	15000
18	No	No	Yes	Yes	Yes	No	Bowland Shale	15000
19	Yes	Yes	Yes	No	No	No	Collyhurst Sandstone	370
20	Yes	Yes	Yes	Yes	No	No	Collyhurst Sandstone	370
21	Yes	Yes	Yes	Yes	Yes	No	Collyhurst Sandstone	280
22	No	Yes	Yes	No	No	No	Collyhurst Sandstone	370
23	No	Yes	Yes	Yes	No	No	Collyhurst Sandstone	370
24	No	Yes	Yes	Yes	Yes	No	Collyhurst Sandstone	280
25	Yes	No	Yes	No	No	Yes	Bowland Shale	15000
26	Yes	No	Yes	Yes	No	Yes	Bowland Shale	15000
27	Yes	No	Yes	Yes	Yes	Yes	Millstone Grit	15000
28	No	No	Yes	No	No	Yes	Bowland Shale	15000
29	No	No	Yes	Yes	No	Yes	Bowland Shale	15000
30	No	No	Yes	Yes	Yes	Yes	Bowland Shale	15000
31	Yes	Yes	Yes	No	No	Yes	Collyhurst Sandstone	390
32	Yes	Yes	Yes	Yes	No	Yes	Collyhurst Sandstone	390
33	Yes	Yes	Yes	Yes	Yes	Yes	Collyhurst Sandstone	300
34	No	Yes	Yes	No	No	Yes	Collyhurst Sandstone	390
35	No	Yes	Yes	Yes	No	Yes	Collyhurst Sandstone	390
36	No	Yes	Yes	Yes	Yes	Yes	Collyhurst Sandstone	300
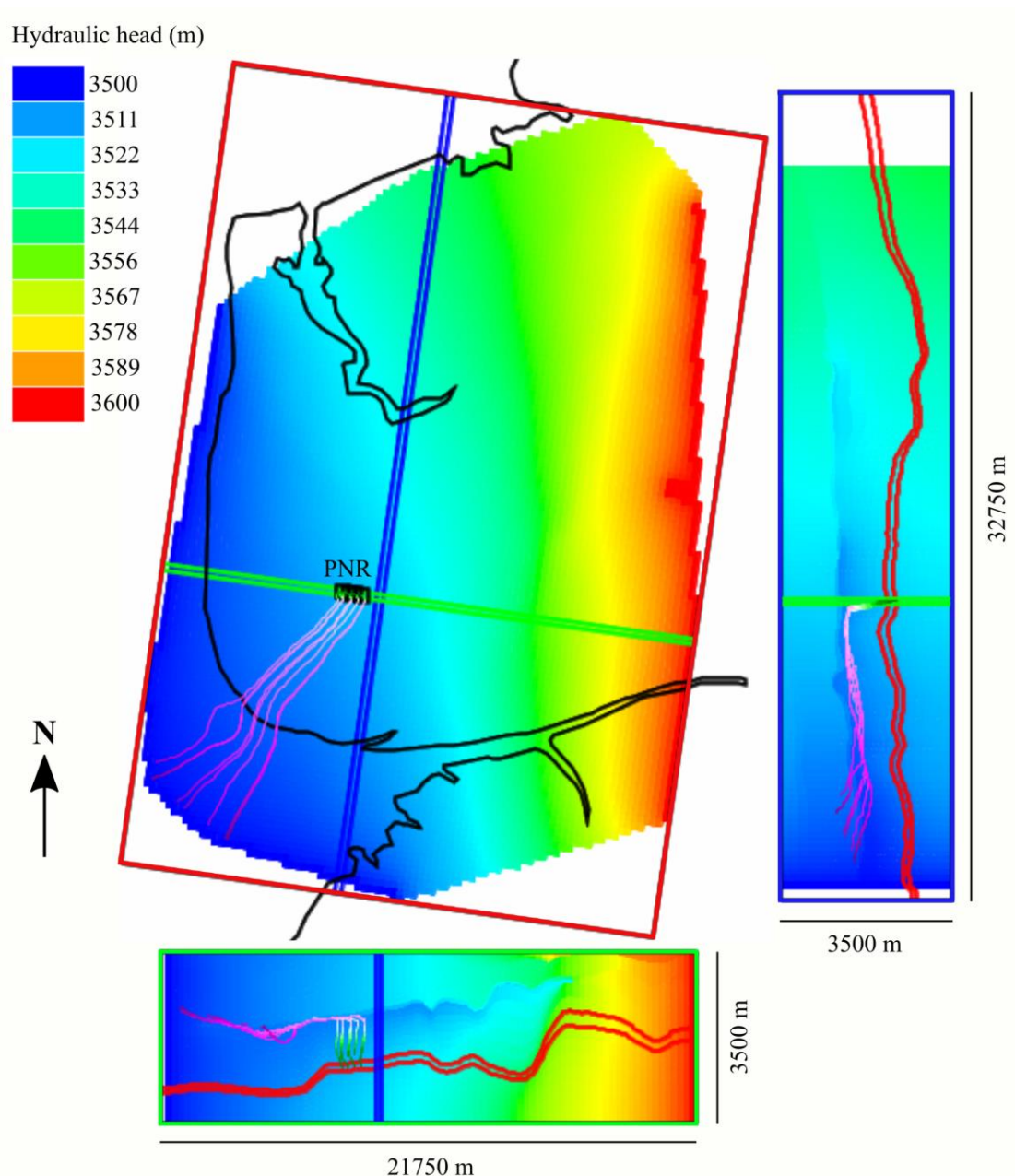
Figure 6.2
Hydraulic head and particle tracks (green to magenta lines) at the end of simulating scenario 9 (red outline – map view, blue outline – west view and green outline – north view). Particles migrated upwards to the Collyhurst Sandstone before travelling laterally south-westward within the Collyhurst Sandstone. Note that although particles appear to have migrated shallower than the Collyhurst Sandstone, this is simply an artefact of the presented cross-sections. Grid cells are not shown for figure clarity.

No scenarios without overpressure resulted in particles reaching the Collyhurst Sandstone within 10000 years. Instead, particles remained within the Bowland Shale (scenarios 1 to 6, 13 to 18 and 25 to 30) (Table 6.4). The exceptions to this were scenarios

3, 15 and 17, where the inclusion of cross-basin flow and a SRV allowed particles to move south-westward into the overlying Millstone Grit (Table 6.4). When cross-basin flow and injection were excluded, particles remained stationary for the 10000 years (scenarios 4, 16 and 28). The addition of injection (maintaining no cross-basin flow) resulted in horizontal particle movement into the immediately adjacent east-west grid cells (scenarios 5, 17 and 29). The further addition of a SRV (still maintaining no cross-basin flow) resulted in particles moving upwards from the injection points to the edge of the SRV or remaining stationary at the release point on the edge of the SRV (scenarios 6, 18 and 30). Particles did not migrate beyond the SRV, and therefore remained within the Bowland Shale. In scenarios with no overpressure the inclusion of cross-basin flow resulted in particles moving further within the Bowland Shale than scenarios without cross-basin flow (scenarios 1, 2, 13, 14, 25 and 26). Particles travelled south-westward for ~1.1 to 1.4 km with a vertical movement of ~0.2 to 0.4 km (Figure 6.3).

When the Woodsfold fault was included in scenarios as a low-permeability barrier, there was no difference to the particle end formation after 10000 years or the time taken to reach the Collyhurst Sandstone (Table 6.4). Likewise, the inclusion of the Haves Ho fault made no difference to the end formation results. However, the travel times to reach the Collyhurst Sandstone in scenarios with both the Haves Ho fault and overpressure present were 20 years longer than scenarios where the Haves Ho fault wasn't present as a low-permeability barrier.
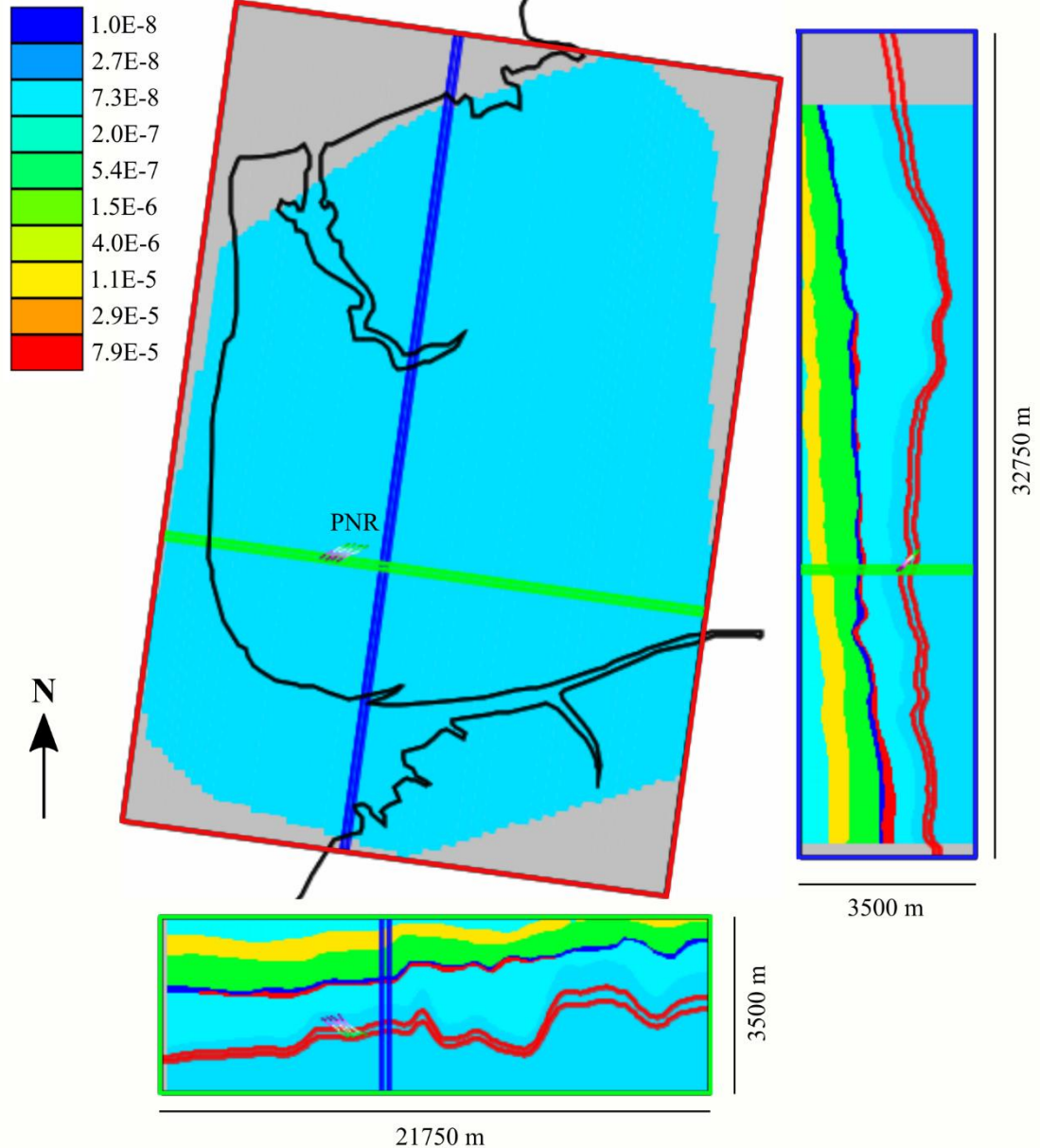
Figure 6.3
Particle tracks (green to magenta lines) for scenario 1 simulation (red outline – map view, blue outline – west view and green outline – north view). Particles remained within the Bowland Shale (lowermost coloured layer) after 10000 year simulation time. Grid cells are not shown for figure clarity.

6.3.2 ANOVA

The single factors of overpressure, SRV and Haves Ho fault were found to have a statistically significant impact on particle travel times to the Collyhurst Sandstone. All three factors had probabilities of <0.0005 of having zero effect (Table 6.5). As measured

189

by the generalised ω^2 method, the overpressure factor explained 50.1% of the variation in travel time to the Collyhurst Sandstone. The mean particle travel time for scenarios with overpressure present was 334 ± 1 years. When overpressure was absent mean travel times were 15000 ± 1 years, which corresponded to the arbitrary time limit chosen for the ANOVA. The SRV and Haves Ho fault explained substantially less of the variation than overpressure (0.0004 and 0.00002%, respectively). For the SRV factor mean travel times decreased by 46 years for scenarios with a SRV present (Table 6.5). For the Haves Ho fault factor mean travel times increased by 10 years when the Haves Ho fault was present as a low-permeability barrier (Table 6.5).

From the 13 possible factor interactions, two interactions were statistically significant: overpressure with a SRV; and overpressure with the Haves Ho fault. When overpressure was absent in both interactions mean travel times were 15000 ± 1 years (Table 6.5). When overpressure was present the inclusion of a SRV reduced mean travel times by 92 years. In contrast, the presence of the Haves Ho fault as a low-permeability barrier increased mean travel times by 20 years (Table 6.5). The interaction between the overpressure and SRV factors explained 0.0007% of the variation in travel time to the Collyhurst Sandstone. The interaction between overpressure and the Haves Ho fault explained 0.00003% of the variation. This result confirmed that overpressure was the most important factor or interaction in the ANOVA and thus the most important hydrogeological factor in controlling particle movement and travel times to the Collyhurst Sandstone.

Table 6.5

Factor and factor interaction results from the ANOVA on particle travel times to the Collyhurst Sandstone.

Factor or factor interaction	P-value	Factor options		Mean (years)	Standard error of mean (years)
Cross-basin flow	0.176	No		7666	1
		Yes		7667	1
Overpressure	<0.0005	No		15000	1
		Yes		334	1
Injection	1.000	No		7667	1
		Yes		7667	0
SRV	<0.0005	No		7690	0
		Yes		7644	1
Woodsfold fault	0.153	No		7666	1
		Yes		7668	0
Haves Ho fault	<0.0005	No		7662	0
		Yes		7672	1
Cross-basin flow *Overpressure	0.332	No	No	15000	1
		No	Yes	333	1
		Yes	No	15000	1
		Yes	Yes	335	1
Cross-basin flow *Woodsfold fault	0.238	No	No	7665	1
		No	Yes	7667	1
		Yes	No	7667	1
		Yes	Yes	7668	1
Cross-basin flow *Injection	1.000	No	No	7666	1
		No	Yes	7666	1
		Yes	No	7667	1
		Yes	Yes	7667	1
Cross-basin flow *SRV	0.238	No	No	7690	1
		No	Yes	7643	1
		Yes	No	7690	1
		Yes	Yes	7645	1
Cross-basin flow *Haves Ho fault	1.000	No	No	7661	1
		No	Yes	7671	1
		Yes	No	7662	1
		Yes	Yes	7672	1
Overpressure *Woodsfold fault	0.238	No	No	15000	1
		No	Yes	15000	1
		Yes	No	333	1
		Yes	Yes	335	1
Overpressure *Injection	1.000	No	No	15000	1
		No	Yes	15000	1
		Yes	No	334	1
		Yes	Yes	334	1
Overpressure *SRV	<0.0005	No	No	15000	1
		No	Yes	15000	1
		Yes	No	380	1
		Yes	Yes	288	1
Overpressure *Haves Ho fault	<0.0005	No	No	15000	1
		No	Yes	15000	1
		Yes	No	324	1
		Yes	Yes	344	1
Woodsfold fault *Injection	1.000	No	No	7666	1
		No	Yes	7666	1
		Yes	No	7668	1
		Yes	Yes	7668	0
Woodsfold fault *SRV	0.153	No	No	7690	1
		No	Yes	7643	1
		Yes	No	7690	0
		Yes	Yes	7645	1
Injection *Haves Ho fault	1.000	No	No	7662	1
		No	Yes	7672	1
		Yes	No	7662	0
		Yes	Yes	7672	1
SRV *Haves Ho fault	1.000	No	No	7685	0
		No	Yes	7695	1
		Yes	No	7639	1
		Yes	Yes	7649	1

6.4   Discussion

6.4.1   *Comparison to Chapter 3 results*

In the 3D scenarios of this chapter no tracked particles reached the Sherwood Sandstone aquifer within the 10000 year simulation time. In contrast, in 18 of the 91 scenarios in Chapter 3 particles reached the aquifer within 10000 years. The following sections compare and discuss the factor results from this chapter and Chapter 3.

6.4.1.1   *Collyhurst Sandstone*

All scenarios from Chapter 3 where particles reached the Sherwood Sandstone had the Collyhurst Sandstone absent from the model domain. The absence of the Collyhurst Sandstone was found to be a statistically significant factor decreasing particle travel times to the Sherwood Sandstone. When the Collyhurst Sandstone was included in the scenarios it allowed eastward horizontal movement of particles within itself, rather than the vertical passage of particles through it and towards the aquifer, i.e. it acted as a deep high-permeability protective formation. All scenarios in the 3D modelling of this chapter had the Collyhurst Sandstone included because its presence at Preston New Road had since been proved by drilling [*Cuadrilla Resources Ltd.*, 2018a]. As in Chapter 3, particles were observed to travel laterally within the Collyhurst Sandstone rather than passing vertically through it and towards the Sherwood Sandstone. The 3D scenario results therefore support the conclusion of Chapter 3 that deep high-permeability formations can be effective barriers to the potential vertical migration of fracking-related fluids. Consequently, identifying and mapping these deep high-permeability formations may be important for predicting the long-term migration routes and receptors of fracking-related fluids. For the Bowland Basin this means better understanding the distribution of the Collyhurst Sandstone, which is present in some areas but absent in others, for example

192

the structural high at Thistleton-1 and east of the Woodsfold fault [*Kirby et al.*, 2000]. In contrast to the 2D scenarios, particles in the Collyhurst Sandstone in the 3D scenarios moved in a south-westwards direction. This difference in particle movement direction likely occurred because of the 3D nature of the boundary conditions and the spatial extent of the modelled low-permeability faults; the faults did not span horizontally across the whole model domain, thereby still allowing a northeast-southwest horizontal hydraulic head gradient to develop across the model domain.

6.4.1.2 Overpressure

Overpressure in this chapter and Chapter 3 was modelled as a vertical hydraulic head gradient generated by a lower boundary condition across the model domains. In Chapter 3 overpressure was a statistically significant factor decreasing particle travel times to the Sherwood Sandstone. The interaction between overpressure and the Collyhurst Sandstone was also statistically significant. The effects of the modelled overpressure were also clear in the 3D scenarios, with overpressure also being a statistically significant factor and accounting for the majority of variation in travel times to the Collyhurst Sandstone. When overpressure was absent from the 3D scenarios particles remained within the Bowland Shale or Millstone Grit for the 10000 year simulation time. In contrast, all scenarios which included overpressure resulted in particles moving to the shallower lying Collyhurst Sandstone. The 3D scenario results therefore supported the conclusion of Chapter 3 that the presence of overpressure increases the vulnerability of shallower formations to fracking-related fluids migrating from below. Nevertheless, the effect of lateral movement within deep high-permeability formations such as the Collyhurst Sandstone may outweigh any vertical migration generated by overpressure, thereby preventing vertical migration to shallow groundwater resources such as fresh water aquifers.

6.4.1.3   SRV

In Chapter 3 the factor of stimulated fracture extent (i.e. the size of the SRV) had three levels: 0, 200 and 600 m. As expected it was found that the greater the stimulated fracture extent, the shorter the mean travel time to the Sherwood Sandstone. In the 3D scenarios of this chapter an SRV was either absent or present, and when one was present the size was fixed for all scenarios. For scenarios without overpressure or cross-basin flow the inclusion of an SRV allowed greater movement of particles within the Bowland Shale. When cross-basin flow was included particles were able to move beyond the Bowland Shale and into the overlying Millstone Grit. In scenarios which included overpressure the addition of a SRV made negligible difference to particle migration routes but did shorten travel times to the Collyhurst Sandstone; in scenario 9 particles reached the Collyhurst Sandstone in 280 years whereas in scenario 8 particles took 370 years to reach the Collyhurst Sandstone (Table 6.4). These results supported the conclusion of Chapter 3 that the extent of the SRV can reduce travel times to shallower formations in the presence of an upward driving force such as overpressure.

6.4.1.4   Low-permeability faults and compartmentalisation

Contrary to common opinion and previous numerical models, low-permeability faults were identified in Chapter 3 as a statistically significant factor decreasing particle travel times to shallow aquifers. In the 2D scenarios low-permeability faults acted to compartmentalise hydraulic head values, thereby discouraging horizontal flow and encouraging vertical flow. The result of compartmentalisation in several scenarios was upward particle migration into the Sherwood Sandstone. In this chapter, 24 of the 36 3D scenarios had the Woodsfold fault included as a low-permeability barrier and, of these 24 scenarios, 12 scenarios also had the Haves Ho fault included as a low-permeability

barrier. The Woodsfold fault was found to be insignificant in the ANOVA and made no difference to particle end formations or travel times to the Collyhurst Sandstone. This result may have occurred because the Woodsfold fault was only modelled as a flow barrier across the central and southern Fylde, thereby still allowing a horizontal hydraulic head gradient to be generated across the model domain. In the 2D model and spatially-limited 3D model of Chapter 3 (see Section 3.4.6.1), the low-permeability faults extended across the whole width of the model domains, thereby limiting the generation of horizontal hydraulic head gradients from the imposed boundary conditions.

The Haves Ho fault was a statistically significant factor in the 3D scenarios of this chapter but inclusion of the Haves Ho fault as a low-permeability barrier increased travel times to the Collyhurst Sandstone by 20 years, contrasting with Chapter 3 where inclusion of low-permeability faults decreased travel times to the Sherwood Sandstone. In the 3D scenarios inclusion of the Haves Ho fault led to lower hydraulic head values to the east of the Haves Ho fault compared to the equivalent scenarios without the Haves Ho fault included (Figure 6.4). The decreased hydraulic head values led to a reduced vertical hydraulic head gradient and therefore resulted in slower particle travel times to the Collyhurst Sandstone. The difference in the 2D and 3D scenario results likely occurred because in the 2D scenarios the Hodder Mudstone, which has a higher permeability than the overlying Bowland Shale [*Cai & Ofterdinger*, 2014], was included to the east of the Haves Ho fault (see Figure. 3.3). The effect of the Hodder Mudstone was to transmit the base overpressure boundary shallower on the east side of the Haves Ho fault. In the 3D scenarios the Hodder Mudstone was not included because of poor borehole constraint and seismic resolution across the Fylde. Consequently, in the 3D scenarios the overpressure boundary was not transmitted shallower on the east side of the Haves Ho fault.
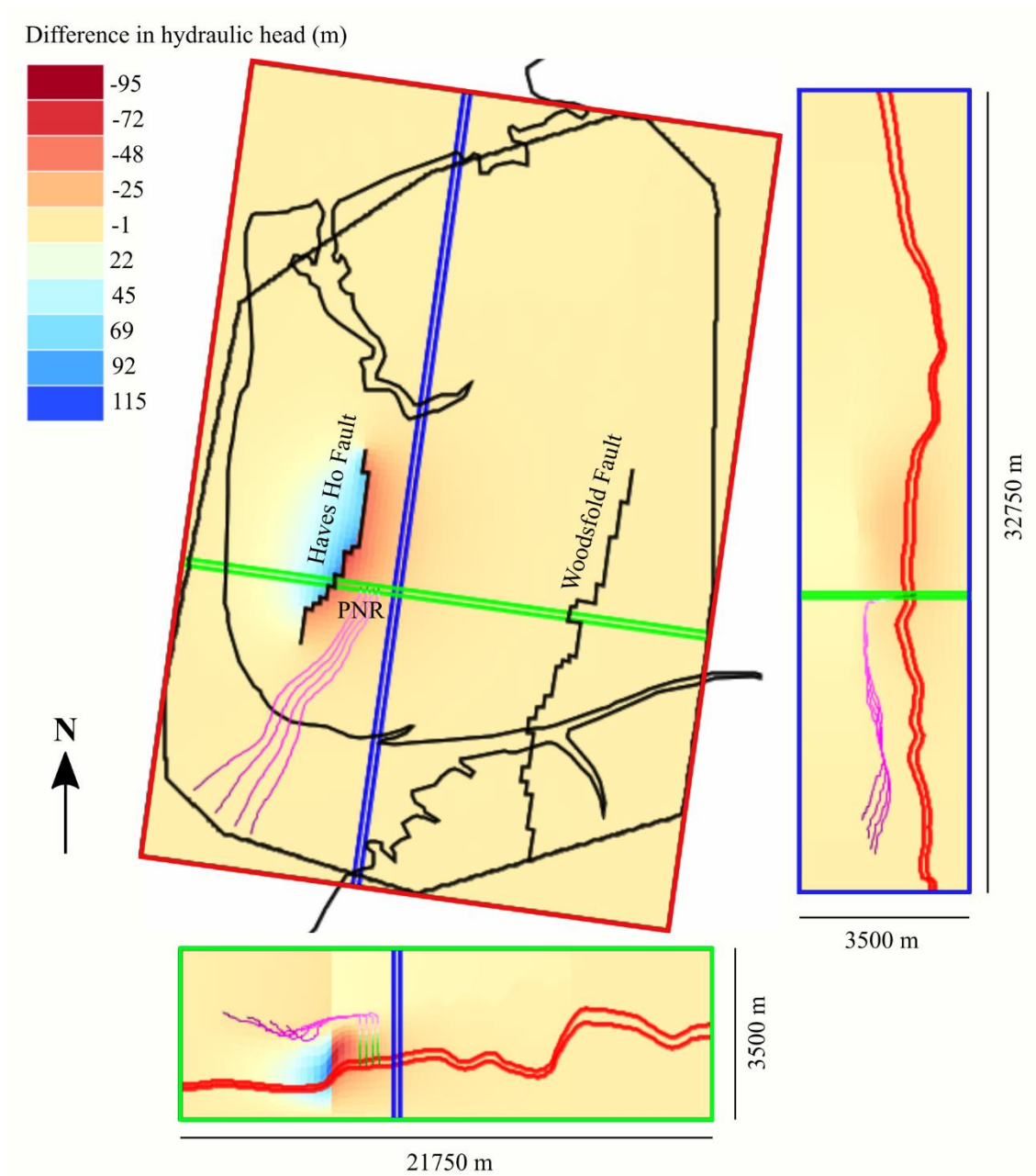
Figure 6.4
Difference in hydraulic head between Scenario 31 (Haves Ho fault included as low-permeability barrier) and Scenario 19 (Haves Ho fault not included as low-permeability barrier) (red outline – map view, blue outline – west view and green outline – north view). Particle tracks for Scenario 31 simulation are shown (green to magenta lines). Grid cells are not shown for figure clarity.

6.4.2   Protective formations in other prospective shale basins

A key result of the 3D modelling, highlighted in Section 6.4.1.1, was the importance of

the Collyhurst Sandstone, a deep high-permeability formation, acting as a protective

formation against the potential upward migration of fracking-related fluids from the Bowland Shale in the Bowland Basin. The Bowland Shale is also considered prospective in several other Early Carboniferous basins in northern England: the Blacon Basin; the Cleveland Basin; the Edale Basin; the Gainsborough Trough; and the Widmerpool Trough (Figure 6.5) [*Andrews*, 2013]. Each prospective basin has different geology due to different depositional and structural histories, with only the Bowland Basin containing the Collyhurst Sandstone. These differences raise the question do other prospective shale basins contain similar deep high-permeability formations that may act as protective formations?

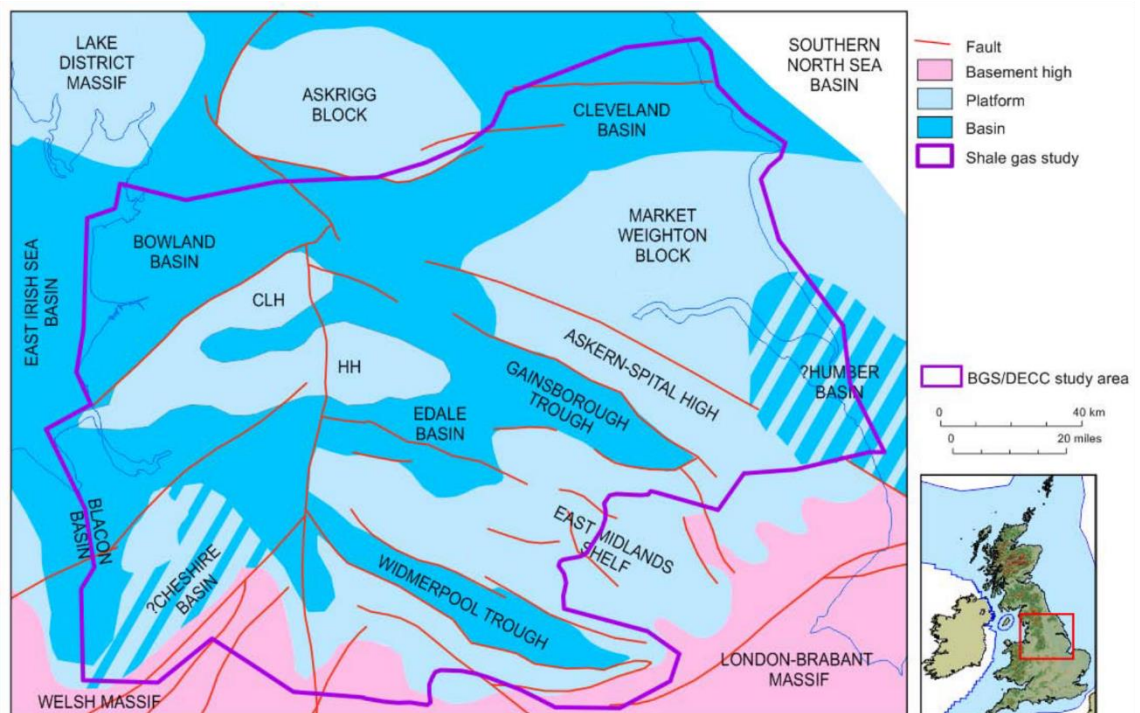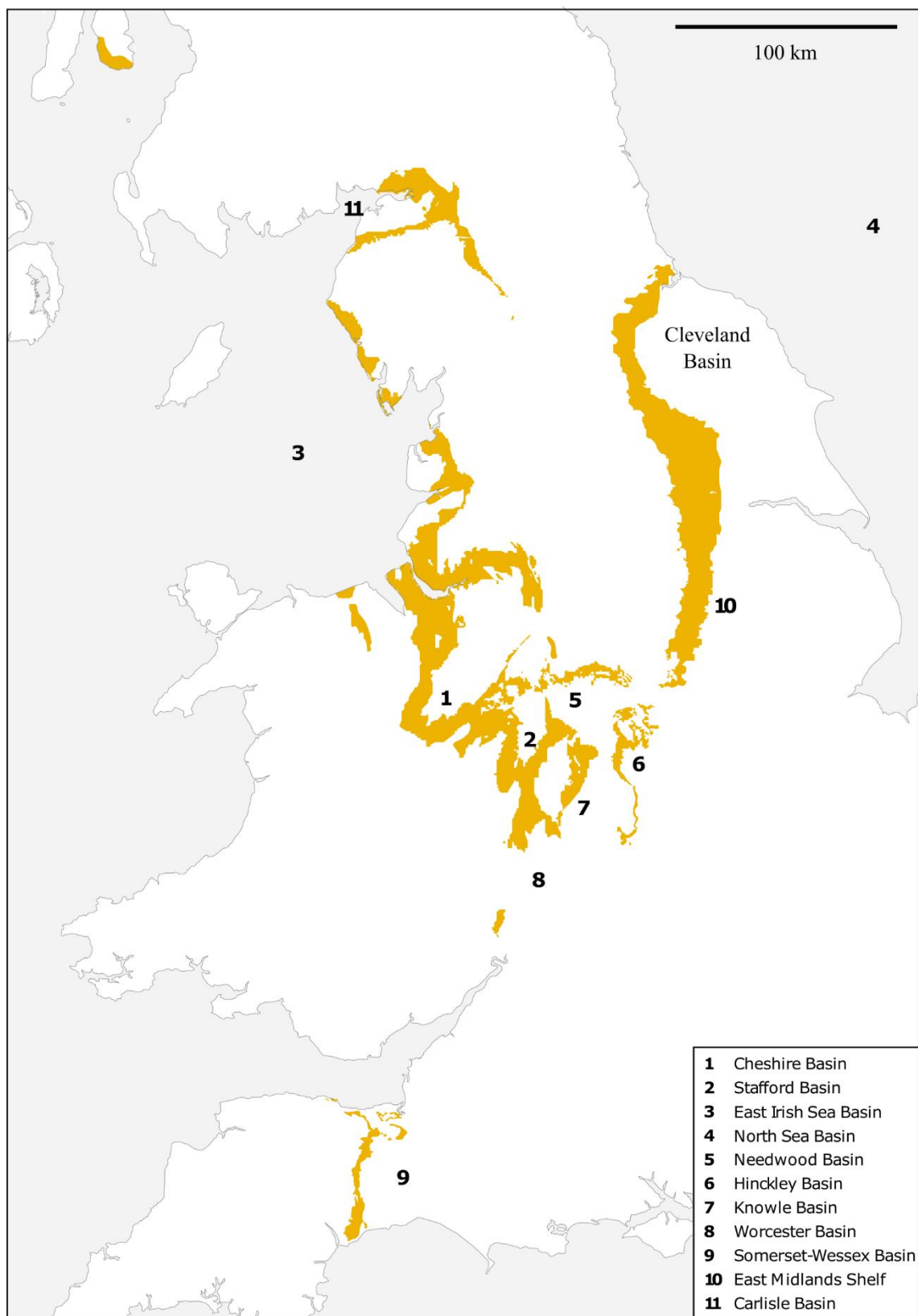*Figure 6.5*
The Early Carboniferous basins and platforms of central Britain. CLH = Central Lancashire High; HH = Holme High. Image from Andrews [2013].

Two prospective basins that may contain an equivalent sandstone formation to the Collyhurst Sandstone are the Gainsborough Trough and Cleveland Basin (Figure 6.5). The Grove-3 and Gainsborough-2 boreholes in the Gainsborough Trough both contain

erosional sandstones of 11.4 and 8.9 m thickness, respectively, at the base of the Permian sequence [*UKOGL*, 2019]. In Grove-3 the sandstone is described as fine to medium grained, moderately well-sorted, friable to loose with log-derived porosities of 30% (not corrected for clay) [*BP Petroleum Development UK Ltd.*, 1982]. This description suggests that the erosional sandstones may also have high permeabilities and, if they were laterally extensive across the Gainsborough Trough, may therefore act as protective formations. Furthermore, overlying the erosional sandstones is the Zechstein sequence, which is composed of Marls and Magnesian Limestone. In the Southern North Sea Gas Basin this sequence is the regional seal [*Glennie*, 1986] and may additionally offer protection onshore for the potential upward migration of fracking-related fluids.

In the Cleveland Basin (Figure 6.5) the basal Permian erosional sandstone appears to be less developed, recorded as 0 m thick in the Kirby Misperton-1 borehole and 2.1 m thick in the Kirby Misperton-8 borehole [*UKOGL*, 2019], thereby reducing its potential as a protective high-permeability formation. However, as in the Gainsborough Trough, the Zechstein sequence is also present in the Cleveland Basin [*UKOGL*, 2019] and may offer protection with its sealing nature. In addition, unlike in the Bowland Basin where the Triassic Sherwood Sandstone is the primary aquifer, the Sherwood Sandstone (169.9 m thick and top depth 1036.8 m below sea level in Kirby Misperton-8) is buried by Jurassic formations in the central Cleveland Basin [*Andrews*, 2013]. The Sherwood Sandstone may therefore act as a deep high-permeability barrier to the overlying Jurassic formations. Groundwater flow in the Sherwood Sandstone may be eastward, driven from onshore outcrops which follow the edge of the Cleveland Basin (Figure 6.6).

Figure 6.6
Sherwood Sandstone Group onshore outcrop. Image adapted from Ambrose et al. [2014].

In contrast, in the Widmerpool Trough the Mercia Mudstone Group is the bedrock geology and directly overlies the Bowland Shale [*Andrews*, 2013]. In the Long Eaton-1 borehole the Mercia Mudstone Group is ~150 m thick [*UKOGL*, 2019]. Protection from potentially upward migrating fracking-related fluids would rely on the low permeability of these formations and the Bowland Shale. Similarly, in the Edale Basin the Millstone Grit outcrops [*Andrews*, 2013] so protection would rely on the thickness and low permeability of the Bowland Shale, rather than a deep high-permeability formation. A deep high-permeability formation is also absent in the Blacon Basin. Formation top depths from the Blacon East-1 borehole indicate that the Lower Mottled Sandstone (part of the Permo-Triassic New Red Sandstone Supergroup) connects the Coal Measures and Superficial Deposits, with no Permian erosional sandstone or Zechstein sequence present [*UKOGL*, 2019]. Protection from potentially upward migrating fracking-related fluids would therefore rely on low permeabilities of the Bowland Shale, interbedded shales within the Millstone Grit and the ~323 m thick Coal Measures.

6.4.3   Model limitations and future work

6.4.3.1   Grid size and particle tracking

The horizontal grid size for the 3D hydrogeological model of the Fylde was set at 250 by 250 m^2, which was five times coarser than the model in Chapter 3. The use of a finer horizontal grid size and more layers in the 3D model would result in more precise particle tracking and predictions of subsurface fluid migration routes. However, this would require greater computational power.

Particle tracking was used to provide an indication of potential migration routes over 10000 years for fracking-related fluids at Preston New Road. The use of particles, for which transport is purely based on hydraulic head gradients and resulting groundwater flow velocities, is a simplification of reality because fracking-related fluids may be

subject to natural attenuation processes during transportation, for example dilution, dispersion, degradation, adsorption and precipitation. Although only chemicals determined as "non-hazardous" by the EA have been identified as suitable for fracking permits, natural attenuation mechanisms may reduce the movement and concentrations of fracking-related fluids. On the other hand, subsurface transformation of chemicals may result in hazardous by-products which could be more mobile [e.g. *Kahrilas et al.*, 2016; *Xiong et al.*, 2018a; 2018b]. Future work could look to integrate chemical and physical effects of fracking-related fluids with 3D basin-scale groundwater models to provide more realistic fluid migration predictions as well as concentrations with respect to environmental standards.

As mentioned in Section 3.4.6.2, fracture flow may be important to consider in alternative parametrisations of the stratigraphic units in the Fylde. However, in contrast to Chapter 3, the constant presence of the Collyhurst Sandstone in the scenarios meant that no particles reached the shallow aquifer. Therefore, whilst preferential fracture flow (if included) may decrease particle travel times through the Bowland Shale and Millstone Grit to the Collyhurst Sandstone, no changes to which hydrogeological factors were, or were not, significant would be expected.

6.4.3.2 Faults

The identification and extent of faults from the seismic reflection data was primarily limited by the quality and 2D nature of the data. As already noted in Chapter 4, the grid coverage by 2D seismic reflection lines in the Bowland Basin is highly non-uniform and the lines also vary in acquisition age (1979 to 1999), acoustic source type (explosive charges and Vibroseis) and processing workflows. As a result, the quality, resolution and depths of the lines vary, complicating the interpretation of horizons and faults across lines. The interpretation and inclusion of the recently released 3D seismic reflection dataset

"Bowland-12" (shot in 2012) would further help interpret faults in the Fylde area surrounding Preston New Road.

The inclusion of faults in the 3D hydrogeological model was also limited by the conversion of the geological model in Petrel to a hydrogeological model in ModelMuse. Horizons were transferred as continuous surfaces with interpreted faults not transferred explicitly. Such an approach was necessarily taken because of the unique nature of the model construction combined with user inexperience. Future work could look to incorporate all interpreted faults in Petrel into ModelMuse. Additionally, a method is needed to incorporate inclined faults in ModelMuse, which preferentially models faults as vertical features using the HFB package.

6.4.3.3   Boundary conditions

The 3D model used constant head boundaries to ensure that the cross-basin flow and overpressure conditions remained constant for the duration of the 10000 year simulations. However, constant head boundaries can influence simulation results because of their ability to allow an infinite amount of water to enter and exit the model. The exit of particles in the Collyhurst Sandstone under the Irish Sea was the result of the constant head boundaries and exiting groundwater, which may not be realistic. Similar to the Sellafield region further north, it is unlikely that substantial flow occurs in the deep subsurface between the Bowland Basin and the East Irish Sea Basin [e.g. *Bath et al.*, 2006]. Although the constant head boundaries provided the simplest boundary conditions to observe the effects of the considered hydrogeological factors, it may be more appropriate in future models of the Bowland Basin to impose more realistic boundary conditions to reflect the more likely hydrogeological regimes. Likewise, the representation of overpressure using a constant head boundary (i.e. constant upward flow forcing particles upwards) does not reflect the ability of shale formations to retain

202

overpressure on geological timescales [*Engelder et al.*, 2014], and thus it remains questioned how best to represent overpressure in groundwater models [*Birdsell et al.*, 2015]. Nevertheless, *Cai and Ofterdinger* [2014] argued that for the Bowland Basin, an upward flux condition at the base of the model domain was appropriate because it produced similar hydraulic head profiles to those observed in two deep boreholes in the nearby Sellafield region.

6.4.3.4   *Fluid effects*

As in Chapter 3 a major simplification of the 3D hydrogeological model and simulations was the exclusion of heat, variable density flow and multiphase flow. Thermal and density gradients in the subsurface can lead to the advection of groundwater, which could enhance or inhibit the migration of fracking-related fluids. For example, fracking fluids are typically low-salinity slickwater whereas formation waters at several kilometres depth are typically high-salinity brines [*Gassiat et al.*, 2013; *Engelder et al.*, 2014]. This difference in fluid salinity, and hence density, makes the initially injected fracking fluid buoyant [*Birdsell et al.*, 2015]. In future groundwater models of the Bowland Basin fluid density effects from salinity may be especially important to include because of the coastal location (potentially leading to sea water intrusion) and shallow brines found in the Sherwood Sandstone and Mercia Mudstone Groups west of the Woodsfold fault [*BGS*, 2018a; *Wilson et al.*, 2019]. Furthermore, it would be appropriate to include multiphase flow because fracking leads to at least two-phase flow within a shale gas reservoir (injected liquid water and chemicals, injected solid proppants, and *in situ* natural gas – phase dependant on subsurface pressure).

6.4.3.5 Groundwater abstractions

No groundwater abstractions were included in the 3D model or simulations but abstractions from the Sherwood Sandstone do occur in the northern and eastern Fylde [*Mott MacDonald*, 1997; 2010]. These shallow abstractions have been the focus of previous groundwater models of the Fylde. The effect of the abstractions on the deeper groundwater system and thus the 3D scenarios presented in this chapter are unknown. There is therefore potential to create further models which include these abstractions and investigate any effects. More generally, because of the growing use of the subsurface, there is an increasing need to develop basin-scale groundwater models that couple shallow and deep groundwater systems, as well as surface water systems, in order to understand potential environmental effects.

6.5   Conclusions

A 3D numerical groundwater model of the Fylde was constructed from geological maps, borehole data and 2D seismic reflection data to investigate how different hydrogeological factors affected the long-term migration of fracking-related fluids from the Bowland Shale at ~2000 m below the surface. The hydrogeological factors considered in factorial scenarios were: cross-basin flow; fluid injection; stimulated reservoir volume; low-permeability faults; and overpressure. Of the 36 scenarios simulated, no scenarios resulted in tracked particles reaching the regional shallow aquifer within the 10000 year simulation time. The study found that the presence of overpressure was the most important statistically significant factor in controlling fluid migration to overlying formations. The shallowest formation reached by tracked particles was the Collyhurst Sandstone, which only occurred when overpressure was included in the scenarios. The Collyhurst Sandstone is a deep high-permeability formation relative to the surrounding

strata and acted to protect overlying formations from upward fluid migration by hydraulically isolating the shale from the overburden and allowing lateral particle movement south-westward. The mapping of deep high-permeability formations in prospective shale basins may therefore be useful for predicting the long-term migration of fracking-related fluids. The inclusion of two low-permeability faults in some scenarios made little difference to tracked particles because the faults did not extend fully across the model domain, thereby not creating hydraulically isolated compartments. Nevertheless, not all known faults were included in the model domain and more complex models may result in different particle migration routes and travel times. This study highlights that data collected for petroleum exploration can also be useful for mitigating potential shallow groundwater resource contamination through the development of 3D basin-scale groundwater models to better understand basin hydraulics and identify important hydrogeological factors.

7 Conclusions, implications and suggestions for further work

7.1 Thesis summary

The potential migration of anthropogenic or natural fluids from unconventional shale reservoirs to shallow groundwater resources along natural geological pathways has been an environmental concern raised with the industrial practice of fracking. High-permeability fault and fracture zones are generally regarded as the highest-risk pathway and so the first aim of this thesis was to determine a horizontal respect distance between fluid injection locations and known faults. The second aim of this thesis was to consider complex geological structure, which previous numerical models had neglected, to investigate hydrogeological factors which might increase or decrease the vulnerability of shallow groundwater resources to the potential upward migration of fracking-related fluids. This second aim was based on a real-life fracking operation in a prospective shale gas basin rather than investigating fluid injection in a simplistic and hypothetical geological scenario. The following sections bring together the main conclusions of the thesis chapters and discuss the implications for fracking operations and, more generally, industrial practices which inject fluids into the subsurface.

7.1.1 Avoiding known faults

It was highlighted at the beginning of this thesis that avoiding known faults, for example those observable on seismic reflection data, was the easiest mitigation measure to reduce the likelihood of injected fluids interacting with faults. Using numerical modelling *Westwood et al.* [2017a] suggested a maximum horizontal respect distance of 433 m between subsurface fluid injection locations and known faults. In Chapter 2 an alternative empirical approach using published microseismic data was employed to determine a horizontal respect distance of 895 m. From a dataset of 109 fracking operations, the empirical risk of detecting microseismicity in shale beyond a horizontal distance of

433 m was 32% and beyond 895 m was 1%. Importantly, the microseismic data showed that fracture stimulation, and therefore potentially injected fluid migration, can extend beyond the 433 m respect distance suggested by *Westwood et al.* [2017a]. Furthermore, the extent of stimulation as defined by the furthest detected microseismic event showed statistically significant relationships with injection volume and rate, suggesting these operational parameters could be adjusted to limit the extent of stimulation in proximity to known faults. Nevertheless, a cautionary approach for nations with limited fracking experience would be to apply a horizontal respect distance of ~900 m between horizontal boreholes orientated perpendicular to the maximum horizontal stress direction and known faults optimally orientated for failure in their regional stress state. The application of horizontal respect distances to known faults could also be employed to enhanced geothermal reservoirs, which also require fluid injection to hydraulically fracture the target reservoir.

7.1.2   *Hydrogeological factors*

Using a 2D numerical model of the Preston New Road fracking site in the Bowland Basin, northwest England, Chapter 3 found four hydrogeological factors that increased the vulnerability of the shallow aquifer to upward fluid migration from the underlying shale reservoir: increased stimulated fracture extent; greater amounts of overpressure; the presence of low-permeability faults; and the absence of deep high-permeability formations above the greatest stimulated fracture extent. The latter two factors are contrary to general opinion, and are therefore not typically considered in environmental risk assessments for fluid injection operations.

7.1.2.1 *Low-permeability faults and compartmentalisation*

Prior to this thesis high-permeability fault and fracture zones were considered the primary risk factor and natural geological pathway for the upward migration of fracking-related fluids from shale reservoirs to shallow aquifers [e.g. *Myers*, 2012; *Birdsell et al.*, 2015]. However, in the 2D model of Chapter 3 it was the scenarios with low-permeability faults, not high-permeability faults that led to tracked particles reaching the shallow aquifer. Low-permeability faults acted to compartmentalise hydraulic head in the model, thereby discouraging horizontal flow whilst encouraging upward flow through strata towards the shallow aquifer. Chapter 6 expanded the 2D model of Chapter 3 to a 3D basin-scale model. In contrast to the 2D model, the inclusion of two low-permeability faults in the 3D model made little difference to scenario results. Considering the results of both Chapters 3 and 6 leads to the conclusion that for compartmentalisation-enhanced upward flow to occur in a geological basin, low-permeability faults must isolate the compartment from regional groundwater flow; isolation occurred in the 2D models but not in the 3D models because of the spatial extent of the modelled faults. In situations where low-permeability faults do not create isolated compartments, low-permeability faults may still influence regional groundwater flow patterns and therefore may still influence the potential long-term migration routes of injected fluids. Furthermore, *Skoumal et al.* [2019] recently recognised the importance of low-permeability barriers and compartmentalisation in the spatial occurrence of injection-induced seismicity. Consequently, there is growing acceptance that identifying low-permeability faults in basins is as important as identifying high-permeability faults.

In Chapter 4 the combination of historic groundwater quality data with seismic reflection data in a prospective basin provided a novel method for identifying compartmentalising low-permeability faults. Given the acquisition and interpretation of

seismic reflection data is a key stage of the petroleum exploration process, it would be in the interests of operators and regulators to also use these data with historic groundwater data to better understand basin hydraulics and therefore enhance environmental risk assessments for groundwater contamination. Nevertheless, in Chapter 4 the spatial extent of groundwater quality and seismic reflection data across the prospective basin limited the identification of low-permeability faults, indicating adequate identification may require supplementing historical groundwater data with dedicated basin-wide groundwater sampling programmes and the acquisition of new seismic data in areas of poor coverage or quality. In the absence of new groundwater data, Chapter 5 investigated if surface water quality data could instead be used to identify compartmentalisation and groundwater-surface water interactions. Variance analysis on surface water quality data could not identify known compartmentalisation in underlying groundwater but could demonstrate regional-scale groundwater-surface water interaction across the studied basin. The absence of a compartmentalisation signature in the surface water data meant there was no chemical evidence to suggest that deeper groundwater in that particular area of the prospective basin was reaching the surface in response to compartmentalisation-enhanced flow. Consequently, compartmentalisation in that area of the prospective basin does not appear to increase the risk of fracking-related contaminants reaching surface waters.

7.1.2.2 *Deep high-permeability formations*

To date environmental risk assessments for fracking operations in England have focussed on low-permeability formations as the key barriers to upward fluid flow [e.g. *Ove Arup and Partners Ltd.*, 2014a]. This focus on low-permeability formations is logical given that conventional petroleum reservoirs are typically sealed above by low-permeability formations such as shales or evaporites. Contrary to this view it was observed in the model

scenarios of Chapters 3 and 6 that deep high-permeability formations between shale reservoirs and shallow aquifers can also play a crucial role in preventing upward fluid migration. When a deep high-permeability formation was included in the model scenarios the effect was to prevent further upward fluid migration by encouraging lateral flow within the high-permeability formation. *Pfunt et al.* [2016] also showed that lateral flow occurred in high-permeability formations above fluid injection points, suggesting this protective mechanism may be common to other prospective basins across the world. Therefore, in addition to mapping low-permeability sealing formations, mapping deep high-permeability formations may also be useful for understanding the long-term migration of injected fluids and assessing contamination risk to shallow groundwater resources.

7.1.2.3 Overpressure

Birdsell et al. [2015] recognised overpressure as a potential driver of upward fluid migration from unconventional shale reservoirs, concluding from their model scenarios that overpressure has a vast range of possible effects depending on how it and borehole production were applied to their model. Overpressure in this thesis was modelled as a permanent lower boundary condition to the model domains, thereby generating a vertical hydraulic head gradient between the bases and tops of the models. Although this contradicts the idea of shales maintaining overpressure over geological time [*Engelder et al.*, 2014], such an approach was straightforward to implement and obtain clear results from. Furthermore, by effectively forcing upward fluid flow such models can be viewed as worst-case scenarios, thereby providing perspective on the results.

In the 2D model of Chapter 3 overpressure was found to be a statistically significant factor controlling particle travel time between the shale reservoir and shallow aquifer. When the protective deep high-permeability formation was excluded from the model,

scenarios with greater amounts of overpressure were more likely to result in particles reaching the aquifer. Chapter 6 supported this result with particles essentially always remaining within the shale formation when overpressure was not included in the scenarios. When overpressure was included in the 3D model scenarios, particles migrated beyond the shale to the deep high-permeability formation, which then prevented further vertical migration to the shallow aquifer. As with the results from Chapter 3, overpressure was found to be a statistically significant factor controlling fluid migration beyond the shale formation. The results of this thesis therefore support the idea that overpressure is a potential driver of upward fluid migration from shale reservoirs to shallow aquifers, but further work is needed to confirm this hypothesis and consider how best to represent overpressure in groundwater models. Similarly to deep high-permeability formations, it may be possible to map or model overpressure in shales across prospective basins and thereby target areas which pose less risk to upward fluid migration.

7.1.3   *Fracking in the Bowland Basin*

The majority of this thesis has focussed on the Bowland Basin as a case study for other prospective shale basins. It therefore seems appropriate to comment on how the findings of this thesis directly relate to fracking operations in the Bowland Basin. The use of EA groundwater quality monitoring data in Chapter 4 showed that the deep (>400 m) groundwater system in the Bowland Basin is poorly understood and large areas remain undrilled and unsampled. This is particularly true for the western Fylde where, although groundwater in the Sherwood Sandstone Group is not currently considered an abstraction resource as in the eastern Fylde, past fracking operations have been focussed to date. The historic focus on groundwater monitoring of the Sherwood Sandstone aquifer in the eastern Fylde has resulted in a regulatory groundwater model [*Mott MacDonald*, 2010] that is too shallow and not extensive enough to cover new uses of the subsurface in the

Bowland Basin. The paucity of groundwater data also means that the hydraulic effects of nearly all of the major basin faults interpreted on seismic reflection data are unknown. Such faults likely influence regional groundwater flow and are therefore important for understanding the potential long-term migration of fracking-related fluids and assessing the risk of groundwater contamination. The surface water quality data analysed in Chapter 5 indicated that the hydraulic effects of known faults are not observable from surface data alone, highlighting the importance of obtaining new groundwater data across the basin. However, the surface water quality data were useful for indicating hydraulic connections between surface waters and groundwater in bedrock formations, thereby enhancing understanding of how and where the surface and subsurface water systems couple.

The 2D and 3D numerical models developed in Chapters 3 and 6, respectively, both indicated that the contamination risk to shallow groundwater from the upward migration of fracking-related fluids along natural geological pathways is low for the Preston New Road site. In the 3D model no tracked particles migrated shallower than the Collyhurst Sandstone and in the worst-case scenario of the 2D model, which used an unlikely hydrogeological configuration and stimulated vertical fractures greater than ever observed using microseismic data, travel times to the shallow aquifer were 130 years without accounting for dilution, dispersion, degradation, adsorption or precipitation effects. The Collyhurst Sandstone was identified as a key protective formation in the basin due to its high permeability relative to the surrounding strata. The Collyhurst Sandstone prevented upward fluid migration by encouraging lateral fluid flow. However, the distribution of the Collyhurst Sandstone in the Bowland Basin is poorly understood and further constraints on its distribution are needed. Furthermore, the geological complexity of the basin means that subsurface structural and stratigraphic interpretations from seismic reflection data are challenging and not always correct. For example, at the Preston New Road site the Millstone Grit was interpreted on seismic reflection data to be present

but on drilling was found to be absent (the Collyhurst Sandstone truncated the Bowland Shales) [*Cuadrilla Resources Ltd.*, 2018a].

Although the modelling results suggested the contamination risk to shallow groundwater from the upward migration of fracking-related fluids along natural geological pathways is low for the Preston New Road site, several caveats regarding the conclusions of the numerical models must be highlighted. Firstly, the neglect of fracture porosity and preferential flow in geological formations of the Bowland Basin likely meant that particle travel times were longer than if fracture flow were accounted for. Thus, whilst the statistical results regarding the hydrogeological factors would likely remain unchanged, particle travel times to the Sherwood Sandstone aquifer or Collyhurst Sandstone might be shorter than currently reported. Secondly, the interaction of the overpressure boundary with the high hydraulic conductivity fault in Chapter 3 may be geologically unrealistic because of the continuous flow of fluid along the fault in response to the constant supply of water from the underlying constant head boundary. Such an interaction contradicts the preservation of shale overpressure over geological timescales. Consequently, modelled groundwater flows and particle tracks in response to this interaction may not represent a real hydrogeological scenario. Finally, the use of constant head boundaries to generate constant cross-basin flow may not be appropriate considering it is unlikely that substantial flow occurs in the deep subsurface from the Bowland Basin to the East Irish Sea Basin. The constant head boundary on the western side of the 3D model domain allowed unlimited groundwater to flow out of the model domain and the exit of particles within the Collyhurst Sandstone. It may be more appropriate in future groundwater models of the Bowland Basin to impose more realistic boundary conditions to reflect the more likely hydrogeological regimes present in the basin.

7.1.4   Reverse vulnerability

Traditionally, groundwater vulnerability to contamination was generally concerned with the downward movement of contaminants from surface applications, for example pesticides [e.g. *Worrall & Kolpin*, 2004]. Environmental risk assessments were therefore based on a top-down approach. Over approximately the last 10 years there has been an increase in global interest in the injection of fluids into the subsurface for energy applications, for example fracking, waste-water disposal, gas storage, geothermal energy, and carbon capture and storage. As a result, groundwater vulnerability must now also be considered using a bottom-up approach (i.e. reverse vulnerability) by assessing the potential for formation or injected fluids to migrate back to the surface or shallow subsurface.

Ultimately, a predictive assessment of the potential upward migration of fluids must utilise numerical modelling. There is therefore a need to develop a new generation of numerical models that couple the deep subsurface with the shallow subsurface and surface. Such models will likely need to combine aspects of petroleum or geothermal reservoir modelling with hydrologic modelling, including both groundwater and surface waters. Likewise, to inform these new models geoscientists will need to draw upon a wide range of data from a variety of sources. For example, seismic reflection surveys, wireline logs and geological mapping data from the coal, petroleum or geothermal industries, and groundwater and surface water quality and flow data from environmental regulatory bodies. This thesis and others [e.g. *Rivard et al.*, 2019] have begun to demonstrate such an integrated approach in the context of fracking and potential groundwater contamination. By combining petroleum exploration and environmental monitoring data, this thesis has developed the first 3D basin-scale groundwater model to address potential upward fluid migration from fracking. Furthermore, through running a series of

215

simulations with differing hydrogeological factors, it was possible to identify key factors

that increased or decreased aquifer vulnerability to upward fluid migration from below.

7.2   Suggestions for further work

7.2.1   *Horizontal respect distances*

The suggested horizontal respect distance of 895 m to known faults was based on a dataset

of only 109 published examples of fracking operations with microseismic data, despite

the number of fracking operations with microseismic data probably being in the region of

tens to hundreds of thousands. If an operator with a substantial collection of microseismic

data allowed access to these data, further work could be undertaken to provide more

robust empirical horizontal respect distances and further investigate the effects of

lithology, ambient stresses, and injection volume and rate. As in Chapter 2 a variance

analysis approach could be used to further identify and understand the influence of

geological and operational factors. A larger dataset of microseismic event distances could

be incorporated into the Bayesian model of Chapter 2 to provide an updated horizontal

respect distance and would also enable comparative respect distances to be calculated

using cumulative distribution functions [e.g. *Davies et al.*, 2012].

7.2.2   *"Unknown" faults*

Although defining a horizontal respect distance is a useful mitigation measure against

fluid interaction with known faults (i.e. those clearly observed on seismic reflection data),

cases of induced seismicity highlight that not all faults are easily detected. For example,

the induced earthquake sequences associated with fluid injection in the PNR-1z and -2

boreholes, which culminated in a M_L 2.9 earthquake, occurred on a previously unknown

fault that was not visible on the 3D seismic reflection data [*Clarke et al.*, 2019]. Therefore,

improvements in fault detection on seismic reflection data could be attempted which could include, but are not limited to, reprocessing of the raw data and subtle attribute mapping [*Townsend et al.*, 1998; *Zhu et al.*, 2019].

7.2.3 Deep groundwater systems

Assessing the long-term migration routes of fluids injected at several kilometres depth requires an understanding of deep groundwater systems. However, environmental groundwater monitoring is commonly focussed on the shallow subsurface (≤400 m), meaning there is often a paucity of data at greater depths and subsequently greater uncertainty in groundwater characteristics such as quality and flow. To improve knowledge of deep groundwater systems in prospective basins, wireline logging data from deep boreholes (e.g. petroleum boreholes) could be utilised. For example, resistivity logs could be used to estimate the conductivity of groundwater, which could also be temperature normalised using bottom hole temperature data. Comparisons between boreholes may even allow interpretation and identification of low-permeability faults and compartmentalisation.

7.2.4 Water temperatures

It is well known that temperature increases with depth in the Earth. In the crust this means that groundwater found at kilometre-scale depths is generally hotter than shallow groundwater and surface waters. Where deep groundwater rises to the surface quickly, heat energy is conserved and can lead to temperature anomalies in shallow groundwater systems or surface waters, for example thermal springs. By this logic temperature measurements of shallow groundwater and surface waters could be used to infer locations where deep groundwater is rising to the surface. Such locations could be targeted for

geothermal energy applications or, in the case of fracking, avoided to reduce the risk of upward migrating fracking-related fluids.

7.2.5 Fluid migration in shale formations

Shale formations are often considered, as in the models of this thesis, relatively homogenous. However, shale formations are highly heterogeneous from the nanoscale to the macroscale. For example, at the macroscale the Bowland and Worston Shale Groups consist of interbedded units of shales, calcareous mudstones, limestones, siltstones and fine sandstones [*Kirby et al.*, 2000]. Each of these units will have different hydraulic properties meaning fluid flow is unlikely to be uniform at the Formation or Group level. Therefore, future research could look to assess if it is appropriate to consider shale formations as homogenous in groundwater models or if heterogeneity at the bed-scale has a critical influence on groundwater flow and contaminant transport. If the latter, it will be important to be able to recognise (and subsequently implement) the presence of bed-scale heterogeneity, which may, or may not be possible using seismic reflection or wireline data. Additional factors to consider in future work regarding fluid migration in shale formations include the effects of overpressure and total organic carbon content, which may favour or inhibit the flow of certain fluids [*Wang & Reed*, 2009].

7.2.6 Numerical modelling

Although the numerical groundwater models presented in this thesis were relatively complex in terms of geological structure, they were simplistic in many other aspects. Further work could look to develop more sophisticated models which include the potentially important effects of heat, variable density flow, multiphase flow and pre-existing anthropogenic influences such as shallow groundwater abstractions. Furthermore, rather than using simple particle tracking as a measure of fluid migration,

there is also scope to include chemical data and attempt to account for the effects of dilution, dispersion, degradation, adsorption, precipitation and preferential fracture flow. Finally, geomechanical modelling could be coupled with groundwater modelling to better reflect subsurface mechanical changes (and therefore hydraulic changes) caused by fluid injection and extraction processes, for example: the creation of hydraulic fractures and extent of the stimulated reservoir volume; compaction caused by borehole production; and pore pressure and poroelastic effects on nearby pre-existing geological fault and fracture zones.

References

Abesser, C., Shand, P., & Ingram, J. (2005). Baseline Report Series: 18. The Millstone Grit of Northern England. British Geological Survey Commissioned Report No. CR/05/015N.

Advanced Resources International, Inc. (2011). World shale gas resources: An initial assessment of 14 regions outside the United States. Report prepared for U.S. Energy Information Administration, Office of Energy Analysis, U.S. Dep. of Energy, Washington, DC 20585.

Allen, D. J., Brewerton, L. J., Coleby, L. M., Gibbs, B. R., Lewis, M. A., MacDonald, A. M., Wagstaff, S. J., & Williams, A. T. (1997). The physical properties of major aquifers in England and Wales. British Geological Survey Technical Report WD/97/34, Environment Agency R&D Publication 8.

Ambrose, K., Hough, E., Smith, N. J. P., & Warrington, G. (2014). Lithostratigraphy of the Sherwood Sandstone Group of England, Wales and south-west Scotland. British Geological Survey Research Report RR/14/01.

Anderson, I., & Underhill, J. R. (2020). Structural constraints on Lower Carboniferous shale gas exploration in the Craven Basin, NW England. *Petroleum Geoscience*.

Anderson, T. W., & Darling, D. A. (1952). Asymptotic theory of certain" goodness of fit" criteria based on stochastic processes. *The annals of mathematical statistics*, 23(2), 193-212.

Andrews, I. J. (2014), The Jurassic shales of the Weald Basin: geology and shale oil and shale gas resource estimation. British Geological Survey for Department of Energy and Climate Change, London, UK.

Andrews, I. J. (2013). The Carboniferous Bowland Shale gas study: geology and resource estimation. British Geological Survey for Department of Energy and Climate Change, London, UK.

Andrews, J. N., Burgess, W. G., Edmunds, W. M., Kay, R. L. F., & Lee, D. J. (1982). The thermal springs of Bath. *Nature*, 298(5872), 339.

Atkinson, T. C., & Davison, R. M. (2002). Is the water still hot? Sustainability and the thermal springs at Bath, England. *Geological Society, London, Special Publications*, 193(1), 15-40.

Baedecker, M. J., & Back, W. (1979). Hydrogeological processes and chemical reactions at a landfill. *Groundwater*, 17(5), 429-437.

Barker W. (2009, January). Increased production through microseismic monitoring of hydraulic fracturing over a multiwell program. In SPE Annual Technical Conference and Exhibition. Society of Petroleum Engineers.

Barker, J. A., Downing, R. A., Gray, D. A., Findlay, J., Kellaway, G. A., Parker, R. H., & Rollin, K. E. (2000). Hydrogeothermal studies in the United Kingdom. *Quarterly Journal of Engineering Geology and Hydrogeology*, 33(1), 41-58.

Bath, A., Richards, H., Metcalfe, R., McCartney, R., Degnan, P., & Littleboy, A. (2006). Geochemical indicators of deep groundwater movements at Sellafield, UK. *Journal of Geochemical Exploration*, 90(1-2), 24-44.

Bath, A. H., McCartney, R. A., Richards, H. G., Metcalfe, R., & Crawford, M. B. (1996). Groundwater chemistry in the Sellafield area: a preliminary interpretation. *Quarterly Journal of Engineering Geology and Hydrogeology*, 29(S1), S39-S57.

BEIS (Department for Business, Energy & Industrial Strategy) (2019). Government ends support for fracking. https://www.gov.uk/government/news/government-ends-support-for-fracking. Last accessed 12th November 2019.

Belcher, W. R., & Sweetkind, D. S. (2010). Death Valley regional groundwater flow system, Nevada and California – Hydrogeologic framework and transient groundwater flow model. U.S. Geological Survey Professional Paper 1711.

Bense, V. F., Gleeson, T., Loveless, S. E., Bour, O., & Scibek, J. (2013). Fault zone hydrogeology. *Earth-Science Reviews*, 127, 171-192.

Bertin, C., & Bourg, A. C. (1994). Radon-222 and chloride as natural tracers of the infiltration of river water into an alluvial aquifer in which there is significant river/groundwater mixing. *Environmental Science & Technology*, 28(5), 794-798.

Birdsell, D. T., Rajaram, H., Dempsey, D., & Viswanathan, H. S. (2015). Hydraulic fracturing fluid migration in the subsurface: a review and expanded modelling results. *Water Resources Research*, 51(9), 7159-7188.

Black, J. H., & Brightman, M. A. (1996). Conceptual model of the hydrogeology of Sellafield. *Quarterly Journal of Engineering Geology and Hydrogeology*, 29(S1), S83-S93.

Bloomfield, J. P., Allen, D. J., & Griffiths, K. J. (2009). Examining geological controls on baseflow index (BFI) using regression analysis: An illustration from the Thames Basin, UK. *Journal of Hydrology*, 373(1-2), 164-176.

Boothroyd, I. M., Almond, S., Qassim, S. M., Worrall, F., & Davies, R. J. (2016). Fugitive emissions of methane from abandoned, decommissioned oil and gas wells. *Science of the Total Environment*, 547, 461-469.

Boothroyd, I. M., Almond, S., Worrall, F., & Davies, R. J. (2017). Assessing the fugitive emission of CH4 via migration along fault zones–Comparing potential shale gas basins to non-shale basins in the UK. *Science of the Total Environment*, 580, 412-424.

Boothroyd, I. M., Almond, S., Worrall, F., Davies, R. K., & Davies, R. J. (2018). Assessing fugitive emissions of CH4 from high-pressure gas pipelines in the UK. *Science of the Total Environment*, 631, 1638-1648.

Bottrell, S. H., West, L. J., & Yoshida, K. (2006). Combined isotopic and modelling approach to determing the source of saline groundwaters in the Selby Triassic sandstone aquifer, UK. *Geological Society, London, Special Publications*, 263(1), 325-338.

BP Petroleum Development (UK) Ltd. (1982). Geological Completion Report Grove-3, PL 178, East Midlands.

Brassington, F. C. (2007). A proposed conceptual model for the genesis of the Derbyshire thermal springs. *Quarterly Journal of Engineering Geology and Hydrogeology*, 40(1), 35-46.

Bredehoeft, J. D., Belitz, K., & Sharp-Hansen, S. (1992). The hydrodynamics of the Big Horn Basin: A study of the role of faults (1). *AAPG bulletin*, 76(4), 530-546.

Briggs, M. A., Hare, D. K., Boutt, D. F., Davenport, G., & Lane, J. W. (2016). Thermal infrared video details multiscale groundwater discharge to surface water through macropores and peat pipes. *Hydrological Processes*, 30(14), 2510-2511.

British Gas PLC. (1991). UK Onshore EXL 042 Lancashire Technical Review.

British Geological Survey (BGS) (2019a). Earthquakes induced by Hydraulic Fracturing Operations near Blackpool, UK. https://earthquakes.bgs.ac.uk/research/BlackpoolEarthquakes.html. Last accessed 23rd September 2019.

British Geological Survey (BGS) (2019b). BGS earthquake database search. https://earthquakes.bgs.ac.uk/earthquakes/dataSearch.html. Last accessed 23rd September 2019.

British Geological Survey (BGS) (2019c). Induced Seismicity around the British Isles in the last 50 days. https://earthquakes.bgs.ac.uk/induced/recent_uk_events.html. Last accessed 16th October 2019.

British Geological Survey (BGS) (2019d). Onshore GeoIndex, http://www.bgs.ac.uk/GeoIndex/home.html. Last accessed 27th May 2019.

British Geological Survey (BGS) (2019e). Current UK ground water use. https://www.bgs.ac.uk/research/ground water/waterResources/Ground waterInUK/2015.html. Last accessed 24th May 2019.

British Geological Survey (BGS) (2018a). Groundwater monitoring in Lancashire. https://www.bgs.ac.uk/research/groundwater/shaleGas/monitoring/waterQualityLancashire.html. Last accessed 16th August 2018.

British Geological Survey (BGS) (2018b). Borehole scans. https://www.bgs.ac.uk/data/boreholescans/home.html. Last accessed 29th May 2018.

British Geological Survey (BGS) (2012). Preston Sheet 75 1:50 000 Series Bedrock and Superficial.

British Geological Survey (BGS) (1990). Garstang Sheet 67 1:50 000 Series Solid Geology.

British Geological Survey (BGS) (1989). Southport Sheet 74 1:50 000 Series Solid and Drift Geology.

British Geological Survey (BGS) (1975). Blackpool Sheet 66 1:50 000 Series Solid and Drift Edition with Bouguer anomalies.

Brownlow, J. W., James, S. C., & Yelderman, J. C. (2016). Influence of hydraulic fracturing on overlying aquifers in the presence of leaky abandoned wells. *Groundwater*, 54(6), 781-792.

Bullen, T. D., Krabbenhoft, D. P., & Kendall, C. (1996). Kinetic and mineralogic controls on the evolution of ground water chemistry and 87Sr/86Sr in a sandy silicate aquifer, northern Wisconsin, USA. *Geochimica et Cosmochimica Acta*, 60(10), 1807-1821.

Burgess, W. G., Edmunds, W. M., Andrews, J. N., Kay, R. L. F., & Lee, D. J. (1980). Investigation of the geothermal potential of the UK. The hydrogeology and hydrochemistry of the thermal water in the Bath–Bristol Basin. Institute of Geological Sciences, London (now British Geological Survey).

Butman, D., & Raymond, P. A. (2011). Significant efflux of carbon dioxide from streams and rivers in the United States. *Nature Geoscience*, 4(12), 839-842.

Cable, J. E., Burnett, W. C., Chanton, J. P., & Weatherly, G. L. (1996). Estimating groundwater discharge into the northeastern Gulf of Mexico using radon-222. *Earth and Planetary Science Letters*, 144(3-4), 591-604.

Cai, Z., & Ofterdinger, U. (2014). Numerical assessment of potential impacts of hydraulically fractured Bowland Shale on overlying aquifers. *Water Resources Research*, 50(7), 6236-6259.

Cathles, L. M. (1990). Scales and effects of fluid flow in the upper crust. *Science*, 248(4953), 323-329.

Chapman, E. C., Capo, R. C., Stewart, B. W., Kirby, C. S., Hammack, R. W., Schroeder, K. T., & Edenborn, H. M. (2012). Geochemical and strontium isotope characterization of produced waters from Marcellus Shale natural gas extraction. *Environmental Science & Technology*, 46(6), 3545-3553.

Chatfield, C. & Collins A. J. (1980). Introduction to Multivariate Analysis. Chapman and Hall, London, 246.

Cheng, Y. (2012). Impact of water dynamics in fractures on the performance of hydraulically fractured wells in gas-shale reservoirs. *Journal of Canadian Petroleum Technology*, 51(02), 143-151.

Clancy, S. A., Worrall, F., Davies, R. J., & Gluyas, J. G. (2018). An assessment of the footprint and carrying capacity of oil and gas well sites: The implications for limiting hydrocarbon reserves. *Science of the Total Environment*, 618, 586-594.

Clarke, H., Eisner, L., Styles, P., & Turner, P. (2014a). Felt seismicity associated with shale gas hydraulic fracturing: The first documented example in Europe. *Geophysical Research Letters*, 41(23), 8308-8314.

Clarke, H., Bustin, M., & Turner, P. (2014b, February). Unlocking the resource potential of the Bowland Basin, NW England. In SPE/EAGE European Unconventional Resources Conference and Exhibition. Society of Petroleum Engineers.

Clarke, H., Verdon, J. P., Kettlety, T., Baird, A. F., & Kendall, J. M. (2019). Real-Time Imaging, Forecasting, and Management of Human-Induced Seismicity at Preston New Road, Lancashire, England. *Seismological Research Letters*, 90(5), 1902-1915.

Cohen, H. A., Parratt, T., & Andrews, C. B. (2013). Potential contaminant pathways from hydraulically fractured shale to aquifers. *Groundwater*, 51(3), 317-319.

Cole, J. J., Prairie, Y. T., Caraco, N. F., McDowell, W. H., Tranvik, L. J., Striegl, R. G., Duarte, C. M., Kortelainen, P., Downing, J. A., Middelburg, J. J., & Melack, J. (2007). Plumbing the global carbon cycle: integrating inland waters into the terrestrial carbon budget. *Ecosystems*, 10(1), 172-185.

Cornford, C., Christie, O., Endresen, U., Jensen, P., & May-Britt, M. Y. H. R. (1988). Source rock and seep oil maturity in Dorset, southern England. In Organic Geochemistry In Petroleum Exploration (399-409). Proceedings of the 13th International Meeting On Organic Geochemistry, Venice, Italy 21–25 September 1987.

Cripps, C., Burker, H. F., Lee, J. R. & Housh, E. (2016) The Fylde, Lancashire: Summary of the Quaternary Geology. British Geological Survey Open Report, OR/16/013.

Cuadrilla Resources Ltd. (2018a). Hydraulic Fracture Plan PNR 2.

Cuadrilla Resources Ltd. (2018b). Hydraulic Fracture Plan PNR 1/1Z. https://cuadrillaresources.com/site/preston-new-road/. Last accessed 7th August 2019.

Cuadrilla Resources Ltd. (2017). Preston New Road 2 Hydraulic Fracture Plan.

Cuadrilla Resources Ltd. (UK), & A. J. Lucas Group (2008). 13th Round Landward Licensing Petroleum Exploration and Development License Application: Unconventional Shale Gas Play Bowland Shale Group – West Lancashire Basin.

Currie, J., Greenstone, M., & Meckel, K. (2017). Hydraulic fracturing and infant health: New evidence from Pennsylvania. *Science Advances*, 3(12), e1603021.

Darling, W. G., Bath, A. H., & Talbot, J. C. (2003). The O and H stable isotope composition of freshwaters in the British Isles. 2, surface waters and groundwater. *Hydrology and Earth System Sciences*, 7, 183-195.

Darrah, T. H., Vengosh, A., Jackson, R. B., Warner, N. R., & Poreda, R. J. (2014). Noble gases identify the mechanisms of fugitive gas contamination in drinking-water wells overlying the Marcellus and Barnett Shales. *Proceedings of the National Academy of Sciences*, 111(39), 14076-14081.

Davies, R., Foulger, G., Bindley, A., & Styles, P. (2013a). Induced seismicity and hydraulic fracturing for the recovery of hydrocarbons. *Marine and Petroleum Geology*, 45, 171-185.

Davies, R. J., Foulger, G. R., Mathias, S., Moss, J., Hustoft, S., & Newport, L. (2013b). Reply: Davies et al. (2012), Hydraulic fractures: How far can they go?. *Marine and Petroleum Geology*, 43, 519-521.

Davies, R. J., Mathias, S. A., Moss, J., Hustoft, S., & Newport, L. (2012). Hydraulic fractures: How far can they go?. *Marine and Petroleum Geology*, 37(1), 1-6.

Davis, S. N. (1964). The chemistry of saline waters by R. A. Krieger. Discussion. *Groundwater*, 2(1), 51.

Deng, K., Liu, Y., & Harrington, R. M. (2016). Poroelastic stress triggering of the December 2013 Crooked Lake, Alberta, induced seismicity sequence. *Geophysical Research Letters*, 43(16), 8482-8491.

Department for Environment, Food and Rural Affairs (DEFRA) (2020). Magic Interactive Map. https://magic.defra.gov.uk/home.htm. Last accessed 14th April 2020.

de Pater, C. J., & Baisch, S. (2011). Geomechanical study of Bowland Shale seismicity, Synthesis report 57.

Dickey, P. A. (1969). Increasing concentration of subsurface brines with depth. *Chemical Geology*, 4(1-2), 361-370.

DiGiulio, D. C., Wilkin, R. T., Miller, C., & Oberley, G. (2011). Investigation of ground water contamination near Pavillion, Wyoming. Office of Research and Development, National Risk Management Research Laboratory.

Dimova, N. T., Burnett, W. C., Chanton, J. P., & Corbett, J. E. (2013). Application of radon-222 to investigate groundwater discharge into small shallow lakes. *Journal of Hydrology*, 486, 112-122.

Eckhardt, K. (2008). A comparison of baseflow indices, which were calculated with seven different baseflow separation methods. *Journal of Hydrology*, 352(1-2), 168-173.

Edmunds, W. M. (2004). Bath thermal waters: 400 years in the history of geochemistry and hydrogeology. *Geological Society, London, Special Publications*, 225(1), 193-199.

Edmunds, W. M. (1971). Hydrogeochemistry of groundwaters in the Derbyshire Dome with special reference to trace constituents. Report of the Institute of Geological Sciences, No.71/7 (now British Geological Survey).

Engelder, T., Cathles, L. M., & Bryndzia, L. T. (2014). The fate of residual treatment water in gas shale. *Journal of Unconventional Oil and Gas Resources*, 7, 33-48.

Environment Agency (2017). Water Quality Archive. http://environment.data.gov.uk/water-quality/index.html. Last accessed 17th November 2017.

Environment Agency (EA) (2013). An Environmental Risk Assessment for shale gas exploratory operations in England. Version 1.

Eukan Consortium (1992). UK Landward Areas Sixth Licensing Round Application Document: Elswick Area, West Lancashire Exploration License Application.

Eukan Energy Ltd. (1994). Development Plan for the Elswick Gasfield, The Fylde, West Lancashire.

Fakcharoenphol, P., Torcuk, M. A., Wallace, J., Bertoncello, A., Kazemi, H., Wu, Y. S., & Honarpour, M. (2013, September). Managing shut-in time to enhance gas flow rate in hydraulic fractured shale reservoirs: a simulation study. In SPE Annual Technical Conference and Exhibition. Society of Petroleum Engineers.

Faul, F., Erdfelder, E., Lang, A.-G., & Buchner, A. (2007). G*Power 3: A flexible statistical power analysis program for the social, behavioral, and biomedical sciences. *Behavior Research Methods*, 39, 175-191.

Ferguson, G., McIntosh, J. C., Grasby, S. E., Hendry, M. J., Jasechko, S., Lindsay, M. B., & Luijendijk, E. (2018). The persistence of brines in sedimentary basins. *Geophysical Research Letters*, 45(10), 4851-4858.

Fisher, Q. J., & Knipe, R. J. (2001). The permeability of faults within siliciclastic petroleum reservoirs of the North Sea and Norwegian Continental Shelf. *Marine and Petroleum Geology*, 18(10), 1063-1081.

Flewelling, S. A., & Sharma, M. (2014). Constraints on upward migration of hydraulic fracturing fluid and brine. *Groundwater*, 52(1), 9-19.

Foulger, G. R., Wilson, M. P., Gluyas, J. G., Julian, B. R., & Davies, R. J. (2018). Global review of human-induced earthquakes. *Earth-Science Reviews*, 178, 438-514.

FracFocus (2019). http://fracfocus.org/water-protection/drilling-usage. Last accessed 23rd September 2019.

Fraser, A. J., & Gawthorpe, R. L. (1990). Tectono-stratigraphic development and hydrocarbon habitat of the Carboniferous in northern England. *Geological Society, London, Special Publications*, 55(1), 49-86.

Frost, C. D., Pearson, B. N., Ogle, K. M., Heffern, E. L., & Lyman, R. M. (2002). Sr isotope tracing of aquifer interactions in an area of accelerating coal-bed methane production, Powder River Basin, Wyoming. *Geology*, 30(10), 923-926.

Gale, J. F., Reed, R. M., & Holder, J. (2007). Natural fractures in the Barnett Shale and their importance for hydraulic fracture treatments. *AAPG bulletin*, 91(4), 603-622.

Gallois, R. (2007). The formation of the hot springs at Bath Spa, UK. *Geological Magazine*, 144(4), 741-747.

Garven, G. (1995). Continental-scale groundwater flow and geologic processes. *Annual Review of Earth and Planetary Sciences*, 23(1), 89-117.

Gaskari, R., & Mohaghegh, S. D. (2006, January). Estimating Major and Minor Natural Fracture Pattern in Gas Shales Using Production Data. Paper presented at SPE Eastern Regional Meeting, Society of Petroleum Engineers, Canton, Ohio, USA.

Gassiat, C., Gleeson, T., Lefebvre, R., & McKenzie, J. (2013). Hydraulic fracturing in faulted sedimentary basins: Numerical simulation of potential contamination of shallow aquifers over long time scales. *Water Resources Research*, 49(12), 8310-8327.

Grapes, T. R., Bradley, C., & Petts, G. E. (2005). Dynamics of river–aquifer interactions along a chalk stream: the River Lambourn, UK. *Hydrological Processes*, 19(10), 2035-2053.

Gawthorpe, R. L. (1987). Tectono-sedimentary evolution of the Bowland Basin, N England, during the Dinantian. *Journal of the Geological Society*, 144(1), 59-71.

Gibbs, R. J. (1970). Mechanisms controlling world water chemistry. *Science*, 170(3962), 1088-1090.

Glennie, K. W. (1986). Development of NW Europe's Southern Permian gas basin. *Geological Society, London, Special Publications*, 23(1), 3-22.

Goodman, P. S., Galatioto, F., Thorpe, N., Namdeo, A. K., Davies, R. J., & Bird, R. N. (2016). Investigating the traffic-related environmental impacts of hydraulic-fracturing (fracking) operations. *Environment International*, 89, 248-260.

Gosselin, D. C., Harvey, F. E., Frost, C., Stotler, R., & Macfarlane, P. A. (2004). Strontium isotope geochemistry of ground water in the central part of the Dakota (Great Plains) aquifer, USA. *Applied Geochemistry*, 19(3), 359-377.

Griffiths, K. J., Shand, P., & Ingram, J. (2003). Baseline Report Series: 8. The Permo-Triassic Sandstones of Manchester and East Cheshire. British Geological Survey Commissioned Report, No. CR/03/265N.

Griggs, D. (1967). Hydrolytic weakening of quartz and other silicates. *Geophysical Journal International*, 14(1-4), 19-31.

Gross, S. A., Avens, H. J., Banducci, A. M., Sahmel, J., Panko, J. M., & Tvermoes, B. E. (2013). Analysis of BTEX groundwater concentrations from surface spills associated with hydraulic fracturing operations. *Journal of the Air & Waste Management Association*, 63(4), 424-432.

Guggenmos, M. R., Daughney, C. J., Jackson, B. M., & Morgenstern, U. (2011). Regional-scale identification of groundwater-surface water interaction using hydrochemistry and multivariate statistical methods, Wairarapa Valley, New Zealand. *Hydrology and Earth System Sciences*, 15(11), 3383-3398.

Gunn, J., Bottrell, S. H., Lowe, D. J., & Worthington, S. R. (2006). Deep ground water flow and geochemical processes in limestone aquifers: evidence from thermal waters in Derbyshire, England, UK. *Hydrogeology Journal*, 14(6), 868-881.

Gussow, W. C. (1954). Differential entrapment of oil and gas: a fundamental principle. *AAPG bulletin*, 38(5), 816-853.

Hackley, K. C., Liu, C. L., & Coleman, D. D. (1996). Environmental isotope characteristics of landfill leachates and gases. *Groundwater*, 34(5), 827-836.

Halinda, D., Sesaro, A. W., Weatherall, G. D., Nugraha, H., & Collecott, D. J. (2013, November). The Microseismic Monitoring of Hydraulic Fracturing Treatments of a CBM Through the Simultaneous Use of Downhole Monitoring Tools in the Stimulated and an Offset Well. A Case Study-Sanga-Sanga CBM, Mahakam Delta, East Kalimantan,

Indonesia. In SPE Unconventional Resources Conference and Exhibition-Asia Pacific. Society of Petroleum Engineers.

Hamaker, S., & Harris, R. (2007). Fault-related ground-water compartmentalization in the East Tintic Mining District, Utah.

Hanor, J. S. (1994). Origin of saline fluids in sedimentary basins. *Geological Society, London, Special Publications*, 78(1), 151-174.

Harbaugh, A. W. (2005). MODFLOW-2005, The U.S. Geological Survey modular ground-water model: the ground-water flow process. U.S. Geological Survey Techniques and Methods 6-A16.

Hawkins, A. B., & Kellaway, G. A. (1991). The hot springs of the Avon Gorge, Bristol, England. In Hot Springs of Bath, Bath City Council, 179-204.

Hedenquist, J. W., & Lowenstern, J. B. (1994). The role of magmas in the formation of hydrothermal ore deposits. *Nature*, 370(6490), 519.

Hem, J. D. (1985). Study and interpretation of the chemical characteristics of natural water. U.S. Geological Survey water-supply paper 2254.

Hird, C., & Clarke, H. (2012). Permeability and Stress Sensitivity Analysis Preese Hall-1 (CBM Solutions). Cuadrilla Resources Preese Hall-1 end of well report LJ/06-5.

Hortle, A. H., Xu, J., & Dance, T. (2009). Hydrodynamic interpretation of the Waarre Fm Aquifer in the onshore Otway Basin: implications for the CO2CRC Otway project. *Energy Procedia*, 1(1), 2895-2902.

Hough, E., Evans, D. J., & Williamson, J. P. (2011). A geological reappraisal of the Preesall Saltfield, Lancashire, United Kingdom: recognizing geological factors relevant to gas storage. Paper presented at SMRI Fall 2011 Technical Conference, York, UK.

Howard, A. S., Warrington, G., Ambrose, K., & Rees, J. G. (2008). A formational framework for the Mercia Mudstone Group (Triassic) of England and Wales. British Geological Survey Research Report, RR/08/04.

Hughes, J. D., Langevin, C. D., & Banta, E. R. (2017). Documentation for the MODFLOW 6 framework. U.S. Geological Survey Techniques and Methods, Book 6, Chap. A57, p.40.

Infrastructure Act (2015). Chapter 7, PART 6 Energy, Section 50, Onshore hydraulic fracturing: safeguards.

Jackson, R. B., Vengosh, A., Darrah, T. H., Warner, N. R., Down, A., Poreda, R. J., Osborn, S. G., Zhao, K., & Karr, J. D. (2013). Increased stray gas abundance in a subset of drinking water wells near Marcellus shale gas extraction. *Proceedings of the National Academy of Sciences*, 110(28), 11250-11255.

Jaffe, W., Lockyer, R., & Howcroft, A. (1997). The Abbeystead Explosion Disaster. *Annals of Burns and Fire Disasters*, 10(3).

Jarvie, H. P., Oguchi, T., & Neal, C. (2002). Exploring the linkages between river water chemistry and watershed characteristics using GIS-based catchment and locality analyses. *Regional Environmental Change*, 3(1-3), 36-50.

Johnston, R., & Shrallow, J. (2011, January). Ambiguity in microseismic monitoring. In 2011 SEG Annual Meeting. Society of Exploration Geophysicists.

Jones, H. K., Morris, B. L., Cheney, C. S., Brewerton, L. J., Merrin, P. D., Lewis, M. A., MacDonald, A. M., Coleby, L. M., Talbot, J. C., McKenzie, A. A., Bird, M. J., Cunningham, J., & Robinson, V. K. (2000). The physical properties of minor aquifers in England and Wales. British Geological Survey Technical Report, WD/00/4. Environment Agency R&D Publication 68.

Kahrilas, G. A., Blotevogel, J., Corrin, E. R., & Borch, T. (2016). Downhole transformation of the hydraulic fracturing fluid biocide glutaraldehyde: implications for

flowback and produced water quality. *Environmental Science & Technology*, 50(20), 11414-11423.

Kamitsuji, R., Nagai, K., Matsuno, Y., Ohsaki, Y., Tamagawa, T., & Tezuka, K. (2009, January). Hydraulic fracturing using heavy brine and microseismic monitoring in Yufutsu oil and gas field. In SPE Hydraulic Fracturing Technology Conference. Society of Petroleum Engineers.

Kilpatrick, J. E., Eisner, L., Williams-Stroud, S., Cornette, B., & Hall, M. (2010, January). Natural fracture characterization from microseismic source mechanisms: a comparison with FMI data. In 2010 SEG Annual Meeting. Society of Exploration Geophysicists.

King, G. E. (2012, January). Hydraulic fracturing 101: what every representative, environmentalist, regulator, reporter, investor, university researcher, neighbor and engineer should know about estimating frac risk and improving frac performance in unconventional gas and oil wells. In SPE hydraulic fracturing technology conference. Society of Petroleum Engineers.

Kirby, G. A., Baily, H. E., Chadwick, R. A., Evans, D. J., Holliday, D. W., Holloway, S., Hulbert, A. G., Pharaoh, T. C., Smith, N. J. P., Aitkenhead, N., & Birch, B. (2000). The structure and evolution of the Craven Basin and adjacent areas. Surface Memoir of the British Geological Survey.

Kissinger, A., Helmig, R., Ebigbo, A., Class, H., Lange, T., Sauter, M., Heitfeld, M., Klünker, J., & Jahnke, W. (2013). Hydraulic fracturing in unconventional gas reservoirs: risks in the geological system, part 2. *Environmental earth sciences*, 70(8), 3855-3873.

Kondash, A. J., Lauer, N. E., & Vengosh, A. (2018). The intensification of the water footprint of hydraulic fracturing. *Science Advances*, 4(8), eaar5982.

Konopelko, A., Sukovatyy, V., Mitin, A., & Rubtsova, A. (2015, October). Microseismic Monitoring of Multistage Hydraulic Fracturing in Complex Reservoirs of the Volgo-Urals Region of Russia. In SPE Russian Petroleum Technology Conference. Society of Petroleum Engineers.

Kratz, M., Hill, A., & Wessels, S. (2012, March). Identifying fault activation in unconventional reservoirs in real time using microseismic monitoring. In SPE/EAGE European Unconventional Resources Conference & Exhibition-From Potential to Production.

Kumar, M., Ramanathan, A. L., & Keshari, A. K. (2009). Understanding the extent of interactions between groundwater and surface water through major ion chemistry and multivariate statistical techniques. *Hydrological Processes*, 23(2), 297-310.

Lacazette, A., & Geiser, P. (2013). Comment on Davies et al., 2012—Hydraulic fractures: How far can they go?. *Marine and Petroleum Geology*, 43, 516-518.

Langevin, C. D., Hughes, J. D., Banta, E. R., Niswonger, R. G., Panday, S., & Provost, A. M. (2017). Documentation for the MODFLOW 6 Groundwater Flow Model. U.S. Geological Survey Techniques and Methods, Book 6, Chap. A55, p.197.

Lees, G. M., & Cox, P. T. (1937). The Geological Basis of the Present Search for Oil in Great Britain by the D'Arcy Exploration Company, Ltd. *Quarterly Journal of the Geological Society*, 93(1-4), 156-194.

Lei, X., Wang, Z., & Su, J. (2019). The December 2018 ML 5.7 and January 2019 ML 5.3 earthquakes in South Sichuan basin induced by shale gas hydraulic fracturing. *Seismological Research Letters*, 90(3), 1099-1110.

Leveille, G. P., Knipe, R., More, C., Ellis, D., Dudley, G., Jones, G., Fisher, Q. J., & Allinson, G. (1997). Compartmentalization of Rotliegendes gas reservoirs by sealing faults, Jupiter Fields area, southern North Sea, *Geological Society, London, Special Publications*, 123(1), 87-104.

Lewis, C. L., Green, P. F., Carter, A., & Hurford, A. J. (1992). Elevated K/T palaeotemperatures throughout Northwest England: three kilometres of Tertiary erosion?. *Earth and Planetary Science Letters*, 112(1-4), 131-145.

Llewellyn, G. T., Dorman, F., Westland, J. L., Yoxtheimer, D., Grieve, P., Sowers, T., Humston-Fulmer, E., & Brantley, S. L. (2015). Evaluating a groundwater supply contamination incident attributed to Marcellus Shale gas development. *Proceedings of the National Academy of Sciences*, 112(20), 6325-6330.

Lunn, D. J., Thomas, A., Best, N., & Spiegelhalter, D. (2000). WinBUGS-a Bayesian modeling framework: concepts, structure, and extensibility. *Statistics and computing*, 10(4), 325-337.

Malone, W. S., Turner, M. G., Mayerhofer, M. J., Northington, N., & Weijers, L. (2009, January). Development of a calibrated fracture-growth model and automated staging routine for the Jonah Field. In SPE Rocky Mountain Petroleum Technology Conference. Society of Petroleum Engineers.

Mather, J. D. (2013). Britain's spa heritage: a hydrogeological appraisal. *Geological Society, London, Special Publications*, 375(1), 243-260.

Matthess, G. (1982). The Properties of Ground water. John Wiley and Sons Inc., New York. p. 71.

Maxwell, S. C., Shemeta, J. E., Campbell, E., & Quirk, D. J. (2008, January). Microseismic deformation rate monitoring. In SPE Annual Technical Conference and Exhibition. Society of Petroleum Engineers.

Maxwell, S. C., Zimmer, U., Gusek, R., & Quirk, D. (2007, January). Hydraulic fracture reorientation across a thrust fault. In 2007 SEG Annual Meeting. Society of Exploration Geophysicists.

Mayerhofer, M. J., Lolon, E., Warpinski, N. R., Cipolla, C. L., Walser, D. W., & Rightmire, C. M. (2010, November). What is stimulated reservoir volume?. In SPE Shale Gas Production Conference. Society of Petroleum Engineers.

Mayerhofer, M. J. Stegent, N. A., Barth, J. O., & Ryan, K. M. (2011, January). Integrating fracture diagnostics and engineering data in the Marcellus shale. In SPE Annual Technical Conference and Exhibition. Society of Petroleum Engineers.

Mayerhofer, M. J. Stegent, N. A., Barth, J. O., & Ryan, K. M. (2011, January). Integrating fracture diagnostics and engineering data in the Marcellus shale. In SPE Annual Technical Conference and Exhibition. Society of Petroleum Engineers.

McDonald, M. G., & Harbaugh, A. W. (1984). A modular three-dimensional finite-difference ground-water flow model. U.S. Geological Survey Open-File Report 83-875.

McKie, T., Jolley, S. J., & Kristensen, M. B. (2010). Stratigraphic and structural compartmentalisation of dryland fluvial reservoirs: Triassic Heron Cluster, Central North Sea. *Geological Society, London, Special Publications*, 347(1), 165-198.

Medici, G., West, L. J., Mountney, N. P., & Welch, M. (2019). Permeability of rock discontinuities and faults in the Triassic Sherwood Sandstone Group (UK): insights for management of fluvio-aeolian aquifers worldwide. *Hydrogeology Journal*, 1-21.

Mohamed, E. A., & Worden, R. H. (2006). Groundwater compartmentalisation: a water table height and geochemical analysis of the structural controls on the subdivision of a major aquifer, the Sherwood Sandstone, Merseyside, UK. *Hydrology and Earth System Sciences Discussions*, 2006, 10(1), 49-64.

Molofsky, L. J., Connor, J. A., Farhat, S. K., Wylie, A. S., & Wagner, T. (2011). Methane in Pennsylvania water wells unrelated to Marcellus shale fracturing. *Oil & Gas Journal*, 109(19), 54-54.

Molofsky, L. J., Connor, J. A., McHugh, T. E., Richardson, S. D., Woroszylo, C., & Alvarez, P. J. (2016). Environmental factors associated with natural methane occurrence in the Appalachian Basin. *Groundwater*, 54(5), 656-668.

Molofsky, L. J., Connor, J. A., Wylie, A. S., Wagner, T., & Farhat, S. K. (2013). Evaluation of methane sources in groundwater in northeastern Pennsylvania. *Groundwater*, 51(3), 333-349.

Mott MacDonald (2010). Fylde Model Upgrade and Scenario Runs: NGMS Upload. Report for the Environment Agency.

Mott MacDonald (1997). Fylde Aquifer/Wyre Catchment Water Resources Study. Final Report for the Environment Agency.

National River Flow Archive (NRFA) (2020). The National River Flow Archive. https://nrfa.ceh.ac.uk/data/search. Last accessed 3rd April 2020.

Neal, C., Rowland, P., Scholefield, P., Vincent, C., Woods, C., & Sleep, D. (2011). The Ribble/Wyre observatory: Major, minor and trace elements in rivers draining from rural headwaters to the heartlands of the NW England historic industrial base. *Science of the Total Environment*, 409(8), 1516-1529.

Neuhaus, C. W., & Miskimins, J. L. (2012, January). Analysis of surface and downhole microseismic monitoring coupled with hydraulic fracture modeling in the Woodford Shale. In SPE Europec/EAGE Annual Conference. Society of Petroleum Engineers.

Neuhaus, C. W., Telker, C., Ellison, M., & Blair, K. (2013, June). Hydrocarbon production and microseismic monitoring-treatment optimization in the Marcellus Shale. In EAGE Annual Conference & Exhibition incorporating SPE Europec. Society of Petroleum Engineers.

NOAA (National Oceanic and Atmospheric Administration) (2019a). Global Climate Report for July 2018. https://www.ncdc.noaa.gov/sotc/global/201807. Last accessed 27th May 2019.

NOAA (National Oceanic and Atmospheric Administration) (2019b). Global Climate Report for June 2018. https://www.ncdc.noaa.gov/sotc/global/201806. Last accessed 27th May 2019.

Myers, T. (2012). Potential contaminant pathways from hydraulically fractured shale to aquifers. *Groundwater*, 50(6), 872-882.

North West Water (NWW) (1986). Lancashire Conjunctive Use Scheme Further Investigations: Wyresdale Tunnel. Final Geological/Geophysical Report.

Oguchi, T., Jarvie, H. P., & Neal, C. (2000). River water quality in the Humber catchment: an introduction using GIS-based mapping and analysis. *Science of the Total Environment*, 251, 9-26.

Oil and Gas Authority (OGA) (2019). Managing onshore induced seismicity. https://www.ogauthority.co.uk/media/5110/oga_managing_onshore_induced_seismicity _infographic.pdf. Last accessed 29th October 2019.

Oil and Gas Authority (OGA) (2017). Guidance for EWTs and HFPs. https://www.ogauthority.co.uk/media/3168/onshore-ewt-and-hfp_january-2017.pdf. Last accessed 7th August 2019.

Olejnik, S., & Algina, J. (2003). Generalized eta and omega squared statistics: measures of effect size for some common research designs. *Psychological methods*, 8(4), 434-447.

Olmstead, S. M., Muehlenbachs, L. A., Shih, J. S., Chu, Z., & Krupnick, A. J. (2013). Shale gas development impacts on surface water quality in Pennsylvania. *Proceedings of the National Academy of Sciences*, 110(13), 4962-4967.

Ordnance Survey (OS) (2019). OS Terrain 50. https://www.ordnancesurvey.co.uk/business-and-government/products/terrain-50.html. Last accessed 27th May 2019.

Osborn, S. G., Vengosh, A., Warner, N. R., & Jackson, R. B. (2011). Methane contamination of drinking water accompanying gas-well drilling and hydraulic fracturing. *Proceedings of the National Academy of Sciences*, 108(20), 8172-8176.

Osborne, M. J., & Swarbrick, R. E. (1997). Mechanisms for generating overpressure in sedimentary basins: a reevaluation. *AAPG bulletin*, 81(6), 1023-1041.

Ove Arup and Partners Ltd. (2014a). Environmental Statement Temporary Shale Gas extraction Preston New Road, Lancashire. Produced for Cuadrilla Bowland Ltd., PNR_ES_Vol1_Environmental Statement.

Ove Arup and Partners Ltd. (2014b). Appendix L – Induced Seismicity Environmental Statement Temporary Shale Gas extraction Preston New Road, Lancashire. Produced for Cuadrilla Bowland Ltd., PNR_ES_Vol2_Appndx L_Induced Seismicity.

Ove Arup and Partners Ltd. (2014c). Appendix K – Hydrogeology and Ground Gas Environmental Statement Temporary Shale Gas extraction Preston New Road, Lancashire. Produced for Cuadrilla Bowland Ltd., PNR_ES_Vol2_Appndx K_Hydrogeology & Gas.

Palat, S., Torbatynia, M., Kanadikirik, K., & Varma, S. (2015, November). Hydrodynamic Modelling of Hydraulic Fracturing Fluid Injection in North Perth Basin Shale Gas Targets. Paper presented at SPE Asia Pacific Unconventional Resources Conference and Exhibition, Society of Petroleum Engineers, Brisbane, Australia.

Palmer, R. C., & Lewis, M. A. (1998). Assessment of groundwater vulnerability in England and Wales. *Geological Society, London, Special Publications*, 130(1), 191-198.

Pfunt, H., Houben, G., & Himmelsbach, T. (2016). Numerical modelling of fracking fluid migration through fault zones and fractures in the North German Basin. *Hydrogeology Journal*, 24(6), 1343-1358.

Piper, A. M. (1944). A graphic procedure in the geochemical interpretation of water-analyses. *Eos, Transactions American Geophysical Union*, 25(6), 914-928.

Pollock, D. W. (2012). User Guide for MODPATH Version 6 – A Particle-Tracking Model for MODFLOW. U.S. Geological Survey Techniques and Methods 6-A41.

Power, O. T. (1978). Gas seep off Anvil Point. Triton, 57.

Rivard, C., Bordeleau, G., Lavoie, D., Lefebvre, R., Ladevèze, P., Duchesne, M.J., Séjourné, S., Crow, H., Pinet, N., Brake, V., & Bouchedda, A. (2019). Assessing potential impacts of shale gas development on shallow aquifers through upward fluid migration: A multi-disciplinary approach applied to the Utica Shale in eastern Canada. *Marine and Petroleum Geology*, 100, 466-483.

Reeves, J. W. (1948). Surface problems in the search for oil in Sussex. *Proceedings of the Geologists' Association*, 59(4), 234-IN8.

Rothwell, J. J., Dise, N. B., Taylor, K. G., Allott, T. E. H., Scholefield, P., Davies, H., & Neal, C. (2010a). A spatial and seasonal assessment of river water chemistry across North West England. *Science of the Total Environment*, 408(4), 841-855.

Rothwell, J. J., Dise, N. B., Taylor, K. G., Allott, T. E. H., Scholefield, P., Davies, H., & Neal, C. (2010b). Predicting river water quality across North West England using catchment characteristics. *Journal of Hydrology*, 395(3-4), 153-162.

Rowe, J., Burley, S., Gawthorpe, R., Cowan, G. T., & Hardman, M. (1993). Palaeofluid flow in the East Irish Sea Basin and its margins. *Geofluids*, 93, 358-362.

Royal Society and Royal Academy of Engineering (2012). Shale gas extraction in the UK: a review of hydraulic fracturing.

Rutqvist, J., Rinaldi, A. P., Cappa, F., & Moridis, G. J. (2015). Modelling of fault activation and seismicity by injection directly into a fault zone associated with hydraulic fracturing of shale-gas reservoirs. *Journal of Petroleum Science and Engineering*, 127, 377-386.

Rutqvist, J., Rinaldi, A. P., Cappa, F., & Moridis, G. J. (2013). Modelling of fault reactivation and induced seismicity during hydraulic fracturing of shale-gas reservoirs. *Journal of Petroleum Science and Engineering*, 107, 31-44.

Sage, R. C., & Lloyd, J. W. (1978). Drift deposit influences on the Triassic Sandstone aquifer of NW Lancashire as inferred by hydrochemistry. *Quarterly Journal of Engineering Geology and Hydrogeology*, 11(3), 209-218.

Saleem, W. A., Baber, S., & Jafri, M. O. (2014, April). Shale Gas Field: Exploration, Exploitation and Development Strategies Globally. In SPE Saudi Arabia Section Technical Symposium and Exhibition. Society of Petroleum Engineers.

Sear, D. A., Armitage, P. D., & Dawson, F. H. (1999). Groundwater dominated rivers. *Hydrological Processes*, 13(3), 255-276.

Selley, R. C. (2012). UK shale gas: the story so far. *Marine and Petroleum Geology*, 31(1), 100-109.

Selley, R. C. (1992). Petroleum seepages and impregnations in Great Britain. *Marine and Petroleum Geology*, 9(3), 226-244.

Selley, R. C., & Stoneley, R. (1987). Petroleum Habitat in South Dorset. In Petroleum Geology of North West Europe, Graham & Trotman, London, 139-148.

Seymour, K. J., Ingram, J. A., & Gebbett, S. J. (2006). Structural controls on groundwater flow in the Permo-Triassic sandstones of NW England. *Geological Society, London, Special Publications*, 263(1), 169-185.

Sibson, R. H. (1974). Frictional constraints on thrust, wrench and normal faults. *Nature*, 249(5457), 542.

Sibson, R. H., Moore, J. M. M., & Rankin, A. H. (1975). Seismic pumping—a hydrothermal fluid transport mechanism. *Journal of the Geological Society*, 131(6), 653-659.

Sicking, C., Vermilye, J., Geiser, P., Lacazette, A., & Thompson, L. (2013). Permeability field imaging from microseismic. *Geophysical Society of Houston Journal*, 3(7), 11-14.

Skoumal, R., Barbour, A. J., Brudzinski, M., Langenkamp, T., & Kaven, J. O. (2019, December). Induced Seismicity in the Delaware Basin. In AGU Fall Meeting Abstracts.

Skoumal, R. J., Brudzinski, M. R., & Currie, B. S. (2015). Earthquakes induced by hydraulic fracturing in Poland Township, Ohio. *Bulletin of the Seismological Society of America*, 105(1), 189-197.

Skoumal, R. J., Ries, R., Brudzinski, M. R., Barbour, A. J., & Currie, B. S. (2018). Earthquakes induced by hydraulic fracturing are pervasive in Oklahoma. *Journal of Geophysical Research: Solid Earth*, 123(12), 10-918.

Smalley, P. C., & Hale, N. A. (1996). Early identification of reservoir compartmentalization by combining a range of conventional and novel data types. *SPE Formation Evaluation*, 11(03), 163-170.

Smerdon, B. D., & Turnadge, C. (2015). Considering the potential effect of faulting on regional-scale groundwater flow: an illustrative example from Australia's Great Artesian Basin. *Hydrogeology Journal*, 23, 949-960.

Sophocleous, M. (2002). Interactions between groundwater and surface water: the state of the science. *Hydrogeology journal*, 10(1), 52-67.

Soulsby, C., Tetzlaff, D., Van den Bedem, N., Malcolm, I. A., Bacon, P. J., & Youngson, A. F. (2007). Inferring groundwater influences on surface water in montane catchments from hydrochemical surveys of springs and streamwaters. *Journal of Hydrology*, 333(2-4), 199-213.

Stoneley, R. (1982). The structural development of the Wessex Basin. *Journal of the Geological Society*, 139(4), 543-554.

Taherdangkoo, R., Tatomir, A., Anighoro, T., & Sauter, M. (2019). Modeling fate and transport of hydraulic fracturing fluid in the presence of abandoned wells. *Journal of contaminant hydrology*, 221, 58-68.

Tellam, J. H. (1995). Hydrochemistry of the saline groundwaters of the lower Mersey Basin Permo-Triassic sandstone aquifer, UK. *Journal of Hydrology*, 165(1-4), 45-84.

The Onshore Hydraulic Fracturing (Protected Areas) Regulations (2016). UK Statutory Instruments 2016, No. 384, Petroleum.

Thornton, G. J. P., & Dise, N. B. (1998). The influence of catchment characteristics, agricultural activities and atmospheric deposition on the chemistry of small streams in the English Lake District. *Science of the Total Environment*, 216(1-2), 63-75.

Townsend, C., Firth, I. R., Westerman, R., Kirkevollen, L., Hårde, M., & Andersen, T. (1998). Small seismic-scale fault identification and mapping. *Geological Society, London, Special Publications*, 147(1), 1-25.

UK Onshore Geophysical Library (UKOGL) (2019). https://ukogl.org.uk/. Last accessed 22nd November 2019.

UK Onshore Geophysical Library (UKOGL) (2012). UKOGL-RG-006.

UK Technical Advisory Group (UKTAG) (2011). Defining & Reporting on Groundwater Bodies.

Underhill, J. R., & Stoneley, R. (1998). Introduction to the development, evolution and petroleum geology of the Wessex Basin. *Geological Society, London, Special Publications*, 133(1), 1-18.

Urbancic, T. I., Schumila, V., Rutledge, J. T., & Zinno, R. J. (1999, January). Determining hydraulic fracture behaviour using microseismicity. In Vail Rocks 1999, The 37th US Symposium on Rock Mechanics (USRMS). American Rock Mechanics Association.

U.S. Energy Information Administration (US EIA) (2019). https://www.eia.gov/dnav/ng/hist/res_epg0_r5302_nus_bcfa.htm. Last accessed 23rd September 2019.

Vengosh, A., Jackson, R. B., Warner, N., Darrah, T. H., & Kondash, A. (2014). A critical review of the risks to water resources from unconventional shale gas development and hydraulic fracturing in the United States. *Environmental Science & Technology*, 48(15), 8334-8348.

Vengosh, A., Warner, N., Jackson, R., & Darrah, T. (2013). The effects of shale gas exploration and hydraulic fracturing on the quality of water resources in the United States. *Procedia Earth and Planetary Science*, 7, 863-866.

Verdon, J. P. (2018, July). Comments on the Scientific Basis, or Lack Thereof, for Hydraulic Fracturing Fault Respect Distances. Report Commissioned by the Oil and Gas Authority.

Wang, F. P., & Reed, R. M. (2009, January). Pore networks and fluid flow in gas shales. In *SPE annual technical conference and exhibition*. Society of Petroleum Engineers.

Ward, R. S., Allen, G., Baptie, B. J., Bateson, L., Bell, R. A., Butcher, A. S., Daraktchieva, Z., Dunmore, R., Fisher, R. E., Horleston, A., Howarth, C. H., Jones, D. G., Jordan, C. J., Kendall, M., Lewis, A., Lowry, D., Miller, C. A., Milne, C. J. Novellino, A., Pitt, J., Purvis, R. M., Smedley, P. L., & Wasikiewicz, J. M. (2018). Preliminary assessment of the environmental baseline in the Fylde, Lancashire. Nottingham, UK, British Geological Survey, OR/18/020.

Warpinski, N. R. (2014, August). A review of hydraulic-fracture induced microseismicity. In 48th US Rock Mechanics/Geomechanics Symposium. American Rock Mechanics Association.

Warpinski, N. R., & Du, J. (2010, January). Source-mechanism studies on microseismicity induced by hydraulic fracturing. In SPE Annual Technical Conference and Exhibition. Society of Petroleum Engineers.

Warpinski, N. R., Wolhart, S. L., & Wright, C. A. (2001, January). Analysis and prediction of microseismicity induced by hydraulic fracturing. In SPE Annual Technical Conference and Exhibition. Society of Petroleum Engineers.

Water Research Centre (WRC) (1972). Interim Report on the Investigation of the Fylde Bunter Aquifer.

Westwood, R. F., Toon, S. M., Styles, P., & Cassidy, N. J. (2017a). Horizontal respect distance for hydraulic fracturing in the vicinity of existing faults in deep geological reservoirs: a review and modelling study. *Geomechanics and Geophysics for Geo-Energy and Geo-Resources*, 1-13.

Westwood, R. F., Toon, S. M., & Cassidy, N. J. (2017b). A sensitivity analysis of the effect of pumping parameters on hydraulic fracture networks and local stresses during shale gas operations. *Fuel*, 203, 843-852.

Whitelaw, P., Uguna, C. N., Stevens, L. A., Meredith, W., Snape, C. E., Vane, C. H., Moss-Hayes, V., & Carr, A. D. (2019). Shale gas reserve evaluation by laboratory

pyrolysis and gas holding capacity consistent with field data. *Nature Communications*, 10(1), 1-10.

Williams-Stroud, S., & Billingsley, R. L. (2010, January). Techniques to estimate fracture effectiveness when mapping low-magnitude microseismicity. In SEG Technical Program Expanded Abstracts. Society of Exploration Geophysicists.

Wilson, A. A. (1990). The Mercia Mudstone Group (Trias) of the East Irish Sea Basin. *Proceedings of the Yorkshire Geological Society*, 48(1), 1-22.

Wilson, A. A., & Evans, W. B. (1990). Geology of the country around Blackpool. British Geological Survey Memoir.

Wilson, M. P., Foulger, G. R., Gluyas, J. G., Davies, R. J., & Julian, B. R. (2017a). HiQuake: The human-induced earthquake database. *Seismological Research Letters*, 88(6), 1560-1565.

Wilson, M. P., Worrall, F., Clancy, S. A., Ottley, C. J., Hart, A., & Davies, R. J. (accepted). Compartmentalisation and groundwater-surface water interactions in a prospective shale gas basin: Assessment using variance analysis and multivariate statistics on water quality data. *Hydrological Processes*.

Wilson, M. P., Worrall, F., Davies, R. J., & Almond, S. (2018). Fracking: How far from faults?. *Geomechanics and Geophysics for Geo-Energy and Geo-Resources*, 4(2), 193-199.

Wilson, M. P., Worrall, F., Davies, R. J., & Hart, A. (2019). Identifying groundwater compartmentalisation for hydraulic fracturing risk assessments. *Environmental Science: Processes & Impacts*, 21(2), 352-369.

Wilson, M. P., Worrall, F., Davies, R. J., & Hart, A. (2017b). Shallow aquifer vulnerability from subsurface fluid injection at a proposed shale gas hydraulic fracturing site. *Water Resources Research*, 53(11), 9922-9940.

Winston, R. B. (2009). ModelMuse-A graphical user interface for MODFLOW-2005 and PHAST. U.S. Geological Survey Techniques and Methods 6-A29.

Winston, R. B. (2000). Graphical User Interface for MODFLOW, Version 4. U. S. Geological Survey Open-File Report 00-315.

Wolhart, S. L., Harting, T. A., Dahlem, J. E., Young, T., Mayerhofer, M. J., & Lolon, E. P. (2006, January). Hydraulic fracture diagnostics used to optimize development in the Jonah field. In SPE Annual Technical Conference and Exhibition. Society of Petroleum Engineers.

Worrall, F., & Kolpin, D. W. (2004). Aquifer vulnerability to pesticide pollution combining soil, land-use and aquifer properties with molecular descriptors. *Journal of Hydrology*, 293(1), 191-204.

Xiong, B., Loss, R. D., Shields, D., Pawlik, T., Hochreiter, R., Zydney, A. L., & Kumar, M. (2018a). Polyacrylamide degradation and its implications in environmental systems. *NPJ Clean Water*, 1(1), 1-9.

Xiong, B., Miller, Z., Roman-White, S., Tasker, T., Farina, B., Piechowicz, B., Burgos, W. D., Joshi, P., Zhu, L., Gorski, C. A., & Zydney, A. L. (2018b). Chemical degradation of polyacrylamide during hydraulic fracturing. *Environmental Science & Technology*, 52(1), 327-336.

Yaliz, A., & Chapman, T. (2003). The Lennox Oil and Gas Field, Block 110/15, East Irish Sea. *Geological Society, London, Memoirs*, 20(1), 87-96.

Yaliz, A., & Taylor, P. (2003). The Hamilton and Hamilton North Gas Fields, Block 110/13a, East Irish Sea. *Geological Society, London, Memoirs*, 20(1), 77-86.

Zhu, J., Perll, C., & Coulman, T. (2019). Enhancing Subsurface Imaging and Reservoir Characterization in the Marcellus Shale Play, Northeast Pennsylvania through Advanced Reprocessing of Wide Azimuth 3D Seismic Data. *Interpretation*, 7(4), 1-46.

Appendix A

This appendix comprises of an additional publication produced during the PhD but which was considered outside the thesis narrative and thus supplementary material. The publication is therefore presented below as a standalone study.

Wilson, M. P., Worrall, F., Davies, R. J., & Hart, A. (2019). A dynamic baseline for dissolved methane in English groundwater. *Science of the Total Environment*, 134854.

Abstract

Elevated dissolved methane (CH_4) concentrations in groundwater are an environmental concern associated with hydraulic fracturing for shale gas. Therefore, determining dissolved CH_4 baselines is important for detecting and understanding any potential environmental impacts. Such baselines should change in time and space to reflect ongoing environmental change and should be able to predict the probability that a change in dissolved CH_4 concentration has occurred. We considered four dissolved CH_4 concentration datasets of English groundwater using a Bayesian approach: two national datasets and two local datasets from shale gas exploration sites. The most sensitive national dataset (the previously published British Geological Survey CH_4 baseline) was used as a strong prior for a larger (2153 measurements compared to 439) but less sensitive (detection limit 1000 times higher) Environment Agency dataset. The use of the strong prior over a weak prior improved the precision of the Environment Agency dataset by 75%. The expected mean dissolved CH_4 concentration in English groundwater based on the Bayesian approach is 0.24 mg/l, with a 95% credible interval of 0.11 to 0.45 mg/l, and a Weibull distribution of $W(0.35\pm0.01, 0.34\pm0.16)$. This result indicates the amount of

CH$_4$ degassing from English groundwater to the atmosphere equates to between 0.7 to 3.1 kt CH$_4$/year, with an expected value of 1.65 kt CH$_4$/year and a greenhouse gas warming potential of 40.3 kt CO$_2$ eq/year. The two local monitoring datasets from shale gas exploration sites, in combination with the national datasets, show that dissolved CH$_4$ concentrations in English groundwater are generally low, but locations with concentrations greater than or equal to the widely used risk action level of 10.0 mg/l do exist. Statistical analyses of groundwater redox conditions at these locations suggest that it may be possible to identify other locations with dissolved CH$_4$ concentrations $\geq$10.0 mg/l using redox parameters such as Fe concentration.

Graphical abstract
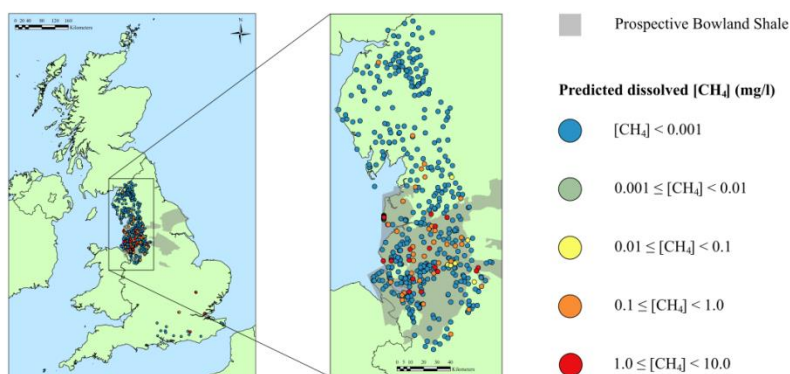
Keywords

Aquifer, Bayesian, CH$_4$, Fracking, Hydraulic fracturing, Shale gas

1. Introduction

Methane (CH$_4$) dissolved in groundwater has no known health effects to humans or animals when consumed. However, gaseous CH$_4$ is known to be a potent greenhouse gas [*IPCC*, 2013], can pose as an asphyxiation hazard in confined spaces, and can create an explosion hazard when concentrations reach 5% by volume in air [*Hooker and Bannon*, 1993]. Because of these hazards and climate change effects, the degassing of CH$_4$ from groundwater, and therefore elevated dissolved CH$_4$ concentrations, have become a topic of environmental concern associated with the hydraulic fracturing (fracking) of unconventional reservoirs, such as shale, to extract commercial quantities of CH$_4$ [*Vengosh et al.*, 2013]. Concerns primarily stem from the United States of America (USA) where there has been considerable debate on whether elevated dissolved CH$_4$ concentrations, widely publicized by the "Gaslands" film, are naturally occurring or the result of stray gas from fracking operations [*Llewellyn et al.*, 2015; *Molofsky et al.*, 2013; 2016; *Osborn et al.*, 2011]. Further concerns may arise from historic industry-related incidents such as the CH$_4$ explosions at Abbeystead (in 1984) and Loscoe (in 1986) as a result of water pumping and landfill waste, respectively [*Exploration Consultants Ltd.*, 1986; *Williams and Aitkenhead*, 1991]. To assess and demonstrate that an industry has impacted an environment it is necessary to show, within a reasonable level of certainty, that an indicator of concern has changed environmental state over and above that which was true without the industrial activity present. Alternatively, that the industrial activity has changed an environmental state beyond some accepted minimum level of harm. Experience from the USA shale gas industry has highlighted that demonstrating the impact, or the ability to confirm the absence of an impact, of fracking on dissolved CH$_4$ concentrations in groundwater requires that a baseline, or pre-intervention control, needs to be established for subsequent observations.

England has a nascent shale gas industry and although a number of companies are developing plans to exploit shale gas reserves, only two sites have been hydraulically fractured to date (note since the time of writing a moratorium has been imposed following induced seismicity). In 2012 the Royal Society and the Royal Academy of Engineering recognized the need to develop a dissolved CH_4 baseline prior to shale gas development [*Mair et al.*, 2012]. In 2017 the British Geological Survey (BGS) contributed to establishing this baseline by publishing dissolved CH_4 concentrations from a range of aquifers across England, Scotland and Wales [*Bell et al.*, 2017]. *Bell et al.* [2017] built on previous dissolved CH_4 sampling results [*Ó Dochartaigh et al.*, 2001; *Gooddy and Darling,* 2005; *Darling and Gooddy,* 2006] to increase the number of BGS sampling locations across Great Britain to 343 sites. Approximately 30% of the 343 sites comprised of private and Environment Agency of England (EA) monitoring sites. However, the EA have numerous other monitoring sites where dissolved CH_4 concentrations in groundwater have been measured and these data are publically available online from the year 2000. These additional dissolved CH_4 concentration measurements were not included in the BGS baseline because of their limited geographical coverage and considerably higher detection limit; and the subsequent difficulty in combining them with the newly acquired BGS CH_4 concentration data [*Rob Ward,* personal communication, 2018]. Therefore, there is a need to create methods which can bring together dissolved CH_4 datasets with different detection limits into a single coherent and consistent framework to make maximum use of all the data available while providing a probabilistic, and thus risk-based, assessment of any impact.

In this study generalised linear modeling within a Bayesian framework [*Gelman et al.*, 2004] is used to combine the BGS and EA dissolved CH_4 concentration data and develop a dynamic baseline for English groundwater. We also collate and incorporate dissolved CH_4 concentrations from local baseline monitoring at two shale gas exploration

sites. This approach is entirely data driven without the need for the parameterisation required in physical models; it is flexible with respect to the distribution chosen to represent the data and can include factors (e.g. location) and covariate information. The Bayesian framework allows differing data sources to be used; one dataset being the prior information to inform the analysis of the next, with the result (the posterior) becoming the prior information for the subsequent dataset. In this way the data are brought together in one framework that can be updated and improved with time, i.e. it provides a dynamic baseline in time and space. Equally, it means that historic data, derived for a variety of purposes, or data from other locations, can be used to strengthen the current monitoring at the current locations of interest: in a Bayesian framework all information has value. Furthermore, all the outputs from a Bayesian analysis come as a probability distribution which means that risk can be assessed. Such a baseline can generate a time series of expected dissolved CH_4 concentrations and indicate the likelihood of an unusually elevated dissolved CH_4 concentration occurring. To further extend our analysis we also investigate whether groundwater redox conditions can be used to predict locations in England with elevated dissolved CH_4 concentrations. These redox conditions may be easier and less expensive to monitor than dissolved CH_4 and may thus better inform where and when more expensive dissolved CH_4 analysis is required.

2. Approach and Methodology

To combine four datasets of dissolved CH_4 concentrations in groundwater with differing detection limits a Bayesian generalised linear modeling approach was taken [*Gelman et al.*, 2004]. This approach uses the concentration distribution of one dataset to inform the sub-detection limit distribution of the other datasets. The output is also probabilistic and can therefore be used as a predictor of likely dissolved CH_4 concentrations. To investigate

271

if groundwater redox conditions could be used to predict locations in England with elevated dissolved CH_4 concentrations, statistical analyses of binomial probability modeling and analysis of variance (ANOVA) were carried out on locations observed to have elevated dissolved CH_4 concentrations.
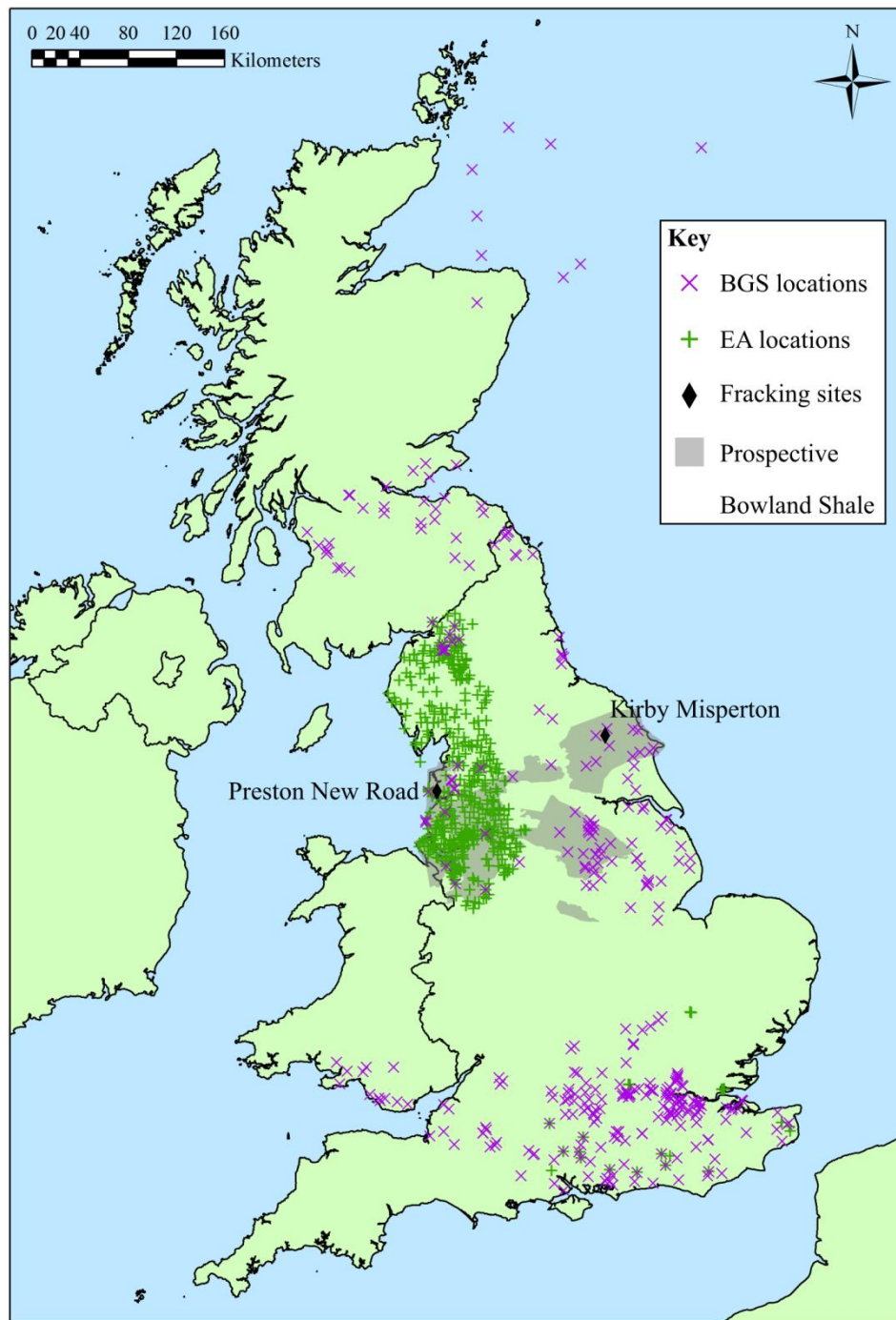
2.1. Dissolved CH_4 concentration datasets

2.1.1. BGS dataset

The BGS dissolved CH_4 concentration data (herein termed the BGS dataset) were downloaded from the supplementary material of *Bell et al.* [2017]. The dataset contains 439 dissolved CH_4 concentration measurements across 336 unique locations in Great Britain (Fig. 1, Table S1). The detection limit for the dataset was ~0.5 μg/l, although in some cases measured dissolved CH_4 concentrations were lower due to favourable gas chromatography conditions during batch analysis [*Bell et al.*, 2017].

2.1.2. EA dataset

Dissolved CH_4 concentrations (in mg/l) in English groundwater were downloaded from the EA Water Quality Archive [*EA*, 2019a] for the years 2000-2017, inclusive. Only those entries with identifiable grid references and location names were used – this dataset is hereafter referred to as the EA dataset (Table S2). Groundwater monitoring was undertaken by the EA for a range of purposes, most commonly as planned investigations and routine monitoring (Table S3). Measurements taken for statutory failures and unplanned reactive monitoring (pollution incidents) were not removed from the dataset because although certain water quality determinands would be expected to be elevated after a pollution incident, CH_4 is not classified as a groundwater pollutant and therefore

dissolved CH_4 measurements may simply have been taken opportunistically when investigating the cause of the incident (we cannot prove otherwise given the available information). Waste monitoring measurements, which might show elevated CH_4 concentrations due to the biogenic breakdown of anthropogenic waste, were also retained in the dataset because these are still important for defining the current status of dissolved CH_4 in groundwater prior to potential widespread shale gas exploitation. The EA dataset contains 2153 dissolved CH_4 concentration measurements from 571 unique locations in England (Fig. 1; Table S2). Approximately 87% of the dissolved CH_4 concentration measurements and ~92% of the unique locations are located in the northwest of England (Cumbria, Lancashire, Greater Manchester, Merseyside and Cheshire) (Fig. 1; Table S4). This geographically focussed sampling is a result of increased dissolved CH_4 sampling in response to the 1984 Abbeystead explosion [*Rob Ward*, personal communication, 2018]. The source of the CH_4 at Abbeystead was attributed to the thermally-mature, organic-rich Bowland Shale [*Exploration Consultants Ltd.*, 1986] and a large area of northwest England is underlain by the Bowland Shale, which is the United Kingdom's (UK) largest prospective shale gas resource [*Andrews*, 2013].

Figure 1
Map of Great Britain showing the dissolved CH$_4$ concentration sampling locations of the BGS and EA datasets. Two shale gas exploration sites with local baseline monitoring of dissolved CH$_4$ concentrations and the prospective area of the Bowland Shale [Andrews, 2013] are also shown.

2.1.3. *Preston New Road and Kirby Misperton datasets*

The law in the UK requires that 12 months of baseline monitoring of dissolved CH_4 concentrations in groundwater must occur at a shale gas exploration site prior to fracking [*Infrastructure Act*, 2015]. In England, at the time of this study, there were two sites (Preston New Road, Lancashire, and Kirby Misperton, North Yorkshire – Fig. 1) where groundwater was being monitored as local baselines prior to fracking. Dissolved CH_4 concentrations for the Preston New Road (PNR) site were compiled from the Cuadrilla Resources Ltd. ePortal [*Cuadrilla Resources Ltd.*, 2019]. This dataset, referred to hereafter as the PNR dataset, consisted of four boreholes at the well pad with monthly dissolved CH_4 concentration measurements in groundwater from two superficial formations (Glacial Till and Middle Sands) within each borehole (Table S5). Where multiple concentration measurements were taken within a month the mean concentration was used. The same approach was used for the Kirby Misperton (KM) site using the monitoring reports submitted to the EA [*EA*, 2019b]. The KM dataset consisted of 11 boreholes (five at the well pad and six at distances 1.7-3.1 km from the well pad) with monthly dissolved CH_4 concentration measurements in single formations: six within the Superficial Deposits/weathered Kimmeridge Clay, two within the un-weathered Kimmeridge Clay, two within the weathered/un-weathered Kimmeridge Clay/Corallian Group, and one within the Corallian Group (Table S6).

2.2. *Bayesian generalised linear modeling*

To create a dynamic baseline, generalised linear modeling within a Bayesian framework [*Gelman et al.*, 2004] was used. Each data point (i.e. a dissolved CH_4 concentration measurement) was assumed to be generated from a particular distribution in the exponential family. *A priori*, four distributions were considered: normal, log-normal,

gamma and Weibull. The latter three distributions are only defined for positive numbers and so there is no possibility that physically impossible negative concentrations would be predicted, as would be the case with a normal distribution. For the BGS and EA datasets only one factor was considered; the difference between all the monitoring locations from which dissolved CH_4 concentration data were available – this factor is henceforward known as the "Location factor". Specific environmental conditions at each location were unknown and the dates of the sampling were not even or consistent within and between the datasets and so no further factors could be included in the analysis. Note that the inclusion of a spatially varying location factor does incorporate unknown spatial variation in environmental conditions across the datasets. For the PNR and KM datasets the sampling at each location within the datasets was sufficient that the difference between the months of sampling could be tested – this factor had 12 levels, one for each month, and is henceforward referred to as "Month factor". Location factor was also considered for the PNR and KM datasets.

Model fit was tested using four approaches. Firstly, that the 95% credible interval (CI) for any factor did not include zero. This is henceforward referred to as being significantly different from zero at a probability of 95%. Secondly, that inclusion of the factor caused the total model deviance to decrease. Thirdly, that the inclusion of an additional factor, interaction or covariate decreased the deviance information criterion (DIC). It is generally true that inclusion of factors, interactions or covariates will decrease the total deviance of a model because inclusion allows greater degrees of freedom for fitting, and so the DIC accounts for the inclusion of more fitting parameters against the additional fit of the model. Fourthly, the fit of the generalised linear model was compared with the original datasets and the fit assessed using the root mean square error (RMSE).

Given the available datasets the analysis was constructed sequentially. Firstly, the four exponential family distributions were fitted to the BGS dataset. Because this was the

first of the four datasets to be considered there were no prior datasets to inform this model. Therefore, a weak uninformative prior distribution was used. A Jeffreys prior [*Jeffreys*, 1946] was chosen as the form of the uninformative prior whereby the expected value was set as the mean of all the dissolved CH_4 concentrations in the BGS dataset. For the Jeffrey prior the standard deviation was set as 100 times the coefficient of variation of the dataset. In this way the Jeffrey prior distribution was centred on the expected value of the data and was almost uniform in distribution. The best-fit model for the BGS dataset was used as the prior distribution for the analysis of the EA dataset – this would represent a strong prior. Because sampling locations differed between the BGS and EA datasets it was not possible to use the BGS dataset as a prior for each location within the EA dataset. To demonstrate the effect of a strong versus weak prior the EA dataset was also analyzed using a Jeffrey prior and the result compared to that when the BGS dataset was used as a strong prior. The best-fit model for the EA dataset was then used as strong prior information for the PNR and KM datasets. In all the datasets those values which were below the analytical detection limit were treated as censored data; the exact value of the dissolved CH_4 concentration was not known but the observation could still provide information. Therefore, censored data were included in the analysis even with varying detection limits within and between the study datasets.

The Bayesian generalised linear modeling was achieved by Markov Chain Monte Carlo (MCMC) simulation to estimate the posterior distribution of the dissolved CH_4 concentrations using WinBUGS (Version 1.4) [*Lunn et al.*, 2000]. The length of the MCMC chain was 30000 cycles after 10000 burn in cycles with samples saved every 10 cycles and with one chain.

2.3. Dissolved CH₄ concentrations ≥10.0 mg/l

In the UK there are no regulatory limits regarding dissolved CH_4 concentrations in groundwater. However, the US Department of the Interior risk action level of 10.0 mg/l [*Eltschlager et al.*, 2001] provides a reference that may assist decision making in other countries [e.g. *Bell et al.*, 2017; *Humez et al.*, 2016; *Schloemer et al.*, 2016]. Consistent with previous studies we adopt 10.0 mg/l as an indicative risk action level in this study and accordingly identify locations with dissolved CH_4 concentrations ≥10.0 mg/l.

2.4. Groundwater redox conditions

Dissolved CH_4 concentrations are expected to show relationships with groundwater redox conditions. Reducing conditions (i.e. a lack of oxygen) can promote CH_4 production by methanogenic bacteria and preserve pre-existing biogenic and thermogenic CH_4 [*Molofsky et al.*, 2016]. Conversely, aerobic conditions may permit rapid consumption of CH_4 by methanotrophic bacteria [*Whittenbury et al.*, 1970]. Therefore, information on groundwater redox conditions could help predict locations with elevated dissolved CH_4 concentrations. For example, in the Appalachian Basin, USA, low nitrate (NO_3^-) and sulfate (SO_4^{2-}) concentrations were associated with higher dissolved CH_4 concentrations and offered strong predictive power when combined with other factors such as sodium (Na)-rich water and upland topography [*Molofsky et al.*, 2016]. To investigate if relationships between redox conditions and dissolved CH_4 concentrations exist in English groundwater, locations in the EA dataset with dissolved CH_4 concentrations ≥10.0 mg/l (henceforward referred to as elevated CH_4 locations) were paired with their nearest neighbouring location where dissolved CH_4 concentrations were <10.0 mg/l (henceforward referred to as low CH_4 locations). The following redox-linked groundwater parameters (henceforward termed "indicators") were extracted from the EA

278

Water Quality Archive for the paired sites: ammonium (NH_4) concentration; biochemical oxygen demand (BOD) as 5 day Allylthiourea (ATU); chemical oxygen demand (COD) as O_2; dissolved oxygen (DO); iron (Fe) concentration; manganese (Mn) concentration; NO_3^- concentration; and SO_4^{2-} concentration. Additionally, calcium (Ca), magnesium (Mg), and Na concentrations were extracted to provide an indication of groundwater type and subsequently determine if the boreholes within a pair sampled the same groundwater body. As a further constraint on groundwater bodies at paired locations, boreholes from the EA dataset were manually matched with boreholes from the BGS Onshore GeoIndex [*BGS*, 2019] using geographic coordinates and location names. The borehole depths and aquifer designations recorded in the BGS Onshore GeoIndex were used as proxies for groundwater bodies sampled by the EA for dissolved CH_4 concentrations.

Two statistical methods were employed to investigate relationships between groundwater redox conditions and dissolved CH_4 concentrations. Firstly, binomial probability modeling was used to predict the probability of association between elevated CH_4 locations and levels of indicators. Dissolved CH_4 concentrations were classified using two levels, either "one or more CH_4 samples ≥ 10.0 mg/l" or "all CH_4 samples <10.0 mg/l", that is elevated or low, respectively. Multiple measured values for the different indicators at each location were mean-averaged to average out irregular timings between groundwater samples and any seasonal variations in groundwater chemistry. The mean-averaged indicators at each elevated CH_4 location were compared to the mean-averaged indicators at the corresponding paired low CH_4 location. A success was recorded when concentrations of NH_4, BOD, COD, Fe and Mn at locations with elevated CH_4 concentrations were higher than their concentration in the corresponding low CH_4 location. Successes for DO, NO_3^- and SO_4^{2-} were recorded when concentrations at elevated CH_4 locations were lower than their concentration in the comparative location. If indicator values were equal in a comparative location pair, this was not counted as a

success. The binomial distribution was then used to assess the probability of the proportion of observed successes and failures. In effect the distribution of indicators between pairs of elevated and low CH_4 locations was treated as modeling a coin toss (binomial distribution). For example, if DO was always lower in the elevated CH_4 locations compared to the paired low CH_4 locations then this would have low probability of occurring by random chance and it could be reasonably concluded that elevated dissolved CH_4 was associated with low DO. By analogy tossing a coin and always coming up heads would be unlikely unless it was a biased coin.

The second statistical method used to investigate any relationships between dissolved CH_4 concentrations and indicators was ANOVA. One-way ANOVA was used where the single factor was the dissolved CH_4 concentration. The dissolved CH_4 concentrations were classified as for the binomial probability modeling, either elevated (≥ 10.0 mg/l) or low (< 10.0 mg/l). Three types of one-way ANOVA were performed: indicators without covariates; indicators with single covariates; and indicators with multiple covariates. The covariates used were the remaining indicators. In this way the ANOVA was used to judge whether or not indicators were significantly different between locations with elevated or low dissolved CH_4 concentrations and, by including or not including covariates, to assess whether differences in indicators could be explained by the behaviour of other indicators. Prior to the ANOVA the normality of each indicator was tested using the Anderson-Darling test and indicator values were log-transformed if necessary and re-tested to confirm improved normality. Statistical significance was judged at the 95% probability of an indicator not having zero effect.

3. Results

3.1. Dissolved CH_4 concentrations in England

The BGS, EA, PNR and KM datasets are provided in the supplementary material (Tables S1, S2, S5 and S6). The EA dataset had approximately five times more dissolved CH_4 concentration measurements than the BGS dataset and on average there were approximately four measurements per unique location in the EA dataset, compared to mostly one measurement per unique location in the BGS dataset (Table 1). The spatial distributions of dissolved CH_4 concentrations from the four datasets are shown in Figure 2. The general detection limit for the BGS dataset (<0.5 µg/l) was three orders of magnitude lower than the EA dataset (<0.5 mg/l) (Fig. 3) and the detection limits for the PNR and KM datasets were <0.01 mg/l and <0.001 mg/l, respectively. The maximum dissolved CH_4 concentration measurement in the EA dataset was 25.9 mg/l, compared to 4.72 mg/l in the BGS dataset, and 36 concentration measurements (over 11 unique locations) were ≥10.0 mg/l (1.7% of the EA dataset) (Table 1). Nine of the 11 locations with a dissolved CH_4 concentration measurement ≥10.0 mg/l were located in the prospective area of the Bowland Shale, although no directional spatial trend was readily observable across England using the currently available data. Both national datasets indicate that dissolved CH_4 concentrations in English groundwater are generally below the risk action level of 10.0 mg/l.

Table 1
Descriptive statistics of dissolved CH_4 concentration measurements in the BGS and EA datasets.

	BGS dataset	EA dataset
Number of dissolved CH_4 concentration measurements	439	2153
Number of unique sampling locations	336	571
Mean number of dissolved CH_4 measurements per unique location	1.3	3.8
Detection limit (mg/l)	<0.0005	<0.5
Maximum dissolved CH_4 concentration (mg/l)	4.72	25.9
Number of dissolved CH_4 measurements ≥10.0 mg/l	0	36
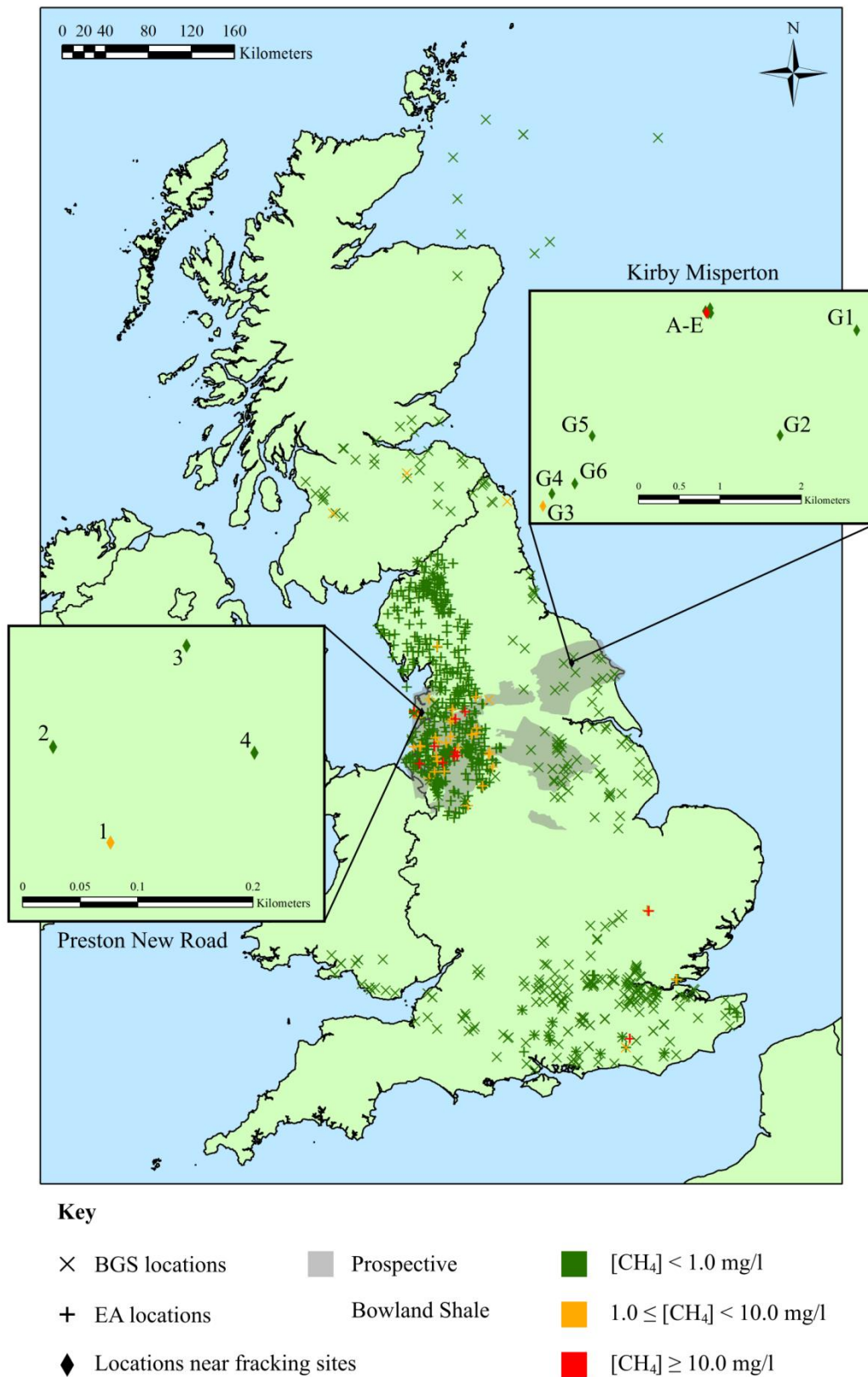
Figure 2
Dissolved CH₄ concentrations for the BGS, EA, PNR and KM datasets (note prospective Bowland Shale is not shown in either inset map for data point clarity). Where more than one dissolved CH₄ concentration measurement is present at a single location, the maximum dissolved CH₄ concentration measured is presented. Monitoring borehole

282

names at shale gas exploration sites correspond to names given in formal site documentation. Prospective area of the Bowland Shale from Andrews [2013].
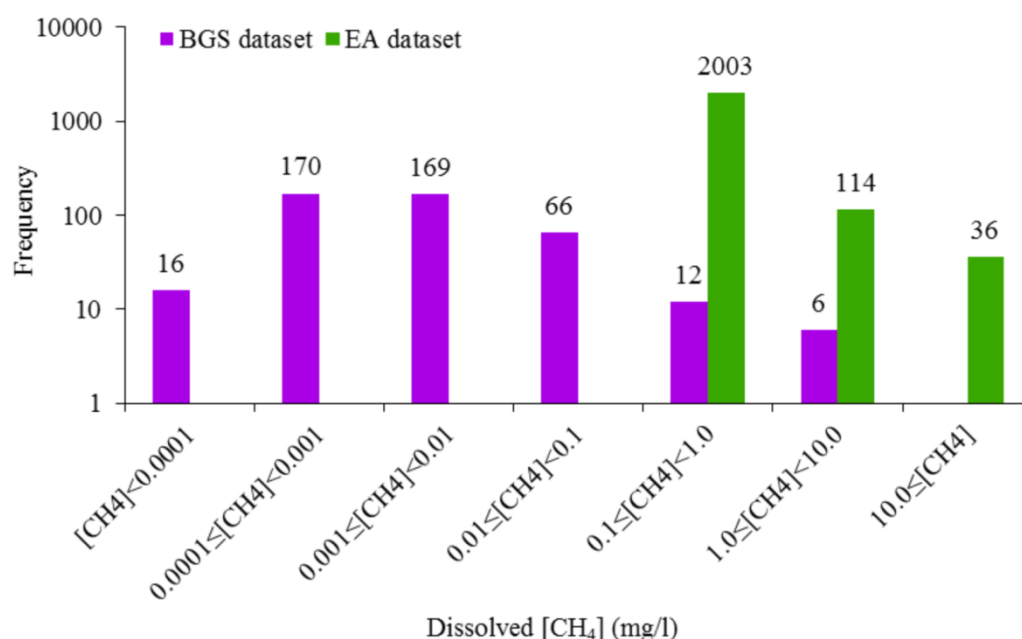
Figure 3
Frequency distributions of dissolved CH4 concentrations in the BGS and EA datasets. Dissolved CH4 concentrations in the EA dataset below the general detection limit of 0.5 mg/l are assigned to the 0.1≤[CH4]<1.0 mg/l category, although their concentrations may be lower.

The PNR dataset contains no dissolved CH_4 concentrations ≥10.0 mg/l in either the Glacial Till or Middle Sands across all four monitoring boreholes (Fig. 4a). The maximum concentration recorded at PNR was 5.75 mg/l in the Middles Sands of Borehole 1 in March 2018 (Table S5). Dissolved CH_4 concentrations at KM were more varied than at PNR but predominantly ranged from below detection limit (<0.001 mg/l) to 0.1 mg/l (Fig. 4b), although the maximum concentration recorded at KM was 67.1 mg/l in the Corallian Group of Borehole E in June 2016 (Table S6). However, this maximum concentration should not necessarily be considered exact because it lies outside the calibration limits of the analytical equipment, i.e. it should be considered as an indicative concentration only [*Envireau Water*, 2017]. Nevertheless, all monthly concentration

results from Borehole E were ≥ 10.0 mg/l (Table S6). The higher dissolved CH_4 concentrations detected at KM compared to PNR may reflect the greater sampling depths at KM, for example samples from Borehole E were from ~200 m below ground level and CH_4 solubility increases with depth. With the exception of Borehole E at KM, dissolved CH_4 concentrations at PNR and KM were not unusual compared to the BGS and EA datasets.
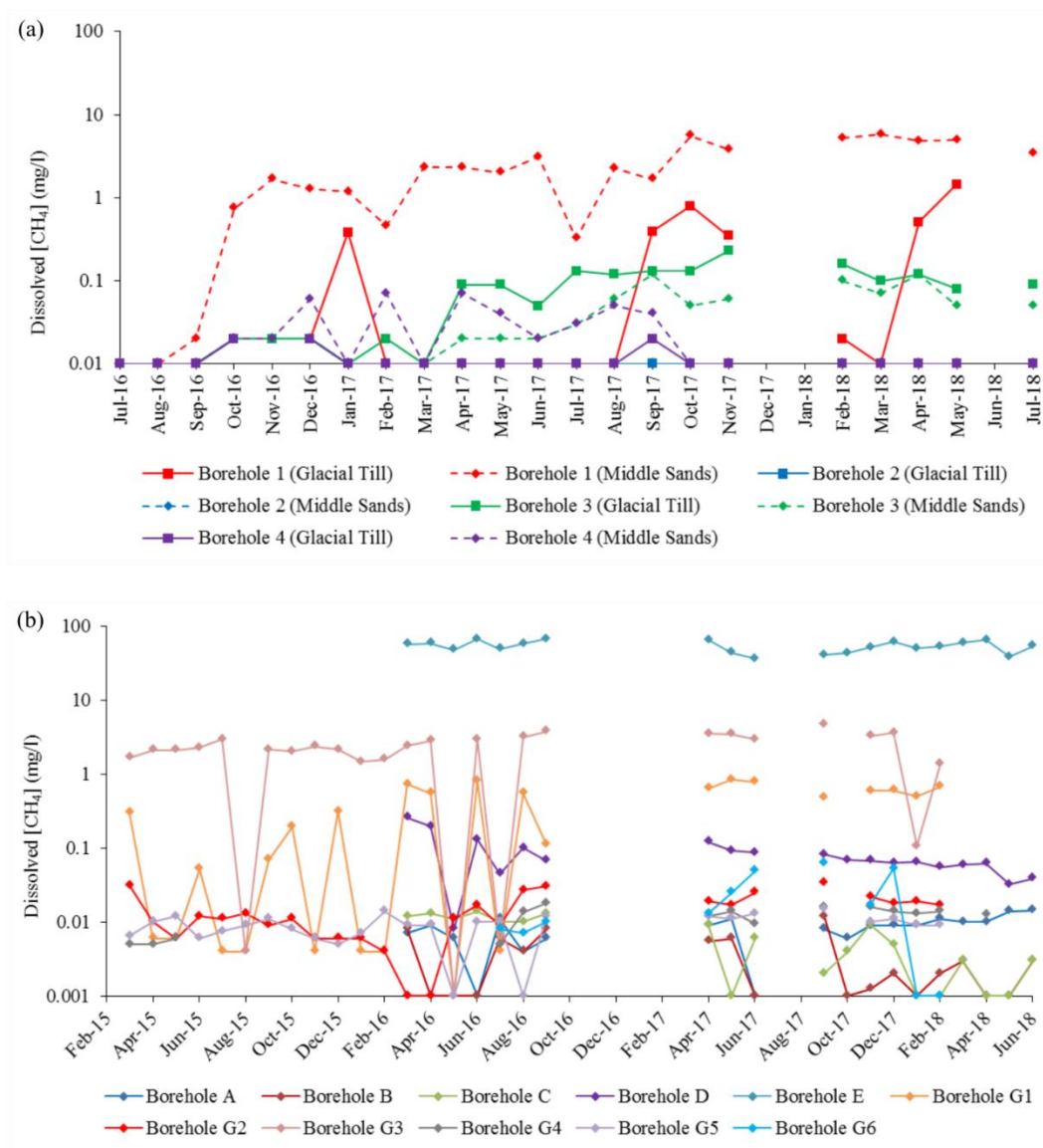
Figure 4
Dissolved CH₄ concentrations in groundwater from local baseline monitoring at the (a) Preston New Road and (b) Kirby Misperton shale gas exploration sites. Gaps show missing data.

3.2. Bayesian generalised linear modeling

3.2.1. BGS and EA datasets

For the BGS dataset the deviances of the distributions were: normal (4242); log-normal (2527); gamma (2087); and Weibull (2076). The Weibull distribution had the lowest deviance and the generalised linear modeling was therefore taken forward using this distribution. The best-fit Weibull distribution was W(0.35±0.01, 0.34±0.16), where the Weibull function has the form W(r, b) where r is the shape factor and b is:

$$b = \lambda^{-r} \ for \ x > 0 \tag{i}$$

where λ is the scale factor. The expected mean, $E(x)$, and variance, $Var(x)$, were:

$$E(x) = b^{-1/r} \ \Gamma\left(1 + \frac{1}{r}\right) = 0.23 \ mg/l \tag{ii}$$

$$Var(x) = \lambda^2 \left[\Gamma\left(1 + \frac{2}{r}\right) - \left(\Gamma\left(1 + \frac{1}{r}\right)\right)^2\right] = 0.7 \ mg/l \tag{iii}$$

The analysis of the BGS dataset provided the strong prior information for the EA dataset. When the strong prior was used for the EA dataset the deviance of the generalised linear model was 1601, compared to 1727 when the weak Jeffrey prior was used. When the predicted values from the weak and strong priors were compared the estimated values from the weak prior were 54% smaller than those predicted from the strong prior. The CI for each location was compared between the weak and strong priors; the CI for the strong prior was on average 58% of the CI for the weak prior (Fig. 5) – and this equates to an increase in equivalent sample size of 75%. With the strong prior the Location factor was significant and this could be used to calculate the expected value (the "average") for each location within the dataset (Figure 6). The distribution of observed and predicted dissolved CH_4 concentrations are plotted in Figure 7. Based upon the EA dataset with the

strong prior, then $E(x) = 0.24$ mg/l and $Var(x) = 0.83$ mg/l, with the 95% CI at 0.11 to 0.45 mg/l.
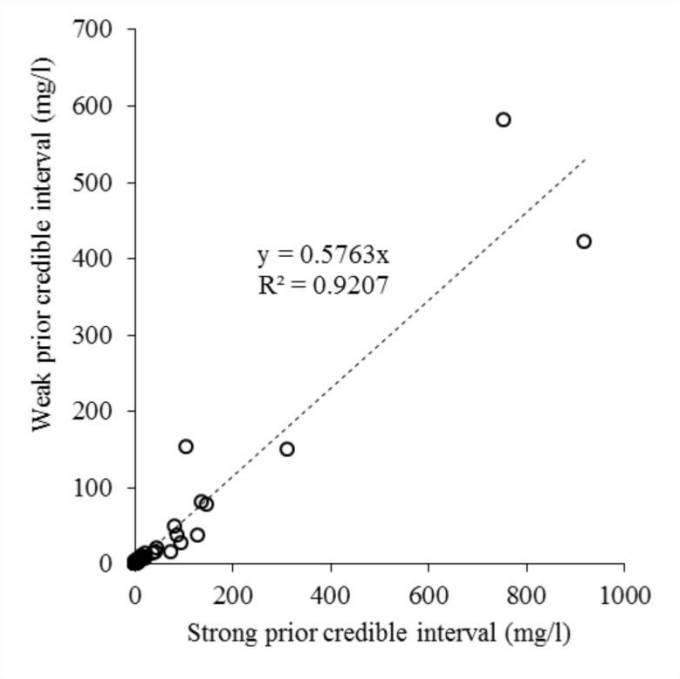
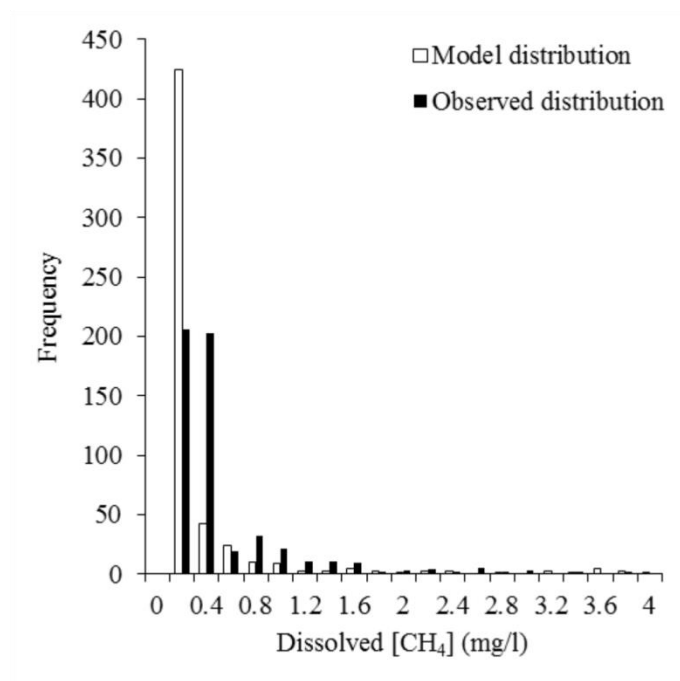*Figure 5*
Comparison of the credible intervals for the EA dataset using the strong and weak priors.
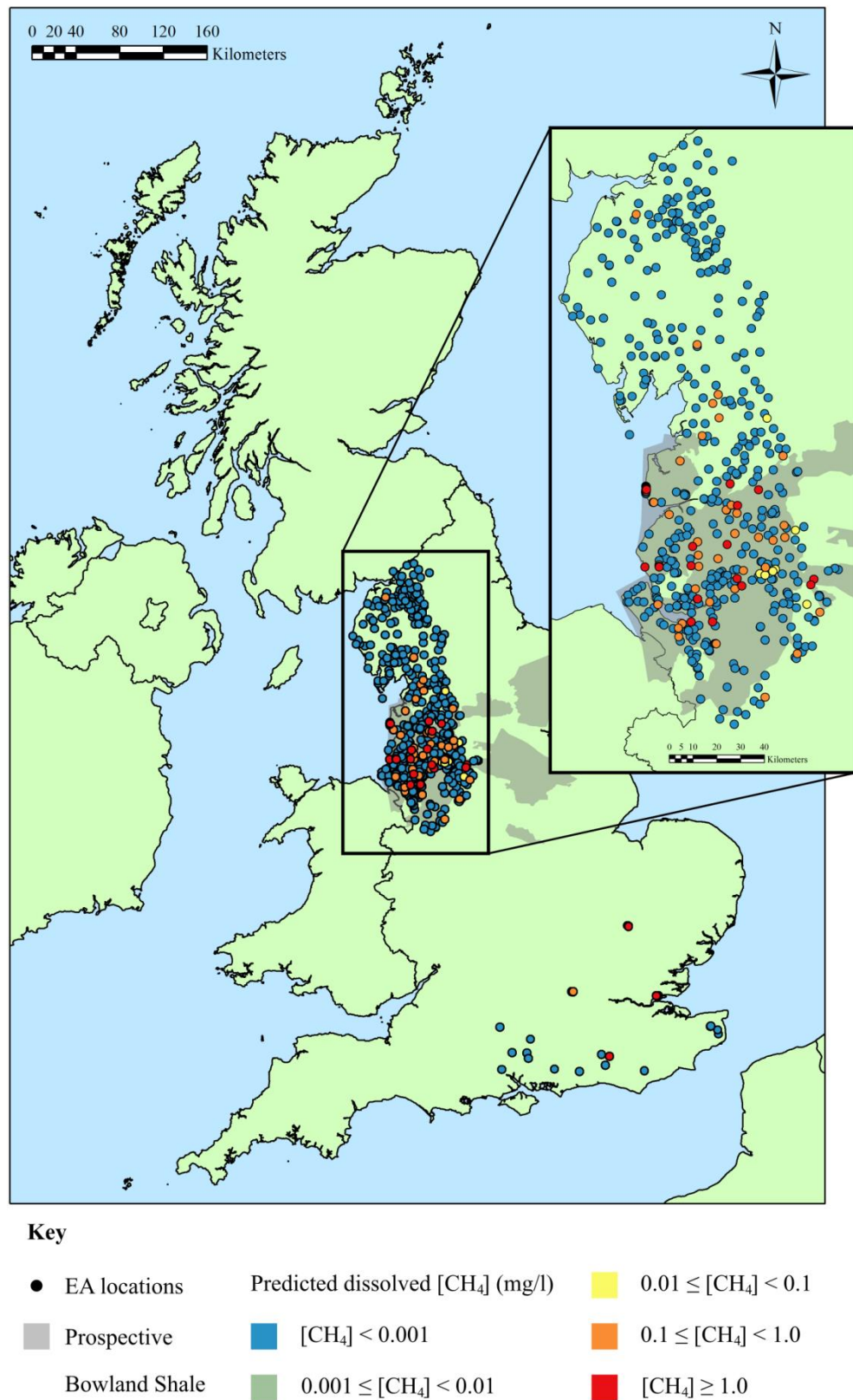
Figure 6
Predicted dissolved CH₄ concentrations for the EA dataset using the strong prior. Inset map shows an enlarged view of northwest England. Prospective area of the Bowland Shale from Andrews [2013].
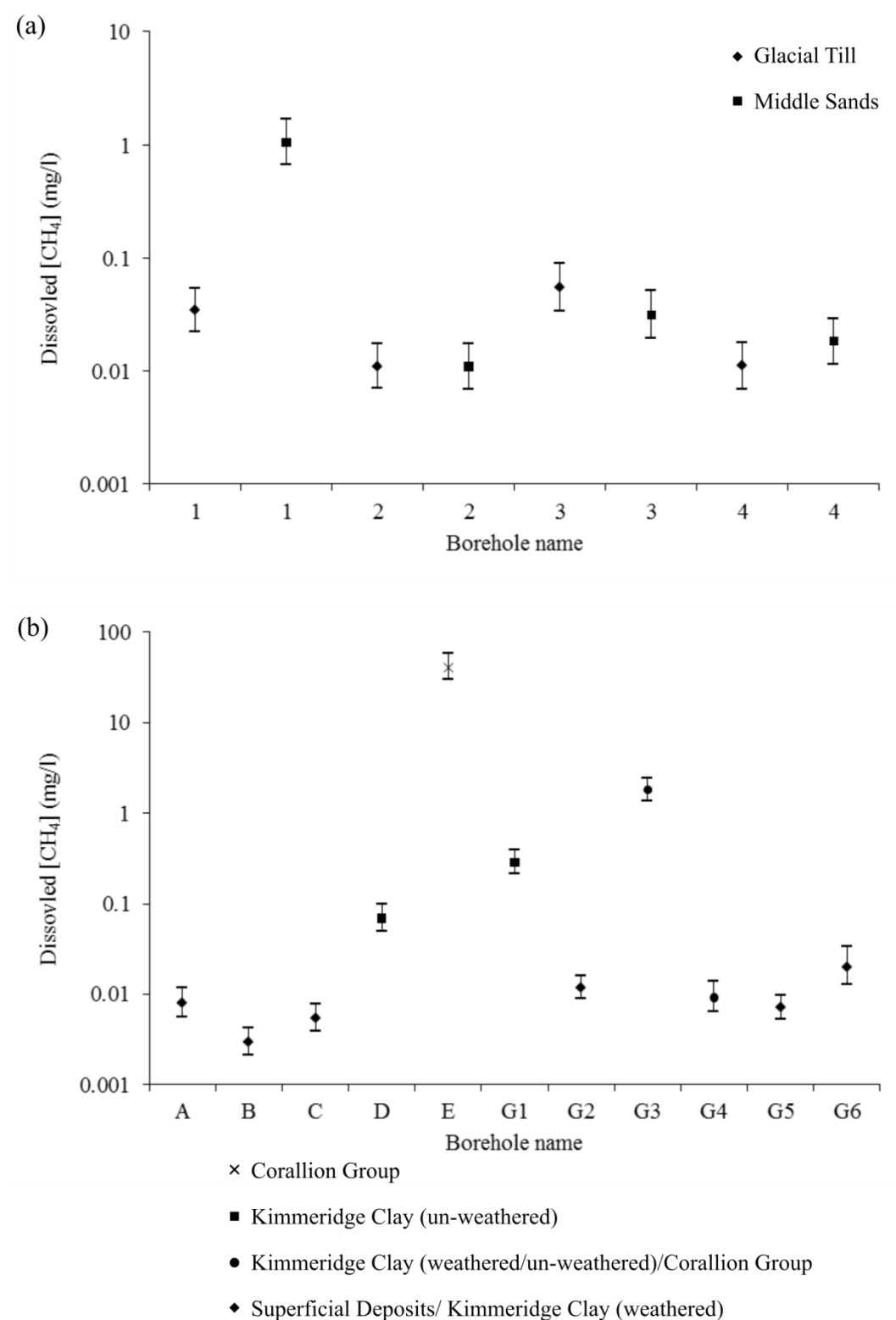
Figure 7
Distributions of the modelled and observed dissolved CH$_4$ concentrations for the EA dataset. Note the x-axis has been limited to 4.0 mg/l even though the observed results extend beyond this.

3.2.2. PNR and KM datasets

When using the weak Jeffreys prior for the PNR dataset the deviance was 661, which improved to 643 on use of the strong prior (the EA dataset with the BGS dataset used as a strong prior). The expected mean dissolved CH$_4$ concentration for the PNR dataset was 0.033 mg/l, with the 95% CI at 0.025 to 0.044 mg/l. The Month factor and its interaction with Location factor proved insignificant, indicating no significant seasonal cycle in the dissolved CH$_4$. The distribution of the data confirmed that the dissolved CH$_4$ concentrations of the Middle Sands in Borehole 1 were indeed significantly different from all the other boreholes (Fig. 8a). For the KM dataset the Month factor and its interactions also proved insignificant. Use of a strong prior made only a small difference to the deviance of the model fit, decreasing from 822 to 820. The expected mean dissolved CH$_4$ concentration for the KM dataset was 0.060 mg/l, with the 95% CI at 0.035 to 0.103 mg/l. The distribution of the data for the boreholes in the KM dataset showed that seven of the

288

11 boreholes were not significantly different from each other, but four boreholes (D, E, G1, and G3) did have significantly higher dissolved CH_4 concentrations (Fig. 8b). However, in this study we can give no particular explanation for this.

Figure 8
Predicted dissolved CH₄ concentrations for groundwater monitoring boreholes at the (a) Preston New Road, and (b) Kirby Misperton shale gas exploration sites. Error bars show 95% credible intervals.

3.3. Relationships between elevated CH₄ concentrations and redox conditions

Thirty six dissolved CH_4 concentration measurements in the EA dataset had concentrations greater than or equal to the risk action level of 10.0 mg/l (Table 2). These 36 concentrations occurred across 11 unique locations and nine of these locations were situated in the prospective area of the Bowland Shale, although no link to thermogenic gas migration from the Bowland Shale can be demonstrated based upon the available data. The percentage of dissolved CH_4 concentration measurements ≥10.0 mg/l from the total number of dissolved CH_4 concentration measurements taken at the 11 locations ranged from 4-100%.

Table 2
Descriptive statistics of unique locations in the EA dataset where dissolved CH_4 concentrations have been measured ≥10.0 mg/l.

EA location name	Geographical area[a]	Number of dissolved CH₄ measurements	Number of dissolved CH₄ measurements ≥10.0 mg/l	Maximum dissolved CH₄ concentration (mg/l)
30006 ad-hoc @ Holiday Moss, Reeds Brow	GMMC	18	12	25.9
30335 ad-hoc @ Bromborough Dock North	GMMC	9	2	12.0
60301 ad-hoc @ Moss Side Farm, Rixton	GMMC	25	1	11.1
60565 ad-hoc @ Arpley Landfill Site, Arpley Meadows	GMMC	37	5	13.6
Blackburn Yarn Dyers ABH	CL	11	3	21.5
Blackpool Pleasure Beach No.1 borehole	CL	3	1	13.9
Brentwood Moss Nurseries Borehole	GMMC	10	4	13.5
Indigo Yarn Company Ltd. borehole	CL	1	1	10.0
Lower Stumble groundwater borehole	SSD	4	3	11.4
Sawston Inv.Spikefields BGS SCO4A 35M BH	CB	2	1	12.4
Whitegate Farm borehole	GMMC	3	3	14.3
Total		123	36	

[a] *Geographical area codes are given in Table S4.*

3.3.1. Groundwater body sampling

Three of the 11 locations with dissolved CH_4 concentrations ≥ 10.0 mg/l showed clear similar relative concentrations of Ca, Mg and Na to their paired low CH_4 location, indicating the corresponding boreholes sampled the same groundwater bodies (Table S7). A further four paired locations also showed similar, although less distinct, relative proportions. However, sampling of the same groundwater body at three of these four paired locations was further supported by the BGS aquifer designations (i.e. aquifer designations were the same for both boreholes in a corresponding pair). We assumed that seven of the 11 pairs sample the same groundwater body within their pairs and therefore ran binomial probability modeling for both the seven and 11 pairs.

3.3.2. Binomial probability modeling

When all 11 paired locations were considered all eight indicators showed probabilities greater than 50% (Table 3), i.e. the observed proportion of successes to failures was more likely than not. However, taking a 95% probability as the significant probability then only NH_4, BOD, DO and Fe showed significant ratios for the elevated and low CH_4 locations. For BOD and DO the probability of success was 100.0%. However, BOD and DO had only one and four trials, respectively, reducing confidence in their results. For those redox indicators present at all 11 paired locations, NH_4 and Fe were the best predictors, both with probabilities of 96.7% (Table 3). When only the seven pairs that likely sampled the same groundwater bodies were considered all eight indicators again showed probabilities greater than 50% (Table 4). Only BOD and DO showed significant ratios for the elevated and low CH_4 locations (100.0%) but had only one and three trials, respectively, again

292

reducing confidence in their results. For those redox indicators present at all seven paired locations Fe, Mn, and SO_4^{2-} were the best predictors, all with probabilities of 93.8% (Table 4).

Table 3
Results of the binomial probability modeling for the 11 paired locations.

Indicator	Number of independent trials	Number of successes (N)	Probability at most N successes (%)
NH_4	11	8	96.7
BOD	1	1	100.0
COD	9	6	91.0
DO	4	4	100.0
Fe	11	8	96.7
Mn	11	7	88.7
NO_3^-	5	3	81.3
SO_4^{2-}	11	7	88.7

Table 4
Results of the binomial probability modeling for the seven paired locations sampling the inferred same groundwater bodies.

Indicator	Number of independent trials	Number of successes (N)	Probability at most N successes (%)
NH_4	7	4	77.3
BOD	1	1	100.0
COD	5	3	81.3
DO	3	3	100.0
Fe	7	5	93.8
Mn	7	5	93.8
NO_3^-	4	3	93.8
SO_4^{2-}	7	5	93.8

3.3.3. Analysis of variance

Prior to ANOVA the Anderson-Darling test suggested that all indicator values should be log-transformed before subsequent analysis – no further transformation was necessary. One-way ANOVA without covariates showed that NH_4, COD, Fe, Mn, and NO_3^- showed statistically significant differences between elevated and low CH_4 locations (Table 5). All statistically significant factors, except NO_3^-, had probabilities <0.0005 of having zero

293

effect. COD explained the highest variation in the data ($R^2 = 15.6\%$) and Mn explained the least variation ($R^2 = 6.3\%$). *A priori* it would be expected that NH_4, BOD, COD, Fe and Mn would be at higher concentrations in boreholes with elevated dissolved CH_4 concentrations, and conversely, that DO, NO_3^- and SO_4^{2-} would all be lower. When the change in mean indicator values going from low to elevated CH_4 locations were considered, COD, Fe and Mn followed the expected pattern (i.e. values increased in elevated CH_4 locations) but NH_4 and NO_3^- did not, despite showing the largest percentage change. This may mean that NH_4 and NO_3^- may not be useful indicators of elevated dissolved CH_4 concentrations. When covariates were considered only one combination improved the fit of the ANOVA and that was when NH_4 was considered with BOD and COD as covariates ($R^2 = 45.0\%$).

Table 5
Results of the ANOVA without covariates and values of the percentage change in mean dissolved CH_4 concentration when going from the low to elevated CH_4 locations (only given for those indicators where a significant difference has been demonstrated). P-values and R^2 values in italics are those found to be significantly different from zero at the 95% probability.

Indicator	P-value	$R^2(\%)$	% increase to elevated CH_4 location
NH_4	*<0.0005*	*14.8*	*-90*
BOD	0.414	0.6	
COD	*<0.0005*	*15.6*	*28*
DO	0.720	0.1	
Fe	*<0.0005*	*13.0*	*22*
Mn	*<0.0005*	*6.3*	*17*
NO_3^-	*0.003*	*11.0*	*99*
SO_4^{2-}	0.620	0.1	

4. Discussion

4.1. Comparison of EA dataset to other studies

Since 2012 a number of published studies related to oil and gas industrial activities have provided measurements of dissolved CH_4 concentrations in groundwater (Table 6). These

range spatially from those covering the 5180 km^2 Wattenberg oil and gas field, Colorado [*Li and Carlson*, 2014], to those which cover whole states and nations [e.g. *Bell et al.*, 2017]. Comparison of the EA dataset to other studies shows that there is little evidence that the EA data were biased towards locations with higher dissolved CH_4 concentrations (Table 6). The EA dataset contains the largest number of dissolved CH_4 concentration measurements of any of the published datasets to date and is also one of the largest in terms of unique sampling locations (Table 6). Despite having one of the highest detection limits (<0.5 mg/l) of the published dissolved CH_4 datasets, the EA dataset has one of the lowest mean dissolved CH_4 concentrations (0.24 mg/l using the Bayesian generalised linear modeling approach) and maximum CH_4 concentrations (25.9 mg/l) (Table 6). Furthermore, the percentage of dissolved CH_4 concentration measurements greater than or equal to the US Department of the Interior risk action level of 10.0 mg/l was also one of the lowest (1.7%); only surpassed by the datasets for Sullivan County (0.8%) [*Reese et al.*, 2014], New York State (0.0%) [*McPhillips et al.*, 2014] and Great Britain (0.0%) [*Bell et al.*, 2017]. These comparisons suggest that although dissolved CH_4 is ubiquitous in English groundwater, including areas with prospective shale gas resources, concentrations are generally low compared to other geographical areas and very rarely above concentrations requiring further investigation. This observation is in agreement with the conclusions of *Bell et al.* [*2017*]. However, the data presented in this study do also highlight that dissolved CH_4 concentrations in English groundwater can exceed 10.0 mg/l.

Table 6

Comparison of published baselines for dissolved CH$_4$ concentrations in groundwater.

Region and study	Number of dissolved CH$_4$ concentration measurements	Number of unique locations	Detection limit (mg/l)	Minimum dissolved CH$_4$ concentration (mg/l)	Median dissolved CH$_4$ concentration (mg/l)[a]	Mean dissolved CH$_4$ concentration (mg/l)[a]	Maximum dissolved CH$_4$ concentration (mg/l)	Number and percentage of dissolved CH$_4$ concentration measurements ≥10.0 mg/l
New York State, USA [*Kappel and Nystrom*, 2012]	239	239	0.001	<0.001	<1.0	Unknown	41.0	21 (8.8%)
Susquehanna County, USA [*Molofsky et al.*, 2013]	1701	1701	0.00005-0.026	<0.00005	0.00076	0.705	43.0	50 (2.9%)
Marcellus Shale, USA [*Darrah et al.*, 2014]	113	113	Unknown	<Detection limit	0.585[b]	8.040[b]	102.164[b]	32 (28.3%)
Barnett Shale, USA [*Darrah et al.*, 2014]	59	20	Unknown	0.716[b]	5.519[b]	13.242[b]	46.962[b]	23 (39.0%)
Sullivan County, USA [*Reese et al.*, 2014]	1882	1882	0.005-0.026	<0.005	0.149	Unknown	16.5	≤15[c] (0.8%)
Wattenberg field, Colorado, USA [*Li and Carlson*, 2014]	223	176	Unknown	<Detection limit	Unknown	4.0	37.1	36 (16.1%)
New York State, USA [*McPhillips et al.*, 2014]	113	113	0.01	0.002	0.007	0.464	8.26	0 (0.0%)
Southwestern Ontario, Canada [*McIntosh et al.*, 2014]	1010	862	1	0	Unknown	Unknown	248	150 (14.9%)
St. Lawrence Lowlands, Quebec, Canada [*Moritz et al.*, 2015]	138	130	0.0006	<0.0006	0.1	3.8	45.9	17 (12.3%)
Chaudière-Appalaches, Canada [*Lefebrve et al.*, 2015]	Unknown	74	Unknown	Unknown	0.2	5.1	31.2	Unknown
Lower Saxony, Germany [*Schloemer et al.*, 2016]	1043	1043	0.0000178[d]	0.0000178[d]	0.00183[d]	Unknown	44.0188[d]	60 (5.8%)
Alberta, Canada [*Humez et al.*, 2016]	179	186	3.333	<3.333	<3.333	5.232	42.9	28 (15.6%)
Great Britain, UK [*Bell et al.*, 2017]	439	336	0.00005-0.005	<0.00005	0.0012	0.0463	4.72	0 (0.0%)
Saint-Édouard, Quebec, Canada [*Bordeleau et al.*, 2018]	Unknown	48	0.006	<0.006	4.9	10.4	82.0	Unknown
EA dataset, England This study	2153	571	0.1-0.5	<0.1	<0.5	0.24[e]	25.9	36 (1.7%)

[a] *May include concentrations below detection limit taken as the detection limit concentration, i.e. "<0.5 mg/l" was taken as "0.5 mg/l".* [b] *Calculated using a CH$_4$ density of 0.657 mg/cm^3 at 1 atm and 298 K.* [c] *Fifteen wells with CH$_4$ concentrations ≥7.0 mg/l.* [d] *Calculated using 0.71 mg/l = 1.0 ml/l at 293 K and 101325 Pa [Schloemer et al., 2016].* [e] *Expected mean from the Bayesian generalised linear modeling.*

4.2. *Dissolved CH₄ flux to atmosphere*

The results of the Bayesian generalised linear modeling for the EA dataset suggest an average dissolved CH_4 concentration of 0.24 mg/l in English groundwater. The solubility of CH_4 in water is 31.0 mg/l at atmospheric pressure and 283 K, with solubility doubling for every 10 m increase in depth [*Bordeleau et al.*, 2018; *Humez et al.*, 2016]. However, the Henry's constant of CH_4 means that in equilibrium with the atmosphere a far lower concentration of dissolved CH_4 would be expected in groundwater:

$$[CH_4] = P_{CH_4} \times K_{HT} \tag{iv}$$

$$K_{HT} = K_{H298} exp\left(A\left(\frac{1}{T} - \frac{1}{298}\right)\right) \tag{v}$$

where T is temperature of the water (K), K_{HT} is Henry's law constant (mol/m³/Pa), K_{H298} is Henry's law constant at 298 K (mol/m³/Pa), $[CH_4]$ is dissolved concentration of CH_4 in water (mol/l), P_{CH_4} is the partial pressure of CH_4 in the atmosphere (Pa) and A is a constant.

Given $P_{CH4} = 1.81 \times 10^{-6} Pa$, $K_{H298} = 1.4 \times 10^{-5} mol/m^3/Pa$ and $A = 1600$ [*Sander*, 2015] then the $[CH_4]$ at equilibrium with air is $4.0 \times 10^{-9}\ mol/l$ ($6.4 \times 10^{-5}\ mg/l$) at 274 K to $2.8 \times 10^{-9}\ mol/l$ ($4.4 \times 10^{-5}\ mg/l$) at 293 K. Therefore, the expected mean concentration for dissolved CH_4 in English groundwater, based on this study, is in excess of that expected at equilibrium with the atmosphere. As a result we would expect almost complete degassing of the CH_4 to the atmosphere upon emergence of groundwater at the surface. The average annual recharge to the main aquifers in England is estimated to be $7 \times 10^9\ m^3/day$ [*EA*, 2007]. If it is assumed that groundwater levels are not changing substantially across England then this same volume must be discharged to surface waters. If it is also assumed that the CH_4 degasses as it emerges to the atmosphere, rather than degassing from the soil profile where it could readily be

oxidised, then given the 95% CI of dissolved CH_4 concentrations predicted from this study (0.11 to 0.45 mg/l), the amount of CH_4 degassing from groundwater would be 0.7 to 3.1 kt CH_4/year with an expected value of 1.65 kt CH_4/yr. This equates to a greenhouse gas warming potential (GWP) of 17 to 74 kt CO_2 eq/yr with an expected value of 40.3 kt CO_2 eq/yr. The UK greenhouse gas inventory estimates a total UK CH_4 flux of 53500 kt CO_2 eq/yr [*DECC*, 2016]. Therefore, CH_4 degassing from groundwater in England potentially contributes ~0.01% to the estimated CH_4 flux in the UK. This estimate is in good agreement with *Gooddy and Darling* [2005] who estimated groundwater contributes a maximum of 0.05% to all UK CH_4 emissions.

4.3. *A dynamic baseline and predicting dissolved CH_4 concentrations*

This study has developed a coherent and transparent approach for combining dissolved CH_4 datasets with different detection limits. The Bayesian approach employed uses all available data to predict distributions of dissolved CH_4 concentrations at national and local scales (e.g. around shale gas sites). Such distributions represent a baseline against which future observations, and especially in this case observations made after fracking operations and shale gas extraction have commenced, can be judged. An advantage of using the Bayesian approach is that the tool automatically updates with new data and so contributes to the development of a dynamic baseline in time and space. In addition, the approach gains value from the whole monitoring network, i.e. maximum information is gained from past and ongoing monitoring. Therefore, this approach gives good value for the money invested in environmental monitoring and can be used to assess information content and informational efficiency of the current monitoring network.

For groundwater determinands with defined environmental quality standards [e.g. *EC,* 2000], individual results from monitoring will be viewed relative to these standards and

the probability that the standard is being exceeded assessed. For determinands such as dissolved CH_4 concentrations, no legal standard exists and such comparisons may not occur. Furthermore, the review period for environmental monitoring is not always clear. Under an operator's permit the operator should review continuously, i.e. dissolved CH_4 concentration data reviewed each time new data are obtained and the regulator informed if there is an issue. The environmental regulator in the UK (the EA in England) may be asked to report at any time to the Secretary of State. However, no fixed review period has currently been set for the UK. In the approach used in this study each new datum can be viewed against a prediction that is based upon all available data, Furthermore, a probability (with uncertainty) is calculated that a new observation is exceptional and not what should be expected, even for locations sampled only once. In the case used here a measurement of dissolved CH_4 concentration would be judged against the predicted distribution as a means of testing whether a CH_4 leak to groundwater has or has not occurred at a shale gas site.

In effect this study has built up a method to improve groundwater baseline assessment at any one site. At the simplest level one could examine the distribution of observed data at any site and compare the latest observation with that distribution. However, this would not be a fair comparison because a local variation might mean that comparing one observation with data from all years would be inappropriate, for example if there was an interannual trend at the site where values in the current year tend to be lower than those in a previous year. Under such circumstances a distribution for the given year would be better than comparing with data from all years. Of course it is unlikely that there will be sufficient observations at a site to give such a reasonable distribution for any month for any year. Therefore, it is preferable if information from other sites could be drawn upon, which is what this Bayesian approach has achieved. An analogous, non-Bayesian approach might be that of weighted regression analysis [*Hirsch et al.*, 2010; 2015].

Our approach could be improved with the use of covariates. This study has considered a range of possible groundwater redox parameters as potential indicators of elevated concentrations of dissolved CH_4. Using binomial probability modeling and ANOVA it was shown that high Fe concentration was a consistently successful indicator of elevated dissolved CH_4 concentrations in English groundwater. This contrasts with research in the Appalachian Basin, USA, which concluded no significant relationship existed between Fe and elevated CH_4 [*Molofsky et al.*, 2016]. Alternatively, *Molofsky et al.* [2016] found that low NO_3^- and SO_4^{2-} concentrations were associated with elevated CH_4 concentrations and offered strong predictive power when combined with other factors of Na-rich water and upland topography. Although our analysis has suggested high Fe concentration may be a good indicator of elevated CH_4 concentrations in English groundwater, more extensive studies using historic data and ongoing groundwater monitoring programmes are needed to investigate this and provide a relationship between concentrations of Fe and dissolved CH_4. Importantly, the redox parameters considered in this study do suggest the possibility that in the future, rather than directly monitoring dissolved CH_4 concentrations, areas with elevated dissolved CH_4 concentrations may be initially identified for further investigation by surveying more readily available and cheaper determinands such as Fe. More expensive analyses measuring dissolved CH_4 concentrations and stable carbon isotopes could then be targeted to confirm elevated CH_4 concentrations and discriminate potential sources [e.g. *Teasdale et al.*, 2019].

5. Conclusions

This study has developed a dynamic baseline for dissolved CH_4 concentrations in English groundwater, from which the potential environmental impact of anthropogenic activities, such as shale gas exploitation, can be assessed. The Bayesian approach used can systematically and transparently bring together multiple monitoring datasets, including

those with differing detection limits, and provide all results within a probabilistic framework with uncertainty. Furthermore, the results from previous analysis can be used as prior information for future analysis, leading to results that develop over time and space. This study used four different datasets of dissolved CH_4 concentrations in groundwater: two nationwide datasets and two local baseline monitoring datasets. By building on the most sensitive national dataset (the previously published British Geological Survey CH_4 baseline for Great Britain) a strong prior distribution was developed. This strong prior was used for the subsequent national dataset (that of the Environment Agency of England), which had approximately five times more dissolved CH_4 concentration measurements but a detection limit three orders of magnitude higher. When the strong prior was used over a weak prior for the subsequent dataset the precision improved by 75%. The expected mean dissolved CH_4 concentration in English groundwater based on the Bayesian approach is 0.24 mg/l, with a variance of 0.83 mg/l, a 95% credible interval of 0.11 to 0.45 mg/l, and a Weibull distribution of $W(0.35\pm0.01, 0.34\pm0.16)$. These results indicate that the amount of CH_4 degassing from English groundwater to the atmosphere equates to between 0.7 to 3.1 kt CH_4/year, with an expected value of 1.65 kt CH_4/year and a greenhouse gas warming potential of 40.3 kt CO_2 eq/year. The two local baseline monitoring datasets were from two shale gas exploration sites in England. These sites, in combination with the national datasets, indicate that dissolved CH_4 concentrations in English groundwater are generally low, but locations with concentrations greater than or equal to the widely used risk action level of 10.0 mg/l do exist. Analyses of groundwater redox conditions at locations with dissolved CH_4 concentrations $\geq$10.0 mg/l suggest that it may be possible to identify other locations with elevated dissolved CH_4 concentrations using redox parameters such as Fe concentration.

Supplementary material

Appendix A (Tables S1-S7)

References

Andrews, I. J. (2013). The Carboniferous Bowland Shale gas study: geology and resource estimation. British Geological Survey for Department of Energy & Climate Change, London, UK.

Bell, R. A., Darling, W. G., Ward, R. S., Basava-Reddi, L., Halwa, L., Manamsa, K., & Dochartaigh, B. Ó. (2017). A baseline survey of dissolved methane in aquifers of Great Britain. *Science of the Total Environment*, 601, 1803-1813.

BGS (British Geological Survey) (2019). British Geoindex Onshore. Available at: BGS Onshore GeoIndex (Last accessed: 05/03/2019).

Bordeleau, G., Rivard, C., Lavoie, D., Lefebvre, R., Malet, X., & Ladevèze, P. (2018). Geochemistry of groundwater in the Saint-Édouard area, Quebec, Canada, and its influence on the distribution of methane in shallow aquifers. *Applied geochemistry*, 89, 92-108.

Cuadrilla Resources Ltd. (2019). Cuadrilla ePortal. Available at: https://www.cuadrillaresourceseportal.com/jan2019.html (Last accessed: 05/03/2019).

Darling, W. G., & Gooddy, D. C. (2006). The hydrogeochemistry of methane: evidence from English groundwaters. *Chemical Geology*, 229(4), 293-312.

Darrah, T. H., Vengosh, A., Jackson, R. B., Warner, N. R., & Poreda, R. J. (2014). Noble gases identify the mechanisms of fugitive gas contamination in drinking-water wells overlying the Marcellus and Barnett Shales. *Proceedings of the National Academy of Sciences*, 111(39), 14076-14081.

DECC (Department of Energy & Climate Change) (2016). 2014 UK greenhouse gas emissions, final figures: statistical release. National Statistics, Department of Energy & Climate Change, London, UK.

EA (Environment Agency) (2007). Underground, under threat – The state of groundwater in England and Wales. Environment Agency, Bristol, UK.

EA (Environment Agency) (2019a). Water Quality Archive. Available at: https://environment.data.gov.uk/water-quality/view/landing (Last accessed: 08/03/2019).

EA (Environment Agency) (2019b). Third Energy – Kirby Misperton (KM8 well) information page. Available at: https://consult.environment-agency.gov.uk/onshore-oil-and-gas/third-energy-kirby-misperton-information-page/ (Last accessed: 05/03/2019).

EC (European Council) (2000). Directive 2000/60/EC of the European Parliament and of the Council of 23 October 2000 establishing a framework for Community action in the field of water policy. Official Journal of the European Communities, 22(2000), L327.

Eltschlager, K. K., Hawkins, J. W., Ehler, W. C., & Baldassare, F. (2001). Technical measures for the investigation and mitigation of fugitive methane hazards in areas of coal mining. US Department of the Interior, Office of Surface Mining Reclamation and Enforcement.

Envireau Water (2017). Baseline Water Quality Data, April – June 2017, Kirby Misperton A Wellsite, North Yorkshire. Envireau Water for Third Energy UK Gas Limited, East Knapton, UK.

Exploration Consultants Ltd. (1986). Lancashire Conjunctive Use Scheme, Further Investigations: Wyresdale Tunnel, Final Geological/Geophysical Report. Exploration Consultants Limited for North West Water, UK.

Gelman, A., Carlin, J. B., Stern, H. S., & Rubin, D. B. (2004). Bayesian Data Analysis (2nd ed.). Boca Raton, FL: Chapman & Hall/CRC.

Gooddy, D. C., & Darling, W. G. (2005). The potential for methane emissions from groundwaters of the UK. *Science of the Total Environment*, 339(1-3), 117-126.

Hirsch, R. M., Moyer, D. L., & Archfield, S. A. (2010). Weighted regressions on time, discharge, and season (WRTDS), with an application to Chesapeake Bay river inputs 1. *Journal of the American Water Resources Association*, 46(5), 857-880.

Hirsch, R. M., Archfield, S. A., & De Cicco, L. A. (2015). A bootstrap method for estimating uncertainty of water quality trends. *Environmental Modeling & Software*, 73, 148-166.

Hooker, P., & Bannon, M. (1993). Methane: its occurrence and hazards in construction. CIRIA Rep. 130.

Humez, P., Mayer, B., Ing, J., Nightingale, M., Becker, V., Kingston, A., Akbilgic, O. & Taylor, S. (2016). Occurrence and origin of methane in groundwater in Alberta (Canada): Gas geochemical and isotopic approaches. *Science of the Total Environment*, 541, 1253-1268.

Infrastructure Act (2015). Part 6 Energy, Onshore hydraulic fracturing: safeguards. Available at: http://www.legislation.gov.uk/ukpga/2015/7/contents/enacted (Last accessed: 05/03/2019).

IPCC (Intergovernmental Panel on Climate Change) (2013). Climate Change 2013: The Physical Science Basis.

Jeffreys, H. (1946). An invariant form for the prior probability in estimation problems. *Proceedings of the Royal Society of London. Series A. Mathematical and Physical Sciences*, 186(1007), 453-461.

Kappel, W. M., & Nystrom, E. A. (2012). Dissolved methane in New York groundwater. US Geological Survey Open-file report 2012-1162.

Lefebvre, R., Ballard, J.-M., Carrier, M.-A., Vigneault, H., Beaudry, C., Berthot, L., Légaré-Couture, G., Parent, M., Laurencelle, M., Malet, X., Therrien, A., Michaud, A., Desjardins, J., Drouin, A., Cloutier, M.H., Grenier, J., Bourgault, M.-A., Larocque, M., Pellerin, S., Graveline, M.-H., Janos, D., & Molson, J. (2015). Portrait des ressources en eau souterraine en Chaudière-Appalaches, Québec, Canada. Projet réalisé conjointement par l'Institut national de la recherche scientifique (INRS), l'Institut de recherche et développement en agroenvironnement (IRDA) et le Regroupement des organismes de bassins versants de la Chaudière-Appalaches (OBV-CA) dans le cadre du Programme d'acquisition de connaissances sur les eaux souterraines (PACES), Rapport final INRS R-1580, soumis au MDDELCC en mars 2015.

Li, H., & Carlson, K. H. (2014). Distribution and origin of groundwater methane in the Wattenberg oil and gas field of northern Colorado. *Environmental science & technology*, 48(3), 1484-1491.

Llewellyn, G. T., Dorman, F., Westland, J. L., Yoxtheimer, D., Grieve, P., Sowers, T., Humston-Fulmer, E. and Brantley, S. L. (2015). Evaluating a groundwater supply

contamination incident attributed to Marcellus Shale gas development. *Proceedings of the National Academy of Sciences*, 112(20), 6325-6330.

Lunn, D. J., Thomas, A., Best, N., & Spiegelhalter, D. (2000). WinBUGS-a Bayesian modeling framework: concepts, structure, and extensibility. *Statistics and computing*, 10(4), 325-337.

Mair, R., Bickle, M., Goodman, D., Koppelman, B., Roberts, J., Selley, R., Shipton, Z., Thomas, H., Walker, A., Woods, E. & Younger, P. (2012). Shale gas extraction in the UK: a review of hydraulic fracturing.

McIntosh, J. C., Grasby, S. E., Hamilton, S. M., & Osborn, S. G. (2014). Origin, distribution and hydrogeochemical controls on methane occurrences in shallow aquifers, southwestern Ontario, Canada. *Applied geochemistry*, 50, 37-52.

McPhillips, L. E., Creamer, A. E., Rahm, B. G., & Walter, M. T. (2014). Assessing dissolved methane patterns in central New York groundwater. *Journal of Hydrology: Regional Studies*, 1, 57-73.

Molofsky, L. J., Connor, J. A., McHugh, T. E., Richardson, S. D., Woroszylo, C., & Alvarez, P. J. (2016). Environmental factors associated with natural methane occurrence in the Appalachian Basin. *Groundwater*, 54(5), 656-668.

Molofsky, L. J., Connor, J. A., Wylie, A. S., Wagner, T., & Farhat, S. K. (2013). Evaluation of methane sources in groundwater in northeastern Pennsylvania. *Groundwater*, 51(3), 333-349.

Moritz, A., Hélie, J. F., Pinti, D. L., Larocque, M., Barnetche, D., Retailleau, S., Lefebvre, R. & Gélinas, Y. (2015). Methane baseline concentrations and sources in shallow aquifers from the shale gas-prone region of the St. Lawrence Lowlands (Quebec, Canada). *Environmental science & technology*, 49(7), 4765-4771.

Ó Dochartaigh, B. E., Smedley, P. L., MacDonald, A. M., Darling, W. G., & Homoncik, S. (2011). Baseline Scotland: groundwater chemistry of the Carboniferous sedimentary aquifers of the Midland Valley. British Geological Survey Report (OR/11/021).

Osborn, S. G., Vengosh, A., Warner, N. R., & Jackson, R. B. (2011). Methane contamination of drinking water accompanying gas-well drilling and hydraulic fracturing. *Proceedings of the National Academy of Sciences*, 108(20), 8172-8176.

Reese, S. O., Neboga, V. V., Pelepko, S., Kosmer, W. J., & Beattie, S. (2014). Groundwater and petroleum resources of Sullivan County, Pennsylvania. Pennsylvania Geological Survey, 4th series, Water Resource Report 71.

Sander, R. (2015). Compilation of Henry's law constants (version 4.0) for water as solvent. *Atmospheric Chemistry & Physics*, 15(8), 4399–4981.

Schloemer, S., Elbracht, J., Blumenberg, M., & Illing, C. J. (2016). Distribution and origin of dissolved methane, ethane and propane in shallow groundwater of Lower Saxony, Germany. *Applied geochemistry*, 67, 118-132.

Teasdale, C. J., Hall, J. A., Martin, J. P., & Manning, D. A. (2019). Discriminating methane sources in ground gas emissions in NW England. *Quarterly Journal of Engineering Geology and Hydrogeology*, 52(1), 110-122.

Vengosh, A., Warner, N., Jackson, R., & Darrah, T. (2013). The effects of shale gas exploration and hydraulic fracturing on the quality of water resources in the United States. *Procedia Earth and Planetary Science*, 7, 863-866.

Whittenbury, R., Phillips, K. C., & Wilkinson, J. F. (1970). Enrichment, isolation and some properties of methane-utilizing bacteria. *Microbiology*, 61(2), 205-218.

Williams, G. M., & Aitkenhead, N. (1991). Lessons from Loscoe: the uncontrolled migration of landfill gas. *Quarterly Journal of Engineering Geology and Hydrogeology*, 24(2), 191-207.

Appendix B

Appendix B Table Captions

Table B1
Microseismic distance and injection data for the 109 fracking operations.

Appendix C

Global Moran's I test

The Global Moran's I test from ArcMap 10.3 is a tool used to evaluate whether a spatial dataset, for example TDS concentrations in groundwater, is spatially autocorrelated (i.e. are the data clustered, dispersed or randomly located) based on the data locations and values. The tool initially calculates the mean value for a dataset. The mean is then subtracted from all location values, creating deviation values at each location. Deviation values from neighbouring locations (specified by the user) are then multiplied together creating cross-products. Comparison of cross-product values of neighbouring locations in relation to the mean value describes whether neighbours show similar or different values of that property. When summed together and normalised by the variance the observed index value is calculated and lies between -1.0 and 1.0. The tool also calculates an expected index, which is used with the observed index, the number of data points and the variance of the dataset to create z-scores and P-values. The z-scores and P-values indicate whether any difference between the observed and expected indexes is statistically significant. If the difference is not statistically significant it cannot be ruled out that the spatial distribution is the result of random spatial processes.

Principal Component Analysis

Principal component analysis is a multivariate statistical technique that can be used for a number of reasons: to reduce the number of variables in a dataset; to identify underlying controls in a dataset; and to orthogonally transform a set of potentially correlated observations, for example major cation and anion concentrations in groundwater, into a number of linearly uncorrelated variables on a new coordinate system. These linearly uncorrelated variables are called principal components. The aim of PCA is to explain the

maximum amount of variance in the observations with the fewest number of linear combinations of the existing variables – these are the principal components. There will always be the same number of principal components as variables in the original dataset, but the first principal component accounts for the largest proportion of the variance in the data and this amount decreases with each following principal component. The number of principal components to be considered can be selected by the eigenvalue of each component or the amount of the cumulative variance explained. Interpretation of principal components in terms of the original observations involves computing the loadings between the principal components and observations – these loadings can be interpreted as if they are correlation coefficients though no direct hypothesis testing of their magnitude exists. From these loadings the relative importance of particular observations in a principal component can be assessed. Principal component values for each observation (scores) can also be plotted graphically, for example PC2 versus PC1, which may help identifying groups and trends that are not obvious in the original data. Furthermore, if the observations have location information, for example groundwater sample locations, the principal component values for each observation location can be plotted spatially to assess spatial relationships.

Appendix C Table Captions

Table C1
Groundwater quality data for the 96 unique sampling locations used in this study. The data for each location are mean values for the years 2000-2016, inclusive, and also include the matched BGS borehole data.

Table C2
The number of samples taken for each groundwater property at each unique sampling location between the years 2000-2016, inclusive.

Appendix D

Appendix D Table Captions

Table D1
Field measurements from the 239 surface water samples.

Table D2
Field measurements and ion concentrations from the 170 ICP analysed surface water samples.

Table D3
Field measurements from the duplicate surface water sampling locations